

# A Mechanistic Approach to Design Smart Scaffolds for Tissue Engineering.

Lorenzo Moroni

## Members of the Committee

<b>Chairman:</b>	Prof. Dr. Ir. P.J. Gellings	University of Twente
<b>Secretary:</b>	Prof. Dr. Ir. A. Blik	University of Twente
<b>Promoters:</b>	Prof. Dr. C.A. van Blitterswijk	University of Twente
<b>Assistant Promoter:</b>	Dr. J.R. de Wijn	University of Twente
<b>Members:</b>	Dr. M.L. Bennink	University of Twente
	Prof. Dr. J. Feijen	University of Twente
	Dr. S.J. Hollister	University of Michigan
	Prof. dr. G.J. Vancso	University of Twente
	Prof. dr. H. Weinans	Erasmus University

## A Mechanistic Approach to Design Smart Scaffolds for Tissue Engineering

Lorenzo Moroni

PhD Thesis, University of Twente, Enschede, The Netherlands.

ISBN: 90-365-2423-7

The research described in this thesis was in part financially supported by the European Commission (FP6 project "INTELLISCAF" GSRD\_2002\_00697).

The research described in this thesis was sponsored by:



© L. Moroni. Neither this book nor its part may be reproduced without permission of the author.

Printed by Gildeprint B.V., Enschede, The Netherlands.

Cover Art: Lorenzo Moroni and Cristina Olivo, adapted from "Dynamic Anatomy" by Burne Hogarth.

# A MECHANISTIC APPROACH TO DESIGN SMART SCAFFOLDS FOR TISSUE ENGINEERING

## DISSERTATION

to obtain

the doctor's degree at the University of Twente,

on the authority of the rector magnificus,

prof. dr. W.H.M. Zijm,

on account of the decision of the graduation committee,

to be publicly defended

on Thursday, December 14<sup>th</sup> 2006, at 13.00

by

Lorenzo Moroni

Born on July 13<sup>th</sup>, 1976

in Milan, Italy

**Promoter:** prof. dr. Clemens A. van Blitterswijk

**Assistant Promoter:** Dr. Joost R. de Wijn

*Success isn't the result of spontaneous combustion. You must set yourself on fire*

Arnold H. Glasgow

A Nonna Matilde

A Mamma e Papá

....and to me, myself, and I

## List of Publications

This Thesis is based on the following publications:

### Peer Reviewed Papers

**Moroni L., de Wijn J.R., van Blitterswijk C.A.** Three-dimensional fiber-deposited PEOT/PBT copolymer scaffolds for tissue engineering: Influence of porosity, molecular network mesh size, and swelling in aqueous media on dynamic mechanical properties. *J Biomed Mater Res A* **2005**; 75:957-965.

**Moroni L., de Wijn J.R., van Blitterswijk C.A.** 3D fiber-deposited scaffolds for tissue engineering: Influence of pores geometry and architecture on dynamic mechanical properties. *Biomaterials* **2006**; 27:974-985.

**Moroni L., Poort G, van Keulen F, De Wijn J, van Blitterswijk CA.** Dynamic Mechanical Properties of 3D Fiber Deposited PEOT/PBT Scaffolds: An Experimental and Numerical Analysis. *J Biomed Mater Res A* **2006**; 78:605-614.

**Moroni L., Schotel R., Sohier J., de Wijn J.R., van Blitterswijk C.A.** Polymer Hollow Fiber Three Dimensional Matrices with Controllable Cavity and Shell Thickness. *Biomaterials*, accepted.

**Moroni L., Licht R., de Boer J., de Wijn J.R., van Blitterswijk C.A.** Fiber Diameter and Texture of Electrospun PEOT/PBT Scaffolds Influence Human Mesenchymal Stem Cells Proliferation and Morphology, and the Release of Incorporated Compounds. *Biomaterials* **2006**; 27:4911-4922.

**Moroni L., Hendriks J.A., Schotel R., de Wijn J.R., van Blitterswijk C.A.** Design of Biphasic Polymeric 3D Fiber Deposited Scaffolds for Cartilage Tissue Engineering, accepted.

**Moroni L. and Hendriks J.A.A., Riesle J., de Wijn J.R., van Blitterswijk C.A.** Three-Dimensional Fiber Deposited Scaffolds with Matching Mechanical Properties Favour Cartilage Regeneration. In submission.

**Moroni L., Curti M., Welti M., Korom S., Weder W., de Wijn J.R., van Blitterswijk C.A.** Anatomical 3D Fiber-Deposited Scaffolds for Tissue Engineering: Designing a Neo-Trachea. In submission.

**Moroni L., Schotel R., de Wijn J.R., van Blitterswijk C.A.** 3D Fiber Deposited-Electrospun Integrated Scaffolds Enhances Cartilage Tissue Formation. In submission.

**Moroni L., Paoluzzi L., Pieper J., de Wijn J.R., van Blitterswijk C.A.** Development of Taylor Made Hybrid Scaffolds for Bone and Osteochondral Tissue Engineering. In submission.

## Other Publications

**Moroni L.**, van Blitterswijk CA. Converge and regenerate. *Nat Mater* **2006**;5(6):437-8.

### Selected Abstracts

**Moroni L.**, Curti M., Welti M., Korom S., Weder W., de Wijn J.R., van Blitterswijk C.A. Anatomical 3D Fiber-Deposited Scaffolds for Tissue Engineering: Designing a Neo-Trachea. *European Society of Tissue Engineering and Regenerative Medicine* **2006**, Rotterdam, The Netherlands.

**Moroni L.**, Schotel R., de Wijn J.R., van Blitterswijk C.A. 3D Fiber Deposited-Electrospun Integrated Scaffolds Enhances Cartilage Tissue Formation. *20<sup>th</sup> European Society for Biomaterials Conference* **2006**, Nantes, France.

**Moroni L.**, Hendriks J.A.A., Schotel R., de Wijn J.R., van Blitterswijk C.A. Biphasic Polymeric Shell-Core 3D Fiber Deposited Scaffolds Enhance Chondrocyte Redifferentiation. *Materials Research Society Spring Meeting* **2006**, San Francisco, USA.

**Moroni L. and Hendriks J.A.A.**, Riesle J., de Wijn J.R., van Blitterswijk C.A. Three Dimensional Fiber Deposited Scaffolds with Matching Biomechanical Properties Favor Cartilage Regeneration. *Regenerate World Congress on Tissue Engineering and Regenerative Medicine* **2006**, Pittsburgh, USA.

**Moroni L.**, Licht R., de Boer J., de Wijn J.R., van Blitterswijk C.A. Nanoporosity of PEOT/PBT Electrospun Scaffolds Enhances Cell Proliferation and Influences Cell Morphology. *Society for Biomaterials Annual Meeting* **2006**, Pittsburgh, USA.

**Moroni L.**, Sohier J., de Wijn J.R., van Blitterswijk C.A. 3D Plotted Scaffolds with Hollow Fibers for Drug Release and Tissue Engineering Applications. *19<sup>th</sup> European Society for Biomaterials Conference* **2005**, Sorrento, Italy.

**Moroni L.**, de Wijn J.R., van Blitterswijk C.A. Dynamic Mechanical Properties of 3D Plotted PEOT/PBT Scaffolds: An Experimental and Numerical Analysis. *19<sup>th</sup> European Society for Biomaterials Conference* **2005**, Sorrento, Italy.

**Moroni L.**, de Wijn J.R., van Blitterswijk C.A. 3D Plotted Scaffolds for Tissue Engineering: Dynamic Mechanical Analysis. *5<sup>th</sup> European Cell & Material Conference* **2004**, Davos, Switzerland.

# Table of Contents

<b>Introduction.....</b>	<b>1</b>
Chapter 1	
General Introduction and Aims.....	3
<b>Characterization and Modelization of 3D Scaffolds.....</b>	<b>37</b>
Chapter 2	
3D Fiber Deposited Scaffolds for Tissue Engineering: Influence of Pores	
Geometry and Architecture on Dynamic Mechanical Properties.....	39
Chapter 3	
3D Fiber Deposited PEOT/PBT Copolymer Scaffolds for Tissue	
Engineering: Influence of Porosity, Molecular Network Mesh Size	
and Swelling in Aqueous Media on Dynamic Mechanical Properties.....	60
Chapter 4	
Dynamic Mechanical Properties of 3D Fiber Deposited PEOT/PBT Scaffolds:	
An Experimental and Numerical Analysis.....	78
<b>Mimicking the Mechanical and PhysicoChemical Behavior of a Tissue....</b>	<b>97</b>
Chapter 5	
3D Fiber Deposited Scaffolds with Enhanced Cell Entrapment Capacity	
and Matching Physico-Chemical Properties Favour Cartilage Regeneration.....	99
<b>Relevance of Anatomically Shaped Scaffolds.....</b>	<b>115</b>
Chapter 6	
Anatomical 3D Fiber Deposited Scaffolds for Tissue Engineering:	
Designing a Neo-Trachea.....	117
<b>Influence of Fiber Dimensions and Textures on Cell Faith.....</b>	<b>135</b>
Chapter 7	
Fiber Diameter and Texture of Electrospun PEOT/PBT Scaffolds Influence	
Human Mesenchymal Stem Cell Proliferation and Morphology, and the	
Release of Incorporated Compounds.....	137
<b>Integrate Conventional and Novel Fabrication Technologies.....</b>	<b>160</b>
Chapter 8	
Design of Biphasic Polymeric 3D Fiber Deposited Scaffolds for Drug Release	
and Tissue Engineering Applications.....	161



---

Chapter 9	
3D Fiber Deposited-Electrospun Integrated Scaffolds Enhance Cartilage Tissue Formation.....	189
Chapter 10	
Development of Taylor Made Hybrid Scaffolds for Osteochondral Tissue Engineering.....	205
<b>General Discussion.....</b>	<b>226</b>
Chapter 11	
General Discussion.....	227
<b>Summary.....</b>	<b>241</b>
<b>Samenvatting.....</b>	<b>244</b>
<b>Riassunto.....</b>	<b>247</b>
<b>Acknowledgements.....</b>	<b>250</b>
<b>Curriculum Vitae.....</b>	<b>255</b>
<b>Selected Colour Figures.....</b>	<b>256</b>



## Introduction

Imagination is more important than knowledge

Albert Einstein (1879 – 1955)



# Chapter 1

## General Introduction and Aims

**T**issue engineering has been defined as an interdisciplinary field that integrates principles of engineering and life sciences to develop biological substitutes that restore, maintain, or improve tissue function [1]. Three main gears are generally needed to achieve tissue regeneration: cell-based therapies, tissue-inducing factors, and biocompatible matrices or scaffolds. These components have been investigated singularly or in combination to create engineered tissues. Since the use of cell-interacting and/or biofactors-releasing scaffolds demonstrated to improve the quality of tissue engineering applications, it is of interest to look at how these scaffolds can be further improved to obtain a better control over the multiple functionalities of a regenerating tissue.

In its broadest meaning scaffolds used in medicine can be traced back until the ancient times of the Incas, as they were used by surgeons to repair cranial defects (cranioplasty) and consisted of molded materials such as gourds, gold, and silver [2]. However, we have to wait until 1668 to have the first successful case reported in literature by Job Janszoon van Meekeren – a surgeon from Amsterdam – where a scaffold or graft was used to repair a bone defect [3]. Since then, many developments have occurred in the field of tissue substitutes or grafts. Among others, Ollier was one of the first to introduce and explain the notions of autograft, allograft, and xenograft [4], where these generally refer to tissue substitutes within the same individual, between individual of the same species, and between individuals of different species respectively. Yet, the concept of scaffolding as a porous matrix or as an implant in which cells can slowly infiltrate and regenerate the local tissue was first introduced by Barth in 1893 [5], and it is only in the last two decades that it has been extensively used to indicate natural or synthetic substrates that can temporarily support cells [6-8] and direct their fate towards appropriate cell-material interactions and release of biological factors [9-11]. Therefore, generally speaking scaffolds for medicine applications can be seen as tissue substitutes, grafts, or porous substrates that interact with cells to promote and maintain during time their differentiation state, in which they express and produce that specific “cocktail” of proteins and growth factors contributing to form a precise functional tissue. More formally, scaffolds are defined in the tissue engineering and biomaterials community as porous structures, usually polymeric, which serves as a substrate and guide for tissue regeneration (Williams Dictionary, 1999).

Within this scenario, the fabrication methods and biomaterials used to make scaffolds for tissue engineering are first critically reviewed. Particular attention will be given to the rapid prototyping techniques and to the polymeric family mainly

used in this research. The aims and synopsis of the thesis will then be introduced to conduct the reader through the book.

## Scaffolds Fabrication Methods

Biomaterial porous scaffolds are generally investigated for tissue engineering and controlled drug delivery applications as three dimensional (3D) means to vehicle medical treatments in specific locations [12-15] and to guide cell attachment, proliferation and differentiation into the tissue to regenerate [16-19]. Beyond the fact that these constructs must be biocompatible and possibly biodegradable and/or bioresorbable, they also have to offer an initial and adequate mechanical support for the seeded cells to integrate with the surrounding tissue, to facilitate regaining the original shape of the treated defect, and to provide the appropriate physico-chemical properties to release a desired biological agent and/or to direct cells fate and the extra cellular matrix (ECM) produced by them into a specific tissue (figure 1). Furthermore, a number of studies lately showed that the ability of scaffolds to control-release at least one biological signal may favor formation of tissues [20-22].

### General Requirements for 3D Scaffolds in Regenerative Medicine

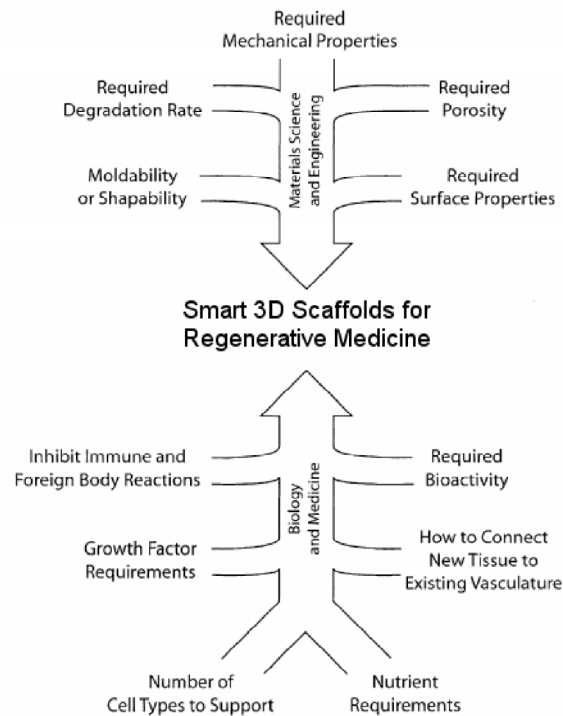


**Figure 1** – Schematic draw of the general material and biological requirements for a 3D scaffold in tissue engineering.

Many different techniques and devices have been developed to fabricate porous 3D scaffolds, each with its own advantages and drawbacks. Table 1 summarizes the main material processing and porosity creation techniques that are currently used to fabricate scaffolds for regenerative medicine. The introduction of rapid prototyping technologies in medical science led to a distinction between porogen- and mold-based “conventional” techniques on the one hand, and model-, electrostatic-, and surface-based “novel” methods on the other. Conventional methods encompass fabrication technologies where the biomaterial is either mixed and molded with porogen agents that are selectively leached to create porosity, or processed to make textile fabrics. Novel model-based methods are based on computer aided design (CAD) and computer aided manufacturing (CAM) to build porous 3D scaffolds in a

Material Processing Techniques	Phase	Biomaterials	Creation Porosity Techniques	Scaffold Fabrication Method
Molding		All	Porogen	Particulate Leaching
Casting Solutions		Polymers		Selective Leaching
(Electro)Spinning		Polymers		Phase Separation
Sintering		All		Gas Foaming
Extrusion	Melts Sturries-Pastes	Polymers All	Textile	Braid
(Photo)Polymerization		Polymers		Woven
			Rapid Prototyping	Knitted
				Non-Woven
				3D printing™
				FDM
				SLS
				SLA

**Table 1** – General material processing and porosity creation techniques associated to the biomaterials used and to the scaffold fabrication method. “All” refers to polymers, ceramics, and metals.

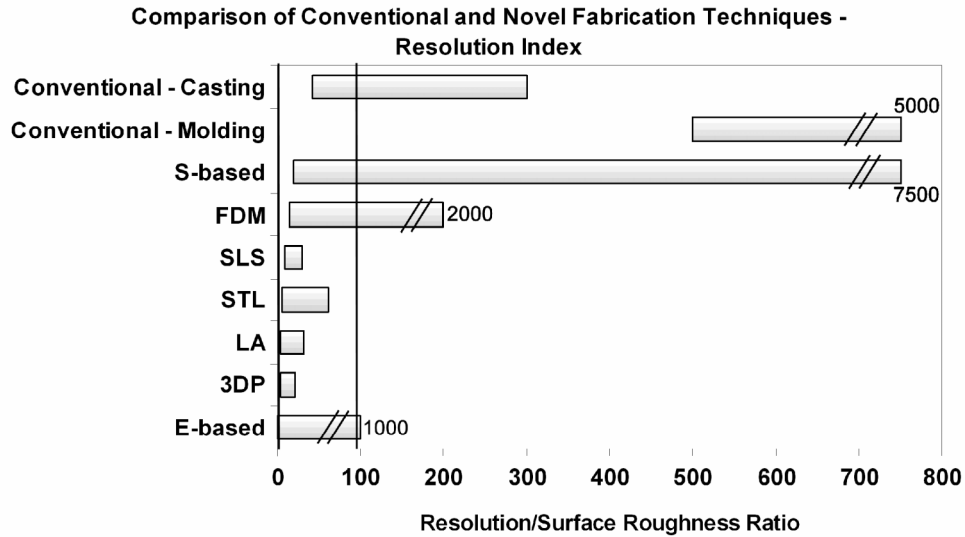


**Figure 2** – Comparison of conventional and novel fabrication techniques in terms of the ratio between the resolution and the surface roughness. S-based = Surface based techniques; FDM = Fused Deposition Modelling; SLS = Selective Laser Sintering; STL = Stereolithography; LA = Laser Ablation; 3DP = 3D Printing; E-based = Electrostatic based techniques.

layer-by-layer controlled manner. In case of electrostatic-based methods, a high voltage electric field is applied to destabilize a fluid biomaterial (solutions, gels, melts, slurries, or pastes) and form 3D scaffolds with micron- and nano-meter features. Figure 2 introduces a comparison of the fabrication techniques in terms of their resolution/surface roughness ratio. Generally, in prototype manufacturing applications this index should be optimized to achieve the minimal surface roughness. In this way a smooth surface as possible is coupled to the current limitation of the technique used. If prototyping is used in tissue engineering, however, surface roughness is desirable up to a certain extent – estimated as one or two order of magnitude lower than the technique resolution – due to its positive influence on cell attachment, morphology, and differentiation. Furthermore, the combination and integration of different conventional and novel technology platforms can be also envisioned to fabricate multifunctional 3D scaffolds that provide an improved interface with cells and with the human body. The most significant techniques are reviewed hereafter.

### ***Conventional Fabrication Methods***

Conventional scaffold fabrication techniques include fiber meshes and bonding, gas foaming, phase separation, freeze drying, and particulate leaching, among others. Fibrous non-woven, woven or knitted scaffolds can be fabricated from polymeric fibers manufactured with standard textile technologies [23-25]. These scaffolds, however, lack structural stability and consequently they can experience high deformations due to cells contractility and motility [26, 27]. To improve the mechanical properties a fiber bonding technique has been developed [28-30], where by applying a heat treatment, the fibers of the scaffolds are joined at the cross-points.

Alternatively, in gas foaming the polymer is saturated with carbon dioxide ( $\text{CO}_2$ ) at critical pressures to achieve high solubility of the gas in the polymer. When the gas pressure is brought back to the atmosphere pressure, the solubility of the  $\text{CO}_2$  in the polymer rapidly decreases, resulting in the formation of gas bubbles or enclosures of variable size [31-33]. A similar approach is applied in phase separation, where a polymer solution is quickly cooled at low temperatures to generate a liquid-liquid phase separation. The solution is quenched and a two-phase solid is formed. The solvent is then removed by sublimation to fabricate the porous scaffold [34-36]. Freeze drying is slightly different from phase separation, since the polymer solution is directly frozen or freeze-dried to yield porous scaffolds [36-38].

Particulate leaching consists of incorporating particles of a specific size (salt crystals or polymeric particles with defined shape and geometry) into a polymer solution, where the solvent used is a non-solvent for the particles. After evaporation of the solvent, a porous scaffold can be produced by leaching out the particles in a medium that is non-solvent for the polymeric scaffold [39-42]. These fabrication techniques have been broadly used to make 3D scaffolds for possible tissue engineering and drug release applications. However, a number of drawbacks can be outlined in their use for an optimal control of tissue formation and drug release profile. Although the pore size and shape of these matrices are controllable to some



extent, not completely interconnected and tortuous pathways are created, which is disadvantageous for nutrient supply and for effective release of biological signals. Pore tortuosity, which can be defined as the ratio of the actual length of the arbitrary pathway that a molecule has to cover to pass through a pore to the shortest linear distance, biases the distribution of viable cells within the scaffolds [43]. Since pore tortuosity is rather high in scaffolds fabricated with conventional techniques, cell viability is limited mostly to 0.5-1 mm in depth [44, 45]. Recent studies found that this phenomenon is also associated to a drop in the oxygen concentration from the outside to the center of the scaffold [46-48]. Furthermore, the incorporation of drugs, growth factors, or other biological agents is hampered by the processing conditions. In thermoplastic technologies the high temperatures involved in the manufacture can compromise the stability of the compound to be integrated, resulting in its denaturation and loss of activity. In solution-based techniques the solvents used can also hinder the stability of the desired biological factor due to a pH change, which will promote aggregation and loss of activity of the factor [34, 49]. In particulate leaching a further arising problem is connected to the efficiency of the agent incorporation, since during the washing step to create the porous scaffold part of the compound is washed away.

### ***Novel Fabrication Methods – Rapid Prototyping***

Among novel scaffold fabrication techniques, rapid prototyping systems appear to be the most promising to satisfy the many of the general requirements for a biomaterial, as they can process a wide number of biomaterials [50-52] in a

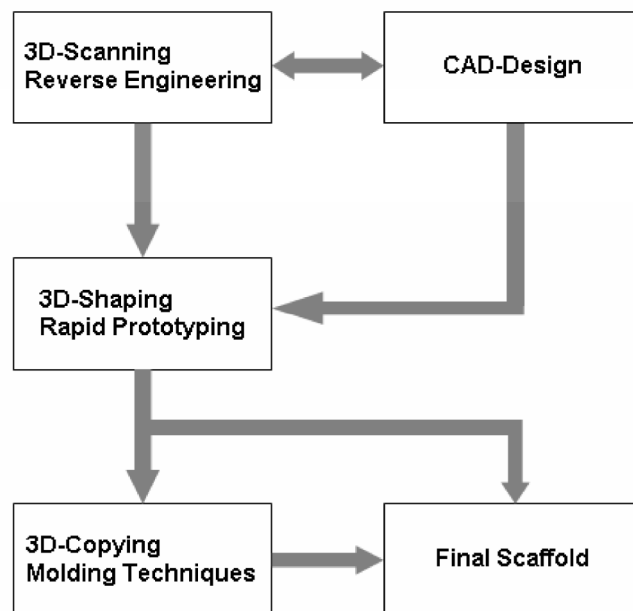


**Figure 3** – Flow chart of CAD model-based novel fabrication technologies.

custom-made shape and with matching mechanical properties in comparison with the specific application considered [53-55]. The outcomes are three-dimensional (3D) scaffolds that possess fine tunable porosity, pore size and shape, and have a completely interconnected pore network, which allows a better cell migration and nutrient perfusion than 3D scaffolds fabricated with conventional techniques [44, 46]. Figure 3 presents the general modeling concept at the base of rapid prototyping. Within the rapid prototyping systems, 3D fiber deposition (3DF) has

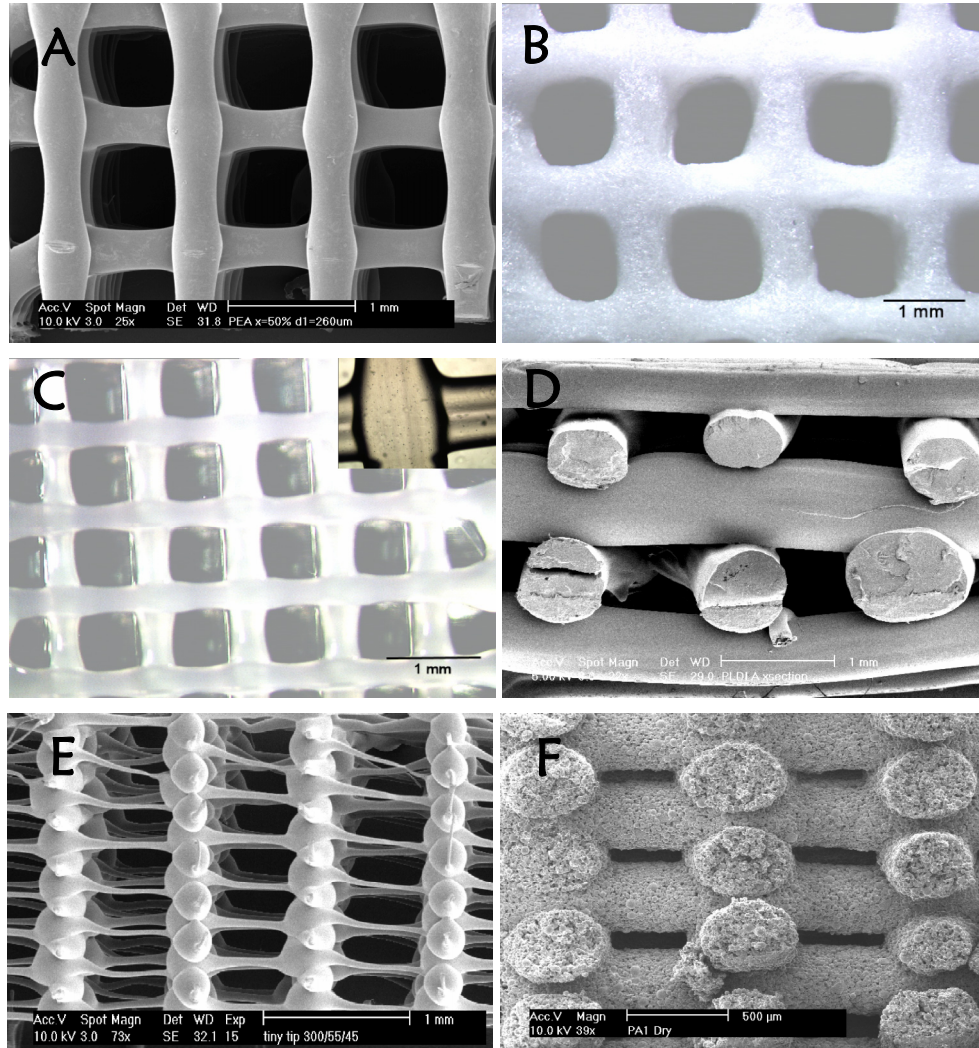


**Figure 4** – Scanning electron (SEM) and optical microscopy (OM) pictures showing some examples of biomaterials processable with 3D fiber deposition technique. (a) thermoplastic polymers (polyester amide – oxide); (b) demineralised bone matrix; (c) hydrogels (lutrol™ - in the insert cells encapsulated in the gel; courtesy of Fedorovich *et al* [60].); (d) PLA; (e) PEOT/PBT; (f) PEOT/PBT microspherical paste. Scale bar: (a-e) 1 mm; (f) 500  $\mu$ m.

been lately investigated by our group to fabricate custom-made scaffolds and to modulate their mechanical properties for tissue engineering applications showing encouraging results [56-59]. In contrast, scaffolds fabricated with conventional techniques can still be shaped with custom-made molds, but it is more difficult to control their mechanical properties, pore size, shape and interconnectivity, resulting in nutrient limitations and cell apoptosis in the center of the construct as previously explained. Briefly, 3DF is a fused deposition modeling (FDM) technique, where molten thermoplastic polymers, hydrogels, and biomaterial pastes are extruded from a CAM controlled robotic unit on a stage in the form of a fiber. These filaments are deposited to form a layer and a 3D scaffold is built with a layer-by-layer strategy, following a CAD pattern. As shown in figure 4, with this technique many different materials – including gels that encapsulate cells [60] – can be processed and organized in different architectures. Different fiber architecture can be achieved, resulting in different pore shapes (figure 5). Moreover, the possibility to acquire computer tomography (CT) or magnetic resonant imaging (MRI) anatomical data from patient datasets offers the fascinating possibility to fabricate anatomically shaped scaffolds, which are custom-made for each specific patient (fig. 6).

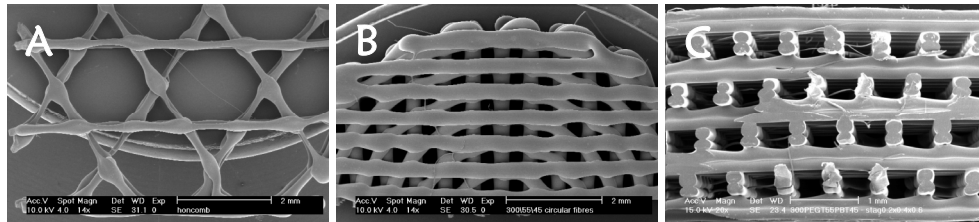


**Figure 5** – SEM micrographs of some possibilities to organize fibers during deposition, resulting in different pore shapes. (a) honeycomb pores; (b) concentric cylindrical fiber deposition; (c) staggered fibers along the cross section development. Scale bar; (a, b) 2 mm; (c) 1 mm.

Many other FDM and extrusion-based tools have been developed to fabricate 3D scaffolds, comprising also multi-dispensing systems that allow depositing different materials at the same time to produce constructs with different physico-chemical properties [61]. This possibility is quite appealing to study the release of multiple compounds from a single scaffold and to exploit the different interactions of the polymers with different cell populations in order to regenerate a more complicated hierarchical structure [62]. Although FDM techniques demonstrated to considerably improve the quality of tissue engineered constructs [59, 63-66], the high temperatures involved during fabrication of molten polymers remain still critical for the direct incorporation of biological factors. A solution could be envisioned if not only metallic [67] or ceramic pastes [68, 69], but also polymeric pastes that can be processed at room temperature will be developed. Alternatively, surface modification techniques could be used to functionalize the fibers and allow grafting of the agents in specific sites [21, 70].

Other direct printing technologies include solid free form (SFF) techniques like 3D printing™ (3DP), selective laser sintering (SLS), and laser ablation (LA). 3DP was one of the first rapid prototyping devices to be developed for tissue engineering

applications. Here, a 3D scaffold is fabricated by depositing in a CAD/CAM controlled manner a jet of solvent on top of a polymer powder-bed. The solvent binds the powder, thus forming a pattern of fibers. The scaffold is then built layer-by-layer [71, 72]. In a similar way, selective laser sintering consists in projecting a laser

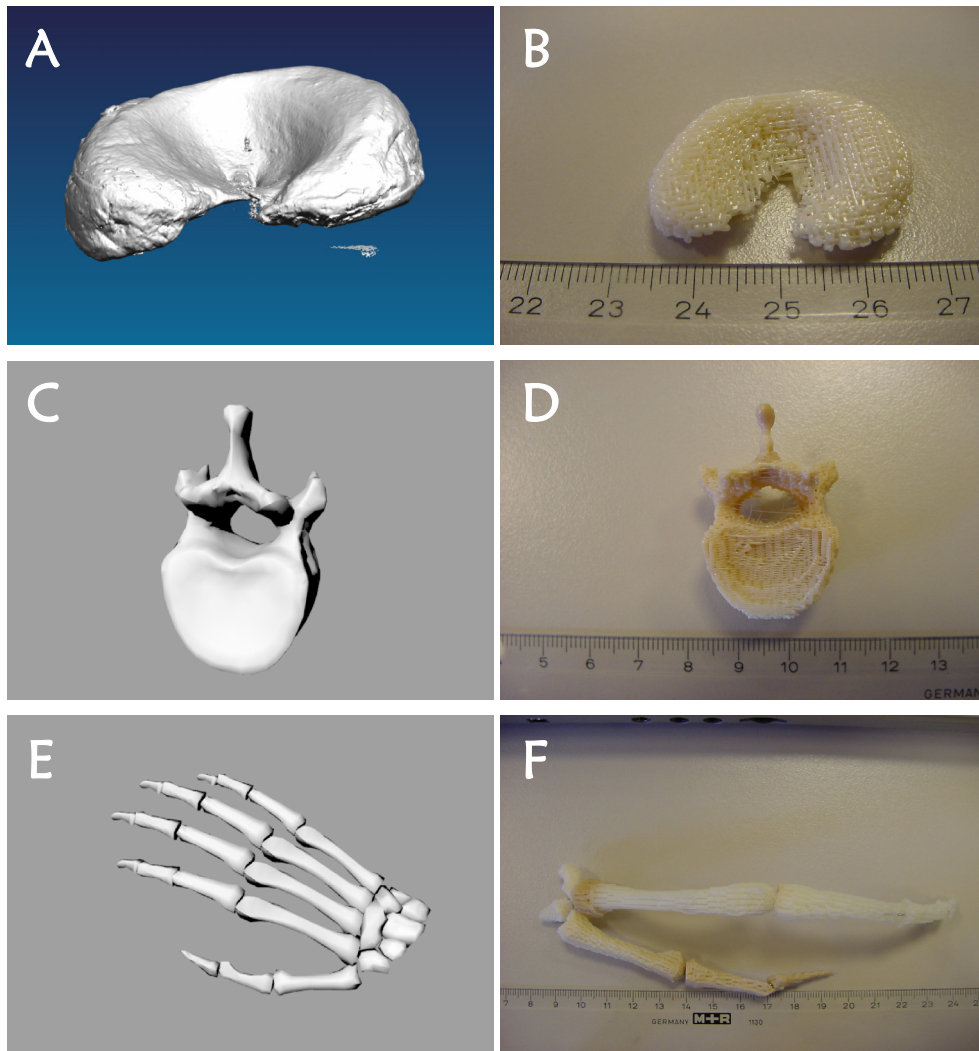


**Figure 6** – Examples of CT/MRI anatomical models (a, c, e) and correspondent anatomically shaped fabricated 3D scaffolds. (a, b) meniscus; (c, d) vertebra; (e, f) finger joints.

beam on a polymeric powder-bed. The laser beam sinters the powder due to the local increase of the temperature above the glass transition temperature of the polymer. The 3D scaffolds are still fabricated in a CAD/CAM fashion [73, 74]. Laser ablation works in the opposite way, as from a solid block of material the porous structure is formed through the ablation of the material hit in specific locations by

the laser beam [75]. If the ablation process is conducted in all of the three directions or if laminated porous films are stacked and bonded on top of each others, a 3D scaffold can be created. These techniques allow the fabrication of periodic structures with well defined, controlled and completely interconnected porosity. They showed the ability to support the formation of improved tissue constructs [16, 18, 74, 76], but still have the disadvantage of using solvents (3DP) or of producing excessive heat (although here localized to the spot where the laser beam hit the polymer, as in SLS and LA), which will affect or compromise the direct incorporation of pharmaceuticals, proteins, or growth factors. Furthermore, extra processing is required to obtain the polymers in powder. A promising modification of SLS that can release active compounds like ribonuclease is surface selective laser sintering (SSLS) [77], although ribonuclease is known to be an exceptionally stable enzyme. Typically, SLS makes use of infrared radiation that hits the polymer particles. The radiation is absorbed volumetrically by the whole particles, which sinters together. SSLS, instead, exploits near-infrared laser. In this case, the radiation is not absorbed by the polymer particles, but by carbon microparticles spread on the surface of the polymer particles. Carbon microparticles are strongly reactive in the near-infrared region and for this reason are used as initiators for the sintering process. Being distributed only on the surface of the polymer particles, sintering happens only superficially.

Biocompatible and biodegradable photosensible polymers that can be used in rapid prototyping techniques like stereolithography (STL) are also investigated. Stereolithography is normally used to produce a negative replica that is filled typically with ceramic or metallic slurries and burnt away during sintering [78]. This step still includes the use of high temperature. Therefore, the use of photosensible polymers in this system would allow the direct fabrication of the scaffold. Incorporation of any biological compounds, however, depends on the sensibility of their activity when hit by the light source (typically UV or blue light) used to start the polymerization.

Many other rapid prototyping technologies have been developed or modified based on existing ones and showed to improve the current resolution limitations with the possibility to directly deposit gels that encapsulate cells or even encompass cell and protein suspensions [79-83]. Rapid prototyping technologies are nowadays a consolidated scaffold fabrication platform and demonstrate encouraging applications for tissue engineering offering a fermenting base to further understand fundamental biological phenomena at the same time improving the quality, the enduring, and the success of regenerative medicine based products.

### ***Novel Fabrication Methods – Electrospinning Technologies***

A desirable characteristic that should be considered in designing and fabricating 3D scaffolds is mimicking the extra cellular matrix (ECM) fibers dimension and topology. With rapid prototyping fabrication techniques this remains still a major challenge. A possible solution to this problem is given by electrospinning (ESP). ESP is a relatively old technique normally employed in polymer technology to spin small diameter fibers [84-86], which recently found applications in tissue engineering as an

electrostatic-based scaffold fabrication method [87-90]. As schematically shown in figure 7, ESP consists of spinning fibers from a biomaterial solution, typically a polymer, by exploiting a high electric field generated by a voltage supply between the solution depot and a collector unit. Depending on the thickness of the fibrous network deposited on the collector, it is possible to fabricate bi-dimensional or three-dimensional structures that can be used to entrap and release drugs [91-93], and/or to seed and culture cells for the regeneration of a specific tissue [93-95]. The particular small dimension of the spun fibers, typically in the same range of ECM

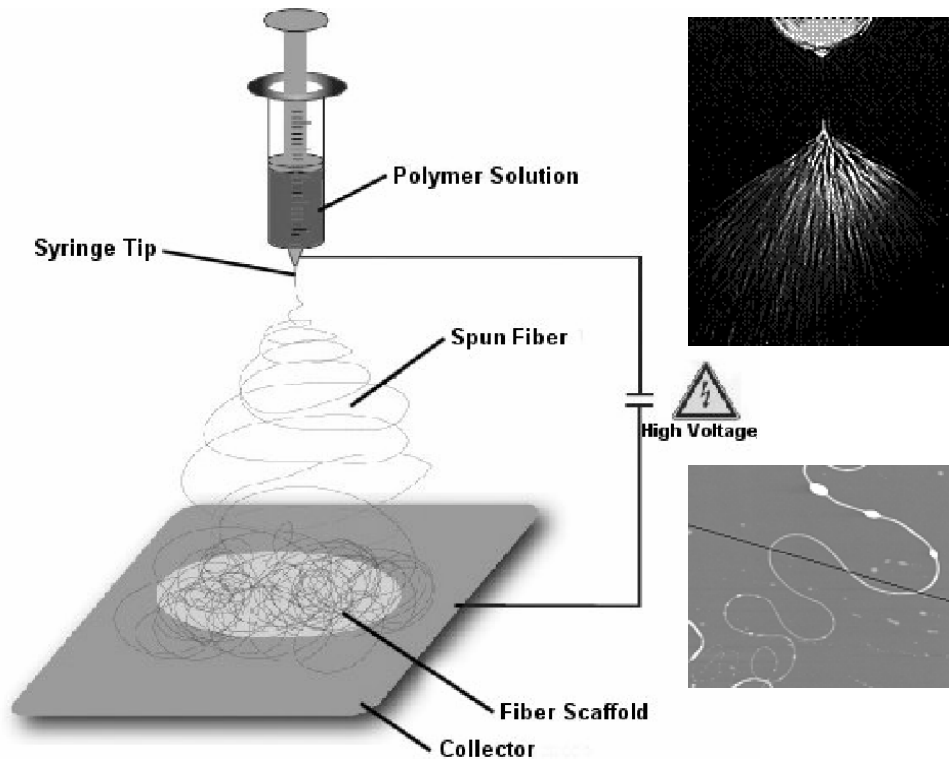


**Figure 7** – Schematic draw of the electrospinning process.

fibrils, makes these structures appealing as they can mimic ECM and possibly influence cells to express the proper proteins and signals. Surface micro- and nano porosity is also another important characteristic of fibrous scaffolds, as it seems to contribute to the creation of a better milieu for the cells for the expression of appropriate ECM components [96-98]. In this respect, electrospinning is an intriguing tool, since the spun fibers can either be made porous or textured [89, 99, 100], or *vice versa* non porous and smooth [89, 101], depending on the chemical properties of the solvent used and on the device settings. Fibers are normally randomly oriented on the collector, but it was shown that it is possible to bias their orientation, e.g. by properly designing the collector plate [102, 103]. Further

sophistication in fiber morphology and architecture included the fabrication of scaffolds with coaxial or hollow nanofibers [103-106]. Cell suspensions and cells directly entrapped in ESP networks have been also successfully processed, thus enlarging the applications of such ECM mimicking matrices as multifunctional tissue engineering scaffolds [107-109].

### ***Novel Fabrication Methods – Surface Based Technologies***

A slightly different set of techniques comprises lithographic tools. These devices find applications in the biomedical field to fabricate 2D or 2.5D – here referred to high aspect ratio features – membranes with specific surface topologies, which have shown to improve cell-material interactions and direct cell fate [110-112]. This can lead to better cell attachment and differentiation [113-115], to an enhancement of the material biocompatibility, and, therefore, to a thinner capsule formation when implanted *in vivo* [116-118]. If the fabricated membranes are stacked and appropriately bonded together, a 3D scaffold can be built [119]. Among lithographic technologies, micropatterning allows the fabrication of custom-made topography with excellent control over the feature shape and size [120-122]. A number of materials have been surface-modified with this system, originally applied to metals and silicon-based materials [123] and more recently extended to polymers [124-126]. Lithography typically consists in the transfer of topological features or patterns onto the surface of silica chips. The patterns are first designed with modelling software and used to create a mask. This mask is shined by a light source in the lithography device, creating selective regions where the light goes through and hit the silica chips, previously coated with a radiation-sensitive material (resist). The pattern transfer is ultimately fixed on the silica by etching the resist. Depending on the light source, lateral resolutions from 1  $\mu\text{m}$  (UV light) to few nanometers (electron beam) can be achieved. Micropatterning or microcontact printing makes use of the patterned silica chip as a master copy to transfer its negative to soft substrates such as silicon or other polymers by either in situ hardening or embossing [97]. A further modification is introduced in colloidal lithography where the masks are made by electrostatically assembling dispersed monolayers of colloidal particles [127]. Depending on the particles size, the resolution can be downscaled to approximately 100 nm. Since microcontact printing and related techniques are based on a stamp transfer mechanism, it is relatively simple to extend their applications to pattern specific biomolecules on top of a biomaterial surface [117, 128-131], thus increasing the degree of multifunctionality of the scaffolds.

A more recent method that exploits a high electric field to induce the formation of patterned material surfaces is electrically induced pattern transfer [132, 133]. In this technique one or more polymer films spun-coated from a solution are placed in between two patterned electrodes. The electrodes are very close ( $d < 1 \mu\text{m}$ ) and separated by a very thin air-gap. The system is, then, heated above the higher glass temperature of the polymeric films. By applying a voltage, a very high electric field is generated due to the very small gap between the two electrodes. This causes instability of the films that occurs at the smallest distance to the patterned electrode

– i.e. the patterns themselves. Therefore, a high aspect ratio replica of the patterned electrode is generated on the polymer film surface.

### *Integration of scaffolds fabrication technological platforms*

The development and integration of novel and/or conventional fabrication techniques is gearing biomaterial design towards multifunctional scaffolds for regenerative medicine. Several combinations of technologies from different scientific disciplines are currently investigated to create and integrate features at different scales, which are of primary importance for the improvement of the current status of tissue engineering applications [134]. An emerging method to precisely analyze which biomaterials are optimal to elicit specific cell-material interactions makes use of micro-array combinatorial approach and may be named as “materiomics” in accordance with the analogous systems to study gene and protein expressions. In this technique, biomaterials can be directly synthesized or chemically patterned in a nano-liter scale to form microarrays that are used to study cell attachment and differentiation [135-138]. Alternatively, series of ligands and/or extracellular matrix components can be deposited in a microarray to study cell faith [139, 140]. In this way, a number of libraries can be compiled containing material- and biomolecule-related cell responses. Depending on the specific tissue engineering application and on the clinical strategy decided, a desired biomolecule-biomaterial couple can be selected. A further improvement of such a method would consist in the inclusion of these biomolecules in biomaterials to combine the material- and the bio-related cell responses in a 3D scaffold.

Other examples of technology platforms integration are offered by the combination of biomaterials processed at different length scales. Here, the rationale is to combine a macrostructure to support cells and tissue development with a synthetic temporary ECM at the micro- and nano-scale. The ECM network would also have the capacity to entrap a higher number of cells, resulting in a considerable improvement of cell seeding efficiency. An interesting possibility to achieve such an improved functional scaffold consists in interspersing sheets of ECM derived microsponges with sheets of synthetic foams, meshes, textiles, or felts [141, 142]. The resulting structures are 3D scaffolds with adjustable thickness, which displays macro- and micro-porosity combined with the flexibility of the constructs. In another approach, the combination of porogen leaching and phase separation techniques allowed the fabrication of nanofibrous scaffolds with interconnected macropores, associating macro- and nano-scale features in the same constructs [143]. A further combination of conventional fabrication techniques consists in coupling gas foaming with ultrasound that resulted in the solvent-free fabrication of a porous 3D scaffold with enhanced pore interconnectivity [144].

Conventional and novel fabrication techniques have been also integrated by associating fiber bonding with electrospinning. The resulting 3D scaffolds comprise a micro- and a nano-fibrillar network, which shows to support a higher cell viability and differentiation into the bone lineage [145]. Similarly, the integration of knitted and ESP fibers proves to support a higher cell attachment and the expression of typical tendons and ligaments markers [146]. Additional examples of conventional



technology combinations with ESP consist in the integration of wet spinning to create multifunctional 3D scaffolds for vascular tissue engineering [147] where the ESP microfibrillar web was deposited on the wet-spun macrofibrillar network to create a structure mimicking vessels. Similarly, ESP nets were modified by immobilizing RGD adhesive peptides on the fibers surface, which enhanced cell attachment, spreading, and proliferation [148]. A particular intriguing integrated technology encompasses ESP scaffolds where fibers are coated by electrochemical deposition with a conductive polymer. In this case it was shown that the release of drugs could be selectively controlled not only by diffusion through the coaxial fibers, but also by applying and releasing an electrical stimulus to the conductive polymer resulting in its expansion and contraction respectively [149].

A great interest has been arisen to use single and multi walled carbon nanotubes (CNTs) as biomaterials for scaffolds in tissue engineering. A few groups have demonstrated a comparable cell viability and attachment with respect to standard biodegradable polymers and, more interestingly, an enhanced adhesion of osteoblasts [150-153] with an improved cytotoxicity as compared to conventional carbon fibers [152]. Composites of CNTs with ceramics and metals are extensively studied and showed to improve the toughness and/or the toughening mechanisms during fracture by deflecting crack formation [154, 155]. A recent combination of CNTs and ESP silk fibers appeared to have an almost 5-fold increase in elastic modulus and could be promising due to the integration of high mechanical (CNTs) and protein adhesion (silk) properties.

All of the above treated techniques belong to a so called “top-down” fabrication approach, where biomaterials are generated by stripping down a complex entity into its component parts. An alternative way to proceed is the “bottom-up” approach, in which materials are assembled molecule by molecule to create novel supramolecular architectures. Self-assembly is surely the most promising “bottom-up” technique for regenerative medicine. Self assembled monolayers (SAMs) have already been studied to selectively control protein and cell adhesion, but they are limited in that they are bi-dimensional structures [156]. A sensible improvement of SAMs is offered by molecular self-assembly of synthetic amphiphilic peptides. Due to their particular polar hydrophilic “head” and non-polar hydrophobic “tail” structure, these molecules voluntarily change their conformation in aqueous solutions and undergo self-assembly to form various semi-enclosed environments through the formation of many non-covalent weak chemical bonds. Depending on the geometry and curvature of the polar head and the shape and length of the non-polar tails it is possible to drive them to form a nanofibrillar 3D network [157]. By combining the desired peptide sequence, which is then synthesized into the correspondent amphiphilic structure, with surface functionalization with the proper biomolecule for a specific application, self-assembled 3D nanofibrillar scaffolds have been fabricated and used for bone [158], cartilage [159], vascular [160], and neural tissue engineering [161], among others [162-166]. Results seem to be promising, although the *in vivo* self-assembly process and *in situ* stabilization mechanisms need to be better understood for a proper control of the technology in regenerative medicine.

## Biomaterials for Scaffolds in Tissue Engineering

Among the biomaterials so far studied, synthetic and natural polymers offer a wide variety of choices to satisfy most of the above mentioned requirements. The mainly used polymers are hereafter considered. Table 2 summarizes some of the properties of these biomaterials and their applications in tissue engineering and drug delivery.

### *Synthetic Polymers*

Within synthetic polymers, linear aliphatic polyesters such as poly(lactic acid) (PLA), poly(glycolic acid) (PGA) and copolymers (PLGA) have been broadly used in tissue engineering. They generally activate a minimal or mild foreign body reaction – and as such are considered as biocompatible – and they are approved by the food and drug administration (FDA) for certain applications. By varying their molecular weight and in case of PLGA also their copolymer ratio, the biodegradation rate and the mechanical properties can be tailored. They have already been studied for drug delivery [14, 20, 167-169] and are suitable for tissue engineering applications [170-175], as the degradation products (lactic and glycolic acids) obtained due to hydrolysis are normally present in the metabolic pathways of the human body. However, their bulk degradation may lead to the formation and accumulation of large amount of degradation products in a short time frame (months vs. years) that cannot be easily disposed off, resulting in local inflammation in tissues [176] and enzymatic hydrolysis [177]. Furthermore, depending on the polymer or copolymer used, if crystal domains are present in the polymer chain they may remain in the body. Another linear aliphatic polyester commonly used in tissue engineering is poly( $\epsilon$ -caprolactone) (PCL). This polymer has found many applications for its good biocompatibility and mechanical properties, but it degrades at a much slower rate than PLA, PGA, and PLGA, which makes it attractive when long-term implants and long-term controlled release applications are desired [174, 178-180].

A different family of thermoplastic polymers that has been recently studied for tissue engineering and drug delivery is poly[poly(ethylene oxide) terephthalate-co-(butylene) terephthalate] (PEOT/PBT). These polyether-ester copolymers (figure 8) exhibit good physical properties like elasticity, toughness and strength in combination with easy processability [181]. These properties result mainly from a

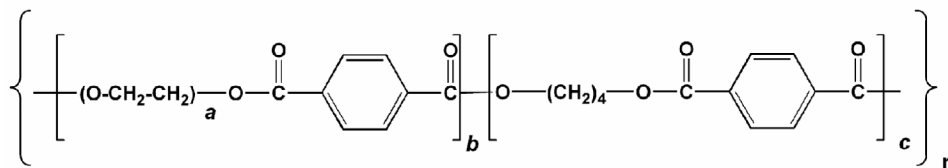


**Figure 8** – Chemical structure of aPEOTbPBTc copolymers, where a is the molecular weight of the initial PEG blocks used in the copolymerization, b and c are the weight percentage of the PEOT and PBT domains resulting at the end of the reaction.

phase separated morphology in which soft, hydrophilic PEO segments at environmental temperatures are physically cross-linked by the presence of hard,

semi crystalline PBT segments. In contrast to chemically cross-linked materials, these cross-links are reversible and will be disrupted at temperatures above their glass transition- or melting point, *vice versa*, which gives the material its good processability. The interest arisen in tissue engineering and drug delivery applications is due to the fact that by varying the molecular weight of the starting PEG segments and the weight ratio of PEOT and PBT blocks it is possible to tailor properties, such as wettability [182], swelling [181, 183, 184], biodegradation rate [184], protein adsorption [185], and mechanical properties [57, 186]. Furthermore, PEOT/PBT copolymers have shown to be biocompatible both *in vitro* and *in vivo* for skin, cartilage, and bone regeneration [46, 187-190] and reached clinical applications (PolyActive™, IsoTis Orthopaedics S.A.) as cement stoppers and bone fillers in orthopedic surgery [191, 192]. Being polyether-esters, degradation occurs in aqueous media by hydrolysis and oxidation, the rate of which varies from very slow for high PBT contents to medium and fast for larger contents of PEOT and longer PEO segments [181, 184]. A further modulation in degradation rate and drug release profile can be achieved by substituting part or all of the terephthalate domains with succinate blocks during the copolymerization reaction [103, 193, 194]. PLA, PGA, PLGA copolymers, PCL, and PEOT/PBT copolymers are equally suitable for many tissue engineering applications. They have proven to be appealing biomaterials to fabricate 3D scaffolds and have been widely used with promising results in regenerative medicine. Albeit they can have multiple properties tailored for specific purposes, some concerns over their degradation mechanism and rate still remain. Among the multitude of other synthetic polymer investigated for controlled release and tissue engineering applications, interesting classes are polyphospho-esters (PPEs) [195, 196], polyphosphazenes (PPAs) [197-200], polyanhydrides (PAs) [201] and polyortho-esters (POEs) [202], as they have shown a surface erosion degradation mechanism [203, 204], which is also known to affect the stability of the scaffolds to a lesser extent and to elicit a lower *in vivo* inflammatory response, as compared to polyesters and polyether-esters previously considered. PPEs display adequate mechanical properties also for hard tissue engineering. Although PPAs, PAs, and POEs have also been used in some cases for hard tissues repair, they might be more suitable for soft tissue engineering due to their generally low mechanical properties. An alternative to the previous polymeric systems is offered by injectable polymers. This class is also very attractive as they can be used in minimally invasive surgery such as arthroscopy, resulting in a decrease in patient discomfort. Furthermore, they can fill irregularly shaped tissue defects [205-207], and cells and bioactive agents can be easily incorporated into them [208-210]. In particular, photopolymerizable systems like poly(propylene fumarate)-diacrylates (PPF-DA) and poly(ethylene glycol)-diacrylates (PEG-DA) based polymers, have been investigated since they can be transdermally hardened *in situ* by applying a light source [211-213]. Alternatively, chemically curable polymers still based on PPF have also been studied as they eliminate the need for light [214]. Despite the advantage of these polymers that is to favor minimally invasive surgery, some issues may still rise from their low mechanical properties and from some remnant toxicity due to the acrylic groups.

	Biocompatibility	Biodegradability	Bulk Mechanical Stiffness (GPa)	Tissue Engineering	Drug Release
PLA	Degradation products in metabolic pathway	Bulk – 5 months to ~ 5 years	2 – 3	Skin; Cartilage; Bone;	Drugs;
PGA	Local Inflammation	Bulk – 1 to ~ 12 months	5 – 7	Ligaments; Tendons; Vessels;	Proteins;
PLGA	Enzymatic Hydrolysis	Bulk – 1 to ~ 12 months	2 – 7	Nerves; Bladder; Liver	Growth Factors
PCL	Hydrolysis Minimal Inflammation	Bulk – more than 3 years	0.4	Skin; Cartilage; Bone;	Model Drugs.
PEOT/PBT	Hydrolysis Mild Foreign Body Reaction No Inflammation.	Bulk – 1 month to ~ 5 years	0.01 – 0.1	Ligaments; Tendons; Vessels; Nerves	Drugs;
PPEs	Hydrolysis Minimal Foreign Body Reaction Minimal Inflammation	Erosion – 1 to more than 3 years	0.4 – 0.7	Skin;	Proteins;
PPAs	Hydrolysis Minimal Foreign Body Reaction Minimal Inflammation	Erosion – 1 week to more than 3 years	180-230 (Shear)	Cartilage; Bone;	Growth Factors
PAs	Hydrolysis Minimal Foreign Body Reaction Minimal Inflammation	Erosion – within 1 month	0.02*10 <sup>-3</sup> – 0.2*10 <sup>-3</sup>	Cartilage; Bone;	Growth Factors;
POEs	Degradation products in metabolic pathway Minimal Inflammation	Erosion – 1 week to ~ 16 months	0.02*10 <sup>-3</sup> – 6*10 <sup>-3</sup>	Nerves;	Genes
PPF-DA	Hydrolysis Minimal Foreign Body Reaction Mild Inflammation	Bulk – 6 months to more than 3 years	0.012*10 <sup>-3</sup> – 4	Liver	Drugs;
PEG-DA	Hydrolysis Minimal Foreign Body Reaction	Bulk – 1 to 3 weeks	0.002 – 0.12	Bone;	Proteins;
Collagen	No or Minimal (cross-linker) Cytotoxicity Mild Foreign Body Reaction Minimal Inflammation	Bulk – 1 day to ~ stable (cross-linker)	0.032*10 <sup>-3</sup> – 0.5*10 <sup>-3</sup>	Nerves;	Growth Factors
Alginate	No or Minimal Foreign Body Reaction No Inflammation	Bulk – 1 day to 3 months	0.1*10 <sup>-3</sup> – 5*10 <sup>-3</sup>	Skin; Vessels;	Proteins;
Chitosan	Hydrolysis No or Minimal Foreign Body Reaction No Inflammation	Bulk – 3 days to 6 months	0.01*10 <sup>-3</sup> – 27*10 <sup>-3</sup>	Genes	Genes
Hyaluronate	Hydrolysis No or Minimal Foreign Body Reaction No Inflammation	Bulk – ~ hours to 1 month	3*10 <sup>-6</sup> – 11	Skin; Cartilage; Bone;	Drugs; Proteins;
			3*10 <sup>-9</sup> – 0.04*10 <sup>-3</sup>	Nerves; Muscle; Pancreas	Growth Factors; Genes
				Skin; Cartilage; Bone;	Proteins;
				Nerves; Vessels;	Growth Factors;
				Liver; Pancreas	Genes
				Skin; Cartilage; Bone;	Drugs;
				Ligaments; Nerves;	Proteins;
				Vessels; Liver	Growth Factors

Table 2 – Principal synthetic and natural polymeric biomaterials used in tissue engineering and their general properties.

### ***Natural Polymers***

Natural polymers also offer a broad selection of materials used for tissue engineering as compared to synthetic ones. Since they are often used in a gel-like phase, these systems are easy to process and biological agents can be readily incorporated during the gel formulation. Collagen is a fibrous protein and a main component of the extra cellular matrix, which has been used for various tissue regenerations [215-219]. In particular, pure collagen type I and type II scaffolds alone, or in combination with glycosaminoglycans (GAGs) have been considered for the repair of many human tissues [218-221]. A further possibility is to use denatured collagen (gelatin) [216], or demineralized bone matrix (DBM) [222-224]. The latter, in particular, has found clinical applications for bone defects either as an injectable gel or as a foamy highly porous scaffold.

Another group of natural polymers that have been investigated for many different tissue engineering applications comprises polysaccharides like alginate [225, 226], chitosan [227, 228], and hyaluronate [229, 230]. Alginate is water soluble and jellifies when cross-linked with calcium ions. This provides a suitable system to include drugs or growth factors directly during gel formation. Chitosan is structurally similar to GAG and has recently attracted more and more attention because of its non-toxicity, bioresorbability, and wound healing abilities [231]. Hyaluronan acid is also abundantly present in the human joint capsules, within the synovium fluid. A change of its chemical structure through an esterification reaction allows the generation of a new set of biomaterials, hyaluronates, with improved properties, increased biocompatibility and fine-tunable degradation rates [232, 233]. These materials have been studied for cartilage and skin regeneration [229, 234, 235] and reached clinical applications for the treatment of deep skin wounds and cartilage [236, 237].

The results obtained with natural polymers showed that it is often possible to mimic the ECM environment, which in several cases significantly influenced seeded cells to proliferate and differentiate in the specific desired tissue to regenerate. However, when compared to synthetic polymers, main concerns over natural polymers are still present due to the potential pathogen transmission and to the lack of constant source.

### **Aims and Approach of this Thesis**

Although an impressive number of biomaterials and of scaffold fabrication technologies have been and are being developed, it is still challenging to find a biomaterial-scaffold technology coupling that satisfies all the requirements generally desirable for tissue engineering. A better control of mechanical and physico-chemical properties, and degradation rate and mechanism needs to be achieved to achieve stable and functional tissue engineered constructs in a long-term application. For instance, it is often the case that when the mechanical properties are suitable, the physico-chemical characteristics of the scaffolds are insufficient due to either biomaterial processing or to the intrinsic chemistry of the material itself. Conversely,

when physicochemical properties are satisfactory, the scaffolds may not display a favorable mechanical behavior. It might be that the most optimal strategy in designing scaffolds for tissue engineering is to integrate different biomaterials and different fabrication technologies to combine mechanical, physicochemical, and biological cues at the macro, micro, and nano scale, as it also appears from the recent studies above mentioned.

The general aim of the work presented hereafter is to introduce a small library of possible solutions that may contribute – if merged together – to match most of the prerequisites desirable for a scaffold. The pursued approach to achieve this goal is developed as follows:

- Characterize and model the mechanical and physicochemical properties of 3D scaffolds and their variation with porosity, pore size, and pore shape.
- Assess the importance of mimicking the mechanical behavior of a tissue, in combination with appropriate physicochemical properties.
- Determine the relevance of anatomically shaped scaffolds as compared to other functional but simpler designs for tissue regeneration.
- Unravel the influence of fiber dimensions and texture on cell faith and on release of incorporated compounds.
- Integrate conventional and novel fabrication technologies together to create multifunctional 3D scaffolds.

PEOT/PBT copolymers were chosen as a biomaterial model to investigate the basic principles that rule the 3D scaffold's fabrication process, mechanical and physicochemical characterization, cell interaction, and tissue development. As previously described, these copolymers exhibit a high versatility in terms of their bulk properties, some compositions being FDA approved and routinely implied in clinical applications. Among the manifold scaffold fabrication techniques 3DF and ESP were selected and mainly studied. Due to their versatility in processing a variety of biomaterials, the scaffolding solutions exemplified in this thesis may be extended to other biomaterials where the fundamental applied principles are still valid.

The goals and corresponding results are presented in the book in the following outline. Chapters 2, 3, and 4 introduce the mechanical and physicochemical characterization and modeling of 3DF scaffolds. Chapter 2 looks at the influence of the fabrication parameters on the viscoelastic behavior of 300PEOT55PBT45 and how these can be fine tuned to match articular cartilage viscoelastic properties. In particular, the modulation of the dynamic stiffness and the equilibrium modulus, as well as of the damping factor and the creep uncovered strain was evaluated and compared to the correspondent values of bovine articular cartilage. Dynamic, static, and frequency scan tests were selected for this purpose. In chapter 3 the influence of the physicochemical properties of the copolymers on the viscoelastic properties of 3D scaffolds are investigated in terms of equilibrium swelling and molecular network mesh size. The influence of the scaffolds porosity on the mechanical behavior is also considered, leading to the formulation of an experimentally derived three-dimensional matrix that correlates the dynamic stiffness of a specific copolymer composition with the correspondent physicochemical properties and scaffold

porosity. Chapter 4 deals with the validation of this experimental correlation matrix with numerical analysis.

Chapter 5 treats a practical exemplification of how the model can be used to select scaffolds with specific physicochemical and mechanical properties. Specifically, the importance of mimicking the dynamic stiffness of articular cartilage with the initial 3D scaffold was assessed and coupled to the influence of the physicochemical properties on cell differentiation.

Chapter 6 aims at studying the effect of anatomically shaped 3DF scaffolds on tissue formation as compared to simplified but still functional designs for tracheal reconstruction. The anatomical scaffolds was built from a computer tomography human dataset and downscaled to the size of a rat trachea compatible to the resolution limitations of the technique. Rat trachea and chondrocytes were purely chosen as a model.

In chapter 7 electrospinning is introduced to fabricate 3D micro and nanofibrillar networks, which display smooth, nano and micro porous surface texture depending on the fabrication parameter. In particular the mechanism of pore formation during fiber spinning is unraveled and the influence of fiber diameter and nanoporosity on human stem cells morphology, seeding, attachment, and proliferation is investigated. The release of incorporated model compounds and the effect of fiber size and texture on the release profile are also considered.

Chapters 8, 9, and 10 pioneer few examples of how to integrate conventional and novel fabrication technique to create multifunctional scaffolds. In chapters 8 the integration of viscous encapsulation – a typical rheological phenomenon that occurs to immiscible molten polymeric blends under specific extrusion conditions – with 3DF allowed the fabrication of shell-core fibrous 3D scaffolds. The shell-core fibers can be designed in such way to combine mechanical properties in the core polymer with physicochemical properties in the shell, thus appropriately directing cell-material interactions. Alternatively, if selective leaching is applied, hollow fibrous 3DF scaffolds are created, which can be used to either increase the available surface for cell adhesion or as reservoir system for controlled drug release. Chapters 9 proposes the integration of ESP networks interspersed in between 3DF scaffolds as a novel construct to enhance cell seeding efficiency and bias cell differentiation. The effect of network density was compared to 3DF scaffolds alone and related to cartilage tissue engineering. Further possibilities to improve the integration process and to direct cell faith of stem cells are also discussed. Chapter 10 presents different 3D hybrid scaffold designs to assembly in a composite PEOT/PBT 3DF polymers as flexible carriers of ceramics and demineralized bone matrices (DBMs). The rationale behind the designs is to improve the brittle mechanical behavior of ceramics by combining them with the polymer and with DBMs that will function as dampers before fracture. Since each single biomaterial component of the 3D hybrid scaffold has been shown to be favorable for bone formation and/or integration in the implant site, bone and osteochondral tissue engineering applications are discussed. Finally chapter 11 gives an overview of the obtained results and of future perspective in scaffolding for tissue engineering and drug delivery applications.

**References:**

- [1] Langer R, Vacanti JP. Tissue engineering. *Science* 1993;260(5110):920-6.
- [2] Sanan A, Haines SJ. Repairing holes in the head: A history of cranioplasty. *Neurosurgery* 1997;40(3):588-603.
- [3] van Meekeren JJ. *Observationes Medico-Chirurgicae*. Amsterdam; 1682.
- [4] Burwell RG. History of bone grafting and bone substitutes with special reference to osteogenic induction. Oxford: Butterworth-Heinemann Ltd; 1994.
- [5] Barth A. Ueber histologische Befunde nach Knochenimplantationen. *Arch Klin Chir* 1893;46:409-17.
- [6] van der Lei B, Wildevuur CR, Nieuwenhuis P, Blaauw EH, Dijk F, Hulstaert CE, Molenaar I. Regeneration of the arterial wall in microporous, compliant, biodegradable vascular grafts after implantation into the rat abdominal aorta. Ultrastructural observations. *Cell Tissue Res* 1985;242(3):569-78.
- [7] Vacanti JP, Morse MA, Saltzman WM, Domb AJ, Perez-Atayde A, Langer R. Selective cell transplantation using bioabsorbable artificial polymers as matrices. *J Pediatr Surg* 1988;23(1 Pt 2):3-9.
- [8] Stone KR, Rodkey WG, Webber R, Mckinney L, Steadman JR. Meniscal Regeneration with Copolymeric Collagen Scaffolds - Invitro and In vivo Studies Evaluated Clinically, Histologically, and Biochemically. *American Journal of Sports Medicine* 1992;20(2):104-111.
- [9] Wu BM, Borland SW, Giordano RA, Cima LG, Sachs EM, Cima MJ. Solid free-form fabrication of drug delivery devices. *Journal of Cont Release* 1996;40(1-2):77-87.
- [10] Yu XJ, Dillon GP, Bellamkonda RV. A laminin and nerve growth factor-laden three-dimensional scaffold for enhanced neurite extension. *Tissue Engineering* 1999;5(4):291-304.
- [11] Healy KE, Rezaia A, Stile RA. Designing biomaterials to direct biological responses. *Bioartificial Organs li: Technology, Medicine, and Materials* 1999;875:24-35.
- [12] Lutolf MP, Hubbell JA. Synthetic biomaterials as instructive extracellular microenvironments for morphogenesis in tissue engineering. *Nat Biotechnol* 2005;23(1):47-55.
- [13] Sohier J, Haan RE, de Groot K, Bezemer JM. A novel method to obtain protein release from porous polymer scaffolds: emulsion coating. *J Control Release* 2003;87(1-3):57-68.
- [14] Nof M, Shea LD. Drug-releasing scaffolds fabricated from drug-loaded microspheres. *J Biomed Mater Res* 2002;59(2):349-56.
- [15] Whang K, Goldstick TK, Healy KE. A biodegradable polymer scaffold for delivery of osteotropic factors. *Biomaterials* 2000;21(24):2545-51.
- [16] Kim SS, Utsunomiya H, Koski JA, Wu BM, Cima MJ, Sohn J, Mukai K, Griffith LG, Vacanti JP. Survival and function of hepatocytes on a novel three-dimensional synthetic biodegradable polymer scaffold with an intrinsic network of channels. *Ann Surg* 1998;228(1):8-13.
- [17] Tsang VL, Bhatia SN. Three-dimensional tissue fabrication. *Adv Drug Deliv Rev* 2004;56:1635-47.



- [18] Sherwood JK, Riley SL, Palazzolo R, Brown SC, Monkhouse DC, Coates M, Griffith LG, Landeen LK, Ratcliffe A. A three-dimensional osteochondral composite scaffold for articular cartilage repair. *Biomaterials* 2002;23(24):4739-51.
- [19] Malda J, Woodfield TB, van der Vloodt F, Wilson C, Martens DE, Tramper J, van Blitterswijk CA, Riesle J. The effect of PEGT/PBT scaffold architecture on the composition of tissue engineered cartilage. *Biomaterials* 2005;26(1):63-72.
- [20] Richardson TP, Peters MC, Ennett AB, Mooney DJ. Polymeric system for dual growth factor delivery. *Nat Biotechnol* 2001;19(11):1029-34.
- [21] Hubbell JA. Hydrogel systems for barriers and local drug delivery in the control of wound healing. *J Control Release* 1996;39:305-313.
- [22] Lee JE, Kim KE, Kwon IC, Ahn HJ, Lee SH, Cho HC, Kim HJ, Seong SC, Lee MC. Effects of the controlled-released TGF-beta 1 from chitosan microspheres on chondrocytes cultured in a collagen/chitosan/glycosaminoglycan scaffold. *Biomaterials* 2004;25(18):4163-4173.
- [23] Cima LG, Vacanti JP, Vacanti C, Ingber D, Mooney D, Langer R. Tissue engineering by cell transplantation using degradable polymer substrates. *J Biomech Eng* 1991;113(2):143-51.
- [24] Freed LE, Vunjak-Novakovic G, Biron RJ, Eagles DB, Lesnoy DC, Barlow SK, Langer R. Biodegradable polymer scaffolds for tissue engineering. *Biotech (NY)* 1994;12(7):689-93.
- [25] Niklason LE, Langer RS. Advances in tissue engineering of blood vessels and other tissues. *Transpl Immunol* 1997;5(4):303-6.
- [26] Smilenov LB, Mikhailov A, Pelham RJ, Marcantonio EE, Gundersen GG. Focal adhesion motility revealed in stationary fibroblasts. *Science* 1999;286(5442):1172-4.
- [27] Kaazempur Mofrad MR, Abdul-Rahim NA, Karcher H, Mack PJ, Yap B, Kamm RD. Exploring the molecular basis for mechanosensation, signal transduction, and cytoskeletal remodeling. *Acta Biomater* 2005;1(3):281-93.
- [28] Mikos AG, Bao Y, Cima LG, Ingber DE, Vacanti JP, Langer R. Preparation of poly(glycolic acid) bonded fiber structures for cell attachment and transplantation. *J Biomed Mater Res* 1993;27(2):183-9.
- [29] Kim BS, Mooney DJ. Engineering smooth muscle tissue with a predefined structure. *J Biomed Mater Res* 1998;41(2):322-32.
- [30] Kim BS, Mooney DJ. Development of biocompatible synthetic extracellular matrices for tissue engineering. *Trends Biotechnol* 1998;16(5):224-30.
- [31] Mooney DJ, Baldwin DF, Suh NP, Vacanti JP, Langer R. Novel approach to fabricate porous sponges of poly(D,L-lactic-co-glycolic acid) without the use of organic solvents. *Biomaterials* 1996;17(14):1417-22.
- [32] Barry JJ, Gidda HS, Scotchford CA, Howdle SM. Porous methacrylate scaffolds: supercritical fluid fabrication and in vitro chondrocyte responses. *Biomaterials* 2004;25(17):3559-68.
- [33] Sproule TL, Lee JA, Li HB, Lannutti JJ, Tomasko DL. Bioactive polymer surfaces via supercritical fluids. *Journal of Supercritical Fluids* 2004;28(2-3):241-248.
- [34] Lo H, Kadiyala S, Guggino SE, Leong KW. Poly(L-lactic acid) foams with cell seeding and controlled-release capacity. *J Biomed Mater Res* 1996;30(4):475-84.
- [35] Whang K, Thomas CK, G. N, K.E. H. A novel method to fabricate bioabsorbable scaffolds. *Polymer* 1995;36:837-842.

- [36] Schoof H, Apel J, Heschel I, Rau G. Control of pore structure and size in freeze-dried collagen sponges. *J Biomed Mater Res* 2001;58(4):352-7.
- [37] Ma PX, Zhang R. Microtubular architecture of biodegradable polymer scaffolds. *J Biomed Mater Res* 2001;56(4):469-77.
- [38] Dagalakis N, Flink J, Stasikelis P, Burke JF, Yannas IV. Design of an artificial skin. Part III. Control of pore structure. *J Biomed Mater Res* 1980;14(4):511-28.
- [39] Mikos AG, Thorsen AJ, L.A. C, Bao Y, Langer R. Preparation and characterization of poly(L-lactic acid) foams. *Polymer* 1994;35:1068-1077.
- [40] Sarazin P, Favis BD. Morphology control in co-continuous poly(L-lactide)/polystyrene blends: a route towards highly structured and interconnected porosity in poly(L-lactide) materials. *Biomacromolecules* 2003;4(6):1669-79.
- [41] Claase MB, Grijpma DW, Mendes SC, De Bruijn JD, Feijen J. Porous PEOT/PBT scaffolds for bone tissue engineering: preparation, characterization, and in vitro bone marrow cell culturing. *J Biomed Mater Res A* 2003;64(2):291-300.
- [42] Ma PX, Choi JW. Biodegradable polymer scaffolds with well-defined interconnected spherical pore network. *Tissue Eng* 2001;7(1):23-33.
- [43] Wu YS, van Vliet LJ, Frijlink HW, van der Voort Maarschalk K. The determination of relative path length as a measure for tortuosity in compacts using image analysis. *European Journal of Pharmaceutical Sciences* 2006;28:433-440.
- [44] Sachlos E, Czernuszka JT. Making tissue engineering scaffolds work. Review: the application of solid freeform fabrication technology to the production of tissue engineering scaffolds. *Eur Cell Mater* 2003;5:29-39; discussion 39-40.
- [45] Muschler GF, Nakamoto C, Griffith LG. Engineering principles of clinical cell-based tissue engineering. *J Bone Joint Surg Am* 2004;86-A(7):1541-58.
- [46] Malda J, Woodfield TB, van der Vloodt F, Kooy FK, Martens DE, Tramper J, van Blitterswijk CA, Riesle J. The effect of PEGT/PBT scaffold architecture on oxygen gradients in tissue engineered cartilaginous constructs. *Biomaterials* 2004;25(26):5773-80.
- [47] Malda J, van den Brink P, Meeuwse P, Grojec M, Martens DE, Tramper J, Riesle J, van Blitterswijk CA. Effect of oxygen tension on adult articular chondrocytes in microcarrier bioreactor culture. *Tissue Eng* 2004;10(7-8):987-94.
- [48] Lewis MC, Macarthur BD, Malda J, Pettet G, Please CP. Heterogeneous proliferation within engineered cartilaginous tissue: the role of oxygen tension. *Biotechnol Bioeng* 2005;91(5):607-15.
- [49] van de Weert M, Hennink WE, Jiskoot W. Protein instability in poly(lactic-co-glycolic acid) microparticles. *Pharm Res* 2000;17(10):1159-67.
- [50] Huttmacher DW. Scaffold design and fabrication technologies for engineering tissues--state of the art and future perspectives. *J Biomater Sci Polym Ed* 2001;12(1):107-24.
- [51] Yang S, Leong KF, Du Z, Chua CK. The design of scaffolds for use in tissue engineering. Part II. Rapid prototyping techniques. *Tissue Eng* 2002;8(1):1-11.
- [52] Yeong WY, Chua CK, Leong KF, Chandrasekaran M. Rapid prototyping in tissue engineering: challenges and potential. *Trends Biotechnol* 2004;22(12):643-52.
- [53] Hollister SJ. Porous scaffold design for tissue engineering. *Nat Mater* 2005;4(7):518-24.

- [54] Taboas JM, Maddox RD, Krebsbach PH, Hollister SJ. Indirect solid free form fabrication of local and global porous, biomimetic and composite 3D polymer-ceramic scaffolds. *Biomaterials* 2003;24(1):181-94.
- [55] Lin CY, Kikuchi N, Hollister SJ. A novel method for biomaterial scaffold internal architecture design to match bone elastic properties with desired porosity. *J Biomech* 2004;37(5):623-36.
- [56] Woodfield TB, Miot S, Martin I, van Blitterswijk CA, Riesle J. The regulation of expanded human nasal chondrocyte re-differentiation capacity by substrate composition and gas plasma surface modification. *Biomaterials* 2006;27(7):1043-53.
- [57] Woodfield TB, Malda J, de Wijn J, Peters F, Riesle J, van Blitterswijk CA. Design of porous scaffolds for cartilage tissue engineering using a three-dimensional fiber-deposition technique. *Biomaterials* 2004;25(18):4149-61.
- [58] Moroni L, de Wijn JR, van Blitterswijk CA. 3D fiber-deposited scaffolds for tissue engineering: Influence of pores geometry and architecture on dynamic mechanical properties. *Biomaterials* 2006;27:974-985.
- [59] Woodfield TB, Van Blitterswijk CA, De Wijn J, Sims TJ, Hollander AP, Riesle J. Polymer scaffolds fabricated with pore-size gradients as a model for studying the zonal organization within tissue-engineered cartilage constructs. *Tissue Eng* 2005;11(9-10):1297-311.
- [60] Fedorovich NE, Ablas J, Creemers LB, Verbout AJ, Dhert WJA. Hydrogels for 3D bone printing. *DPTE Proceedings* 2006:38.
- [61] Yan Y, Xiong Z, Hu Y, Wang S, Zhang R, Zhang C. Layered manufacturing of tissue engineering scaffolds via multi-nozzle deposition. *Mater Letters* 2003;57:2623-2628.
- [62] Smith CM, Stone AL, Parkhill RL, Stewart RL, Simpkins MW, Kachurin AM, Warren WL, Williams SK. Three-dimensional bioassembly tool for generating viable tissue-engineered constructs. *Tissue Eng* 2004;10(9-10):1566-76.
- [63] Hutmacher DW, Ng KW, Kaps C, Sittinger M, Klaring S. Elastic cartilage engineering using novel scaffold architectures in combination with a biomimetic cell carrier. *Biomaterials* 2003;24:4445-58.
- [64] Hutmacher DW, Garcia AJ. Scaffold-based bone engineering by using genetically modified cells. *Gene* 2005;347(1):1-10.
- [65] Schantz JT, Brandwood A, Hutmacher DW, Khor HL, Bittner K. Osteogenic differentiation of mesenchymal progenitor cells in computer designed fibrin-polymer-ceramic scaffolds manufactured by fused deposition modeling. *J Mater Sci Mater Med* 2005;16(9):807-19.
- [66] Hoque ME, Hutmacher DW, Feng W, Li S, Huang MH, Vert M, Wong YS. Fabrication using a rapid prototyping system and in vitro characterization of PEG-PCL-PLA scaffolds for tissue engineering. *J Biomater Sci Polym Ed* 2005;16(12):1595-610.
- [67] Li JP, de Wijn JR, Van Blitterswijk CA, de Groot K. Porous Ti(6)Al(4)V scaffold directly fabricating by rapid prototyping: Preparation and in vitro experiment. *Biomaterials* 2005.
- [68] Michna S, Wu W, Lewis JA. Concentrated hydroxyapatite inks for direct-write assembly of 3-D periodic scaffolds. *Biomaterials* 2005;26(28):5632-9.

- [69] Smay JE, Cesarano III J, Tuttle BA, Lewis JA. Directed Colloidal Assembly of Linear and Annulate Lead of Zirconia Titanate Arrays. *J Am Ceram Soc* 2005;87(2):293-295.
- [70] Hubbell JA. Materials science. Enhancing drug function. *Science* 2003;300(5619):595-6.
- [71] Giordano RA, Wu BM, Borland SW, Cima LG, Sachs EM, Cima MJ. Mechanical properties of dense polylactic acid structures fabricated by three dimensional printing. *J Biomater Sci Polym Ed* 1996;8(1):63-75.
- [72] Pfister A, Landers R, Laib A, Hubner U, Schmelzeisen R, Mullhaupt R. Biofunctional Rapid Prototyping for Tissue-Engineering Applications: 3D Bioplotting versus 3D Printing. *J Polym Sci Part A: Polym Chem* 2004;42:624-638.
- [73] Tan KH, Chua CK, Leong KF, Cheah CM, Gui WS, Tan WS, Wiria FE. Selective laser sintering of biocompatible polymers for applications in tissue engineering. *Biomed Mater Eng* 2005;15(1-2):113-24.
- [74] Williams JM, Adewunmi A, Schek RM, Flanagan CL, Krebsbach PH, Feinberg SE, Hollister SJ, Das S. Bone tissue engineering using polycaprolactone scaffolds fabricated via selective laser sintering. *Biomaterials* 2005;26(23):4817-27.
- [75] Takesada M, Vanagas E, Tuzhilin D, Kudryashov I, Suruga S, Murakami H, Sarukura N, Matsuda K, Mononobe S, Saiki T, Yoshimoto M, Koshihara S. Micro-Character Printing on a Diamond Plate by Femtosecond Infrared Optical Pulses. *Jpn J Appl Phys* 2003;42:4613-4616.
- [76] Voskerician G, Gingras PH, Anderson JM. Macroporous condensed poly(tetrafluoroethylene). I. In vivo inflammatory response and healing characteristics. *J Biomed Mater Res A* 2006;76(2):234-42.
- [77] Antonov EN, Bagratashvili VN, Whitaker MJ, Barry JJA, Shakesheff KM, Konovalov AN, Popov VK, Howdle SM. Three-Dimensional Bioactive and Biodegradable Scaffolds Fabricated by Surface-Selective Laser Sintering. *Adv Mater* 2005;17:327-330.
- [78] Chu TM, Orton DG, Hollister SJ, Feinberg SE, Halloran JW. Mechanical and in vivo performance of hydroxyapatite implants with controlled architectures. *Biomaterials* 2002;23(5):1283-93.
- [79] Gratson GM, Xu M, Lewis JA. Microperiodic structures: direct writing of three-dimensional webs. *Nature* 2004;428(6981):386.
- [80] Vozzi G, Flaim C, Ahluwalia A, Bhatia S. Fabrication of PLGA scaffolds using soft lithography and microsyringe deposition. *Biomaterials* 2003;24(14):2533-40.
- [81] Roth EA, Xu T, Das M, Gregory C, Hickman JJ, Boland T. Inkjet printing for high-throughput cell patterning. *Biomaterials* 2004;25(17):3707-15.
- [82] Boland T, Mironov V, Gutowska A, Roth EA, Markwald RR. Cell and organ printing 2: fusion of cell aggregates in three-dimensional gels. *Anat Rec A Discov Mol Cell Evol Biol* 2003;272(2):497-502.
- [83] Wang XH, Yan YN, Pan YQ, Xiong Z, Liu HX, Cheng B, Liu F, Lin F, Wu RD, Zhang RJ, Lu QP. Generation of three-dimensional hepatocyte/gelatin structures with rapid prototyping system. *Tissue Engineering* 2006;12(1):83-90.
- [84] Taylor G. Electrically Driven Jets. *Proc R Soc London, Ser A* 1969;313:453-475.
- [85] Doshi J, Reneker D. Electrospinning Process and Applications of Electrospun Fibers. *J of Electrostatic* 1995;35:151-160.

- [86] Larrondo L, Manley R. Electrostatic Fiber Spinning from Polymer Melts. I. Experimental Observations on Fiber Formation and Properties. *J Polym Sci: Pol Phys Ed* 1981;19:909-920.
- [87] Kidoaki S, Kwon IK, Matsuda T. Mesoscopic spatial designs of nano- and microfiber meshes for tissue-engineering matrix and scaffold based on newly devised multilayering and mixing electrospinning techniques. *Biomaterials* 2005;26(1):37-46.
- [88] Li WJ, Tuli R, Huang X, Laquerriere P, Tuan RS. Multilineage differentiation of human mesenchymal stem cells in a three-dimensional nanofibrous scaffold. *Biomaterials* 2005;26(25):5158-66.
- [89] Kwon IK, Kidoaki S, Matsuda T. Electrospun nano- to microfiber fabrics made of biodegradable copolyesters: structural characteristics, mechanical properties and cell adhesion potential. *Biomaterials* 2005;26(18):3929-39.
- [90] Min BM, Lee G, Kim SH, Nam YS, Lee TS, Park WH. Electrospinning of silk fibroin nanofibers and its effect on the adhesion and spreading of normal human keratinocytes and fibroblasts in vitro. *Biomaterials* 2004;25(7-8):1289-97.
- [91] Jiang H, Hu Y, Li Y, Zhao P, Zhu K, Chen W. A facile technique to prepare biodegradable coaxial electrospun nanofibers for controlled release of bioactive agents. *J Control Release* 2005;108(2-3):237-43.
- [92] Cui W, Li X, Zhu X, Yu G, Zhou S, Weng J. Investigation of Drug Release and Matrix Degradation of Electrospun Poly(DL-lactide) Fibers with Paracetamol Inoculation. *Biomacromolecules* 2006;7(5):1623-9.
- [93] Li C, Vepari C, Jin HJ, Kim HJ, Kaplan DL. Electrospun silk-BMP-2 scaffolds for bone tissue engineering. *Biomaterials* 2006;27(16):3115-24.
- [94] Badami AS, Kreke MR, Thompson MS, Riffle JS, Goldstein AS. Effect of fiber diameter on spreading, proliferation, and differentiation of osteoblastic cells on electrospun poly(lactic acid) substrates. *Biomaterials* 2006;27(4):596-606.
- [95] Li WJ, Tuli R, Okafor C, Derfoul A, Danielson KG, Hall DJ, Tuan RS. A three-dimensional nanofibrous scaffold for cartilage tissue engineering using human mesenchymal stem cells. *Biomaterials* 2005;26(6):599-609.
- [96] Mrksich M. What can surface chemistry do for cell biology? *Curr Opin Chem Biol* 2002;6(6):794-7.
- [97] Curtis A, Wilkinson C. Topographical control of cells. *Biomaterials* 1997;18(24):1573-83.
- [98] Boyan BD, Lossdorfer S, Wang L, Zhao G, Lohmann CH, Cochran DL, Schwartz Z. Osteoblasts generate an osteogenic microenvironment when grown on surfaces with rough microtopographies. *Eur Cell Mater* 2003;6:22-7.
- [99] Bognitzki M, Czado W, Frese T, Schaper A, Hellwig M, Steinhart M, Greiner A, Wendorff J. Nanostructured Fibers via Electrospinning. *Adv Mater* 2001;13(1):70-72.
- [100] McCann JT, Marquez M, Xia Y. Highly porous fibers by electrospinning into a cryogenic liquid. *J Am Chem Soc* 2006;128(5):1436-7.
- [101] Matsuda T, Ihara M, Inoguchi H, Kwon IK, Takamizawa K, Kidoaki S. Mechanoactive scaffold design of small-diameter artificial graft made of electrospun segmented polyurethane fabrics. *J Biomed Mater Res A* 2005;73(1):125-31.
- [102] Li D, Ouyang G, McCann JT, Xia YN. Collecting electrospun nanofibers with patterned electrodes. *Nano Letters* 2005;5(5):913-916.

- [103] van Dijkhuizen-Radersma R, Roosma JR, Sohler J, Peters FL, van den Doel M, van Blitterswijk CA, de Groot K, Bezemer JM. Biodegradable poly(ether-ester) multiblock copolymers for controlled release applications: An in vivo evaluation. *J Biomed Mater Res A* 2004;71(1):118-27.
- [104] Loscertales IG, Barrero A, Marquez M, Spretz R, Velarde-Ortiz R, Larsen G. Electrically forced coaxial nanojets for one-step hollow nanofiber design. *Journal of the American Chemical Society* 2004;126(17):5376-5377.
- [105] Sun Z, Zussman E, Yarin A, Wendorff J, Greiner A. Compound Core-Shell Polymer Nanofibers by Co-Electrospinning. *Adv Mater* 2003;15(22):1929-1932.
- [106] Yu JH, Fridrikh SV, Rutledge GC. Production of submicrometer diameter fibers by two-fluid electrospinning. *Advanced Materials* 2004;16(17):1562-1566.
- [107] Jayasinghe SN, Qureshi AN, Eagles PAM. Electrohydrodynamic jet processing: An advanced electric-field-driven jetting phenomenon for processing living cells. *Small* 2006;2(2):216-219.
- [108] Eagles PA, Qureshi AN, Jayasinghe SN. Electrohydrodynamic jetting of mouse neuronal cells. *Biochem J* 2006;394(Pt 2):375-8.
- [109] Stankus JJ, Guan JJ, Fujimoto K, Wagner WR. Microintegrating smooth muscle cells into a biodegradable, elastomeric fiber matrix. *Biomaterials* 2006;27(5):735-744.
- [110] Clark P, Connolly P, Curtis AS, Dow JA, Wilkinson CD. Topographical control of cell behaviour. I. Simple step cues. *Development* 1987;99(3):439-48.
- [111] Clark P, Connolly P, Curtis AS, Dow JA, Wilkinson CD. Topographical control of cell behaviour: II. Multiple grooved substrata. *Development* 1990;108(4):635-44.
- [112] Flemming RG, Murphy CJ, Abrams GA, Goodman SL, Nealey PF. Effects of synthetic micro- and nano-structured surfaces on cell behavior. *Biomater* 1999;20(6):573-88.
- [113] Boyan BD, Hummert TW, Dean DD, Schwartz Z. Role of material surfaces in regulating bone and cartilage cell response. *Biomaterials* 1996;17(2):137-46.
- [114] Thapa A, Miller DC, Webster TJ, Haberstroh KM. Nano-structured polymers enhance bladder smooth muscle cell function. *Biomaterials* 2003;24(17):2915-26.
- [115] Thapa A, Webster TJ, Haberstroh KM. Polymers with nano-dimensional surface features enhance bladder smooth muscle cell adhesion. *J Biomed Mater Res A* 2003;67(4):1374-83.
- [116] Gehrke TA, Walboomers XF, Jansen JA. Influence of transforming growth factor-beta3 on fibrous capsule formation around microgrooved subcutaneous implants in vivo. *Tissue Eng* 2000;6:505-17.
- [117] Ito Y. Surface micropatterning to regulate cell functions. *Biomaterials* 1999;20(23-24):2333-42.
- [118] Zinger O, Zhao G, Schwartz Z, Simpson J, Wieland M, Landolt D, Boyan B. Differential regulation of osteoblasts by substrate microstructural features. *Biomaterials* 2005;26(14):1837-47.
- [119] Papenburg B, Vogelaar L, Bolhuis-Versteeg L, Lammertink R, Grijpma D, Poot A, Stamatialis D, Wessling M. Advanced Polymeric Scaffolds for Tissue Engineering. *DPTE Proceedings* 2006:47-48.
- [120] Jackman RJ, Brittain ST, Adams A, Prentiss MG, Whitesides GM. Design and fabrication of topologically complex, three-dimensional microstructures. *Science* 1998;280(5372):2089-91.

- [121] Csucs G, Michel R, Lussi JW, Textor M, Danuser G. Microcontact printing of novel co-polymers in combination with proteins for cell-biological applications. *Biomaterials* 2003;24(10):1713-20.
- [122] Kam L, Shain W, Turner JN, Bizios R. Correlation of astroglial cell function on micro-patterned surfaces with specific geometric parameters. *Biomaterials* 1999;20(23-24):2343-50.
- [123] Rogers J, Bao Z, Meier M, Dodabalapur A, Schueller OJA, Whitesides G. Printing, molding, and near field photolithography methods for patterning organic lasers, smart pixels and simple circuits. *Synthetic Metals* 2000;115:5-11.
- [124] Lu L, Kam L, Hasenbein M, Nyalakonda K, Bizios R, Gopferich A, Young JF, Mikos AG. Retinal pigment epithelial cell function on substrates with chemically micropatterned surfaces. *Biomaterials* 1999;20(23-24):2351-61.
- [125] Lu L, Yaszemski MJ, Mikos AG. Retinal pigment epithelium engineering using synthetic biodegradable polymers. *Biomaterials* 2001;22(24):3345-55.
- [126] van Kooten TG, Whitesides JF, von Recum A. Influence of silicone (PDMS) surface texture on human skin fibroblast proliferation as determined by cell cycle analysis. *J Biomed Mater Res* 1998;43(1):1-14.
- [127] Denis FA, Hanarp P, Sutherland DS, Dufrêne YF. Fabrication of nanostructured polymer surfaces using colloidal lithography and spin-coating. *Nanolett* 2002;2:1419-25.
- [128] Goldmann T, Gonzalez JS. DNA-printing: utilization of a standard inkjet printer for the transfer of nucleic acids to solid supports. *J Biochem Biophys Methods* 2000;42(3):105-10.
- [129] Jung DR, Kapur R, Adams T, Giuliano KA, Mrksich M, Craighead HG, Taylor DL. Topographical and physicochemical modification of material surface to enable patterning of living cells. *Crit Rev Biotechnol* 2001;21(2):111-54.
- [130] Kane RS, Takayama S, Ostuni E, Ingber DE, Whitesides GM. Patterning proteins and cells using soft lithography. *Biomaterials* 1999;20(23-24):2363-76.
- [131] Park TH, Shuler ML. Integration of cell culture and microfabrication technology. *Biotechnol Prog* 2003;19(2):243-53.
- [132] Schäfer E, Thurn-Albrecht T, Russell TP, Steiner U. Electrically induced and structure formation and pattern transfer. *Nature* 2000;403:874-77.
- [133] Morariu MD, Voicu NE, Schäfer E, Lin Z, Russell TP, Steiner U. Hierarchical structure formation and pattern replication induced by an electric field. *Nat Mater* 2003;2:48-52.
- [134] Stevens MM, George JH. Exploring and engineering the cell surface interface. *Science* 2005;310(5751):1135-8.
- [135] Anderson DG, Levenberg S, Langer R. Nanoliter-scale synthesis of arrayed biomaterials and application to human embryonic stem cells. *Nat Biotechnol* 2004;22(7):863-6.
- [136] Anderson DG, Putnam D, Lavik EB, Mahmood TA, Langer R. Biomaterial microarrays: rapid, microscale screening of polymer-cell interaction. *Biomaterials* 2005;26(23):4892-7.
- [137] Simon CG, Jr., Eidelman N, Kennedy SB, Sehgal A, Khatri CA, Washburn NR. Combinatorial screening of cell proliferation on poly(L-lactic acid)/poly(D,L-lactic acid) blends. *Biomaterials* 2005;26(34):6906-15.

- [138] Faid K, Voicu R, Bani-Yaghoub M, Tremblay R, Mealing G, Py C, Barjovanu R. Rapid fabrication and chemical patterning of polymer microstructures and their applications as a platform for cell cultures. *Biomed Microdevices* 2005;7(3):179-84.
- [139] Orner BP, Derda R, Lewis RL, Thomson JA, Kiessling LL. Arrays for the combinatorial exploration of cell adhesion. *J Am Chem Soc* 2004;126(35):10808-9.
- [140] Flaim CJ, Chien S, Bhatia SN. An extracellular matrix microarray for probing cellular differentiation. *Nat Methods* 2005;2(2):119-25.
- [141] Brown LJ, Chun I, Dhanaraj S, Malaviya P, Melican MC, Rezanian A, Zhang L. Hybrid biologic-synthetic bioabsorbable scaffolds. *US* 2003/0023316.
- [142] Chen G, Sato T, Ushida T, Hirochika R, Shirasaki Y, Ochiai N, Tateishi T. The use of a novel PLGA fiber/collagen composite web as a scaffold for engineering of articular cartilage tissue with adjustable thickness. *J Biomed Mater Res A* 2003;67(4):1170-80.
- [143] Chen V, Ma P. Nano-fibrous poly(L-lactic acid) scaffolds with interconnected spherical macropores. *Biomaterials* 2004;25:2065-2073.
- [144] Wang XX, Li W, Kumar V. A method for solvent-free fabrication of porous polymer using solid-state foaming and ultrasound for tissue engineering applications. *Biomaterials* 2006;27(9):1924-1929.
- [145] Tuzlakoglu K, Bolgen N, Salgado AJ, Gomes ME, Piskin E, Reis RL. Nano- and micro-fiber combined scaffolds: a new architecture for bone tissue engineering. *J Mater Sci Mater Med* 2005;16(12):1099-104.
- [146] Sahoo S, Ouyang H, Goh JC, Tay TE, Toh SL. Characterization of a novel polymeric scaffold for potential application in tendon/ligament tissue engineering. *Tissue Eng* 2006;12(1):91-9.
- [147] Williamson MR, Black R, Kielty C. PCL-PU composite vascular scaffold production for vascular tissue engineering: Attachment, proliferation and bioactivity of human vascular endothelial cells. *Biomaterials* 2006;27(19):3608-3616.
- [148] Kim TG, Park TG. Biomimicking extracellular matrix: cell adhesive RGD peptide modified electrospun poly(D,L-lactic-co-glycolic acid) nanofiber mesh. *Tissue Eng* 2006;12(2):221-33.
- [149] Abidian MR, Kim DH, Martin DC. Conducting-polymer nanotubes for controlled drug release. *Advanced Materials* 2006;18(4):405-+.
- [150] Zanello LP, Zhao B, Hu H, Haddon RC. Bone cell proliferation on carbon nanotubes. *Nano Letters* 2006;6(3):562-567.
- [151] Price RL, Ellison K, Haberstroh KM, Webster TJ. Nanometer surface roughness increases select osteoblast adhesion on carbon nanofiber compacts. *J Biomed Mater Res* 2004;70A(1):129-138.
- [152] Price RL, Haberstroh KM, Webster TJ. Improved osteoblast viability in the presence of smaller nanometre dimensioned carbon fibres. *Nanotech* 2004;15(8):892-900.
- [153] Correa-Duarte MA, Wagner N, Rojas-Chapana J, Morszeck C, Thie M, Giersig M. Fabrication and biocompatibility of carbon nanotube-based 3D networks as scaffolds for cell seeding and growth. *Nano Letters* 2004;4(11):2233-2236.
- [154] Zhan GD, Kuntz JD, Wan JL, Mukherjee AK. Single-wall carbon nanotubes as attractive toughening agents in alumina-based nanocomposites. *Nat Mater* 2003;2(1):38-42.
- [155] Wang XT, Padture NP, Tanaka H. Contact-damage-resistant ceramic/single-wall carbon nanotubes and ceramic/graphite composites. *Nat Mater* 2004;3(8):539-544.



- [156] Mrksich M, Dike LE, Tien J, Ingber DE, Whitesides GM. Using microcontact printing to pattern the attachment of mammalian cells to self-assembled monolayers of alkanethiolates on transparent films of gold and silver. *Exp Cell Res* 1997;235(2):305-13.
- [157] Zhang SG. Fabrication of novel biomaterials through molecular self-assembly. *Nature Biotechnology* 2003;21(10):1171-1178.
- [158] Hartgerink JD, Beniash E, Stupp SI. Self-assembly and mineralization of peptide-amphiphile nanofibers. *Science* 2001;294(5547):1684-8.
- [159] Kisiday J, Jin M, Kurz B, Hung H, Semino C, Zhang S, Grodzinsky AJ. Self-assembling peptide hydrogel fosters chondrocyte extracellular matrix production and cell division: implications for cartilage tissue repair. *Proc Natl Acad Sci U S A* 2002;99(15):9996-10001.
- [160] Welsh ER, Tirrell DA. Engineering the extracellular matrix: a novel approach to polymeric biomaterials. I. Control of the physical properties of artificial protein matrices designed to support adhesion of vascular endothelial cells. *Biomacromolecules* 2000;1(1):23-30.
- [161] Holmes TC, de Lacalle S, Su X, Liu G, Rich A, Zhang S. Extensive neurite outgrowth and active synapse formation on self-assembling peptide scaffolds. *Proc Natl Acad Sci U S A* 2000;97(12):6728-33.
- [162] Zhang S, Holmes TC, DiPersio CM, Hynes RO, Su X, Rich A. Self-complementary oligopeptide matrices support mammalian cell attachment. *Biomaterials* 1995;16(18):1385-93.
- [163] Lee SB, Koepsel R, Stolz DB, Warriner HE, Russell AJ. Self-assembly of biocidal nanotubes from a single-chain diacetylene amine salt. *J Am Chem Soc* 2004;126(41):13400-5.
- [164] Semino CE, Merok JR, Crane GG, Panagiotakos G, Zhang S. Functional differentiation of hepatocyte-like spheroid structures from putative liver progenitor cells in three-dimensional peptide scaffolds. *Differentiation* 2003;71(4-5):262-70.
- [165] Harrington DA, Cheng EY, Guler MO, Lee LK, Donovan JL, Claussen RC, Stupp SI. Branched peptide-amphiphiles as self-assembling coatings for tissue engineering scaffolds. *J Biomed Mater Res A* 2006;78A(1):157-167.
- [166] Gimi B, Leong T, Gu Z, Yang M, Artemov D, Bhujwala ZM, Gracias DH. Self-assembled three dimensional radio frequency (RF) shielded containers for cell encapsulation. *Biomed Microdevices* 2005;7(4):341-5.
- [167] Uhrich KE, Cannizzaro SM, Langer RS, Shakesheff KM. Polymeric systems for controlled drug release. *Chem Rev* 1999;99(11):3181-98.
- [168] Jang JH, Shea LD. Controllable delivery of non-viral DNA from porous scaffolds. *J Control Release* 2003;86(1):157-68.
- [169] Sengupta S, Eavarone D, Capila I, Zhao G, Watson N, Kiziltepe T, Sasisekharan R. Temporal targeting of tumour cells and neovasculature with a nanoscale delivery system. *Nature* 2005;436(7050):568-72.
- [170] Anderson JM, Langone JJ. Issues and perspectives on the biocompatibility and immunotoxicity evaluation of implanted controlled release systems. *J Control Release* 1999;57(2):107-13.
- [171] Babensee JE, McIntire LV, Mikos AG. Growth factor delivery for tissue engineering. *Pharm Res* 2000;17(5):497-504.

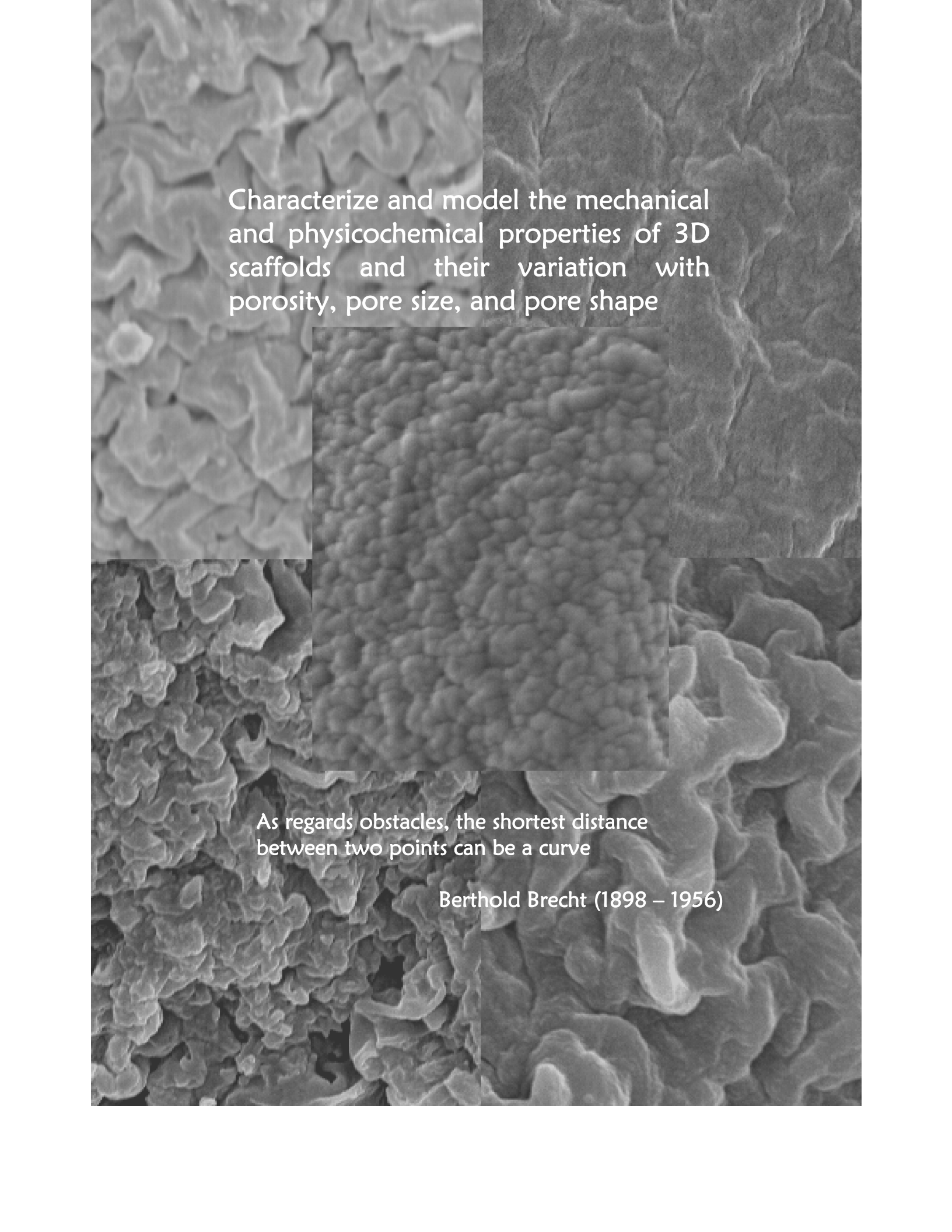
- [172] Chu CR, Douchis JS, Yoshioka M, Sah RL, Coutts RD, Amiel D. Osteochondral repair using perichondrial cells. A 1-year study in rabbits. *Clin Orthop Relat Res* 1997(340):220-9.
- [173] Freed LE, Marquis JC, Nohria A, Emmanuel J, Mikos AG, Langer R. Neocartilage formation in vitro and in vivo using cells cultured on synthetic biodegradable polymers. *J Biomed Mater Res* 1993;27(1):11-23.
- [174] Honda M, Yada T, Ueda M, Kimata K. Cartilage formation by cultured chondrocytes in a new scaffold made of poly(L-lactide-epsilon-caprolactone) sponge. *J Oral Maxillofac Surg* 2000;58(7):767-75.
- [175] Sarazin P, Roy X, Favis BD. Controlled preparation and properties of porous poly(L-lactide) obtained from a co-continuous blend of two biodegradable polymers. *Biomaterials* 2004;25(28):5965-78.
- [176] Bostman O, Hirvensalo E, Vainionpaa S, Makela A, Vihtonen K, Tormala P, Rokkanen P. Ankle fractures treated using biodegradable internal fixation. *Clin Orthop Relat Res* 1989(238):195-203.
- [177] Fu K, Pack DW, Klibanov AM, Langer R. Visual evidence of acidic environment within degrading poly(lactic-co-glycolic acid) (PLGA) microspheres. *Pharm Res* 2000;17(1):100-6.
- [178] Wang PY. Compressed poly(vinyl alcohol)-polycaprolactone admixture as a model to evaluate erodible implants for sustained drug delivery. *J Biomed Mater Res* 1989;23(1):91-104.
- [179] Hutmacher DW, Schantz T, Zein I, Ng KW, Teoh SH, Tan KC. Mechanical properties and cell cultural response of polycaprolactone scaffolds designed and fabricated via fused deposition modeling. *J Biomed Mater Res* 2001;55(2):203-16.
- [180] Choi SH, Park TG. Synthesis and characterization of elastic PLGA/PCL/PLGA tri-block copolymers. *J Biomater Sci Polym Ed* 2002;13(10):1163-73.
- [181] Bezemer JM, Grijpma DW, Dijkstra PJ, van Blitterswijk CA, Feijen J. A controlled release system for proteins based on poly(ether ester) block-copolymers: polymer network characterization. *J Control Release* 1999;62(3):393-405.
- [182] Olde Riekerink MB, Claase MB, Engbers GH, Grijpma DW, Feijen J. Gas plasma etching of PEO/PBT segmented block copolymer films. *J Biomed Mater Res A* 2003;65(4):417-28.
- [183] van Dijkhuizen-Radersma R, Peters FL, Stienstra NA, Grijpma DW, Feijen J, de Groot K, Bezemer JM. Control of vitamin B12 release from poly(ethylene glycol)/poly(butylene terephthalate) multiblock copolymers. *Biomaterials* 2002;23(6):1527-36.
- [184] Deschamps AA, Claase MB, Sleijsler WJ, de Bruijn JD, Grijpma DW, Feijen J. Design of segmented poly(ether ester) materials and structures for the tissue engineering of bone. *J Control Release* 2002;78(1-3):175-86.
- [185] Mahmood TA, de Jong R, Riesle J, Langer R, van Blitterswijk CA. Adhesion-mediated signal transduction in human articular chondrocytes: the influence of biomaterial chemistry and tenascin-C. *Exp Cell Res* 2004;301(2):179-88.
- [186] Moroni L, de Wijn JR, van Blitterswijk CA. Three-dimensional fiber-deposited PEOT/PBT copolymer scaffolds for tissue engineering: Influence of porosity, molecular network mesh size, and swelling in aqueous media on dynamic mechanical properties. *J Biomed Mater Res A* 2005;75:957-965.

- [187] van Blitterswijk CA, van den Brink J, Leenders H, Bakker D. The effect of PEO ratio on degradation, calcification and bone bonding of PEO/PBT copolymer (PolyActive). *Cell and Materials* 1993;3:23-26.
- [188] Bakker D, van Blitterswijk CA, Hesselings SC, Grote JJ. Effect of implantation site on phagocyte/polymer interaction and fibrous capsule formation. *Biomaterials* 1988;9(1):14-23.
- [189] Beumer GJ, van Blitterswijk CA, Ponec M. Degradative behaviour of polymeric matrices in (sub)dermal and muscle tissue of the rat: a quantitative study. *Biomaterials* 1994;15(7):551-9.
- [190] Beumer GJ, van Blitterswijk CA, Ponec M. Biocompatibility of a biodegradable matrix used as a skin substitute: an in vivo evaluation. *J Biomed Mater Res* 1994;28(5):545-52.
- [191] Bulstra SK, Geesink RG, Bakker D, Bulstra TH, Bouwmeester SJ, van der Linden AJ. Femoral canal occlusion in total hip replacement using a resorbable and flexible cement restrictor. *J Bone Joint Surg Br* 1996;78(6):892-8.
- [192] Mensik I, Lamme EN, Riesle J, Brychta P. Effectiveness and Safety of the PEGT/PBT Copolymer Scaffold as Dermal Substitute in Scar Reconstruction Wounds (Feasibility Trial). *Cell Tissue Bank* 2002;3(4):245-53.
- [193] van Dijkhuizen-Radersma R, Roosma JR, Kaim P, Metairie S, Peters FL, de Wijn J, Zijlstra PG, de Groot K, Bezemer JM. Biodegradable poly(ether-ester) multiblock copolymers for controlled release applications. *J Biomed Mater Res A* 2003;67(4):1294-304.
- [194] van Dijkhuizen-Radersma R, Metairie S, Roosma JR, de Groot K, Bezemer JM. Controlled release of proteins from degradable poly(ether-ester) multiblock copolymers. *J Control Release* 2005;101(1-3):175-86.
- [195] Wang J, Mao HQ, Leong KW. A novel biodegradable gene carrier based on polyphosphoester. *J Am Chem Soc* 2001;123(38):9480-1.
- [196] Wang S, Wan AC, Xu X, Gao S, Mao HQ, Leong KW, Yu H. A new nerve guide conduit material composed of a biodegradable poly(phosphoester). *Biomaterials* 2001;22(10):1157-69.
- [197] Caliceti P, Veronese FM, Lora S. Polyphosphazene microspheres for insulin delivery. *Int J Pharm* 2000;211(1-2):57-65.
- [198] Aldini NN, Caliceti P, Lora S, Fini M, Giavaresi G, Rocca M, Torricelli P, Giardino R, Veronese FM. Calcitonin release system in the treatment of experimental osteoporosis. Histomorphometric evaluation. *J Orthop Res* 2001;19(5):955-61.
- [199] Ambrosio AM, Allcock HR, Katti DS, Laurencin CT. Degradable polyphosphazene/poly(alpha-hydroxyester) blends: degradation studies. *Biomaterials* 2002;23(7):1667-72.
- [200] Cohen S, Bano MC, Cima LG, Allcock HR, Vacanti JP, Vacanti CA, Langer R. Design of synthetic polymeric structures for cell transplantation and tissue engineering. *Clin Mater* 1993;13(1-4):3-10.
- [201] Leong KW, Kost J, Mathiowitz E, Langer R. Polyanhydrides for controlled release of bioactive agents. *Biomaterials* 1986;7(5):364-71.
- [202] Choi NS, Heller J. Drug Delivery devices manufactured from poly(orthoesters) and poly(orthocarbonates). *US Patent* 1978;4.093.709.

- [203] Burkoth AK, Burdick J, Anseth KS. Surface and bulk modifications to photocrosslinked polyanhydrides to control degradation behavior. *J Biomed Mater Res* 2000;51(3):352-9.
- [204] Andriano KP, Tabata Y, Ikada Y, Heller J. In vitro and in vivo comparison of bulk and surface hydrolysis in absorbable polymer scaffolds for tissue engineering. *J Biomed Mater Res* 1999;48(5):602-12.
- [205] Kuo CK, Ma PX. Ionically crosslinked alginate hydrogels as scaffolds for tissue engineering: part 1. Structure, gelation rate and mechanical properties. *Biomaterials* 2001;22(6):511-21.
- [206] Fisher JP, Holland TA, Dean D, Engel PS, Mikos AG. Synthesis and properties of photocross-linked poly(propylene fumarate) scaffolds. *J Biomater Sci Polym Ed* 2001;12(6):673-87.
- [207] Burdick JA, Peterson AJ, Anseth KS. Conversion and temperature profiles during the photoinitiated polymerization of thick orthopaedic biomaterials. *Biomaterials* 2001;22(13):1779-86.
- [208] Mann BK, Gobin AS, Tsai AT, Schmedlen RH, West JL. Smooth muscle cell growth in photopolymerized hydrogels with cell adhesive and proteolytically degradable domains: synthetic ECM analogs for tissue engineering. *Biomaterials* 2001;22(22):3045-51.
- [209] Mann BK, Schmedlen RH, West JL. Tethered-TGF-beta increases extracellular matrix production of vascular smooth muscle cells. *Biomaterials* 2001;22(5):439-44.
- [210] Elbert DL, Pratt AB, Lutolf MP, Halstenberg S, Hubbell JA. Protein delivery from materials formed by self-selective conjugate addition reactions. *J Control Release* 2001;76(1-2):11-25.
- [211] He S, Yaszemski MJ, Yasko AW. Synthesis of biodegradable poly(propylene fumarate) networks with poly(propylene fumarate)-diacrylate macromers as crosslinking agents and characterization of their degradation products. *Polymer* 2000;42:1251-1260.
- [212] He S, Yaszemski MJ, Yasko AW, Engel PS, Mikos AG. Injectable biodegradable polymer composites based on poly(propylene fumarate) crosslinked with poly(ethylene glycol)-dimethacrylate. *Biomaterials* 2000;21(23):2389-94.
- [213] Elbert DL, Hubbell JA. Conjugate addition reactions combined with free-radical cross-linking for the design of materials for tissue engineering. *Biomacromolecules* 2001;2(2):430-41.
- [214] Behravesh E, Yasko AW, Engel PS, Mikos AG. Synthetic biodegradable polymers for orthopaedic applications. *Clin Orthop Relat Res* 1999(367 Suppl):S118-29.
- [215] Bell E, Rosenberg M, Kemp P, Gay R, Green GD, Muthukumar N, Nolte C. Recipes for reconstituting skin. *J Biomech Eng* 1991;113(2):113-9.
- [216] Choi YS, Hong SR, Lee YM, Song KW, Park MH, Nam YS. Studies on gelatin-containing artificial skin: II. Preparation and characterization of cross-linked gelatin-hyaluronate sponge. *J Biomed Mater Res* 1999;48(5):631-9.
- [217] Pachence JM. Collagen-based devices for soft tissue repair. *J Biomed Mater Res* 1996;33(1):35-40.
- [218] Mueller SM, Shortkroff S, Schneider TO, Breinan HA, Yannas IV, Spector M. Meniscus cells seeded in type I and type II collagen-GAG matrices in vitro. *Biomaterials* 1999;20(8):701-9.

- [219] Nehrer S, Breinan HA, Ramappa A, Young G, Shortkroff S, Louie LK, Sledge CB, Yannas IV, Spector M. Matrix collagen type and pore size influence behaviour of seeded canine chondrocytes. *Biomaterials* 1997;18(11):769-76.
- [220] Nehrer S, Breinan HA, Ramappa A, Hsu HP, Minas T, Shortkroff S, Sledge CB, Yannas IV, Spector M. Chondrocyte-seeded collagen matrices implanted in a chondral defect in a canine model. *Biomaterials* 1998;19(24):2313-28.
- [221] Yannas IV. Applications of ECM analogs in surgery. *J Cell Bioch* 1994;56(2):188-91.
- [222] Chakkalakal DA, Strates BS, Garvin KL, Novak JR, Fritz ED, Mollner TJ, McGuire MH. Demineralized bone matrix as a biological scaffold for bone repair. *Tissue Eng* 2001;7(2):161-77.
- [223] Mauney JR, Jaquiere C, Volloch V, Heberer M, Martin I, Kaplan DL. In vitro and in vivo evaluation of differentially demineralized cancellous bone scaffolds combined with human bone marrow stromal cells for tissue engineering. *Biomaterials* 2005;26(16):3173-85.
- [224] Peterson B, Whang PG, Iglesias R, Wang JC, Lieberman JR. Osteoinductivity of commercially available demineralized bone matrix. Preparations in a spine fusion model. *J Bone Joint Surg Am* 2004;86-A(10):2243-50.
- [225] Shapiro L, Cohen S. Novel alginate sponges for cell culture and transplantation. *Biomaterials* 1997;18(8):583-90.
- [226] Terada S, Yoshimoto H, Fuchs JR, Sato M, Pomerantseva I, Selig MK, Hannouche D, Vacanti JP. Hydrogel optimization for cultured elastic chondrocytes seeded onto a polyglycolic acid scaffold\*. *J Biomed Mater Res A* 2005;75(4):907-16.
- [227] Chenite A, Chaput C, Wang D, Combes C, Buschmann MD, Hoemann CD, Leroux JC, Atkinson BL, Binette F, Selmani A. Novel injectable neutral solutions of chitosan form biodegradable gels in situ. *Biomaterials* 2000;21(21):2155-61.
- [228] Madhally SV, Matthew HW. Porous chitosan scaffolds for tissue engineering. *Biomaterials* 1999;20(12):1133-42.
- [229] Solchaga LA, Gao J, Dennis JE, Awadallah A, Lundberg M, Caplan AI, Goldberg VM. Treatment of osteochondral defects with autologous bone marrow in a hyaluronan-based delivery vehicle. *Tissue Eng* 2002;8(2):333-47.
- [230] Segura T, Anderson BC, Chung PH, Webber RE, Shull KR, Shea LD. Crosslinked hyaluronic acid hydrogels: a strategy to functionalize and pattern. *Biomaterials* 2005;26(4):359-71.
- [231] Chandy T, Sharma CP. Chitosan--as a biomaterial. *Biomater Artif Cells Artif Organs* 1990;18:1-24.
- [232] Brun P, Cortivo R, Zavan B, Vecchiato N, Abatangelo G. In vitro reconstructed tissues on hyaluronan-based temporary scaffolding. *J Mater Sci Mater Med* 1999;10(10/11):683-8.
- [233] Campoccia D, Doherty P, Radice M, Brun P, Abatangelo G, Williams DF. Semisynthetic resorbable materials from hyaluronan esterification. *Biomaterials* 1998;19(23):2101-27.
- [234] Aigner J, Tegeler J, Hutzler P, Campoccia D, Pavesio A, Hammer C, Kastenbauer E, Naumann A. Cartilage tissue engineering with novel nonwoven structured biomaterial based on hyaluronic acid benzyl ester. *J Biomed Mater Res* 1998;42(2):172-81.

- [235] Chen WY, Abatangelo G. Functions of hyaluronan in wound repair. *Wound Repair Regen* 1999;7(2):79-89.
- [236] Giuggioli D, Sebastiani M, Cazzato M, Piaggese A, Abatangelo G, Ferri C. Autologous skin grafting in the treatment of severe scleroderma cutaneous ulcers: a case report. *Rheumatology (Oxford)* 2003;42(5):694-6.
- [237] Pavesio A, Abatangelo G, Borrione A, Brocchetta D, Hollander AP, Kon E, Torasso F, Zanasi S, Marcacci M. Hyaluronan-based scaffolds (Hyalograft C) in the treatment of knee cartilage defects: preliminary clinical findings. *Novartis Found Symp* 2003;249:203-17; discussion 229-41.



Characterize and model the mechanical and physicochemical properties of 3D scaffolds and their variation with porosity, pore size, and pore shape

As regards obstacles, the shortest distance between two points can be a curve

Berthold Brecht (1898 – 1956)





## Chapter 2

# 3D Fiber Deposited Scaffolds for Tissue Engineering: Influence of Pores Geometry and Architecture on Dynamic Mechanical Properties

L. Moroni <sup>a, b, \*</sup>, J.R. de Wijn <sup>a, b</sup>, C.A. van Blitterswijk <sup>a</sup>

<sup>a, \*</sup> Institute for BioMedical Technology (BMTI), University of Twente, P.O. Box 217, 7500 AE Enschede, The Netherlands. E-mail: l.moroni@tnw.utwente.nl

<sup>b</sup> IsoTis S.A., P.O. Box 98, 3720 AB Bilthoven, The Netherlands

### Abstract

One of the main issues in tissue engineering is the fabrication of scaffolds that closely mimic the biomechanical properties of the tissues to be regenerated. Conventional fabrication techniques are not sufficiently suitable to control scaffold structure to modulate mechanical properties. Within novel scaffold fabrication processes 3D fiber deposition (3DF) showed great potential for tissue engineering applications because of the precision in making reproducible 3D scaffolds, characterized by 100% interconnected pores with different shapes and sizes. Evidently, these features also affect mechanical properties. Therefore, in this study we considered the influence of different structures on dynamic mechanical properties of 3DF scaffolds. Pores were varied in size and shape, by changing fibre diameter, spacing and orientation, and layer thickness. With increasing porosity, dynamic mechanical analysis (DMA) revealed a decrease in elastic properties such as dynamic stiffness and equilibrium modulus, and an increase of the viscous parameters like damping factor and creep unrecovered strain. Furthermore, the Poisson's ratio was measured, and the shear modulus computed from it. Scaffolds showed an adaptable degree of compressibility between sponges and incompressible materials. As comparison, bovine cartilage was tested and its properties fell in the fabricated scaffolds range. This investigation showed that viscoelastic properties of 3DF scaffolds can be modulated to accomplish mechanical requirements for tailored tissue engineered applications.

**Keywords:** rapid prototyping, dynamic mechanical analysis, scaffolds, tissue engineering.

## Introduction

Rapid Prototyping techniques have recently attracted more and more interest for applications in tissue engineering as powerful tools to fabricate scaffolds. These scaffolds are built layer by layer, through material deposition on a stage, either in a molten phase (known as Fused Deposition Modeling (FDM)) [1-10] or in droplets together with a binding agent (referred to as 3D Printing) [2-4,11-15]. The 3D outcomes of this process are usually 100% interconnected porous scaffolds per definition, since during fabrication the layers are deposited as interpenetrating networks (material and void, see figure 1). Scaffolds have a defined structure and architecture, and can be built with a customized shape by CAD-CAM techniques. This flexibility and versatility in creating scaffolds gives us the opportunity to use rapid prototyping devices to generate improved scaffolds and to study the influence of different structural phenomena on tissue reconstruction. Within this respect, fused deposition modeling (FDM) techniques [2, 5, 10] have been lately used for tissue engineering purposes, offering appealing solutions for scaffold fabrication. Among these devices 3D plotting [16, 17] and 3D fiber deposition (3DF) [18] has been recently developed and used for tissue engineering purposes, the latter being a system for the extrusion of highly viscous polymers. 3DF is, essentially, a fused deposition technique in which an extrudate of molten polymer is deposited from a XYZ motor drive syringe on a stationary stage by applying pressure.

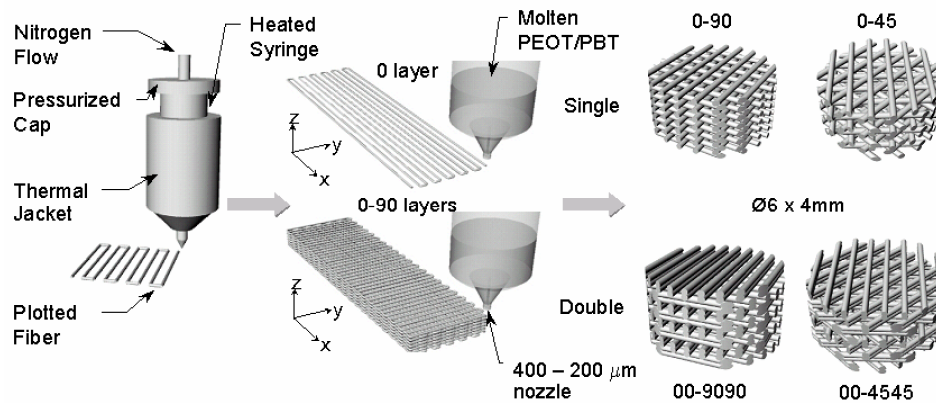


**Figure 1** – Draw of a Bioplotter device and 3DF fabrication process. 0-90 and 0-45 scaffolds architectures in single and double layer versions are presented. Modified from Woodfield et al. [18].

From a mechanical point of view, one of the main paradigms in tissue engineering and biomechanical science has always been that a scaffold should mimic the biomechanical properties of the organ or tissue to be replaced [14, 15, 19, 20]. Nevertheless, to our knowledge no systematic study has been conducted to assess whether the exact match of mechanical properties is indeed so crucial for optimal tissue regeneration. For instance, since mechanical properties are intimately related to the porosity of porous structures, it might be that a stiffer and less porous scaffold

will provide a better integration with the surrounding natural tissue, or - in contrast - that a more flexible and porous one will allow cells to attach and proliferate in a more efficient way. It is here where rapid prototyping offers possibilities to compromise such different requirements into one scaffold, because it adds freedom of varying structural parameters to the non-variable bulk mechanical properties of the material used.

Hence, the aim of this paper was to investigate the dynamic and static mechanical properties of scaffolds with a number of different structural features that can modulate their viscoelastic properties in order to mimic a large collection of natural tissues [21-25]. For this purpose, block-copolymers of polyethyleneoxide-terephthalate (PEOT) and polybutylene-terephthalate (PBT) have been investigated. These polyether-ester multiblock copolymers belong to a class of materials known as thermoplastic elastomers which exhibit good physical properties like elasticity, toughness and strength in combination with easy processability [26], as previously explained in chapter 1. This family of copolymers has already been of great interest for tissue engineering and drug delivery applications, because by varying the molecular weight of the starting PEG segments and the weight ratio of PEOT and PBT blocks it is possible to tailor-make properties, such as wettability [27], swelling [26, 28, 29], biodegradation rate [29], protein adsorption [30], and mechanical properties [18]. Furthermore, PEOT/PBT block copolymers have shown to be extensively biocompatible both in vitro and in vivo [31-34] and reached clinical applications (PolyActive™, IsoTis Orthopaedics S.A.) as cement stoppers and bone fillers in orthopedic surgery [35, 36]. Being polyether-esters degradation occurs in aqueous media by hydrolysis and oxidation, the rate of which varying from very low for high PBT contents to medium and high for larger contents of PEOT and longer PEO segments [26, 29].

The 3DF scaffolds response was assessed by dynamic mechanical analysis (DMA) since it allows tailoring of test conditions that can more closely simulate the physiological environment of the specific tissue to repair, and it enables scaffolds viscoelastic characterization [37-41]. By varying fiber diameter, fiber spacing and layer thickness in the internal structure of a scaffold, the mechanical properties change. This is due, among other factors, to a correspondent change of the overall porosity of the scaffold. Fiber orientation or deposition angle are also parameters to consider. If the angle step with which two subsequent layers are deposited or if the number of layers plotted with the same orientation on top of each other is varied, a different mechanical behavior will result at constant porosity. Bovine articular cartilage was tested as a reference to show how a scaffold structure can be tailored to mimic the biomechanical behavior of a specific tissue. Therefore, the combination of 3DF and DMA is shown in this study to be a powerful tool to achieve optimized scaffolds for tissue engineering applications.

## Materials and Methods

### *Scaffold Fabrication*

Poly(ethylene oxide terephthalate)-poly(butylene terephthalate) (PEOT/PBT) block copolymers were obtained from IsoTis S.A. (Bilthoven, The Netherlands). Their chemical composition is represented by the notation aPEOTbPBTc, where a is the molecular weight of the starting poly(ethylene glycol) PEG segments used in the polymerization process, while b and c refer to the weight ratio between PEGT and PBT blocks, respectively. For this study, 300PEOT55PBT45 co-polymer was used.

3D scaffolds were fabricated with a Bioplotter device (Envisiontec GmbH, Germany), essentially an XYZ plotter construction as previously described by Landers et al [17]. A few modifications enabled the extrusion of highly viscous 300PEOT55PBT45 melts, as shown in figure 1. Briefly, the polymer was placed in a stainless steel syringe and heated at  $T = 190\text{ }^{\circ}\text{C}$  through a heated cartridge unit, mounted on the "X"-mobile arm of the apparatus. When the polymer reached a molten phase, a nitrogen pressure of 5 Bars was applied to the syringe through a pressurized cap. Rectangular block models were loaded on the Bioplotter CAD/CAM software and plotted layer by layer, through the extrusion of the polymer on a stage as a fiber. The scaffold was then characterized by varying the fiber diameter (d1) (through the nozzle diameter or the deposition speed), the spacing between fibers in the same layer (d2), the layer thickness (d3) and the configuration of the deposited fibers within the whole architecture, which are all parameters set on the CAD/CAM software controlling the Bioplotter. The nozzles used to extrude polymer fibers were stainless steel Luer Lock hypodermic needles with internal diameter (ID) of  $400\text{ }\mu\text{m}$  and  $200\text{ }\mu\text{m}$ , shortened to a length of approximately 16.2 mm. The corresponding plotted fibers had a diameter d1 of  $260\text{ }\mu\text{m}$  and  $170\text{ }\mu\text{m}$ , respectively. The fiber spacing d2 was set to  $600\text{ }\mu\text{m}$ ,  $800\text{ }\mu\text{m}$  and  $1000\text{ }\mu\text{m}$ , and the layer thickness d3 was originally set to  $150\text{ }\mu\text{m}$ ,  $250\text{ }\mu\text{m}$  and  $350\text{ }\mu\text{m}$ . Since the adhesion of fibers between two subsequent layers was compromised for a layer thickness larger than 60% of the fiber diameter value,  $d3 = 275\text{ }\mu\text{m}$  was chosen as the largest value for  $d1 = 170\text{ }\mu\text{m}$  set of scaffolds. The architecture was changed by plotting fibers with  $45^{\circ}$  and  $90^{\circ}$  angle steps between two successive layers (called 0-45 and 0-90 configurations respectively) and by modifying the fiber orientation after one or after two printed layers (referred to as single and double layers configurations respectively). The deposition speed was varied between 100 mm/min and 300 mm/min in order to assess its influence on fiber diameter and overall porosity of the scaffolds.

For comparison with more conventional techniques, scaffolds were also made by salt leaching, whereby a mixture of polymer powder and salt particles was compression molded into blocks and the salt removed by leaching in water. The average pore size of these scaffolds was  $182\text{ }\mu\text{m}$ , with a maximum pore size of  $600\text{ }\mu\text{m}$  and an overall porosity of 75% [42-43].

***Scaffold Characterization***

Cylindrical plugs of 6 mm in diameter by 4 mm in height were cored out in the “Z-direction” from the rectangular 3D plotted blocks, and taken as samples for the mechanical analysis. Scaffolds geometry and architecture were characterized by scanning electron microscopy (SEM) analysis with a Philips XL 30 ESEM-FEG. Samples were gold sputtered (Carrington) before SEM analysis. The porosity of 3D plotted scaffolds was calculated following the theoretical approach by Landers et al [17]:

$$P = 1 - \frac{V_{\text{scaffold}}}{V_{\text{cube}}} = 1 - \frac{\pi \cdot d_1^2}{4 \cdot d_2 \cdot d_3} \quad (1)$$

where P is the scaffold porosity, d1 the fiber diameter, d2 the fiber spacing and d3 the layer thickness, within each different structure (see also tables 1 and 2). Porosity was also experimentally measured – e.g. in case of the salt leached scaffolds – by analyzing the mass and the volume of each scaffold, as:

$$P = 1 - \frac{M}{V} \cdot \frac{1}{\rho} \quad (2)$$

where, M and V are the measured mass and volume of the scaffolds, while  $\rho$  is the specific density of 300PEOT55PBT45 (1.2 g/cm<sup>3</sup>). Since, there was only a small difference (< 1%) between theoretical and experimental porosities (data not shown), we decided to refer to the theoretical one, as more conformal to the fabrication parameters of the Bioplotter.

***Bovine Articular Cartilage Harvest***

Bovine articular cartilage plugs of the same dimension as the 3D scaffolds specimens were punched out from the knee of a 6-month old calf. The obtained samples were perpendicularly sectioned. Once the knee was opened, cartilage plateaus were kept hydrated with phosphate-buffered saline (PBS) (Gibco-BRL), while the cylindrical plugs were punched out from the femoral condyle with a coring drill. The samples were then stored in PBS and mechanically tested during the same day.

***Dynamic Mechanical Analysis***

A DMA instrument (Perkin Elmer 7e) was used to evaluate the viscoelastic properties of the 3D scaffolds and of the bovine articular cartilage cylindrical plugs. For each structural and architectural configuration three samples were tested in all the experiments performed. In the case of bovine articular cartilage, six plugs were tested to level out the differences between the different regions of the femoral

plateau, where the samples were taken. Cylindrical fixtures were chosen to test the specimens along their compression axis, in the “Z-direction”.

Dynamic stress and creep recovery tests were performed on scaffolds for mechanical characterization. In the dynamic stress test, scaffolds were loaded with a dynamic force varying from 3.5N to 4.5N, which is well in the middle of the linear part of the static stress-strain curve. A ramp of 50mN/min at a constant frequency of 1Hz was used, as depicted in figure 2. Dynamic stiffness, or storage modulus, and damping factor, or  $\tan \delta$ , were calculated.

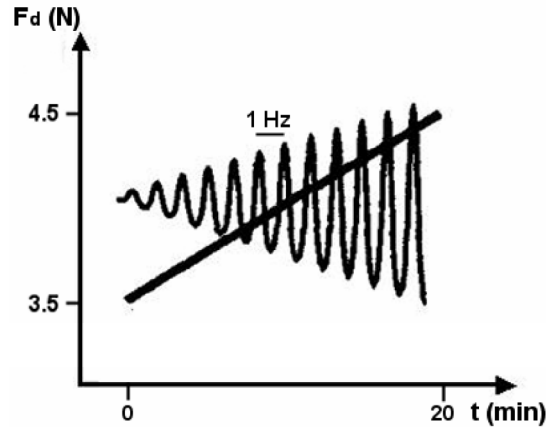


**Figure 2** – Schematic diagram of the dynamic force applied on 3D scaffolds during viscoelastic assessment. The resulting force is the sum of the two depicted curves.

In the creep recovery test, samples were pre-loaded with a recovery force of 100mN for two minutes. Then, a force of 3.5N was applied instantaneously and kept for three minutes, after which the loading condition was returned to the recovery value. This set up was cycled for three times to ensure that no significant difference was experienced after each loading cycle, in terms of equilibrium modulus and unrecovered creep strain. The same experiment was repeated with a loading force of 4.5N to assess creep and recovery properties of the fabricated scaffolds in the minimum and maximum force range applied in the dynamic stress analysis.

For a frequency scan test, a force of 100mN was applied and kept constant, while a variable load of 80 mN was superimposed with a frequency sweep from 0.1Hz to 15Hz. The elastic modulus and dynamic viscosity were measured and related to the viscoelastic behavior of the scaffolds as the frequency increases.

To consider the influence of an aqueous environment and possible perfusion effects, the tests were done in three different environmental conditions: in a nitrogen atmosphere, in PBS and in a synovium-like fluid. This last wet setting consisted of a 3% (w/v) solution of polyvinylpyrrolidone (PVP) in de-ionized water. The dynamic viscosity of the solution was measured with Brookfield viscosimeter and determined as 0.01 Pa\*s, which is in the range of natural synovium fluid [44]. Bovine articular cartilage was tested only in wet milieus. Scaffolds were soaked both in PBS and in

PVP-solution over night, before loading. The temperature was set to 37 °C for all the experiments.

### *Poisson's Ratio optical measurement*

Poisson's ratios of scaffolds, bulk polymer and bovine articular cartilage were measured through an optical technique as described by Jurvelin *et al* [45]. Briefly, samples were placed between non-rotating tips of a micrometer under a stereomicroscope. Original height and diameter were measured. Then, a compressive strain of 10% was applied to the specimens through the micrometer and the final height and diameter were determined, after leaving the samples equilibrating for 1h. Dimensional measurements were performed through imaging analysis (Scion Image, Scion Corporation) of micrographs acquired with a video camera (Sony progressive 3CCD) and a frame grabber (PCImage SRGB, Matrix Vision) connected to the stereomicroscope. Poisson's ratios were then computed as:

$$\nu = -\frac{\Delta D/D}{\Delta L/L} \quad (3)$$

where  $\nu$  is the Poisson's ratio, D and L are the samples original diameter and height respectively, while  $\Delta D$  and  $\Delta L$  the variation of diameter and length between the unstrained and the strained configurations.

From the measured experimental values of dynamical stiffness and Poisson's ratio, scaffolds shear modulus was indirectly calculated through the formula:

$$G = \frac{E}{2 \cdot (1 - \nu)} \quad (4)$$

where G is the scaffold shear modulus and E the dynamic stiffness.

## Results

### *Scaffolds Characterization*

300PEOT55PBT45 3D scaffolds with different pore architecture and geometry were fabricated. Pore architecture was dependent on fiber orientation and deposition (Fig. 3). A fiber deposition angle of 90° created quadrangular pores (Fig. 3A-C), while a 45° angle step generated polygonal pores (Fig. 3D-F). Furthermore, the deposition of two successive layers with the same fiber orientation resulted in doubling the pore height (Fig. 3C and 3F). The pore geometry was defined by fiber diameter and spacing (d1 and d2), and layer thickness (d3) (Fig. 3C). A decrease of the fiber diameter from 260 μm to 170 μm and a decrease of the layer thickness from 350 μm to 150 μm corresponded to a decrease of the pore height. Analogously, a decrease of the fiber spacing from 1000 μm to 600 μm lead to a decrease of the pore width. The pore height was mainly defined by the layer thickness, while the pore width was defined by the difference between fiber spacing and fiber diameter.

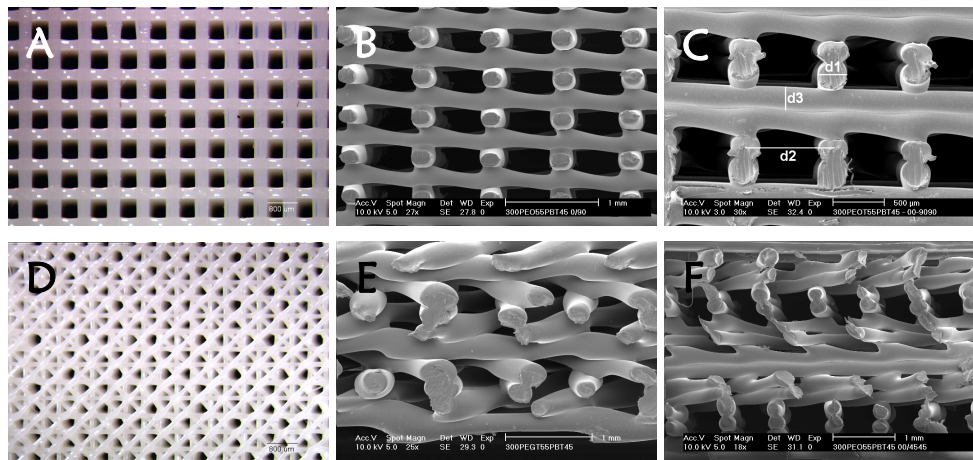


**Figure 3** – Optical Microscopy pictures of scaffolds surface and SEM micrographs of cross sections. (d, e, f) 0-45 and (a, b, c) 0-90 architecture configurations in (b, e) single and (c, f) double layer versions. (c) represents graphically the fiber diameter and spacing (d1 and d2) and the layer thickness d3 of a 3DF scaffold.

The effect of deposition speed ( $V$ ) on fiber diameter and ultimately on scaffold porosity is depicted in figure 4. A decrease of  $V$  from 300 mm/min to 100 mm/min resulted in an increase of the fiber diameter from 268  $\mu\text{m}$  to 432  $\mu\text{m}$ , which corresponded to a decrease of the scaffold's porosity from 75% to 29%. The variation of all the parameters above introduced, one by one, allowed to create a set of scaffolds within a porosity range from 29% up to 91%.

SEM analysis revealed a significant consistency between the theoretical and real values of fiber diameter, fiber spacing, and layer thickness for all the scaffolds processed. The fiber diameter (d1) was  $268 \pm 32 \mu\text{m}$  when the larger Bioplottter tip (ID = 400  $\mu\text{m}$ ) was used and  $170 \pm 15 \mu\text{m}$  when the smaller one was used (ID = 200  $\mu\text{m}$ ). The fiber spacing (d2) was  $605 \pm 12 \mu\text{m}$ ,  $807 \pm 28 \mu\text{m}$ , and  $1001 \pm 0.00 \mu\text{m}$ . The layer thickness (d3) was  $148 \pm 10 \mu\text{m}$ ,  $257 \pm 11 \mu\text{m}$ , and  $344 \pm 11 \mu\text{m}$ . All the scaffolds produced had 100% pore interconnectivity and no layer delamination phenomenon occurred in the porosity range analyzed.

### *Dynamic Mechanical Properties*

3D plotted scaffolds were tested to characterize their viscoelastic behavior. Tables 1 and 2 summarize the obtained data from DMA on some of the deposited scaffolds with different porosity, and on articular bovine cartilage. With increasing porosity and/or by changing the scaffold architecture, the dynamic stiffness increased from a minimum value of  $0.186 \pm 0.005 \text{ MPa}$  to a maximum of  $13.7 \pm 2.63 \text{ MPa}$  (table 1, columns 3-5), while the equilibrium modulus varied from  $0.04 \pm 0.005 \text{ MPa}$  to  $8 \pm 0.81 \text{ MPa}$  (table 1, columns 6-8). Analogously, the Damping factor decreased from  $0.202 \pm 0.015$  to  $0.075 \pm 0.012$  (table 2, columns 3-5), while the creep uncovered strain changed from  $49.67 \pm 15.9\%$  to  $0.36 \pm 0.13\%$  in the same porosity series (table 2, columns 6-8). Dynamic stiffness and equilibrium modulus of bovine



articular cartilage were higher under synovium-like fluid conditions and measured as  $9.64 \pm 1.81$  MPa and  $0.64 \pm 0.16$  MPa, respectively. Damping factor and creep unrecovered strain were  $0.175 \pm 0.03\%$  and  $46.91 \pm 9.86\%$ . DMA showed an increase in dynamic stiffness and equilibrium modulus with decreasing fiber spacing

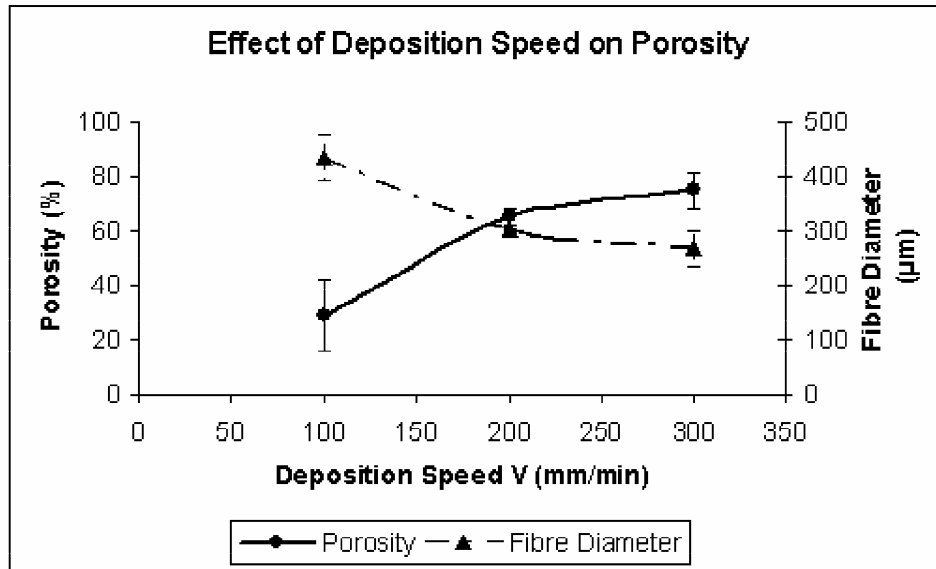


**Figure 4** – Effect of deposition speed on scaffolds porosity and fiber diameter in a 00-9090 layer configuration with an ID =  $400 \mu\text{m}$  nozzle.

and layer thickness (Figs. 5a and 5b). Inversely, the damping factor and the uncovered creep strain decreased, which resulted in a less plastic behavior of the scaffolds (Figs. 5c and 5d). The influence of the architecture on the mechanical properties of the scaffolds was also studied (Fig. 6). By varying the layer configuration from single to double layer printed versions and from 0-90 to 0-45 fiber orientation, the dynamic stiffness and the equilibrium modulus decreased (Figs. 6a and 6b), while the damping factor and the unrecovered creep strain increased (Figs. 6c and 6d), although the porosity remained constant to 75%. These results were then used to make a comparison with the mechanical data on bovine articular cartilage. A frequency scan of bovine articular cartilage, solid material and 3DF scaffolds has also been performed and depicted in figure 7. This test further assessed the modulation of viscoelastic properties of 300PEOT55PBT45 along a frequency span typical of physiological conditions [21], since bovine articular cartilage values were found in between solid material and 3DF scaffolds.

Results from the optical measurement of Poisson's ratio of scaffolds with different architectures are shown in figure 8. A modulation from 0.117 to 0.478 by varying the scaffolds architecture or by increasing their porosity was measured.

Porosity (%)	Scaffold Structure ( $\mu\text{m}$ )	E' (MPa) - Dry	E' (MPa) - PBS	E' (MPa) - PVP	Ha (MPa) - Dry	Ha (MPa) - PBS	Ha (MPa) - PVP
28,9	d1=260 - d2=800 - d3=150 - V=100	13.7 $\pm$ 2.63	-	-	8 $\pm$ 1.47	-	-
41	d1=260 - d2=600 - d3=150	8.66 $\pm$ 0.81	8.74 $\pm$ 2.44	9.7 $\pm$ 0.5	6.88 $\pm$ 0.81	4.88 $\pm$ 0.23	6.33 $\pm$ 1.47
55,8	d1=260 - d2=800 - d3=150	6.63 $\pm$ 0.88	7.1 $\pm$ 0.66	5.28 $\pm$ 1.35	4.73 $\pm$ 0.88	2.35 $\pm$ 0.12	3.27 $\pm$ 1.12
64,2	d1=260 - d2=1000 - d3=150	2.6 $\pm$ 0.23	2.75 $\pm$ 2.68	2.6 $\pm$ 0.02	0.66 $\pm$ 0.25	2 $\pm$ 0.12	1.59 $\pm$ 0.02
78,7	d1=260 - d2=1000 - d3=250	0.815 $\pm$ 0.11	1.21 $\pm$ 1.08	1.01 $\pm$ 0.99	0.24 $\pm$ 0.11	0.43 $\pm$ 0.08	0.58 $\pm$ 0.3
85,4	d1=170 - d2=600 - d3=275	0.589 $\pm$ 0.11	-	-	0.04 $\pm$ 0.005	-	-
91,2	d1=170 - d2=1000 - d3=275	0.262 $\pm$ 0.09	-	-	0.13 $\pm$ 0.01	-	-
Bovine Cartilage (65-80)	-	-	9.3 $\pm$ 0.9	9.64 $\pm$ 1.81	-	0.49 $\pm$ 0.05	0.64 $\pm$ 0.16

**Table 1** – Elastic properties of few different 3DF PEOT/PBT scaffolds with a 00-9090 architecture and bovine articular cartilage, tested with DMA.

Porosity (%)	Scaffold Structure ( $\mu\text{m}$ )	Tan $\delta$ - Dry	Tan $\delta$ - PBS	Tan $\delta$ - PVP	$\epsilon$ (%) - Dry	$\epsilon$ (%) - PBS	$\epsilon$ (%) - PVP
28,9	d1=260 - d2=800 - d3=150 - V=100	0.08 $\pm$ 0.014	-	-	0.36 $\pm$ 0.13	-	-
41	d1=260 - d2=600 - d3=150	0.075 $\pm$ 0.011	0.065 $\pm$ 0.004	0.064 $\pm$ 0.002	0.55 $\pm$ 0.001	0.72 $\pm$ 0.27	0.71 $\pm$ 0.28
55,8	d1=260 - d2=800 - d3=150	0.077 $\pm$ 0.002	0.084 $\pm$ 0.005	0.067 $\pm$ 0.0007	0.91 $\pm$ 0.07	1.12 $\pm$ 0.62	0.7 $\pm$ 0.43
64,2	d1=260 - d2=1000 - d3=150	0.107 $\pm$ 0.011	0.111 $\pm$ 0.05	0.091 $\pm$ 0.01	2.37 $\pm$ 0.93	1.49 $\pm$ 0.27	1.7 $\pm$ 0.1
78,7	d1=260 - d2=1000 - d3=250	0.182 $\pm$ 0.009	0.155 $\pm$ 0.05	0.121 $\pm$ 0.019	14.56 $\pm$ 1.07	7.59 $\pm$ 1.26	17.38 $\pm$ 0.59
85,4	d1=170 - d2=600 - d3=275	0.18 $\pm$ 0.003	-	-	49.67 $\pm$ 15.9	-	-
91,2	d1=170 - d2=1000 - d3=275	0.169 $\pm$ 0.014	-	-	44.72 $\pm$ 8.44	-	-
Bovine Cartilage (65-80)	-	-	0.164 $\pm$ 0.005	0.175 $\pm$ 0.03	-	27.16 $\pm$ 12.05	46.91 $\pm$ 9.86

**Table 2** – Plastic properties of few different 3DF PEOT/PBT scaffolds with a 00-9090 architecture and bovine articular cartilage, tested with DMA.

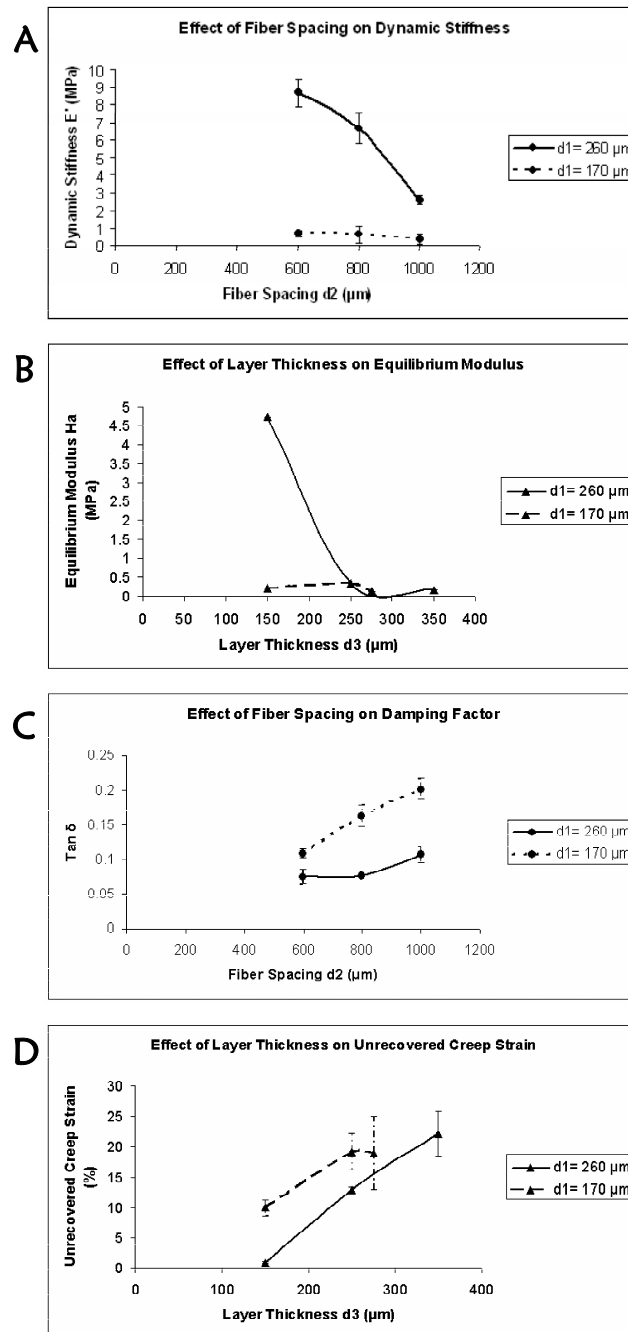


**Figure 5** – Effect of (a, c) fibre spacing and (b, d) layer thickness on, respectively, elastic and plastic behaviour of 300PEGT55PBT45 3D scaffolds. Analogous trend were found concerning the influence of layer thickness and fibre spacing on the elastic and plastic behaviour, respectively. 00-9090 scaffold configuration was fixed.

Correspondently, the shear modulus  $G'$  increased from  $0.96 \pm 0.26$  MPa to  $8.81 \pm 1.1$  MPa (Fig. 9). Poisson's ratio of cartilage was 0.305 (Fig. 8), and the shear modulus was  $6.93 \pm 1.3$  MPa (Fig. 9). All the viscoelastic parameters were measured along the main compression axis of the structures, in the "Z-direction". Therefore, from the mechanical characterization performed we cannot infer any information in the other directions, since both the fabricated scaffolds and natural cartilage are anisotropic structures.

## Discussion

In this study, the modulation of the viscoelastic properties of 3D fiber deposited PEOT/PBT scaffolds has been investigated. Bovine articular cartilage was also studied as a reference to show how 3DF scaffolds can mimic a natural tissue. Firstly, SEM analysis revealed a very good consistency between the machine settings and the actual parameters. Variations of fiber diameter, fiber spacing and layer thickness were due to a decrease of polymer melt viscosity over time as a result of thermal degradation. This implied a faster polymer flow out of the tip during printing, and consequently a slight increase of fiber diameter at a specific deposition speed. Nevertheless, scaffolds presented 100% interconnected pores and were reproducible with the same characteristics each time they were processed.

3DF constructs were mechanically characterized through DMA for different geometrical and architectural configurations. From a mechanical point of view, these scaffolds were treated and analyzed following a solid-state mechanics approach. However, it has to be noted that the macroporous structure plays a determinant role on the properties of the whole scaffold. It is, indeed, the organization and the volume of macropores that drives the modulation of mechanical properties from the bulk material. Dynamic stress and creep recovery tests determined the constructs' dynamic (dynamic stiffness and damping factor) and quasi-static (equilibrium modulus and creep unrecovered strain) behavior, respectively. Dynamic stiffness and equilibrium modulus increased with decreasing fiber spacing and layer thickness. Inversely, the damping factor and the creep unrecovered strain decreased, illustrating a less plastic behavior of the scaffolds (see figure 5). The observed trends are directly related to the scaffold porosity. In fact, a decrease of fiber diameter, fiber spacing or layer thickness results in an increase of deposited polymer and a consequent decrease of pore volume within the same scaffold volume. A similar trend was also obtained by decreasing the fiber deposition speed. In this case, a decrease in the deposition speed resulted in a larger polymer flow per traveled distance, which implied a larger fiber diameter and lead to a decrease of porosity. As shown in tables 1 and 2, a slight increase in dynamic stiffness and equilibrium modulus, and a consequent small decrease in the viscous factors was generally experienced from dry to wet conditions. Such an environment, as in a physiological setting, introduces a second phase during dynamical load. The final measurement is then the sum of the response of the material itself and that of a fluid phase being transported in and out of the solid phase through the pores. The result is an increase of the apparent stiffness at higher fluid phase viscosities. In the

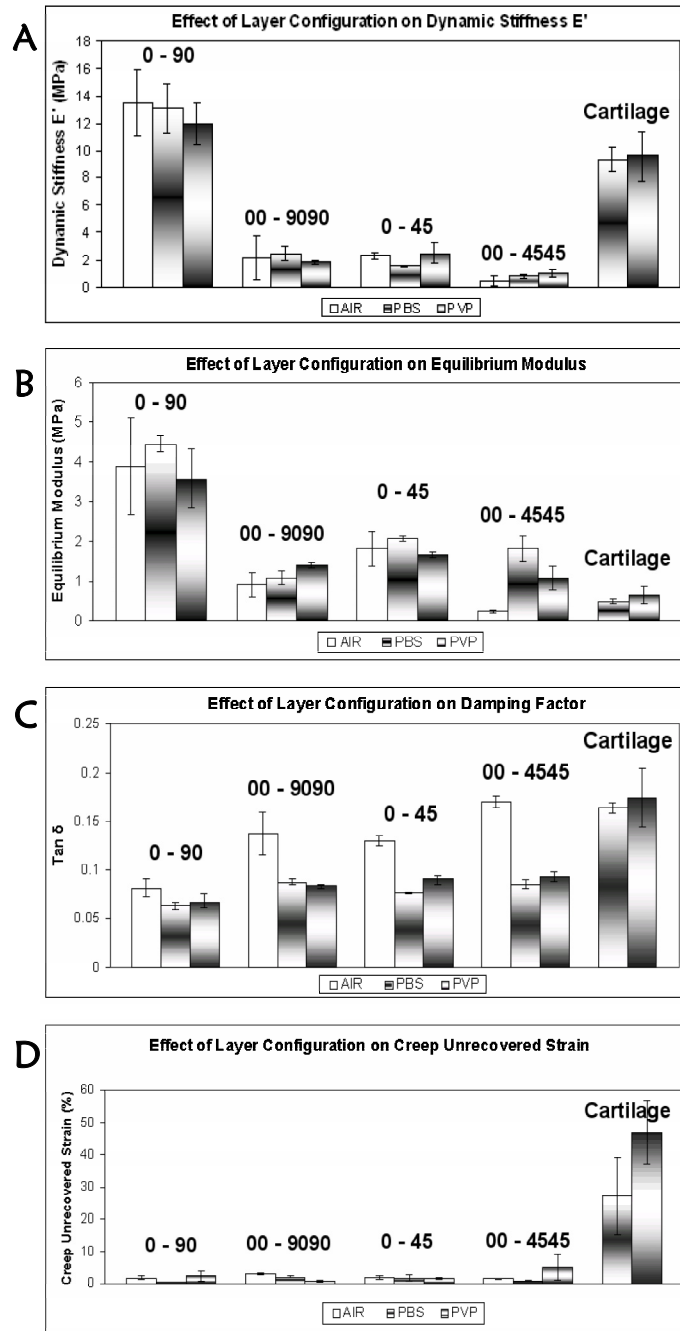


**Figure 6** – Effect of scaffold architecture at a constant porosity  $P = 73\%$  on (a, b) elastic and (c, d) plastic behaviour of 3DF scaffolds in different media. Bovine articular cartilage was also tested with the same loading protocol as a reference.

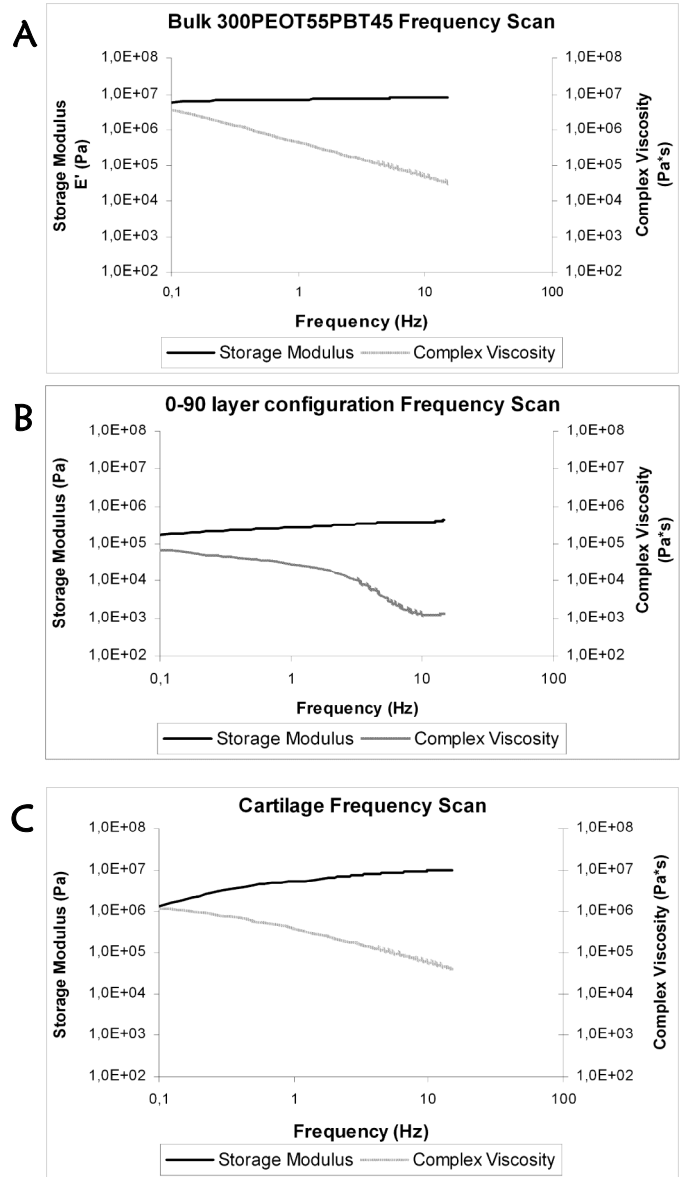


**Figure 7** – Frequency Scan diagram for 300PEGT55PBT45 bulk and 0-90 scaffolds, and bovine articular cartilage. An increase of applied load frequency generates a decrease of dynamic viscosity and an increase of dynamical stiffness, which is characteristic of viscoelastic materials. Similar behaviour was shown for all the other scaffold architectures.

case of the viscous factors such a biphasic liquid-solid system implied a decrease of damping and unrecovered creep strain, because part of the lost energy during load

is dissipated by the liquid component. This viscoelastic behavior is also encountered in many natural tissues and is strictly connected to the macro porous structure of the constructs. In fact, a larger pore volume leads to an increase of the mechanical response of the fluid component, since more liquid will be pumped through the pores of the scaffold.

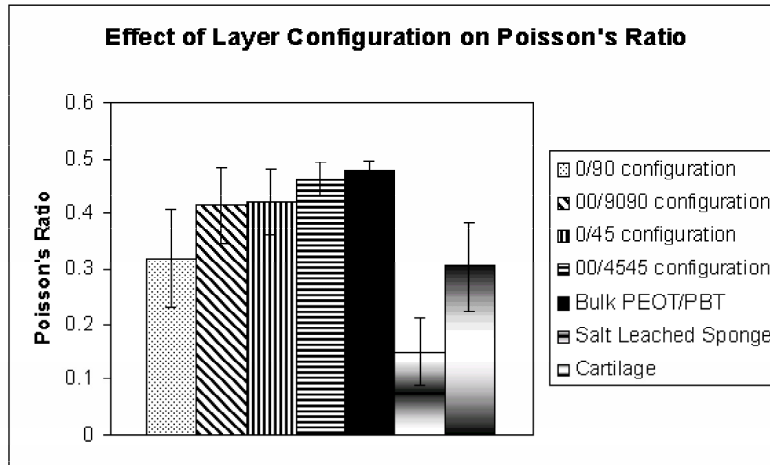


**Figure 8** – Influence of scaffold architecture on Poisson's ratio optical measurement. Bulk and salt leached PEOT/PBT scaffold, and bovine articular cartilage were also tested as references to show architectural compressibility modulation.

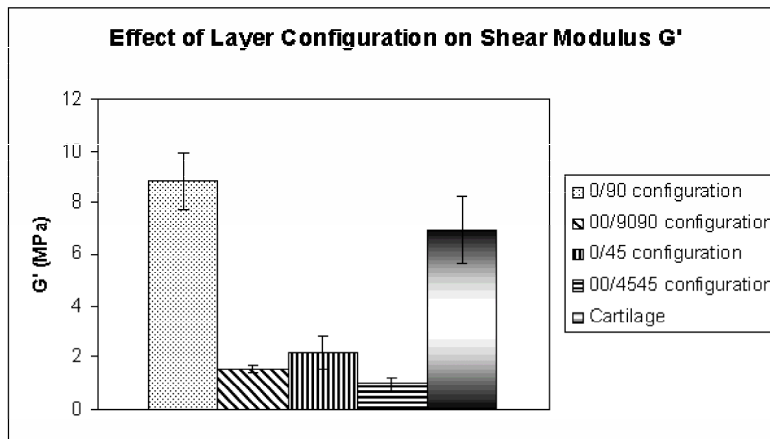


**Figure 9** – Effect of scaffold architecture on shear modulus, indirectly calculated from Poisson's ratio and dynamical stiffness measurements.

The modulation of PEOT/PBT 3DF scaffolds viscoelastic properties was also found for different pore architecture, while the porosity was kept constant. Interestingly, a



change in the scaffold from single to double layer configuration and from 0-90 to 0-45 fiber deposition resulted in a more flexible and plastic construct, while the porosity was constant (see figure 6). In the first case, we could infer that an increase in the pore size along the compression axis led to a mechanically weaker structure. In the second case the local increase of contact points between fibers implied a larger contact area and, thus, a decrease of the local stress experienced by the structure. This was reflected in lower values of storage and equilibrium modulus. Again, a decrease in dynamic stiffness was accompanied by an increase of the damping factor, which implied a more plastic behavior of the scaffolds. However, while the equilibrium modulus varied in a similar way as the dynamic stiffness, the creep unrecovered strain didn't significantly change with the architecture and was considerably low for the fixed porosity analyzed.

A further assessment of the mechanical modulation of PEOT/PBT scaffolds was given by the frequency scan test (Fig. 7). In this case, the higher the frequency with which the force was dynamically applied, the higher was the storage modulus (dynamic stiffness), but the lower the dynamic viscosity. A comparison between frequency scans of bulk polymer, scaffolds, and bovine articular cartilage reveals an enhanced viscoelastic behavior for the 3D structure as compared to the bulk one, the plastic nature of bovine articular cartilage being even more pronounced than the copolymer.

Concerning the compressibility of the scaffold, the Poisson's ratio has been measured for solid material, salt leached and 3DF copolymer scaffolds. Poisson's ratios generally vary between 0 and 0.5. In this range, the lower its value, the more compressible is a material. A comparison of the measured ratios between the fabricated scaffolds revealed a compressibility that is controlled by their architecture and structure. In particular, a tendency to higher values of Poisson's ratio for double layer and 0-45 configurations of the scaffolds could be detected with respect of single layer and 0-90 versions. Therefore, doubling the printed layers with the same angle orientation or decreasing the angle orientation step to 45 degrees resulted in less compressible scaffolds at constant porosity (see figure 8).

Similar implications as for dynamic stiffness and equilibrium modulus can be found for the shear modulus. Doubling the printed layers with the same angle orientation or changing the layer orientation angle step from 90 to 45 degrees, led to less stiff scaffolds (figure 9). An increase in pore dimension along the compression axis implied a more flexible structure in that direction and apparently also in the perpendicular plane, where the shear stress is experienced. A larger contact area between the fibers, as previously described, characterizes the 0-45 scaffold configuration. Apparently, this affects the local stress field so that a lower shear modulus is found.

A first comparison between the mechanical parameters measured for 3D scaffolds and bovine cartilage revealed that a 0-90 layer configuration of the deposited fibers was most effective in mimicking the biomechanical behavior of the natural tissue with this specific copolymer. It is certainly true that in this scenario the great freedom that 3D fiber deposition offers as a fabrication device, allows one to customize and render scaffolds for a wide variety of tissue engineering applications. It was the aim of this investigation to show how a number of mechanical

parameters of 3D scaffolds can be controlled, simply by varying their structure and architecture. Evidently, the bulk properties of the material used plays a major role on the overall behavior of 3D porous scaffolds. In this respect, the PEOT/PBT copolymers give the possibility to look at the effect of bulk properties on 3D porous constructs by changing the copolymer composition. Therefore, our following studies will be directed to superimpose bulk polymer properties of other PEOT/PBT copolymers on the current structural findings.

## Conclusions

This study shows how viscoelastic properties of 3D fiber deposited PEOT/PBT blocks copolymer scaffolds could be modulated to accomplish mechanical requirements for tailored tissue engineered applications. The modulation was not only dependent on porosity, but also on fiber deposition and orientation. The scaffold architecture is relevant from a biological point of view, since pores size and shape influence cells attachment and ingrowth. The 3DF-Biplotter device is able to fabricate structures with high reproducibility and flexibility, and it offers a wide variety of solutions in terms of different architectural and geometrical configurations. DMA enables tailoring 3D fiber deposition fabrication parameters in order to optimize scaffolds architecture and structure.

## Acknowledgements

Discussion on 3D fiber deposition with T.B.F. Woodfield was really appreciated. We are also grateful to P. Kaim for measuring the dynamic viscosity of the synovium-like fluid. F. Peters was very helpful in setting the DMA equipment.

## References:

- [1] Cooke MN, Fisher JP, Dean D, Rimnac C, Mikos AG. Use of stereolithography to manufacture critical-sized 3D biodegradable scaffolds for bone ingrowth. *J Biomed Mater Res: Appl Biomater* 2002;64B:65-69.
- [2] Hutmacher DW. Scaffold design and fabrication technologies for engineering tissues – state of the art and future perspectives. *J Biomater Sci Polymer edn*, Vol. 12, No. 1, 2002: 107-124.
- [3] Hutmacher DW. Scaffolds in tissue engineering bone and cartilage. *Biomaterials* 2000;21: 2529-2543.
- [4] Sachlos E, Czernuszka JT. Making tissue engineering scaffolds work. Review on the application of solid freeform fabrication technology to the production of tissue engineering scaffolds. *Eur Cells and Mater*, 2003;5:29-40.
- [5] Hutmacher DW, Schantz T, Zein I, Ng KW, Teoh SH, Tan KC. Mechanical properties and cell cultural response of polycaprolactone scaffolds designed and fabricated via fused deposition modelling. *J Biomed Mater Res* 2001;55A:203-216.
- [6] Vozzi G, Flaim C, Ahluwalia A, Bhatia S. Fabrication of PLGA scaffolds using soft lithography and microsyringe deposition. *Biomaterials* 2003;24:2533-2540.

- [7] Vozzi G, Previti A, De Rossi D, Ahluwalia A. Microsyringe-based deposition of two-dimensional and three-dimensional polymer scaffolds with a well-defined geometry for application to tissue engineering. *Tissue Engineering*, 2002;8(6):1089-1098.
- [8] Woodfield TBF, Bezemer JM, Pieper JS, van Blitterswijk CA, Riesle J. Scaffolds for tissue engineering of cartilage. *Critical Reviews in Eukaryotic Gene Expression*, 2002;12(3):209-236.
- [9] Yang S, Leong KF, Du Z, Chua CK. The design of scaffolds for use in tissue engineering. Part II. Rapid prototyping techniques. *Tissue Engineering*, 2002;8(1):1-11.
- [10] Zein I, Hutmacher DW, Tan KC, Teoh SH. Fused deposition modelling of novel scaffold architectures for tissue engineering applications. *Biomaterials* 2002;23:1169-1185.
- [11] Sachs E, Brancazio D, Bredt JF, Tuerck H, Lee Sang-J-On J, Curodeau A, Khanuja S, Cima M, Fan A, Michaels SP, Lauder A. Three-dimensional printing techniques. International Patent WO 9325336, 1993.
- [12] Giordano RA, Wu BM, Borland SW, Cima LG, Sachs EM, Cima MJ. Mechanical properties of dense polylactic acid structures fabricated by three dimensional printing. *J Biomater Sci Polymer Edn*, 1996;8(1):63-75.
- [13] Kim SS, Utsunomiya H, Koski JA, Wu BM, Cima MJ, Sohn J, Mukai K, Griffith LG, Vacanti JP. Survival and function of hepatocytes on a novel three-dimensional synthetic biodegradable polymer scaffold with intrinsic network of channels. *Ann Surg*, 1998 ; 228(1):8-13.
- [14] Sherwood JK, Riley SL, Palazzolo R, Brown SC, Monkhouse DC, Griffith LG, Landeen LK, Ratcliffe A. A three-dimensional osteochondral composite scaffold for articular cartilage repair. *Biomaterials*, 2002;23:4739-4751.
- [15] Taboas JM, Maddox RD, Krebsbach PH, Hollister SJ. Indirect solid free form fabrication of local and global porous, biomimetic and composite 3D polymer-ceramic scaffolds. *Biomaterials*, 2003;24:181-194.
- [16] Landers R, Hübner U, Schmelzeisen R, Müllhaupt R. Rapid prototyping of scaffolds derived from thermoreversible hydrogels and tailored for application in tissue engineering. *Biomaterials*, 2002;23: 4437-4447.
- [17] Landers R, Pfister A, Hübner U, John H, Schmelzeisen R, Müllhaupt R. Fabrication of soft tissue engineering scaffolds by means of rapid prototyping techniques. *J Mater Sci*, 2002;37: 3107-3116.
- [18] Woodfield TBF, Malda J, de Wijn J, Péters F, Riesle J, van Blitterswijk CA. Design of porous scaffolds for cartilage tissue engineering using a three-dimensional fibre-deposition technique. *Biomaterials* 2004;25:4149-4161.
- [19] Hollister SJ, Maddox RD, Taboas JM. Optimal design and fabrication of scaffolds to mimic tissue properties and satisfy biological constraints. *Biomaterials*, 2002;23:4095-4103.
- [20] Lin ASP, Barrows TH, Cartmell SH, Guldborg RE. Microarchitectural and mechanical characterization of oriented porous polymer scaffolds. *Biomaterials* 2003;24:481-489.
- [21] van Mow C, Ratcliffe A, Poole AR. Cartilage and diarthrodial joints as paradigms for hierarchical materials and structures. *Biomaterials*, 1992;13(2).

- [22] Laasanen MS, Töyräs J, Korhonen RK, Rieppo J, Saarakkala S, Nieminen MT, Hirvonen J, Jurvelin JS. Biomechanical properties of knee articular cartilage. *Biorheol*, 2003;40:133-140.
- [23] Doerhing TC, Carew EO, Vesely I. The effect of strain rate on the viscoelastic response of aortic valve tissue: a direct-fit approach. *Ann Biomed Eng*, 2004;32(2):223-232.
- [24] Elhadj S, Chan R, Forsten-Williams K. Implementation of an optical method for the real-time determination of uniaxial strain and vessel mechanics. *IEEE Trans Biomed Eng*, 2004; 51(3):536-538.
- [25] Yeni YN, Christopherson GT, Turner AS, Les CM, Fyhrie DP. Apparent viscoelastic anisotropy as measured from nondestructive oscillatory tests can reflect the presence of a flaw in cortical bone. *J Biomed Mater Res*, 2004;69A(1):124-130.
- [26] Bezemer JM, Grijpma DW, Dijkstra PJ, van Blitterswijk CA, Feijen J. A controlled release system for proteins based on poly(ether ester) block-copolymers: polymer network characterization. *J Cont Rel*. 1999 ;62(3):393-405.
- [27] Olde Riekerink M, Claase M, Engbers G, Grijpma D, Feijen J. Gas Plasma etching of PEO/PBT segmented block copolymer films. *J Biomed Mater Res*, 2003;65A(4):417-428.
- [28] van Dijkhuizen-Radersma R, Peters FL, Stienstra NA, Grijpma DW, Feijen J, de Groot K, Bezemer JM. Control of vitamin B12 release from poly(ethylene glycol)/poly(butylene terephthalate) multiblock copolymers. *Biomaterials*, 2002;23(6):1527-36.
- [29] Deschamps AA, Claase MB, Sleijster WJ, de Bruijn JD, Grijpma DW, Feijen J. Design of segmented poly(ether ester) materials and structures for the tissue engineering of bone. *J Cont Rel*, 2002;78:175-86.
- [30] Mahmood TA, de Jong R, Riesle J, Langer R, van Blitterswijk CA. Adhesion-mediated signal transduction in human articular chondrocytes: the influence of biomaterial chemistry and tenascin-C. *Exp Cell Res*, 2004;301(2):179-188.
- [31] van Blitterswijk CA, van de Brink J, Leenders H, Bakker D. The effect of PEO ratio on degradation, calcification and bone bonding of PEO/PBT copolymer (PolyActive). *Cell and Mater*, 1993;3:23-36.
- [32] Beumer GJ, van Blitterswijk CA, Ponec M. Degradation behavior of polymeric matrices in (sub)dermal and muscle tissue of the rat: a quantitative study. *Biomaterials*, 1994;15:551-559.
- [33] Beumer GJ, van Blitterswijk CA, Ponec M. Biocompatibility of degradable matrix induced as a skin substitute: an in vivo evaluation. *J Biomed Mater Res*, 1994;28:545-552.
- [34] Bakker D, van Blitterswijk CA, Hesselink SC, Grote JJ, Deams WT. Effect of implantation site on phagocyte/polymer interaction and fibrous capsule formation. *Biomaterials*, 1988;9:14-21.
- [35] Mensik I, Lamme EN, Riesle J, Brychta P. Effectiveness and safety of the PEGT/PBT copolymer scaffold as dermal substitute in scar reconstruction wounds (feasibility trial). *Cell Tissue Bank*, 2002;3(4):245-53.
- [36] Bulstra SK, Geesink RG, Bakker D, Bulstra TH, Bouwmeester SJ, van der Linden AJ. Femoral canal occlusion in total hip replacement using a resorbable and flexible cement restrictor. *J Bone Joint Surg Br.*, 1996;78(6):892-898.

- [37] Jones DS. Dynamical mechanical analysis of polymeric systems of pharmaceutical and biomedical significance. *International Journal of Pharmaceutics* 1999;179:167-178.
- [38] Lewis G. Key issues involved with the use of miniature specimens in the characterization of the mechanical behaviour of polymeric biomaterials – a review. *J Biomed Mater Res (Appl Biomater)*, 2002;63B:455-466.
- [39] Meyvis TKL, Stubbe BG, van Steenbergen MJ, Hennink WE, De Smedt SC, Demeester J. A comparison between the use of dynamic mechanical analysis and oscillatory shear rheometry for the characterisation of hydrogels. *Internat J of Pharmac*. 2002;244:163-168.
- [40] Nazhat SN, Kellomäki M, Törmälä P, Tanner KE, Bonfield W. Dynamic mechanical characterization of biodegradable composites of hydroxyapatite and polylactides. *J Biomed Mater Res (Appl Biomater)*, 2001;58B:335-343.
- [41] Menard KP. *Dynamic mechanical analysis. A practical Introduction*. CRC Press LLC, 1999.
- [42] Malda J, Woodfield TBF, van der Vloodt F, Wilson C, Martens DE, Tramper J, van Blitterswijk CA, Riesle J. The effect of PEGT/PBT Scaffold Architecture on the Composition of Tissue Engineered Cartilage. *Biomaterials*, 2004;26(1):63-72.
- [43] Du C, Klasens P, Haan RE, Bezemer J, Cui FZ, de Groot K, Layrolle P. Biomimetic calcium phosphate coatings on Polyactive 1000/70/30. *J Biomed Mater Res* 2002;59(3):535-546.
- [44] Mazzucco D, McKinley G, Scott RD, Spector M. Rheology of joint fluid in total knee arthroplasty patients. *J Orthop Res*, 2002;20:1157-1163.
- [45] Jurvelin JS, Buschmann MD, Hunziker EB. Optical and mechanical determination of Poisson's ratio of adult bovine humeral articular cartilage. *J Biomechanics*, 1997;30(3):235-241.

# Chapter 3

## 3D Fiber Deposited PEOT/PBT Copolymer Scaffolds for Tissue Engineering: Influence of Porosity, Molecular Network Mesh Size and Swelling in Aqueous Media on Dynamic Mechanical Properties

L. Moroni <sup>a\*</sup>, J.R. de Wijn <sup>a</sup>, C.A. van Blitterswijk <sup>a</sup>

<sup>a,\*</sup> Institute for BioMedical Technology (BMTI), University of Twente, P.O. Box 217, 7500 AE Enschede, The Netherlands. E-mail: l.moroni@tnw.utwente.nl

### Abstract

**A**mong novel scaffold fabrication techniques, 3D fiber deposition (3DF) has lately emerged as a means to fabricate well-defined and custom-made scaffolds for tissue regeneration, with 100% interconnected pores. The mechanical behavior of these constructs is dependent not only on different three-dimensional architectural and geometric features, but also on the intrinsic chemical properties of the material used. These affect the mechanics of the solid material and eventually of 3D porous constructs derived from them. For instance, poly(ethylene oxide terephthalate)-poly(butylene terephthalate) (PEOT/PBT) block copolymers are known to have mechanical properties, depending on the PEOT/PBT weight ratio in block form and on the molecular weight of blocks of poly(ethylene glycol) (PEG) blocks. These differences are enhanced even more by their different swelling properties in aqueous media. Therefore, in this paper we have studied the influence of copolymer compositions in terms of their swelling on dynamic mechanical properties of solid material and porous 3DF scaffolds. The molecular weight of the starting PEG blocks used in the copolymer synthesis varied from 300 g/mol to 1000 g/mol. The PEOT/PBT weight ratio in the blocks used varied from 55/45 to 80/20. This corresponded to an increase of the swelling ratio  $Q$  from 1.06 to 2.46, and of the mesh size  $\xi$  from  $\sim 9 \text{ \AA}$  to  $\sim 47 \text{ \AA}$ . With increased swelling, dynamic mechanical analysis (DMA) revealed a decrease in elastic response and an increase of viscoelasticity. Thus, by coupling structural and chemical characteristics, the viscoelastic properties of PEOT/PBT 3DF scaffolds may be fine tuned to achieve mechanical requirements for a variety of engineered tissues. Ultimately, the combination of 3DF and DMA may be useful to validate the hypothesis that mimicking the biomechanical behavior of a specific tissue for its optimal replacement is an important issue for at least some tissue engineering applications.

**Keywords:** rapid prototyping, 3D fiber deposition, dynamic mechanical analysis, swelling ratio, mesh size.

## Introduction

Since many natural tissues demonstrate constrained viscoelastic properties [1-5], it is relevant from a biological point of view to study whether scaffolds can be fabricated so as to modulate this behavior. The mechanical response of scaffolds depends in the first place on the properties of the solid material employed. Furthermore, when scaffolds are fabricated with a three-dimensional porous architecture the effect of porosity is superimposed on the mechanical properties of the solid material. Scaffold behavior will thus depend on the void fraction, fabric architecture and material properties. The intrinsic chemical composition of the material used is therefore relevant. In the particular case of polymeric scaffolds, their composition can be changed in order to fine tune mechanical properties. This can be accomplished by varying the polymer chemistry or adding two or more polymers to form copolymer blocks.

Within this picture, block-copolymers of polyethyleneoxide-terephthalate (PEOT) and polybutylene-terephthalate (PBT) have been investigated. These polyether-ester multiblock copolymers belong to a class of materials known as thermoplastic elastomers which exhibit good physical properties like elasticity, toughness and strength in combination with easy processing, as described in chapter 1. This class of polymers have been extensively studied for *in vitro* and *in vivo* biocompatibility [6-9] and found clinical applications (PolyActive™, IsoTis Orthopaedics S.A.) as cement stoppers and bone fillers in orthopedic surgery [10, 11]. Being polyether-esters degradation occurs in aqueous media, by hydrolysis and oxidation, at a rate that varies from very low for high PBT contents to medium and high for larger contents of PEOT and longer PEO segments [12-14]. Similarly, by varying the PEOT/PBT ratio and the length of the PEO segments, a series of copolymers can be obtained covering a wide range of mechanical properties with different abilities to swell in aqueous media [12, 13]. The swelling capacity is due to the hydrophilic nature of PEO and proportional to the polymeric network mesh size, i.e., the effective length of the soft segments between the physical cross-links [12]. This is an important parameter not only determining mechanical properties but also the diffusion rate of pharmaceutical compounds in controlled release systems. In this respect dynamic mechanical analysis (DMA) is valuable to measure the viscoelastic behavior of scaffolds fabricated out of these hydrogels (as these polymers are sometimes referred to) and allows the tailoring of test conditions in order to simulate the physiological environment of the tissue to be reconstructed [15-19]. Several rapid prototyping techniques offer the possibility of directly fabricating scaffolds with different geometric structures and with different material properties. These scaffolds are built layer by layer through material deposition on a stage via computer aided design (CAD) models and computer-controlled tooling processes (CAM), either as a molten thermoplast (known as fused deposition modeling techniques) [20, 21] or as droplets together with a binding agent (referred to 3D printing techniques) [22, 23]. Among these rapid prototyping devices 3D plotting [24-26] and 3D fiber deposition (3DF) [27, 28] has been recently developed and used for tissue engineering purposes, the latter being a modified system of 3D plotting for the extrusion of

highly viscous polymers. 3DF is, essentially, a fused deposition technique in which an extrudate of molten polymer is deposited from a servomechanically controlled syringe that applies pressure onto a stationary stage. The outcomes of this process are scaffolds with pores which are interconnected per definition, since during fabrication the layers are deposited as interpenetrating networks (material and void, see figure 1). These scaffolds have a defined structure and architecture, and can be built with a customized shape by CAD-CAM techniques. In contrast, conventional techniques require a percolating distribution of a porogen agent in the material to achieve 100% interconnectivity. For instance, salt leaching is based on the statistical occurrence of contacts between salt crystal, which limits pore size and shape depending on the crystal dimension and distribution within the material. The greater flexibility of 3D fiber deposition in creating scaffolds gives the opportunity to use this device to study the influence of different structural phenomena on tissue reconstruction.

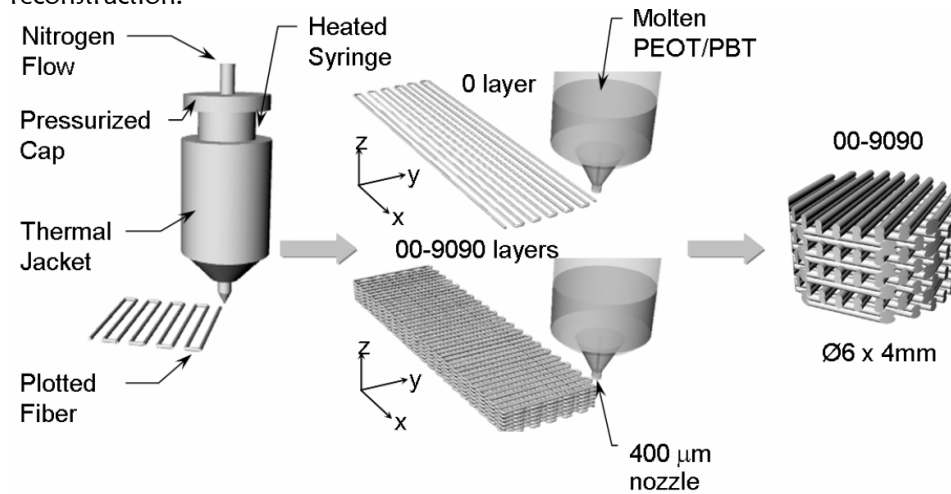


**Figure 1** – The Bioplotter fabrication process. Scheme adapted with permission from Woodfield et al [27].

In this study we focus on the effects of the copolymer swelling ratio on viscoelastic properties such as equilibrium or dynamic modulus and damping factors of solid material and porous 3DF scaffolds. Besides the obvious need for a minimum of strength these viscoelastic properties, especially the stiffness, are considered to be of primary importance for initial performance of scaffolds in tissue engineering applications [29]. With constant porosity, we assume that reduced swelling, and short and soft segments interspersing larger hard blocks will give a stiffer and less plastic structure. In contrast, greater swelling of the polymer with long and soft segments separating smaller hard blocks will result in a more flexible, if not deformable, scaffold. The data obtained can be used to generate a set of multi dimensional matrixes, where viscoelastic parameters are expressed as functions of porosity and material swelling ratio, and then compared to the corresponding parameters of the natural tissues into which they will be grafted or replace. This tool should be helpful to design an optimal scaffold [30-33] for a specific tissue



engineering application, in terms of porosity, swelling ratio and mechanical properties.

## Materials and Methods

### *Scaffolds Fabrication*

aPEOTbPBTc co-polymers were obtained from IsoTis S.A. (Bilthoven, The Netherlands). In this investigation, the molecular weight of starting PEG blocks was (a) 300 g/mol, 600 g/mol and 1000 g/mol, while PEOT/PBT ratio (b and c) was 55/45, 70/30 and 80/20 in weight percentage.

3D scaffolds were fabricated with a Bioplotter device (Envisiontec GmbH, Germany), which is a XYZ plotter construction as previously described by Landers *et al.* [24, 26]. Few modifications were performed before this device was used to extrude highly viscoelastic fibers or filaments. Briefly, polymer granules were loaded in a stainless steel syringe and heated at a temperature T (180°-200°C), through a thermal cartridge unit mounted on the mobile “X”-arm of the apparatus. When the polymer reached the molten phase, a nitrogen pressure P was applied to the syringe through a pressure cap. Nitrogen was used in order to minimize the copolymer oxidation. Table 1 introduces values for T and P used to fabricate 3D scaffolds with different copolymer compositions. Rectangular block models were CAD-designed with Rhinoceros software (Delft Spline, The Netherlands), loaded on the Bioplotter CAM software and deposited layer by layer, through the extrusion of the polymer as a filament onto a stage. The scaffold was then rendered by the filament diameter and spacing, and by the layer thickness, which in turn determined the pore size and overall porosity. The nozzle used to extrude the molten polymer was a stainless steel Luer Lock hypodermic needle with internal diameter (ID) of 400  $\mu\text{m}$ , and shortened to a length of 16.2 mm. This needle diameter has been chosen because experimentally it appeared to be the best compromise in terms of feasible scaffold porosities and fabrication time. The resolution in terms of dimensional accuracy is limited by the filament diameter, which is dependent on the needle diameter. The smallest needle diameter that could be used for the highly viscous polymer melts and a maximum nitrogen pressure of 6 bars had an internal diameter of 150  $\mu\text{m}$ .

Solid compression molded scaffolds were also fabricated as reference for the 3D scaffolds characterization. Briefly, for each composition 4 grams of copolymer were melted at T = 180 °C and left to cool at room temperature under a pressure of 5 bars. Cylindrical samples 6 mm in diameter by 4 mm in height were punched out using a cork drill in the “Z-direction” from solid and 3D scaffolds for mechanical characterization.

### *Bovine Articular Cartilage Harvest*

Bovine articular cartilage plugs of the same dimension as the 3D scaffold specimens were punched out from the knee of a 6-month old calf. The specimens obtained were perpendicularly sectioned. Once the knee was opened, cartilage plateaus were

kept hydrated with phosphate-buffered saline (PBS) (Gibco-BRL), while the cylindrical plugs were cored from the femoral condyle. The samples were then stored in PBS and mechanically tested during the same day.

### ***Scaffolds Characterization***

Scaffold geometry and architecture were characterized by scanning electron microscopy (SEM) analysis. The porosity of 3D plotted scaffolds was calculated following the theoretical approach by Landers *et al.* [24]:

$$P = 1 - \frac{V_{\text{scaffold}}}{V_{\text{cube}}} = 1 - \frac{\pi}{4} \cdot \frac{1}{\frac{d_2}{d_1}} \cdot \frac{1}{\frac{d_3}{d_1}} \quad (1)$$

where P is the scaffold porosity, d1 the filament diameter, d2 the filament spacing and d3 the layer thickness, within each different structure.

Porosity was also experimentally measured by analyzing the mass and the volume of each scaffold, as:

$$P = 1 - \frac{M}{V} \cdot \frac{1}{\rho} \quad (2)$$

where, M and V are the measured mass and volume of the scaffolds, while  $\rho$  is the specific density for all the PEOT/PBT block copolymers tested. Since there were only small differences (< 1%) between theoretical and experimental porosity we referred to the theoretical one, as more conformal to the fabrication parameters of the Bioplotter. Porosities were measured in the dry unswollen state, but differentiation of equations (1) and (2) shows that swelling has no influence on the porosity.

For a physico-chemical characterization of the fabricated scaffolds, the number average molecular weight  $M_n$  of the copolymer used was measured with Gel Permeation Chromatography (GPC), before and after plotting. Samples were dissolved in and eluted with 0.02M sodiumtrifluoroacetate (NaF<sub>3</sub>Ac) in hexafluoroisopropanol (HFIP) through a Polymer Labs (PL) HFIP gel guard column (50 x 7.5 mm) and two PL HFIP gel analytical columns (300 x 7.5 mm). Flow rate was 1ml/min and a refraction index detector was used. The molecular weights ( $M_n$  and  $M_w$ ) were determined relative to polymethylmethacrylate (PMMA) standards. To measure the volume swelling ratio Q, the scaffolds were put in PBS at 37 °C and left for three days to reach a swollen equilibrium state. Q was calculated as [13]:

$$Q = 1 + \frac{\rho \cdot (M_{\text{swollen}} - M_{\text{dry}})}{M_{\text{dry}}} \quad (3)$$

where  $\rho$  was taken for simplicity as 1.2 g/ml for all the compositions,  $M_{\text{swollen}}$  is the scaffold equilibrium wet weight, and  $M_{\text{dry}}$  is the scaffold dry weight. The swollen weight was measured after having blotted the scaffolds with a tissue and after having expelled the water from the pores by applying pressurized air. The polymeric network mesh sizes were also calculated from the swelling ratios and the equilibrium moduli, according to rubber elasticity theories [12, 34, 35]:

$$\sigma = R \cdot T \cdot \varphi_p^{1/3} \cdot v_e \cdot \left( \alpha - \frac{1}{\alpha^2} \right) \quad (4)$$

where  $\alpha$  is the reduced stress,  $R$  is the universal gas constant,  $T$  is the absolute temperature,  $\varphi_p$  is the polymer volume fraction in the equilibrium swollen state considered as  $1/Q$ ,  $v_e$  is the elastically effective network chain concentration and  $\alpha$  is the ratio of deformed to undeformed length of the sample. Equation 4 is based on the affine deformation assumption (network nodes displace similar as sample length under deformation), as formulated by Treloar *et al* [35]. Thus,  $v_e$  is obtained from the measured equilibrium modulus  $H_a$ :

$$\frac{\sigma}{\left( \alpha - 1/\alpha^2 \right)} \cong \frac{H_a}{3} = R \cdot T \cdot \frac{1}{Q}^{1/3} \cdot v_e \quad (5)$$

From  $v_e$  the cross-links molecular weight is derived according to rubber elasticity theories [34] and solute diffusion rate considerations in controlled release systems [12, 36]:

$$v_e = \frac{1}{\bar{v} \cdot M_c} \cdot \left( 1 - 2 \cdot \frac{M_c}{M_n} \right) \quad (6)$$

where  $\bar{v}$  is the specific volume of the dry polymer (0.83 cm<sup>3</sup>/g),  $M_n$  is the number average molecular weight (g/mol), and  $M_c$  is the molecular weight of the chains between cross-links. Then, the mesh size is computed as [12, 36, 37]:

$$\xi = \left( \frac{1}{Q} \right)^{-1/3} \cdot l \cdot (n \cdot C_\infty)^{1/2} \quad (7)$$

where  $l$  is the bond length (approximated to 1.5 Å, which is the average of one carbon-carbon bond and two carbon-oxygen bonds),  $C_\infty$  is the characteristic ratio (3.8 for PEG) [38], and  $n$  is the average number of bonds between cross-links, determined by:

$$n = 3 \cdot \frac{x_{\text{PEG}} \cdot M_c}{M_r} \quad (8)$$

where,  $x_{\text{PEG}}$  is the weight fraction of PEG in the copolymer and  $M_r$  is the molecular weight of the repeating unit of PEG (44 g/mole).

### *Dynamic Mechanical Analysis*

A DMA instrument (Perkin Elmer 7e) was used to measure viscoelastic properties of the 3D fabricated scaffolds. For each configuration three samples were analyzed for all the experiments performed. Cylindrical fixtures were chosen to test the specimens and evaluate their behavior as a whole structure along their compression axis, in the “Z-direction”.

Scaffolds and cartilage plugs were loaded with a dynamic force varying from 3.5N to 4.5N in a dynamic stress experiment. More specifically, a starting force of 3.5N was applied and then continuously increased to 4.5N with a sinusoidal loading ramp of 50mN/min, at a constant frequency of 1Hz. Dynamic stiffness and damping factor were calculated by the instrument software (Pyris).

In a creep and recovery test the scaffolds were tested to analyze their equilibrium properties. Samples were first pre-loaded with a recovery force of 100mN for two minutes. Then, a force of 3.5N was applied instantaneously and kept for three minutes, after which the loading condition was set back to the recovery value. This protocol was cycled three times to assess if there was any difference, after each loading cycle, in terms of equilibrium modulus and unrecovered creep strain values. The same experiment was repeated with a loading force of 4.5N to assess creep and recovery properties of the fabricated scaffolds in the minimum and maximum force range applied during the dynamic stress test.

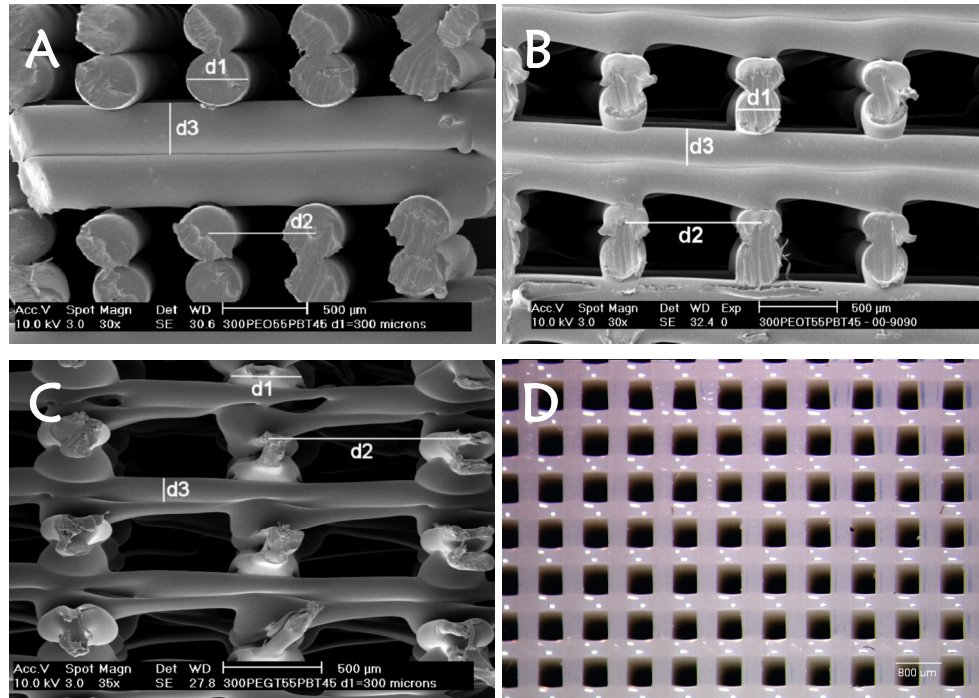
The tests were conducted under wet conditions: a synovium-like fluid was prepared as a 3% (w/v) solution of polyvinylpyrrolidone (PVP) in de-ionized water. This was done to simulate the physiological environment of articular cartilage. Scaffolds were soaked in PVP-solution overnight, before loading. The temperature was 37 °C during all of the experiments.

## **Results**

### *Scaffolds Characterization*

aPEOTbPBTc 3D scaffolds with different pore geometry and swelling ratio were fabricated. An increase in the molecular weight of the starting soft PEG blocks from 300 g/mol to 1000 g/mol, and an increase in the relative percentage of soft blocks versus the hard ones in the final copolymers from 55/45 to 80/20, corresponded to an increase of the overall swelling ratio  $Q$  of the scaffolds [12-14]. Copolymer filaments were deposited with a diameter  $d_1 = 260 \mu\text{m}$ , while filament spacing  $d_2$  was  $600 \mu\text{m}$ ,  $800 \mu\text{m}$  and  $1000 \mu\text{m}$ , and layer thickness  $d_3$  was  $150 \mu\text{m}$ ,  $250 \mu\text{m}$  and  $350 \mu\text{m}$ . Figure 2 illustrates the resulting structures. Variation in the fabrication

parameters resulted in a modulation of 3DF scaffolds porosity from 41% to 85%. Scaffolds with the same geometrical specification built with different copolymer ratios and PEG molecular weights had similar porosity.



Porosity, Mesh  
Size & Swelling

**Figure 2** – SEM and optical microscope micrographs of 300PEOT55PBT45 3D fiber deposited scaffolds. Cross sections and surface (d) of three different pore geometries are shown. Filament diameter  $d1 = 260 \mu\text{m}$ . (a)  $d2 = 600 \mu\text{m}$  and  $d3 = 350 \mu\text{m}$ ; (b)  $d2 = 800 \mu\text{m}$  and  $d3 = 250 \mu\text{m}$ ; (c)  $d2 = 1000 \mu\text{m}$  and  $d3 = 150 \mu\text{m}$ . Scale bar: (a-c)  $500 \mu\text{m}$ ; (d)  $800 \mu\text{m}$ .

SEM analysis revealed consistency between the theoretical and real values of filament diameter, filament spacing and layer thickness among all of the fabricated scaffolds. Filament diameter  $d1$  varied from  $261 \pm 8 \mu\text{m}$  to  $292 \pm 9 \mu\text{m}$  (Table 1), depending on the copolymer composition. Filament spacing measured  $605 \pm 12 \mu\text{m}$ ,  $807 \pm 28 \mu\text{m}$ , and  $1001 \pm 0.00 \mu\text{m}$ . Layer thickness was  $148 \pm 10 \mu\text{m}$ ,  $257 \pm 11 \mu\text{m}$ , and  $344 \pm 11 \mu\text{m}$ , respectively for all the copolymer compositions. The fluctuations in the values were due to the time the copolymers stayed in the syringe. Slight thermal degradation caused the polymer melt viscosity to decrease with time. Scaffolds presented 100% interconnected pores and were reproducible with the same characteristics each time they were processed.

	300/55/45	300/70/30	1000/70/30	300/80/20	600/80/20	1000/80/20
T (Celsius)	190	160	180	140	150	160
P (Bars)	5	4.5	5	4	4.5	4.5
Filament Diameter ( $\mu\text{m}$ )	268 $\pm$ 32	261 $\pm$ 8	292 $\pm$ 12	285 $\pm$ 23	290 $\pm$ 16	292 $\pm$ 9

**Table 1** – Process parameters and geometrical characterization of 3DF scaffolds with different copolymer compositions. Deposition speed was constant at  $V = 300$  mm/min.

Porosity, Mesh  
Size & Swelling

The physico-chemical parameters characterizing the copolymers used are shown in Table 2. GPC analysis revealed that the number average molecular weight did not change much before and after plotting. Therefore,  $M_n$  values of the solid materials were used to calculate the molecular weight between the cross-links  $M_c$ .  $M_n$  varied from 50.67 kg/mol to 46.76 kg/mol with increasing PEOT/PBT block ratios from 55/45 to 80/20, respectively, and from 46.76 kg/mol to 57.79 kg/mol with increasing the length of the starting PEG segments from 300 g/mol to 1000 g/mol. Consequently,  $M_c$  varied from 250 g/mol for 300PEOT55PBT45 to 2550 g/mol for 1000PEOT80PBT20. The equilibrium swelling ratio  $Q$  of solid scaffolds varied from  $1.06 \pm 0.01$  to  $2.31 \pm 0.05$  in the same copolymer range.  $Q$  was found to be slightly higher for 3DF scaffolds, varying from  $1.13 \pm 0.01$  to  $2.46 \pm 0.21$ . This did not considerably affect the calculated mesh size  $\xi$  that ranged from 9 Å to 47 Å depending on 3DF scaffold swelling ratios, or from 9.27 Å to 46 Å when solid swelling ratios were used.

Copolymer Compositions	Q - Solid	Q - 3D Scaffolds	Mn (Kg/mole) - Solid	Mn (Kg/mole) - 3D Scaffolds	Ha (MPa) - Solid	Mc (g/mole)	$\xi$ (Å)
300PEOT55PBT45	1.06 $\pm$ 0.01	1.14 $\pm$ 0.01	50.67	44.6	97.16	250	9
300PEOT70PBT30	1.09 $\pm$ 0.03	1.54 $\pm$ 0.09	48.45	46.18	42.7	450	16
1000PEOT70PBT30	1.715 $\pm$ 0.005	1.76 $\pm$ 0.02	57.43	57.56	29.6	710	20
300PEOT80PBT20	1.13 $\pm$ 0.01	1.72 $\pm$ 0.04	46.76	45	20.1	740	22
600PEOT80PBT20	1.695 $\pm$ 0.005	2.3 $\pm$ 0.01	50	53.1	12.6	1660	37
1000PEOT80PBT20	2.31 $\pm$ 0.05	2.46 $\pm$ 0.21	57.79	61.1	10.3	2550	47

**Table 2** – Network characterization of swollen PEOT/PBT copolymers as solid material and 3DF scaffolds in PBS at 37°C.

### *Dynamic Mechanical Properties*

The dynamic mechanical properties of solid material and 3DF scaffolds of different copolymer compositions were determined with DMA. A correlation between the solid equilibrium modulus  $H_a$  and the equilibrium swelling ratio  $Q$  was found, with a correlation coefficient  $r^2 = 0.97$  (Fig. 3):

$$H_a = 145.7 \cdot \left(\frac{1}{Q}\right)^{1/3} - 107.7 \quad (9)$$

In the case of 3DF porous scaffolds, a general trend between the swelling ratio and the viscoelastic parameters was found within the porosity range analyzed (see figures 4 and 5). In particular, with increasing swelling ratio and porosity the dynamic stiffness decreased from  $9.7 \pm 0.5$  MPa to  $0.13 \pm 0.06$  MPa, while the damping factor  $\tan \delta$  increased from  $0.064 \pm 0.0045$  to  $0.197 \pm 0.0042$ . Analogous behavior was found for the equilibrium modulus and the unrecovered creep strain, respectively. The equilibrium modulus decreased from  $6.33 \pm 1.47$  MPa to  $0.15 \pm 0.001$  Mpa, while the unrecovered creep strain increased from  $0.7 \pm 0.43\%$  to  $85.97 \pm 27.15\%$ . The dynamic stiffness and damping factor of bovine articular cartilage were measured as  $9.64 \pm 1.81$  MPa and  $0.175 \pm 0.03$ , while equilibrium modulus and creep unrecovered strain were  $0.64 \pm 0.16$  MPa and  $46.91 \pm 9.86\%$ , respectively.

Effect of Swelling Ratio on Equilibrium Modulus

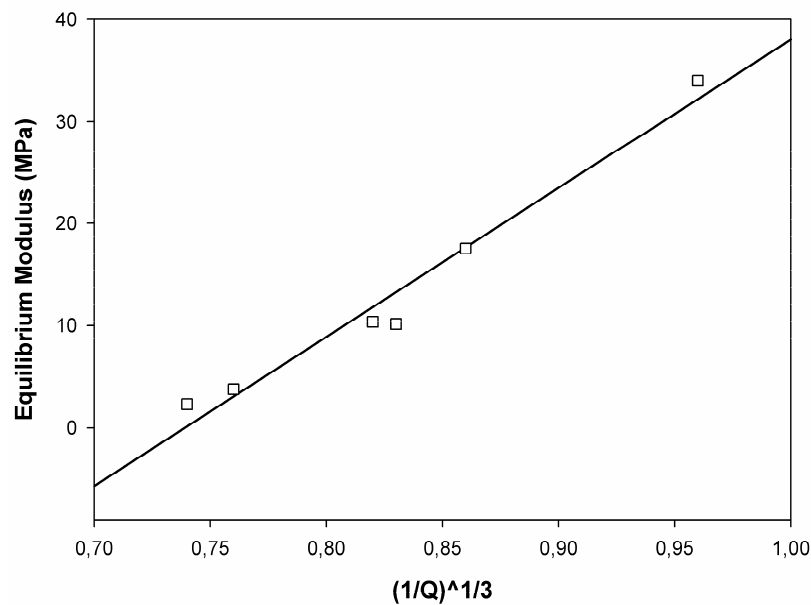


**Figure 3** – Correlation between the solid copolymer equilibrium modulus  $H_a$  and the equilibrium swelling ratio  $Q$ , as theoretically introduced in equation (4).  $R^2 = 0.97$ .

Effect of Swelling Ratio on Dynamic Stiffness of 3D Porous Scaffolds

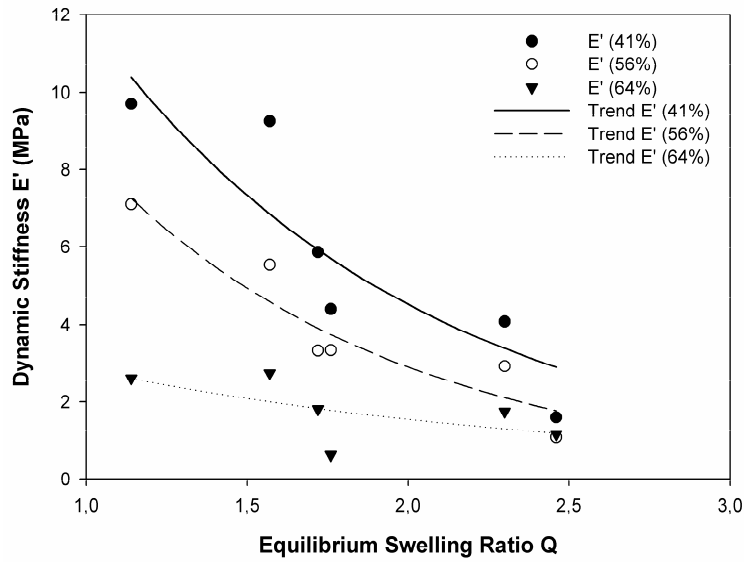


**Figure 4** – General effect of the swelling ratio on the dynamic stiffness of 3DF porous scaffolds. A few different porosities are depicted to exemplify the variation in stiffness with porosity.

Effect of Swelling Ratio on Damping Factor of 3D Porous Scaffolds

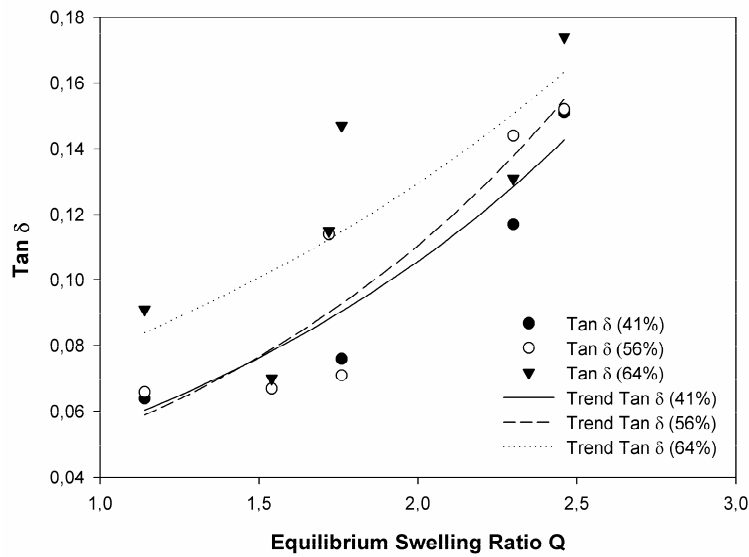


**Figure 5** – General effect of the swelling ratio on the damping factor  $\tan \delta$  of 3DF scaffolds. A few different porosities are presented to illustrate the correlation of damping with porosity.



A linear correlation was found for the equilibrium swelling ratio  $Q$  and the mesh size  $\xi$  of 3DF scaffolds ( $r^2 = 0.96$ , figure 6). Such a relationship is described by:

$$\xi = 28.4 \cdot Q - 26.5 \quad (10)$$

Therefore, the viscoelastic parameters can also be related to the network mesh size and porosity. Scaffold mechanical properties, swelling ratio (or mesh size) and porosity can thus be used to construct a reliable multi-dimensional correlation matrix. This can be used to fine tune scaffolds to mimic a natural tissue. Figure 7 introduces an example of such a matrix. Dynamic stiffness values for bovine articular cartilage, cancellous bone [39], and skin [40] are also depicted to demonstrate how the matrix can be used to compare mechanical properties of synthetic scaffolds with potential for repair or replacement of defective tissue.

Porosity, Mesh  
Size & Swelling

Linear Correlation between Swelling Ratio and Mesh Size for 3D Porous Scaffolds

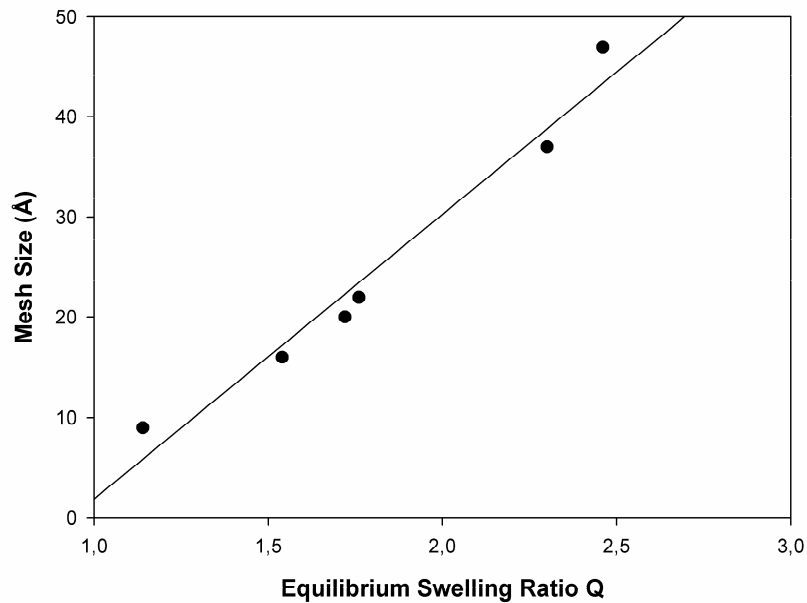


**Figure 6** – Linear Correlation between polymer network mesh size and equilibrium swelling ratio.  $R^2 = 0.96$ .

## Discussion

The intrinsic and structural properties of solid and 3D porous plotted PEOT/PBT copolymer scaffolds have been evaluated and correlated with their mechanical behavior. This family of copolymers has already been of great interest for tissue

engineering and drug delivery applications, because by varying the molecular weight of the starting PEG segments and the weight ratio of PEOT and PBT blocks it is possible to tailor properties, such as wettability [41], swelling [12-14], biodegradation rate [14], protein adsorption [42], and mechanical properties [27]. As expected, an increase in the molecular weight of the starting PEG blocks and an increase of the PEOT weight ratio in the composition led to an enhancement of the materials swelling capacity, reflected by the increase of  $M_c$  and  $\xi$  (table 2). Slightly higher values of  $Q$  were observed for 3DF scaffolds with respect to the solid material. This might be due to a better water uptake capacity of the copolymers in a filament shape, which results in a higher surface to volume ratio than solid materials. For what concerns the mechanical behavior of the different copolymer compositions, a correlation between the solid PEOT/PBT equilibrium modulus  $H_a$  and its volume equilibrium swelling ratio  $Q$  was found, where  $H_a$  is related to  $(1/Q)^{1/3}$  (figure 3). This is in agreement with the theory of rubber elasticity introduced by Treloar et al [35]. Therefore, solid PEOT/PBT copolymers appear to behave as rubbery polymers, with very low plasticity. When porosity is superimposed on the solid material by structuring it into a scaffold, the plastic behavior is enhanced, even though the damping factors remain relatively low (e.g. see figure 5).

From a molecular point of view, by increasing the length of the starting PEG soft segments, the dynamical stiffness and the equilibrium modulus decreased, while the damping factor and the unrecovered creep strain increased. Therefore, an increase of swelling ratio for the 3DF scaffolds appears to result in a less stiff and more plastic mechanical behavior. This softening is consistent with the physico-chemical structure of the materials used. An increase of the length of the PEG soft blocks generates bigger soft PEOT domains, at constant ratio between PEOT and PBT blocks in the copolymer. Similarly, an increase of PEOT weight percentage in the copolymers with constant length of the starting PEG soft segments led to a decrease of the elastic moduli and a corresponding increase of the viscous factors as damping and creep. Again, larger numbers of soft regions with respect to the hard ones in the whole structure of the material entailed an enhanced plastic behavior. With constant copolymer composition, the mechanical parameters were related in an exponential way to porosity.

Furthermore, a linear correlation between the equilibrium swelling ratio  $Q$  and the molecular network mesh size  $\xi$  was found for 3D scaffolds. Remarkably, this confirms the relationship between the polymer water uptake capability and the chain network mesh size as already has been shown by Bezemer et al. [12] for solid PEOT/PBT films and by Canal *et al.* [37] for polyvinylalcohol hydrogel systems with  $Q < 10$ , suggesting that from a strictly physico-chemical point of view solid material and 3D porous scaffolds can be treated with a similar approach. The experimental relationship is also in agreement with the theory of rubber elasticity, as given by equations (4) to (8), from which a more general positive correlation is calculated between  $\xi$  and  $Q$  of hydrogel systems, where  $\xi$  depends on  $Q^n$  with  $n \leq 1$ . The mesh size identifies the mean distance between successive cross-links and, therefore, determines the maximum size of solutes that can diffuse through the network [12].

Similarly, a larger network mesh size is expected to result in a material with a more flexible and plastic behavior.

By coupling geometric and architectural features with chemical properties of the copolymers used, it was possible to create multi-dimensional correlation matrices that can be used to optimize 3D fiber deposited scaffolds in terms of mechanical properties for a specific tissue engineering application (Fig. 7). Since a dynamic loading condition is the most realistic setting to characterize the mechanical behavior of materials and tissues in use, dynamic stiffness has been chosen to exemplify these matrices. Dynamic stiffness appears to be modulated by scaffold porosity and swelling ratio. Values for articular cartilage, cancellous bone [39], and skin [40] are also included in figure 7 as an example of matching mechanical properties. From a strictly practical clinical point of view, the prevailing stresses are too high to consider this copolymer family for in vivo bone tissue engineering. These scaffolds would fail under a severe physiological loading. In the case of trabecular bone, its stiffness (between 90 MPa and 400 MPa [43]) could be sustained by a stiff PEOT/PBT composition such as solid 300PEOT55PBT45. Yet, it is not only the intrinsic stiffness of the scaffold but also its organization and architecture that affects its integrity with the surrounding environment. A PEOT/PBT scaffold with a porous irregular structure typical of trabecular bone would fail under physiological load, since the superimposition of porosity on the structure would dramatically reduce its final in vivo stiffness and strength.

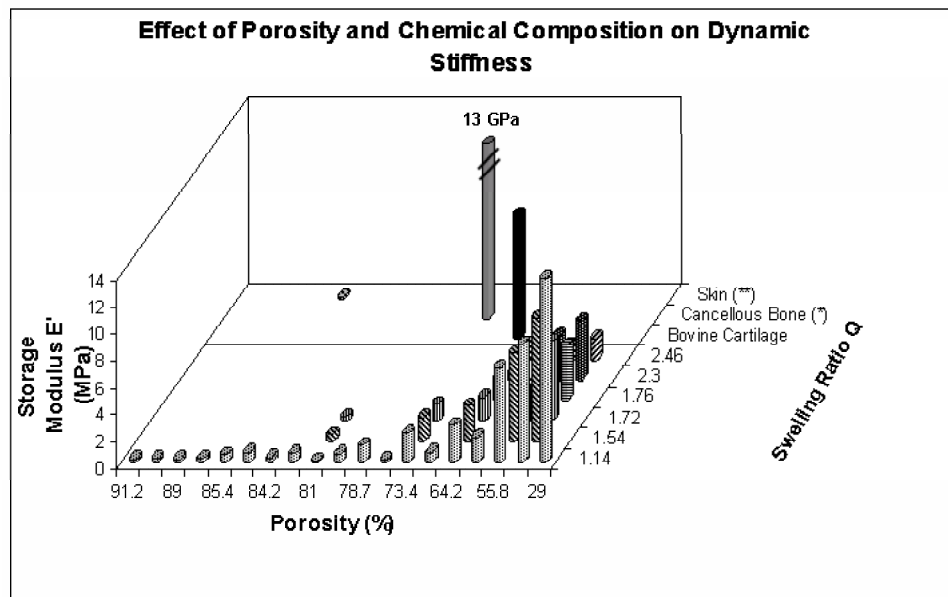


**Figure 7** – Multi-dimensional mechanical matrix: effect of porosity and swelling ratio of PEOT/PBT 3DF scaffolds on dynamic stiffness. Similar matrix can be generated for equilibrium modulus, damping factor, and unrecovered creep strain. Cancellous Bone and skin storage modulus values are from Einhorn *et al.* [39] and Dirillidou *et al.* [40], respectively.

However, the importance of such a mimicking process remains to be validated in terms of tissue regeneration. Further studies will be performed in the future to validate the assumed relevance of scaffolds dynamic mechanical properties on newly engineered tissue.

## Conclusions

### Porosity, Mesh Size & Swelling

3DF polymeric scaffolds have been characterized through DMA, in terms of their viscoelasticity. Overall structure porosity is the main factor that modulates the viscoelasticity of 3D constructs, but the chemical composition of the PEOT/PBT copolymers used in our study appeared to be another important determinant of their mechanical properties. As swelling increases there is a decrease in the elastic moduli and an increase in the other viscoelastic parameters. If mimicking the biomechanical behavior of the tissue to be grown is a key point in tissue engineering, coupling 3DF techniques and DMA allows us to create a powerful system to select the most favorable scaffold for a specific application. We have generated a wide range of 3DF scaffolds in terms of architectural and geometric features, the viscoelastic properties of which are correlated with the overall porosity and the chemical composition of the copolymer used. Nevertheless, the role of scaffolds mechanical properties for the performance in tissue engineering applications remains an open question. It will be interesting to determine whether the optimal internal structure and polymeric composition of a fabricated scaffold in terms of cell attachment and viability, will also be most closely approaching the natural tissue's mechanical properties.

## References:

- [1] van Mow C, Ratcliffe A, Poole AR. Cartilage and diarthrodial joints as paradigms for hierarchical materials and structures. *Biomaterials* 1992;13:67-97.
- [2] Laasanen MS, Töyräs J, Korhonen RK, Rieppo J, Saarakkala S, Nieminen MT, Hirvonen J, Jurvelin JS. Biomechanical properties of knee articular cartilage. *Biorheology* 2003;40:133-140.
- [3] Doerhing TC, Carew EO, Vesely I. The effect of strain rate on the viscoelastic response of aortic valve tissue: a direct-fit approach. *Ann Biomed Eng* 2004;32(2):223-232.
- [4] Elhadj S, Chan R, Forsten-Williams K. Implementation of an optical method for the real-time determination of uniaxial strain and vessel mechanics. *IEEE Trans Biomed Eng* 2004;51(3):536-538.
- [5] Yeni YN, Christopherson GT, Turner AS, Les CM, Fyhrie DP. Apparent viscoelastic anisotropy as measured from nondestructive oscillatory tests can reflect the presence of a flaw in cortical bone. *J Biomed Mater Res* 2004;69:124-130.
- [6] van Blitterswijk CA, van de Brink J, Leenders H, Bakker D. The effect of PEO ratio on degradation, calcification and bone bonding of PEO/PBT copolymer (PolyActive). *Cells Mater* 1993;3(23):23-36.

- [7] Beumer GJ, van Blitterswijk CA, Ponec M. Degradation behavior of polymeric matrices in (sub)dermal and muscle tissue of the rat: a quantitative study. *Biomaterials* 1994;15:551-559.
- [8] Beumer GJ, van Blitterswijk CA, Ponec M. Biocompatibility of degradable matrix induced as a skin substitute: an in vivo evaluation. *J Biomed Mater Res* 1994;28:545-552.
- [9] Bakker D, van Blitterswijk CA, Hesselting SC, Grote JJ, Deams WT. Effect of implantation site on phagocyte/polymer interaction and fibrous capsule formation. *Biomaterials* 1988;9:14-21.
- [10] Mensik I, Lamme EN, Riesle J, Brychta P. Effectiveness and safety of the PEGT/PBT copolymer scaffold as dermal substitute in scar reconstruction wounds (feasibility trial). *Cell Tissue Bank* 2002;3(4):245-53.
- [11] Bulstra SK, Geesink RG, Bakker D, Bulstra TH, Bouwmeester SJ, van der Linden AJ. Femoral canal occlusion in total hip replacement using a resorbable and flexible cement restrictor. *J Bone Joint Surg Br* 1996;78(6):892-898.
- [12] Bezemer JM, Grijpma DW, Dijkstra PJ, van Blitterswijk CA, Feijen J. A controlled release system for proteins based on poly(ether ester) block-copolymers: polymer network characterization. *J Control Release* 1999;62(3):393-405.
- [13] van Dijkhuizen-Radersma R, Peters FL, Stienstra NA, Grijpma DW, Feijen J, de Groot K, Bezemer JM. Control of vitamin B12 release from poly(ethylene glycol)/poly(butylene terephthalate) multiblock copolymers. *Biomaterials* 2002;23(6):1527-36.
- [14] Deschamps AA, Claase MB, Sleijsler WJ, de Bruijn JD, Grijpma DW, Feijen J. Design of segmented poly(ether ester) materials and structures for the tissue engineering of bone. *J Control Release* 2002;78(1-3):175-86.
- [15] Jones DS. Dynamical mechanical analysis of polymeric systems of pharmaceutical and biomedical significance. *International J of Pharmaceutics* 1999;179:167-178.
- [16] Lewis G. Key issues involved with the use of miniature specimens in the characterization of the mechanical behaviour of polymeric biomaterials – a review. *J Biomed Mater Res* 2002;63B:455-466.
- [17] Meyvis TKL, Stubbe BG, van Steenbergen MJ, Hennink WE, De Smedt SC, Demeester J. A comparison between the use of dynamic mechanical analysis and oscillatory shear rheometry for the characterisation of hydrogels. *International Journal of Pharmaceutics* 2002;244:163-168.
- [18] Nazhat SN, Kellomäki M, Törmälä P, Tanner KE, Bonfield W. Dynamic mechanical characterization of biodegradable composites of hydroxyapatite and polylactides. *J Biomed Mater Res* 2001;58B:335-343.
- [19] Menard KP. *Dynamic mechanical analysis. A practical Introduction*. CRC Press LLC; 1999.
- [20] Hutmacher DW, Schantz T, Zein I, Ng KW, Teoh SH, Tan KC. Mechanical properties and cell cultural response of polycaprolactone scaffolds designed and fabricated via fused deposition modelling. *J Biomed Mater Res* 2001;55:203-216.
- [21] Sachlos E, Czernuszka JT. Making tissue engineering scaffolds work. Review on the application of solid freeform fabrication technology to the production of tissue engineering scaffolds. *European Cells and Materials* 2003;5:29-40.

- [22] Giordano RA, Wu BM, Borland SW, Cima LG, Sachs EM, Cima MJ. Mechanical properties of dense polylactic acid structures fabricated by three dimensional printing. *J Biomater Sci Polymer Edn* 1996;8(1):63-75.
- [23] Yang S, Leong KF, Du Z, Chua CK. The design of scaffolds for use in tissue engineering. Part II. Rapid prototyping techniques. *Tissue Engineering* 2002;8(1):1-11.
- [24] Landers R, Müllhaupt R. Desktop manufacturing of complex objects, prototypes and biomedical scaffolds by means of computer-assisted design combined with computer-guided 3D plotting of polymers and reactive oligomers. *Macromol Mater Eng* 2002;282:17-21.
- [25] Landers R, Hübner U, Schmelzeisen R, Müllhaupt R. Rapid prototyping of scaffolds derived from thermoreversible hydrogels and tailored for application in tissue engineering. *Biomaterials* 2002;23:4437-4447.
- [26] Landers R, Pfister A, Hübner U, John H, Schmelzeisen R, Müllhaupt R. Fabrication of soft tissue engineering scaffolds by means of rapid prototyping techniques. *J Mater Sci* 2002;37:3107-3116.
- [27] Woodfield TBF, Malda J, de Wijn J, Péters F, Riesle J, van Blitterswijk CA. Design of porous scaffolds for cartilage tissue engineering using a three-dimensional fibre-deposition technique. *Biomaterials* 2004;25:4149-4161.
- [28] Malda J, Woodfield TBF, van der Vloodt F, Wilson C, Martens DE, Tramper J, van Blitterswijk CA, Riesle J. The effect of PEGT/PBT Scaffold Architecture on the Composition of Tissue Engineered Cartilage. *Biomaterials* 2004;26:63-72.
- [29] Lin CY, Kikuchi N, Hollister SJ. A novel method for biomaterial scaffold internal architecture design to match bone elastic properties with desired porosity. *J Biomech* 2004;37:623-636.
- [30] Sherwood JK, Riley SL, Palazzolo R, Brown SC, Monkhouse DC, Griffith LG, Landeen LK, Ratcliffe A. A three-dimensional osteochondral composite scaffold for articular cartilage repair. *Biomaterials* 2002;23:4739-4751.
- [31] Taboas JM, Maddox RD, Krebsbach PH, Hollister SJ. Indirect solid free form fabrication of local and global porous, biomimetic and composite 3D polymer-ceramic scaffolds. *Biomaterials* 2003;24:181-194.
- [32] Hollister SJ, Maddox RD, Taboas JM. Optimal design and fabrication of scaffolds to mimic tissue properties and satisfy biological constraints. *Biomaterials* 2002;23:4095-4103.
- [33] Lin ASP, Barrows TH, Cartmell SH, Guldberg RE. Microarchitectural and mechanical characterization of oriented porous polymer scaffolds. *Biomaterials* 2003;24:481-489.
- [34] Flory PJ. *Principles of Polymer Chemistry*. Ithaca: Cornell University Press; 1953. Chapters 11 and 13.
- [35] Treloar LRG. *The physics of rubber elasticity*. Oxford: Clarendon Press, 2<sup>nd</sup> edition; 1958. Chapter 4.
- [36] Peppas NA and Barr-Howel BD. Characterization of the cross-linked structure of hydrogels, in: Peppas NA, editor. *Hydrogels in Medicine and Pharmacy*, Vol. I. Boca Raton: CRC Press; 1986. p 27-56.
- [37] Canal T and Peppas NA. Correlation between mesh size and equilibrium degree of swelling of polymeric networks. *J Biomed Mater Res* 1989;23:1183-1193.
- [38] Brandrup J and Immergut EH. *Polymer Handbook*. New York: John Wiley and Sons; 1975.

- [39] Einhorn TA. Biomechanics of Bone. Principles of Bone Biology. Academic Press;1996. p 25-37.
- [40] Diridollou S, Patat F, Gens F, Vaillant L, Black D, Lagarde JM, Gall Y, Berson M. In vivo model of the mechanical properties of the human skin under suction. *Skin Res Technol* 2000;6(4):214-221.
- [41] Olde Riekerink M, Claase M, Engbers G, Grijpma D, Feijen J. Gas Plasma etching of PEO/PBT segmented block copolymer films. *J Biomed Mater Res* 2003;65:417-428.
- [42] Mahmood TA, de Jong R, Riesle J, Langer R, van Blitterswijk CA. Adhesion-mediated signal transduction in human articular chondrocytes: the influence of biomaterial chemistry and tenascin-C. *Exp Cell Res* 2004;301(2):179-188.
- [43] Athanasious KA, Zhu CF, Lanctot BS, Agrawal CM, Wang X. Fundamentals of Biomechanics in Tissue Engineering of Bone. *Tissue Engineering* 2000;6(4):361-381.

# Chapter 4

## Dynamic Mechanical Properties of 3D Fiber Deposited PEOT/PBT Scaffolds: An Experimental and Numerical Analysis

Experimental &  
Numerical

L. Moroni <sup>a\*</sup>, G. Poort<sup>b</sup>, F. Van Keulen<sup>b</sup>, J.R. de Wijn <sup>a</sup>, C.A. van Blitterswijk <sup>a</sup>

<sup>a,\*</sup> Institute for BioMedical Technology (BMTI), University of Twente, P.O. Box 217, 7500 AE Enschede, The Netherlands. E-mail: l.moroni@tnw.utwente.nl

<sup>b</sup> Structural Optimisation and Computational Mechanics Group, Department of Mechanical Engineering and Marine Technology, Delft University of Technology, Delft, The Netherlands

### Abstract

**M**echanical properties of three-dimensional (3D) scaffolds can be appropriately modulated through novel fabrication techniques like 3D fiber deposition (3DF), by varying scaffold's pores size and shape. Dynamic stiffness, in particular, can be considered as an important property to optimize the scaffold structure for its ultimate in vivo application to regenerate a natural tissue. Experimental data from dynamic mechanical analysis (DMA) reveal a dependence of the dynamic stiffness of the scaffold on the intrinsic mechanical and physico-chemical properties of the material used, and on the overall porosity and architecture of the construct. The aim of this study was to assess the relationship between the above-mentioned parameters, through a mathematical model, which was derived from the experimental mechanical data. As an example of how mechanical properties can be tailored to match the natural tissue to be replaced, articular bovine cartilage and pig knee meniscus cartilage dynamic stiffness were measured and related with the modeled 3DF scaffolds dynamic stiffness. The dynamic stiffness of 3DF scaffolds from Poly(Ethylene Oxide Terephthalate)-Poly(Butylene Terephthalate) (PEOT/PBT) copolymers was measured with DMA. With increasing porosity, the dynamic stiffness was found to decrease in an exponential manner. The influence of the scaffold architecture (or pore shape) and of the molecular network properties of the copolymers was expressed as a scaffold characteristic coefficient  $\alpha$ , which modulates the porosity effect. This model was validated through an FEA numerical simulation performed on the structures that were experimentally tested. The relative deviation between the experimental and the finite element model was less than 15% for all of the constructs with a dynamic stiffness higher than 1 MPa. Therefore, we conclude that the mathematical model introduced can be used to predict the dynamic stiffness of a porous PEOT/PBT



scaffold, and to choose the biomechanically optimal structure for tissue engineering applications.

**Keywords:** 3D scaffolds, Poly(Ethylene Oxide Terephthalate)-Poly(Butylene Terephthalate), porosity, architecture, swelling, tissue engineering.

## Introduction

Rapid prototyping techniques have been extensively used to fabricate three-dimensional (3D) scaffolds for tissue engineering purposes [1-5]. The versatility of these techniques [6-9] and the precision in the structures obtained make them very appealing systems to customize scaffolds towards specific applications [10-14]. 3D plotting [15-17] and 3D fiber deposition (3DF), in particular, in which a scaffold is fabricated in a computer controlled pattern on a stage as layers of fibers, have been demonstrated to be very effective in terms of pore interconnectivity, shape and size, at the same time keeping a good reproducibility of the structures generated [18-21]. The ability to modulate the geometric and architectural features of constructs allows us to consider using this technique as a powerful tool to thoroughly study the effect of porosity and architecture on the mechanical properties of these scaffolds.

Copolymers of poly(ethylene oxide terephthalate)-poly(butylene terephthalate) (PEOT/PBT) comprise a family of resorptive polymers with specific hydrogel characteristics. These polyether-ester multiblock copolymers belong to a class of materials known as thermoplastic elastomers which display good physical properties to function during tissue regeneration like elasticity, strength and toughness, in combination with easy processing. These properties derive mainly from the phase-separated morphology of these copolymers, in which soft, hydrophilic PEO segments at handling temperatures are physically cross-linked by the presence of hard, semi crystalline PBT segments. In contrast to chemically cross-linked materials, these cross-links are reversible and will be disrupted at temperatures above their glass transition- or melting-point which gives the material its good handling properties. By controlling the PEOT/PBT ratio, the characteristic dimension (mesh size, figure 2) of the molecular network can be varied to obtain polymers with a broad range of biodegradation rate, hydrophilicity, swelling, and, consequently, mechanical properties. This class of polymers has been extensively investigated for *in vitro* and *in vivo* biocompatibility [22-25] and used in the clinic as cement restrictors and bone fillers in orthopaedic surgery (PolyActive™, IsoTis OrthoBiologics S.A.) [26, 27]. Being polyether-esters degradation occurs in aqueous media, by hydrolysis and oxidation, at a rate that varies from very low for high PBT contents to medium and high for larger contents of PEOT and longer PEO segments [28-30]. *In vivo* the degraded fragments of the copolymer are phagocytosed by macrophages, which play a major role in their removal.

We have previously shown how the viscoelastic properties of PEOT/PBT 3DF scaffolds depend on overall porosity, fiber deposition and mesh size of the molecular network through dynamic mechanical analysis (DMA) [20, 21]. With increasing porosity and with increasing mesh size, the decrease of the compressive modulus, further referred to as dynamic stiffness, and of the equilibrium modulus

experienced by DMA follows an exponential trend. Conversely, the damping factor and the unrecovered creep strain appear to increase in an exponential manner. In this paper we focus on the assessment of this mathematical model, derived from the experimental data, through a numerical investigation of the scaffold's mechanical properties by finite element analysis (FEA). The analysis has been restricted to dynamic stiffness, since it can be considered the most important mechanical parameter in characterizing a scaffold for its final *in vivo* application. Since mimicking the mechanical behavior of the natural tissue to be replaced is a general requirement in designing a scaffold, an example of how the dynamic stiffness of the modeled 3DF scaffolds can be tailored to match articular bovine cartilage and porcine knee meniscus cartilage throughout their resorption is studied. Articular bovine cartilage was chosen because of the similar mechanical properties as compared with human articular cartilage, while porcine knee meniscus cartilage was chosen because of the similar dimension with respect to human knee meniscus. The scaffold stiffness as resulting from the numerical analysis approach is dependent on FEA parameters such as the total area of the scaffold taken into consideration for the computation, the number of elements generated during meshing, and the number of serial slices stacked together to generate the simulation model of the scaffolds. The results of the numerical analysis were compared with the experimental data to assess their consistency and to test the mathematical model.

## Materials and Methods

### *Scaffold Fabrication*

aPEOTbPBTc copolymers were obtained from IsoTis S.A. (Bilthoven, The Netherlands). The molecular weight of starting PEG blocks (a) was set to 300 g/mol, 600 g/mol and 1000 g/mol, while PEOT/PBT ratio (b and c) was set to 55/45, 70/30 and 80/20.

3DF scaffolds were produced with a Bioplotter device (Envisiontec GmbH, Germany), which is essentially an XYZ plotting device that was previously described by Landers *et al.* [15-17] and by our group [18-21]. A few modifications were done to enable the extrusion of highly viscous PEOT/PBT fibers (see figure 1). Briefly, the polymer was put in a stainless steel syringe and heated at  $T = 190\text{ }^{\circ}\text{C}$  through a thermostated cartridge unit, fixed on the "X"-mobile arm of the apparatus. When the polymer reached a molten phase, a nitrogen pressure of 5 Bars was applied to the syringe through a pressurized cap. Rectangular block models were loaded on the Bioplotter CAM software and deposited, layer by layer, through the extrusion of the polymer on a stage as a fiber. Scaffolds were then rendered by varying the fiber diameter (through the nozzle diameter or the deposition speed), the spacing between fibers in the same layer, the layer thickness and the configuration of the deposited fibers within the whole architecture. The nozzles used to extrude the polymer filaments were stainless steel Luer Lock needles with internal diameter (ID) of  $400\text{ }\mu\text{m}$  and  $200\text{ }\mu\text{m}$ , shortened to a length of 16 mm. This resulted in extruded fibers with a diameter  $d_1$  of  $260\text{ }\mu\text{m}$  and  $170\text{ }\mu\text{m}$ , respectively. The fiber spacing  $d_2$

was set to 600  $\mu\text{m}$ , 800  $\mu\text{m}$  and 1000  $\mu\text{m}$ , and the layer thickness  $d_3$  was originally set to 150  $\mu\text{m}$ , 250  $\mu\text{m}$  and 350  $\mu\text{m}$ . Since the adhesion of fibers between two subsequent layers was compromised at layer thicknesses larger than 60% of the fiber diameter value,  $d_3 = 275 \mu\text{m}$  was chosen as the largest value for the set of scaffolds with  $d_1 = 170 \mu\text{m}$ . The architecture was changed by depositing fibers with 45° or 90° orientation steps between two successive layers (called 0-45 and 0-90 configurations respectively) and by modifying the fiber orientation after one or after two deposited layers (referred to as single and double layer configurations respectively), as depicted in figure 1. The deposition speed was also varied between 100 mm/min and 300 mm/min, resulting in a decrease of both the fiber diameter and the overall porosity of the scaffolds.

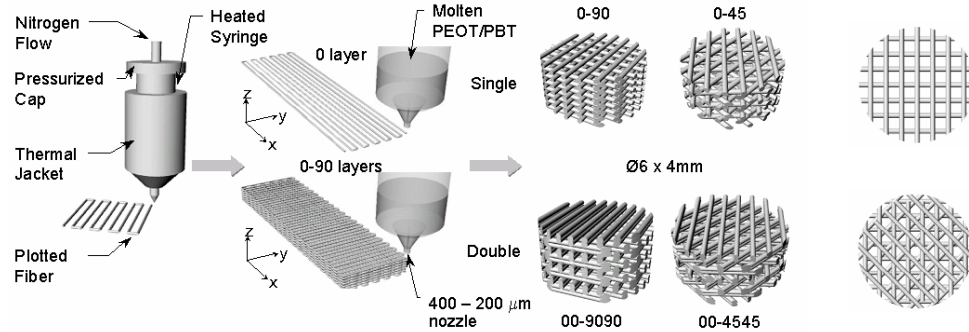


**Figure 1** – Drawing of a Bioplotter device and 3DF fabrication process. 0-90 and 0-45 scaffold architectures in single and double layer versions are illustrated. Inserts shows the quadrangular (top) and polygonal (bottom) pore shapes.

Solid non-porous scaffolds were also fabricated by injection molding, as a reference for the 3D scaffold characterization. Briefly, for each composition 4 grams of polymer were molten at  $T = 180 \text{ }^\circ\text{C}$  in a stainless steel mold and left to cool down at room temperature under a pressure of 5 bars. Solid sheets with the same dimensions as the 3D scaffolds were then obtained.

### ***Scaffold Characterization***

Cylindrical samples of 6 mm in diameter by 4 mm in height were punched out using a cork drill in the “X, Y, and Z-directions” from the rectangular 3DF blocks for mechanical analysis. Scaffold geometry and architecture were characterized by scanning electron microscopy (SEM) with a Philips XL 30 ESEM-FEG. The fiber diameter ( $d_1$ ) and spacing ( $d_2$ ), and the layer thickness ( $d_3$ ) were measured for three different samples and for all the fibers deposited for each scaffold configuration. The porosity of the scaffolds was calculated as [15, 20]:

$$P = 1 - \frac{V_{\text{scaffold}}}{V_{\text{cube}}} = 1 - \frac{\pi}{4} \cdot \frac{1}{\frac{d_2}{d_1}} \cdot \frac{1}{\frac{d_3}{d_1}} \quad (1)$$

where P is the scaffold porosity, d1 the fiber diameter, d2 the fiber spacing and d3 the layer thickness, within each different structure. The fabricated constructs were also physico-chemically characterized in terms of their copolymeric network mesh size  $\xi$  (figure 2), which was calculated as explained in previous reports [21, 28].

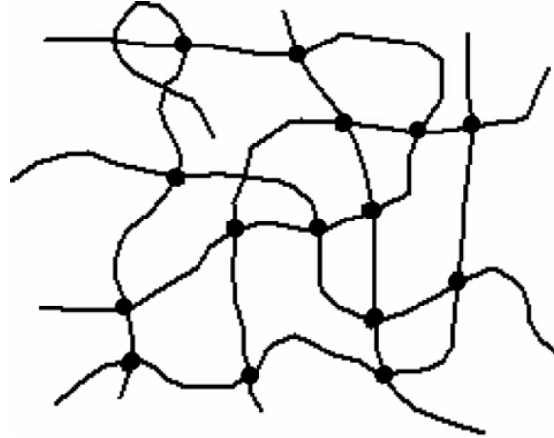


**Figure 2** – Scheme of the molecular network mesh size, defined as the mean statistical distance between two cross-links (●), which in PEOT/PBT copolymers are the hard, semi-crystalline PBT units. Adapted with permission from Bezemer et al [26].

Microcomputed tomography was performed on PEOT/PBT scaffolds to describe their structure and to generate a stack of images for the numerical analysis. A desktop MicroCT ( $\mu$ CT-40, Scanco Medical, Switzerland) with a resolution of 20  $\mu$ m in all the three spatial dimensions (x-ray voltage 45 kVp) was used. The number of slices was approximately 200 for all the samples evaluated and dependent on their actual height. Each slice was 1024x1024 pixels, covering a length of 4 mm. For the evaluation, volumes of interest slightly smaller than the diameter of the cylinders were chosen to exclude crushed boundaries.

### ***Porcine Knee Meniscus and Bovine Articular Cartilage Harvest***

Porcine knee meniscus and bovine articular cartilage plugs of the same dimension as the 3D scaffolds specimens were punched out of the meniscus of a 6-month old male pig and of the knee of a 6-month old male calf in a direction perpendicular to the articulation, respectively. The specimens obtained were perpendicularly sectioned. Once the knee was opened, the menisci and the cartilage plateaus were kept hydrated with phosphate-buffered saline (PBS) (Gibco-BRL), while the cylindrical plugs were cored from the lateral and medial menisci for the pig, and

from the femoral condyle for the calf. The samples were then stored in PBS and mechanically tested during the same day.

### *Dynamic Mechanical Analysis*

A DMA instrument (Perkin Elmer 7e, The Netherlands) was used to assess the viscoelastic properties along the X, Y, and Z-axis of the 3D scaffolds fabricated as depicted in figure 3. As described elsewhere [20], 3D scaffolds were loaded with a compressive force varying from 3.5N to 4.5N in a dynamic stress experiment. A starting force of 3.5N was applied and then continuously increased to 4.5N with a sinusoidal loading ramp of 50mN/min, at a constant frequency of 1Hz. Dynamic stiffness and damping factor were measured.

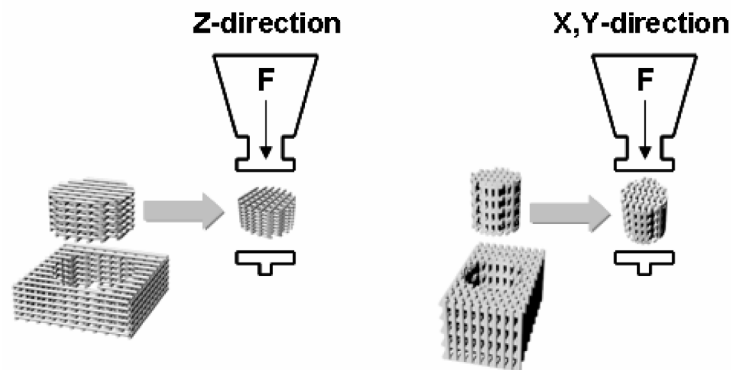


**Figure 3** – Scheme of the mechanical testing unit and the scaffold position during X, Y, and Z-direction testing.

The scaffolds were also analyzed on equilibrium properties in a creep and recovery experiment. Samples were pre-loaded with a force of 100mN for two minutes. Then, a force of 3.5N was applied instantaneously and maintained for three minutes, after which the loading condition was set back to the recovery value. This protocol was cycled for three times to detect possible differences after each loading cycle in terms of equilibrium modulus and unrecovered creep strain values. The same experiment was repeated with a loading force of 4.5N to assess creep and recovery properties of the fabricated scaffolds in the minimum and maximum force range applied in the dynamic stress test.

The samples were analyzed in wet conditions: a synovium-like fluid was prepared after a 3% (w/v) solution of N-polyvinylpyrrolidone (PVP) in de-ionized water. This was done to achieve a closer physiological environment with respect to articular and meniscal cartilage, whose mechanical properties can be appropriately mimicked by PEOT/PBT 3D scaffolds [21]. Scaffolds were soaked in PVP-solution over night, before loading. The temperature was set to 37 °C for all the experiments. For each configuration three different samples were analyzed for each experiment performed and for each testing direction (X, Y, and Z).

Porcine knee menisci and bovine articular cartilage samples were tested following the same protocol explained above, but only along the longitudinal direction of the cylindrical samples. Three samples were tested for both the animals and for each experimental condition.

### ***Mathematical Model***

An exponential function was considered to correlate the scaffold's porosity, architecture and molecular network mesh size with the dynamic stiffness, chosen as the most important mechanical parameter for tissue engineering applications. In particular, we assumed that the porosity has a predominant influence on the mechanical behavior of 3D scaffolds. The contribution of internal architecture and intrinsic physicochemical properties of the polymers, like the molecular network mesh size  $\xi$ , to the mechanical variation has been modeled as a scaffold characteristic coefficient  $\alpha$ , which modulates the porosity influence. Therefore, the relationship between the dynamic stiffness and the porosity of the scaffolds can be described as:

$$E' = E_0 \cdot e^{-\alpha P} \quad (2)$$

where,  $E'$  and  $E_0$  are the dynamic stiffness of the 3DF scaffolds and the solid material respectively,  $P$  is scaffold porosity, and  $\alpha$  is the scaffold characteristic coefficient. Single-factor of variance (ANOVA) was employed to assess the statistical significance of the exponential function fit to the experimental data ( $p < 0.05$ ). A Durbin-Watson statistical analysis was also found to check if the residual did not significantly autocorrelate (null hypothesis accepted for  $1.59 < d < 2.5$ ).

### ***Numerical Analysis***

Finite element (FE) simulations were performed to obtain the apparent stiffness of the scaffolds. As described by van Rietbergen *et al.* [31], the stiffness tensor describing the linear relation between stress and strain is obtained by simulating three compression and three shear tests. The microCT scans of the PEOT/PBT scaffolds were segmented by applying a threshold level to distinguish between voids and material. Representative volume elements (RVE) were selected from the segmented images and were then converted into voxel-based FE models and analyzed. The FEA elements used were 8 node hexahedral elements with cubic shape and linear elastic analyses were performed.

The resulting stiffness tensor depends on the size of the RVE that is modeled because of the boundary conditions, the compression and shear tests. As the RVE becomes larger, the effect of the boundaries diminishes and the resulting apparent stiffness converges. Preferably the RVE is as small as possible to limit computational requirements, while retaining the accuracy of the results. Hence, several RVE sizes were analyzed to obtain the appropriate RVE size. Specifically, RVE size was varied from 62x62 pixels (a fiber-pore unit of the scaffold structure) to 312x312 pixels

(whole scaffold structure). The stiffness tensors were rotated to the orthotropic coordinate system and the apparent stiffness of the scaffolds was determined.

## Results and Discussion

### *Scaffolds Characterization*

PEOT/PBT scaffolds with different pore architecture and geometry were fabricated. Pore architecture was dependent on fiber orientation and deposition. A fiber deposition angle of  $90^\circ$  created quadrangular pores, while a  $45^\circ$  angle generated polygonal pores. Furthermore, the deposition of two successive layers with the same filament orientation resulted in doubling the pore height. The pore geometry was defined by fiber diameter, spacing ( $d_1$  and  $d_2$ ) and layer thickness  $d_3$ . The pore height was mainly defined by the layer thickness, while the pore width was defined by the difference between fiber spacing and fiber diameter. The effect of the deposition speed  $V$  on the fiber diameter and thus on the porosity was also considered.

From SEM analysis the fiber diameter  $d_1$  was measured as  $268 \pm 32 \mu\text{m}$  for the larger Bioplotter tip ( $ID = 400 \mu\text{m}$ ) and  $170 \pm 15 \mu\text{m}$  for the smaller one used ( $ID = 200 \mu\text{m}$ ). The fiber spacing was  $605 \pm 12 \mu\text{m}$ ,  $807 \pm 28 \mu\text{m}$ , and  $1001 \pm 0.00 \mu\text{m}$ . The layer thickness was  $148 \pm 10 \mu\text{m}$ ,  $257 \pm 11 \mu\text{m}$ , and  $344 \pm 11 \mu\text{m}$ . The variation of all the mentioned parameters introduced above allowed generating a set of scaffolds within a porosity range from  $29 \pm 2\%$  up to  $91 \pm 1\%$ , as calculated from equation (1). The deviations can be related to the resident time the polymer stays in the syringe, which caused a decrease of polymer melt viscosity due to slight thermal degradation, as determined from flow rate versus time experiments (data not shown). Figure 4 shows few examples of the fabricated scaffolds.

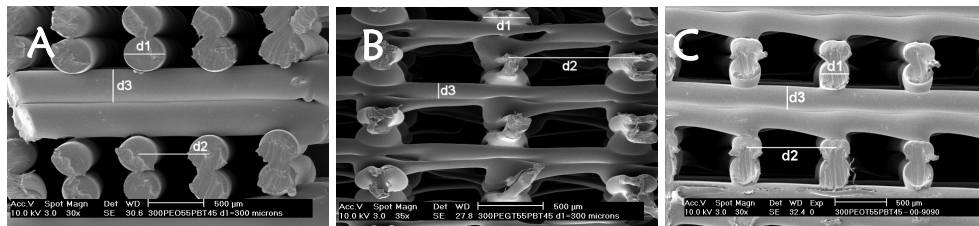


**Figure 4** – SEM micrographs of 300PEGT55PBT45 3D fiber deposited scaffolds. Cross sections of three different pore geometries are shown. Fiber diameter  $d_1 = 260 \mu\text{m}$ . (a)  $d_2 = 600 \mu\text{m}$  and  $d_3 = 350 \mu\text{m}$ ; (b)  $d_2 = 800 \mu\text{m}$  and  $d_3 = 250 \mu\text{m}$ ; (c)  $d_2 = 1000 \mu\text{m}$  and  $d_3 = 150 \mu\text{m}$ . Scale bar:  $500 \mu\text{m}$ .

Microcomputed tomography, SEM, and optical microscopy analysis of scaffold sections revealed 100% pore interconnectivity. Figure 5 illustrates the pores accessibility of 3DF scaffolds, analysed with microCT. Pores were completely interconnected for a porosity range between 29% and 91%, and for all the scaffolds architectures fabricated. With decreasing porosity microCT showed an increase of surface area per unit volume ( $S_v$ ) from  $1.94 \text{ mm}^{-1}$  to  $11.3 \text{ mm}^{-1}$ .  $S_v$  didn't change

noticeably within the different scaffold architectures considered. This is related to their constant porosity, which was previously demonstrated [20].

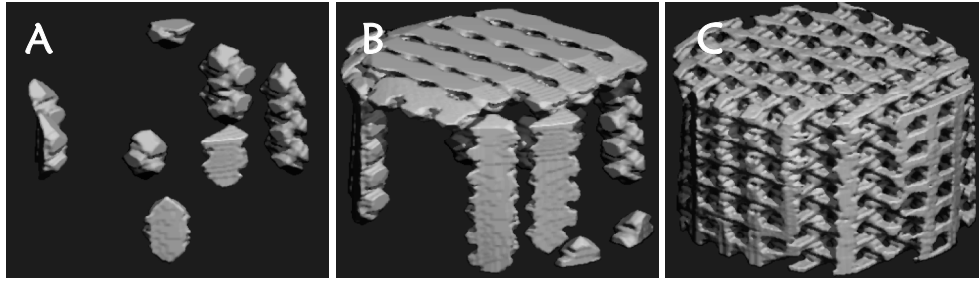


**Figure 5** – Microcomputed tomography (microCT) reconstruction of the pore network in a 3D scaffold. (a) and (b) show the pore accessibility reconstruction. (c) represents the microCT reconstruction of the 3DF scaffold.

### *Mathematical Model*

The dynamic stiffness fit the exponential model introduced in equation (2) with respect to scaffold porosity, with a correlation coefficient  $r^2 = 0.99$ . The exponential function decay significantly fitted the experimental data ( $p < 0.05$ ) and the residuals were not found to autocorrelate ( $1.59 < d < 2.5$ ) for any of the architectures fabricated or the copolymers analyzed. Figure 6 shows the correlation between the experimental data and the exponential curve for 300PEOT55PBT45. The scaffold characteristic coefficient  $\alpha$  increased from 0.027 to 0.073 by changing the fiber deposition orientation of 300PEOT55PBT45 scaffolds from a 0-90 to a 00-4545 configuration, as shown in table 1. In a similar way, by changing the copolymer composition, with the architecture fixed to the 00-9090 configuration,  $\alpha$  varied from 0.062 for 300PEOT55PBT45 with a molecular network mesh size of 9 Å, to 0.415 for 1000PEOT80PBT20 with a molecular network mesh size of 47 Å, as shown in table 2. The variation of  $\alpha$  for different copolymer compositions can be attributed to their different hydrogel-like behavior in a dynamic setting. A higher mesh size, resulting in a higher swelling ratio, implies a higher uptake of the synovium-like fluid by the polymer, which contributes to the final dynamic stiffness of the construct. Not only the bulk stiffness of the copolymer, but also the dynamic permeation of the fluid through the scaffold has its influence on the eventual elastic response. From the coefficient computed for the different 300PEOT55PBT45 architectures and for the different copolymers with a 00-9090 configuration, it is possible to derive the  $\alpha$  parameters for the other compositions with different architectures. From a theoretical point of view, the stiffness of a three-dimensional elastic open-cell foam scales with the square of the apparent density, as formulated by Gibson et al. [32], and experimentally assessed by Woesz et al [33]. Being the apparent density directly proportional to the porosity of a 3D construct, the same scale law is expected. However, when a power law regression was used a



Architecture	$E'_0$ (MPa)	$\alpha$
0-90	97	0,027
00-9090	97	0,062
0-45	97	0,0465
00-4545	97	0,073

**Table 1** – Characterization of the scaffold intrinsic coefficient  $\alpha$  (range 0.027 – 0.073,  $E'_0=97.16$  MPa), for different architectures.

Copolymer Compositions	Symbols	Swelling Ratio Q	Mesh Size $\xi$ (Å)	$E'_0$ (MPa)	$\alpha$
300PEOT55PBT45	●	1,14	9	97	0,062
300PEOT70PBT30	○	1,54	16	42,8	0,04
1000PEOT70PBT30	▼	1,76	20	29,6	0,046
300PEOT80PBT20	▽	1,72	22	20,1	0,034
600PEOT80PBT20	■	2,3	37	12,6	0,028
1000PEOT80PBT20	□	2,46	47	10,3	0,0415

**Table 2** – Characterization of the calculated intrinsic polymeric network and the correspondent values of the scaffold intrinsic coefficient  $\alpha$  (range 0.028 – 0.062), for the copolymer compositions analyzed. The symbols refer to the different PEOT/PBT compositions analyzed and depicted in figure 9.  $\xi$  standard deviations were always smaller than 1% and not included in the table.

lower correlation coefficient was found with respect of the exponential fit above introduced. This might be due to the different structure of the scaffold examined here, which is comprised of a highly organized interpenetrating fiber network and, therefore, not similar to the random structure typical of foams. The dynamic nature of the stiffness calculated with DMA might also contribute to the exponential decay with increasing porosity, although to our knowledge no other study has validated this behavior.

An example of how this model can be used is depicted in figure 7 for different scaffold architectures and in figure 8 for different copolymers. We measured bovine articular cartilage with DMA as  $9.64 \pm 1.81$  MPa and pig knee meniscal cartilage as  $1.93 \pm 0.387$  MPa. If mimicking the dynamic stiffness of articular or meniscal cartilage is considered as a goal in tissue engineering, a specific combination of scaffold porosity, scaffold architecture, and a specific copolymer composition can be obtained from the model for an optimal match of the original tissue biomechanics. Such a mechanical modulation of PEOT/PBT 3DF scaffolds may also cover a wider

range of tissues, so that different applications for softer tissues like vessels, liver, skin or tendons and ligaments can be envisaged as well.

### Porosity Influence on Dynamic Stiffness of 300PEGT55PBT45 3D Scaffolds

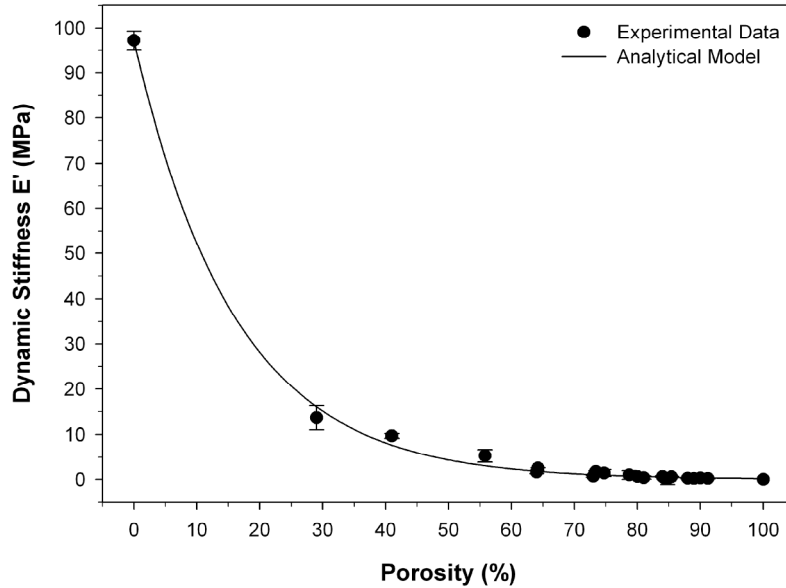


**Figure 6** – Fit of the experimental dynamic stiffness with an exponential decay curve.  $R^2 = 0.99$ ; ( $p < 0.05$ ).

Extending the models perspective in three dimensions, a relationship between dynamic stiffness, porosity and polymeric mesh size can be obtained by feeding the data into a three-dimensional Gaussian fit regression:

$$E' = 355.7 \cdot e^{-0.5 \cdot \left[ \left( \frac{P + 38.3}{31.4} \right)^2 + \left( \frac{\xi + 6.1}{13.6} \right)^2 \right]} \quad (3)$$

with a correlation coefficient  $r^2 = 0.96$ , as shown in figure 9. The coefficients are related to polymeric intrinsic parameters, such as the elastically effective network chain concentration  $\nu_e$ , the number average molecular weight  $M_n$  and the cross-link molecular weight  $M_c$ .

#### *Numerical Analysis*

A numerical Analysis was performed with a finite element program to validate the model obtained from the experimental data. The material parameters given to the

## Mathematical Model of Porosity Effect on Dynamic Stiffness: Architecture

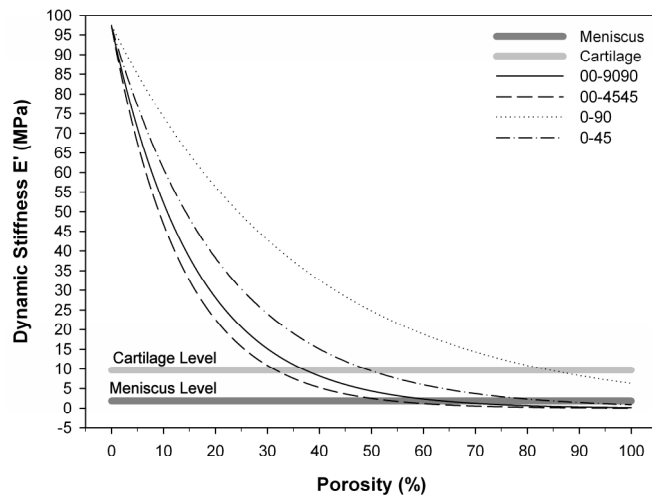


**Figure 7** – Mathematical model of the porosity effect on dynamic stiffness. 300PEOT55PBT45 scaffolds with different architectures in terms of angle deposition (0-45 and 0-90) and stacked layers (00-4545 and 00-9090) are presented in comparison with articular bovine cartilage and with porcine knee meniscus dynamic stiffness;  $n=3$ , ( $p < 0.05$ ).

## Mathematical Model of Porosity Effect on 3D Scaffolds Dynamic Stiffness: Mesh Size

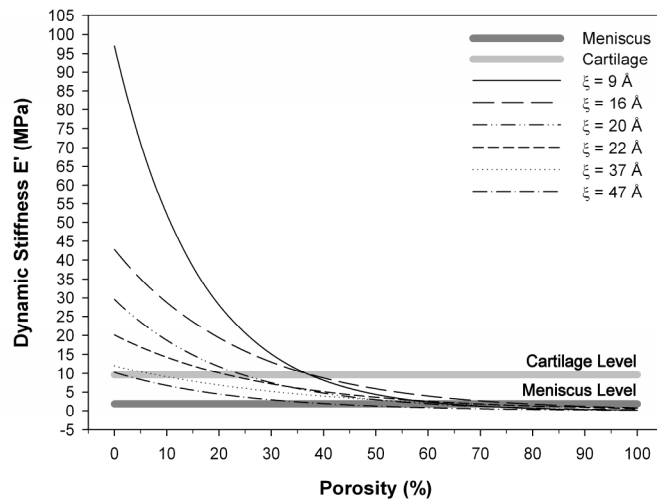


**Figure 8** – Mathematical model of the porosity effect on dynamic stiffness. Scaffolds from the copolymers with increasing molecular network mesh size  $\xi$ , are compared with articular bovine cartilage and with pig knee meniscus dynamic stiffness. The same architecture (00-9090) was used for all of the copolymers used;  $n=3$ , ( $p < 0.05$ ).

## Three-Dimensional Mathematical Matrix

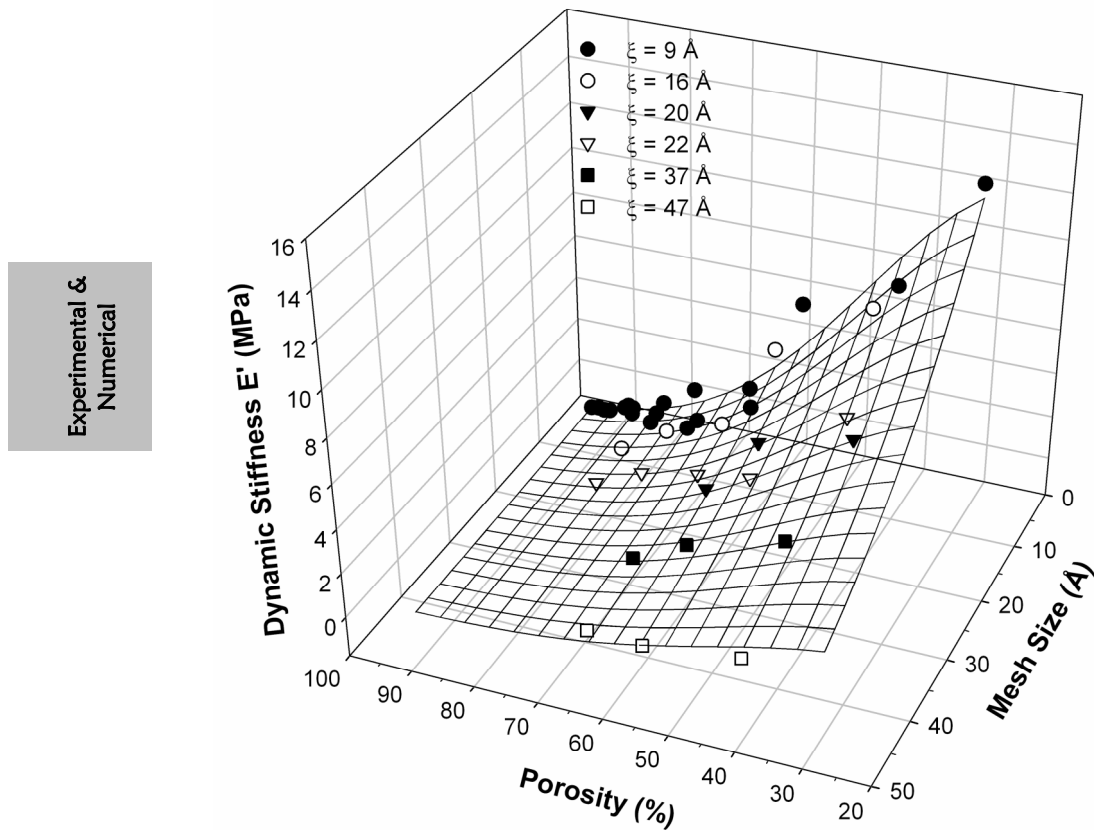


**Figure 9** – Mathematical model of the porosity and mesh size effects on dynamic stiffness for 00-9090 scaffold architecture: solid (0% porosity) stiffness values have been excluded to simplify the curve (symbols refer to the experimental data for the PEOT/PBT compositions analyzed and shown in table 2);  $n=3$ , ( $p < 0.05$ ).

FEA software as input are the bulk modulus, measured by DMA of the non porous solid compression molded scaffolds, and the Poisson's ratio, measured by an optical and mechanical determination, as previously described [20]. By varying these parameters any composition can be assumed to be present in the model. Therefore, 300PEOT55PBT45 was mainly analyzed in a range of porosity restricted to values from 40% to 80%, as representing a set of typical porous constructs used for tissue engineering applications.

Figures 10 and 11 present a comparison between the experimental and the numerical values for the various geometrical and architectural scaffold features analyzed. With decreasing porosity in the range considered, the experimental dynamic stiffness ranged from  $8.66 \text{ MPa} \pm 0.81 \text{ MPa}$  to  $0.315 \text{ MPa} \pm 0.059 \text{ MPa}$ , while the numerical computed values of the apparent stiffness decreased from  $9.00 \text{ MPa}$  to

1.01 MPa (figure 10). Analogously, for scaffolds with the same porosity but different architecture the experimental dynamic stiffness changed from 13.49 MPa  $\pm$  2.41 MPa for the 0-90 configuration to 0.46 MPa  $\pm$  0.36 MPa for the 00-4545 configuration. The apparent stiffness values converged in the numerical analysis,

#### Numerical Evaluation of Experimental Dynamic Stiffness

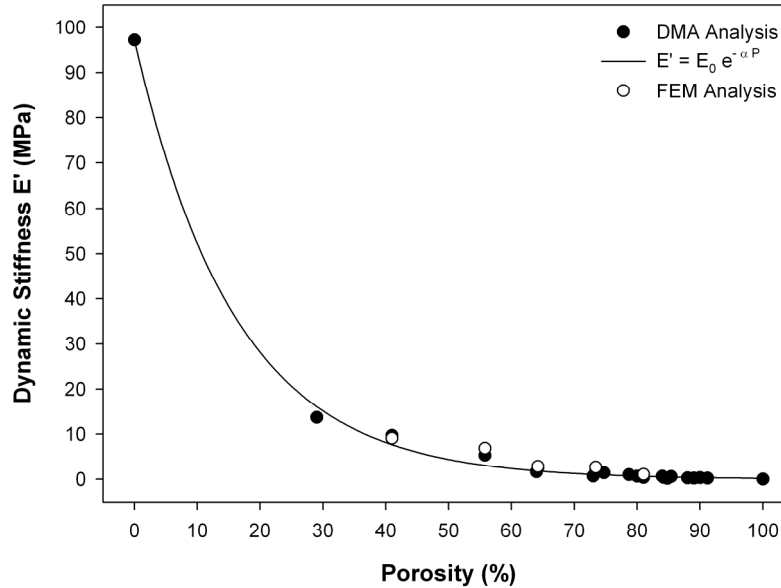


**Figure 10** – Comparison between numerical analysis and experimental data for dynamic stiffness values of 00-9090 architecture scaffolds with increasing porosities.

decreasing from 13.47 MPa to 0.675 MPa, respectively (figure 11). A better convergence to the experimental data was found by increasing the number of slices stacked to create the model and the RVE size, which resulted in an increase of the number of finite elements generated in the mesh. More precisely, for the best convergence obtained the number of elements varied from 1,856,732 for the highest to 670,090 for the lowest porosity. Similarly, by varying the fiber architecture the optimal number of elements changed from 3,286,921 for a 0-90 configuration to 324,131 for a 0-45 deposition. The deviation was less than 15% for almost all the computed 3D scaffolds, as compared to the experimental data. This deviation consistently increased, but only did so for porosities higher than 80%. Since the FEM numerical program was designed for linear elastic materials, such an increase in the relative deviation with increasing porosity might be explained by the correspondent increase of the viscous or plastic response of PEOT/PBT scaffolds [20, 21].

Numerical Evaluation of Experimental Dynamic Stiffness

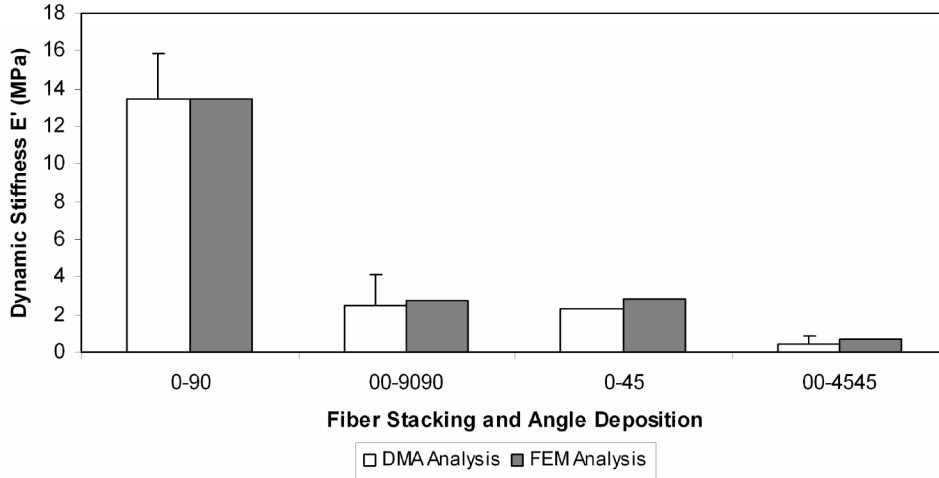


Figure 11 – Comparison between numerical analysis and experimental data for dynamic stiffness values of scaffolds with different architecture and similar porosities.

Numerical Analysis of 3DF Scaffolds Dynamic Stiffness

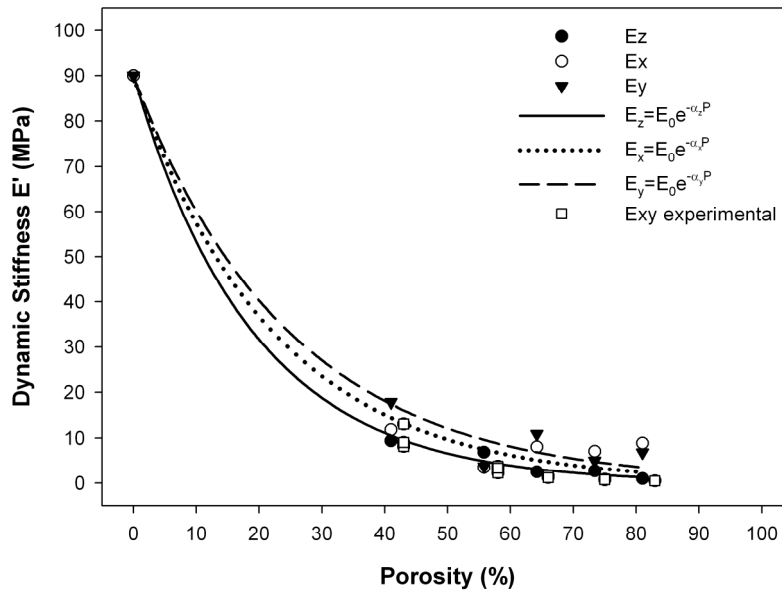
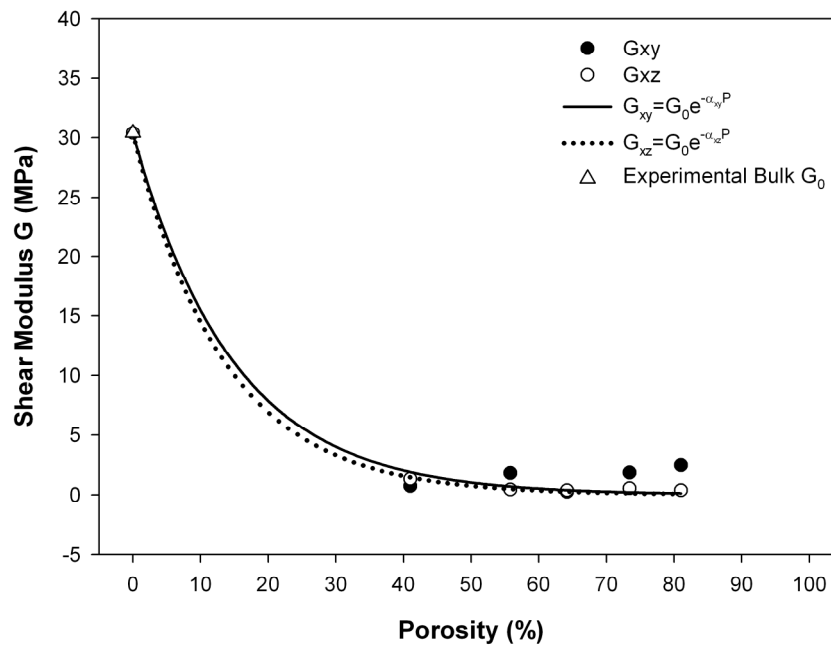


Figure 12 – Numerical dynamic stiffness components along the three axes x, y, and z. A general trend obtained by fitting the numerical values in the exponential model suggested quasi-isotropy of the scaffolds. 0% porosity (solid) values are obtained experimentally with DMA. Experimental data for x and y are also presented to show the consistency between experimental and numerical data in the three dimensions. Experimental values ( $\square$ ) are slightly shifted to the right for clarity;  $n=3$ .

Experimental & Numerical

Figure 12 and 13 introduce the values of the dynamic stiffness and of the shear modulus in the three dimensions, obtained from the whole modulus tensor generated by the FEM program. If the numerical results in the x and y directions were fit with an exponential function, as experimentally observed for the z direction, a quasi-isotropic behavior of the scaffolds was suggested, since the values of the scaffold characteristic coefficient  $\alpha$  didn't differ considerably. Such isotropy is more and more evident with increasing porosity. This was unexpected, because the fiber architecture in the constructs was not homogeneous in all the three directions. However, experimental dynamic stiffness measured in x and y directions confirmed the numerical results. We could, therefore, conclude that the intrinsic anisotropy of the fabricated structure diminishes considerably in the porosity range observed. Numerical shear modulus also fit in the exponential model previously described. Nonetheless, it must be noted that the computed shear modulus values were one order of magnitude lower as compared to the dynamic stiffness and no experimental data could be obtained to assess this trend.

### Numerical Analysis of 3DF Scaffolds Shear Modulus



**Figure 13** – Components of the numerical shear modulus. A general trend obeying the exponential decay obtained through the mathematical model is depicted.

## Conclusions

FEM numerical analysis has been proven to be a reliable tool to precisely characterize elastic properties of 3DF scaffolds. Furthermore, by experimental DMA it was possible to create a mathematical model that predicts the dynamic stiffness of scaffolds varying in porosity, architecture and intrinsic physico-chemical properties, such as the molecular network mesh size.

Eventually, the numerical simulation demonstrates consistency with this mathematical model. The dynamic stiffness of articular bovine and meniscal pig cartilage has been previously measured [20, 21, 34] and used as a comparison with PEOT/PBT porous scaffolds to show a practical use of the model. The mechanical properties of many different soft and hard tissues could be mimicked by these copolymers, simply by varying the scaffold porosity, the scaffold architecture and/or the copolymer composition. The combination of 3DF and of the PEOT/PBT polymer family leads to the generation of a set of useful scaffolds that can be fine-tuned to match the biomechanical properties for different tissue engineering applications.

## Acknowledgements

The authors would like to thank Dr. H. Weinans from the laboratory for orthopedics at the Erasmus University of Rotterdam for providing us the finite element software that we used to perform our simulations.

## References:

- [1] Hutmacher DW. Scaffold design and fabrication technologies for engineering tissues – state of the art and future perspectives. *J Biomater Sci Polymer Ed* 2002;12:107-124.
- [2] Hutmacher DW. Scaffolds in tissue engineering bone and cartilage. *Biomaterials* 2000;21:2529-2543.
- [3] Sachlos E, Czernuszka JT. Making tissue engineering scaffolds work. Review on the application of solid freeform fabrication technology to the production of tissue engineering scaffolds. *European Cells and Materials* 2003;5:29-40.
- [4] Woodfield TBF, Bezemer JM, Pieper JS, van Blitterswijk CA, Riesle J. Scaffolds for tissue engineering of cartilage. *Critical Reviews in Eukaryotic Gene Expression* 2002;12:209-236.
- [5] Yang S, Leong KF, Du Z, Chua CK. The design of scaffolds for use in tissue engineering. Part II. Rapid prototyping techniques. *Tissue Engineering* 2002;8:1-11.
- [6] Cooke MN, Fisher JP, Dean D, Rimnac C, Mikos AG. Use of stereolithography to manufacture critical-sized 3D biodegradable scaffolds for bone ingrowth. *J Biomed Mater Res* 2002;64B:65-69.
- [7] Zein I, Hutmacher DW, Tan KC, Teoh SH. Fused deposition modelling of novel scaffold architectures for tissue engineering applications. *Biomaterials* 2002;23:1169-1185.



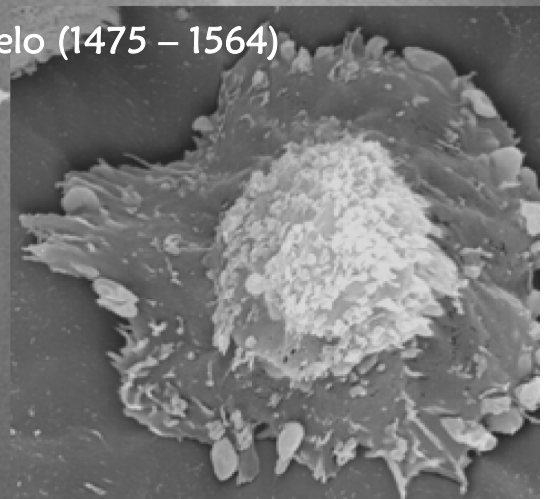
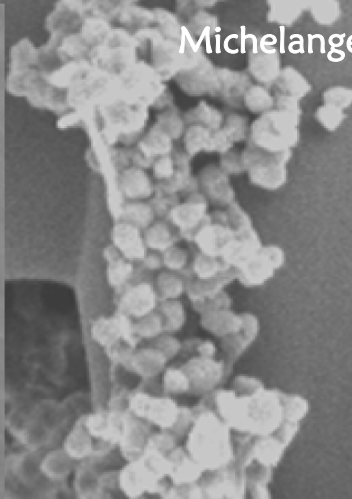
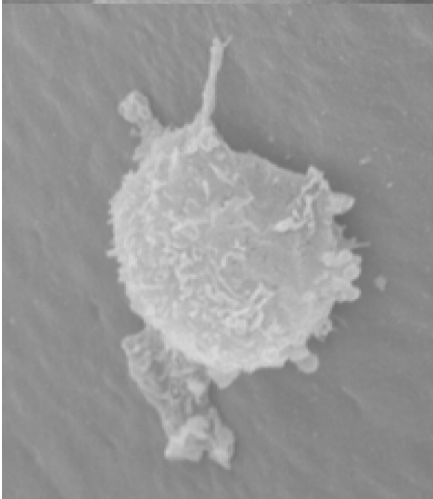
- [8] Kim SS, Utsunomiya H, Koski JA, Wu BM, Cima MJ, Sohn J, Mukai K, Griffith LG, Vacanti JP. Survival and function of hepatocytes on a novel three-dimensional synthetic biodegradable polymer scaffold with intrinsic network of channels. *Ann Surg* 1998;228:8-13.
- [9] Vozzi G, Flaim C, Ahluwalia A, Bhatia S. Fabrication of PLGA scaffolds using soft lithography and microsyringe deposition. *Biomaterials* 2003;24:2533-2540.
- [10] Vozzi G, Previti A, De Rossi D, Ahluwalia A. Microsyringe-based deposition of two-dimensional and three-dimensional polymer scaffolds with a well-defined geometry for application to tissue engineering. *Tissue Engineering* 2002;8:1089-1098.
- [11] Hutmacher DW, Schantz T, Zein I, Ng KW, Teoh SH, Tan KC. Mechanical properties and cell cultural response of polycaprolactone scaffolds designed and fabricated via fused deposition modelling. *J Biomed Mater Res* 2001;55:203-216.
- [12] Giordano RA, Wu BM, Borland SW, Cima LG, Sachs EM, Cima MJ. Mechanical properties of dense polylactic acid structures fabricated by three dimensional printing. *J Biomater Sci Polymer Edn* 1996;8:63-75.
- [13] Sherwood JK, Riley SL, Palazzolo R, Brown SC, Monkhouse DC, Griffith LG, Landeen LK, Ratcliffe A. A three-dimensional osteochondral composite scaffold for articular cartilage repair. *Biomaterials* 2002;23:4739-4751.
- [14] Taboas JM, Maddox RD, Krebsbach PH, Hollister SJ. Indirect solid free form fabrication of local and global porous, biomimetic and composite 3D polymer-ceramic scaffolds. *Biomaterials* 2003;24:181-194.
- [15] Landers R, Müllhaupt R. Desktop manufacturing of complex objects, prototypes and biomedical scaffolds by means of computer-assisted design combined with computer-guided 3D plotting of polymers and reactive oligomers. *Macromol. Mater. Eng.* 2002;282:17-21.
- [16] Landers R, Hübner U, Schmelzeisen R, Müllhaupt R. Rapid prototyping of scaffolds derived from thermoreversible hydrogels and tailored for application in tissue engineering. *Biomaterials* 2002;23:4437-47.
- [17] Landers R, Pfister A, Hübner U, John H, Schmelzeisen R, Müllhaupt R. Fabrication of soft tissue engineering scaffolds by means of rapid prototyping techniques. *J Mater Sci* 2002;37:3107-3116.
- [18] Woodfield TBF, Malda J, de Wijn J, Péters F, Riesle J, van Blitterswijk CA. Design of porous scaffolds for cartilage tissue engineering using a three-dimensional fibre-deposition technique. *Biomaterials* 2004;25:4149-4161.
- [19] Malda J, Woodfield TBF, van der Vloodt F, Wilson C, Martens DE, Tramper J, van Blitterswijk CA, Riesle J. The effect of PEGT/PBT Scaffold Architecture on the Composition of Tissue Engineered Cartilage. *Biomaterials* 2004;26:63-72.
- [20] Moroni L, de Wijn J, van Blitterswijk CA. 3D fiber deposited scaffolds for tissue engineering: influence of pore geometry and architecture on dynamic mechanical properties. *Biomaterials* 2006;27:974-985.
- [21] Moroni L, de Wijn J, van Blitterswijk CA. 3D Fiber Deposited PEOT/PBT Copolymer Scaffolds for Tissue Engineering: Influence of Porosity, Molecular Network Mesh Size and Swelling in Aqueous Media on Dynamic Mechanical Properties. *J Biomed Mater Res* 2005;75A:957-965.

- [22] van Blitterswijk CA, van de Brink J, Leenders H, Bakker D. The effect of PEO ratio on degradation, calcification and bone bonding of PEO/PBT copolymer (PolyActive). *Cells Mater* 1993;3:23-36.
- [23] Beumer GJ, van Blitterswijk CA, Ponec M. Degradation behavior of polymeric matrices in (sub)dermal and muscle tissue of the rat: a quantitative study. *Biomaterials* 1994;15:551-559.
- [24] Beumer GJ, van Blitterswijk CA, Ponec M. Biocompatibility of degradable matrix induced as a skin substitute: an in vivo evaluation. *J Biomed Mater Res* 1994;28:545-552.
- [25] Bakker D, van Blitterswijk CA, Hesselting SC, Grote JJ, Deams WT. Effect of implantation site on phagocyte/polymer interaction and fibrous capsule formation. *Biomaterials* 1988;9:14-21.
- [26] Mensik I, Lamme EN, Riesel J, Brychta P. Effectiveness and safety of the PEGT/PBT copolymer scaffold as dermal substitute in scar reconstruction wounds (feasibility trial). *Cell Tiss Bank* 2002;3:245-253.
- [27] Bulstra SK, Geesink RG, Bakker D, Bulstra TH, Bouwmeester SJ, van der Linden AJ. Femoral canal occlusion in total hip replacement using a resorbable and flexible cement restrictor. *J Bone Joint Surg Br* 1996;78:892-898.
- [28] Bezemer JM, Grijpma DW, Dijkstra PJ, van Blitterswijk CA, Feijen J. A controlled release system for proteins based on poly(ether ester) block-copolymers: polymer network characterization. *J Control Release* 1999;62:393-405.
- [29] van Dijkhuizen-Radersma R, Peters FL, Stienstra NA, Grijpma DW, Feijen J, de Groot K, Bezemer JM. Control of vitamin B12 release from poly(ethylene glycol)/poly(butylene terephthalate) multiblock copolymers. *Biomaterials* 2002;23:1527-36.
- [30] Deschamps AA, Claase MB, Sleijster WJ, de Bruijn JD, Grijpma DW, Feijen J. Design of segmented poly(ether ester) materials and structures for the tissue engineering of bone. *J Control Release* 2002;78:175-86.
- [31] Van Rietbergen B, Weinans H, Huiskes R, Odgaard A. A new method to determine trabecular bone elastic properties and loading using micromechanical finite element models. *J of Biomech* 1995;28:69-81.
- [32] Gibson LJ, Ashby MF. *Cellular Solids – structure and properties*, 2<sup>nd</sup> edn. Cambridge Univ Press, 1997.
- [33] Woesz A, Stampfl J, Fratzl P. Cellular Solids beyond the Apparent Density – an Experimental Assessment of Mechanical Properties. *Adv Eng Mater* 2004;6:134-138.
- [34] Sweigart MA, Zhu CF, Burt DM, de Holl PD, Agrawal CM, Clanton TO, Athanasiou KA. Intraspecies and Interspecies Comparison of the Compressive Properties of the Medial Meniscus. *Ann Biomed Eng* 2004;32:1569-1579.

Assess the importance of mimicking the mechanical behavior of a tissue, in combination with appropriate physicochemical properties

Sto ancora imparando

Michelangelo (1475 – 1564)





# Chapter 5

## Three Dimensional Fiber Deposited Scaffolds with Enhanced Cell Entrapment Capacity and Matching Physico-Chemical Properties Favour Cartilage Regeneration

J. A. A. Hendriks<sup>a, b, \*</sup> and L. Moroni<sup>a, \*</sup>, J. Riesle<sup>b</sup>, J. R. de Wijn<sup>a</sup>, C.A. van Blitterswijk<sup>a</sup>

<sup>a, \*</sup> Institute for BioMedical Technology (BMTI), University of Twente, P.O. Box 217, 7500 AE Enschede, The Netherlands. E-mail: l.moroni@tnw.utwente.nl; j.a.a.hendriks@tnw.utwente.nl

<sup>b</sup> CellcoTec N.V., Prof. Bronkhorstlaan 10D, 3723 MB Bilthoven, The Netherlands

Matching  
Cartilage

### Abstract

An important tenet in designing scaffolds for tissue engineering application or cell therapy is that they should mimic the biomechanical properties of the tissues to be replaced. We hypothesized that this can be achieved by controlling scaffold's pore architecture and volume with 3D fiber deposition (3DF). In addition to mimicking mechanical properties one would also like to determine the contribution of tissue formation to the mechanical properties of a construct during culture and its dependence on scaffold composition and structure. It has been shown that depending on the material, matching the scaffolds mechanical properties to cartilage can compromise the porosity, which hampers tissue formation. Therefore, the aim of this investigation was to assess whether 3DF scaffolds with controlled pore volume and at the same time matching mechanical properties, are indeed effective to support cartilage tissue formation. Next to this, we studied mechanical stability of the constructs in time during culture. Previously it was established that co-culturing primary chondrocytes with expanded chondrocytes in micromass culture and in vivo enhanced cartilage tissue formation. In this study primary and expanded chondrocytes (1:5) were cultured on scaffolds in vitro for 4 weeks. DNA, Glycosaminoglycans (GAG) and dynamic stiffness of the constructs were measured at day 1, 7 and 28 to assess the relative amount of cells, the cartilage specific matrix build up and the constructs stability. Cell morphology and matrix distribution was analyzed by ESEM. A higher amount of cartilage specific matrix (ECM) was formed on lower pore volume scaffolds after 28 days of culture. Furthermore, a less protein adhesive composition supported chondrocytes rounded morphology, which contributed to cartilagenous differentiation. Interestingly, the dynamic stiffness of a hybrid construct remained approximately at the same value

\* Equally contributing authors.

after culture, suggesting a comparable kinetics of tissue formation and scaffold degradation in low pore volume scaffolds. These results imply that 3DF scaffolds with low pore volume and appropriate physico-chemical properties support chondrocyte differentiation. Both formed tissue and scaffold were shown to contribute to the dynamic stiffness of the constructs during culture.

**Keywords:** rapid prototyping, pore volume, physico-chemical properties, dynamic stiffness, cartilage.

## Introduction

In tissue engineering, scaffolds have been shown to deliver an essential contribution to treatments of chondral defects. These constructs have to possess sufficient biocompatibility, to be possibly biodegradable, to provide mechanical stability and to constitute an appropriate substrate for cells to direct these into the proper lineage [1-5]. They can also act as a delivery vehicle for cells and it has been shown that some scaffolds deliver instructive signals to enhance chondrogenesis of cells [6-8]. Polyethyleneoxide-terephthalate (PEOT)/polybutylene-terephthalate (PBT) copolymers are interesting candidates to make scaffolds for tissue engineering as they comply at least partially with the above mentioned criteria. These polyether-ester multi-block copolymers are thermoplastic elastomers which display satisfactory physical properties like elasticity, toughness and strength in combination with easy processability [9-12].

Previous results from our group showed that both architecture and composition of the PEOT/PBT scaffolds influence cartilage specific matrix formation of chondrocytes [13-16]. On two-dimensional more protein adhesive surfaces like 300/55/45 (a/b/c, where a is the molecular weight of PEG units used in the copolymerization, while b and c are the PEOT and PBT weight fractions in the final copolymer) a direct relationship between a spread chondrocyte morphology and reduced differentiation capacity has been shown [15]. In contrast, on less protein adhesive surfaces (e.g. 1000/70/30) chondrocytes take a spherical morphology, aggregate and enhanced differentiation is apparent [16]. When 3D scaffolds are fabricated with conventional techniques, like compression moulding and salt leaching, the achievement of mechanically matching structures to cartilage infers a low pore volume. The pore network of these scaffolds is often tortuous and not completely interconnected, resulting in a scarce nutrient perfusion. This can be overcome by a rapid prototyping technique such as 3D fiber deposition (3DF), as the resulting scaffolds have a completely interconnected pore network and scaffold's pore architecture and volume can be controlled [13, 17].

Human articular cartilage thickness has been shown to range between 0.5 and 7.1 mm at various locations in the knee. For in vitro or in vivo studies in cartilage tissue engineering, scaffold thickness ranged typically between 1-5 mm [18]. In general, cells from an immature animal model are used to study correlation between limiting factors such as nutrient gradients, pore volume and interconnectivity of a scaffold and homogenous cartilage tissue formation [19]. However, matching scaffold's thickness for cartilage repair with chondrocytes from adult model origin might not be just a matter of scaling up. Oxygen tension has shown to decrease throughout

such clinically relevant size scaffolds [20, 21]. Albeit no difference in oxygen tension was shown between 3DF and compression moulded (CM) scaffolds with the same porosity (80%), tissue formation with chondrocytes from immature origin showed to be enhanced in 3DF scaffolds compared to CM scaffolds. So far, with CM techniques manufactured 1000/70/30 scaffolds with matching mechanical properties of cartilage hampered porosity and pore interconnectivity to such an extent that cartilage tissue formation was obstructed. Therefore, the aim of this study was to examine the influence of scaffold's pore volume and polymeric composition on matrix build up by mature articular chondrocytes. Next to this we examined the influence of extra cellular matrix build up in chorus with scaffold degradation on mechanical stability of scaffolds. For this purposes, 3D scaffolds were fabricated by a rapid prototyping technique such as 3DF, since with this method it is possible to achieve scaffolds with low pore volume and high pore interconnectivity. Recently, we found that co-culturing of primary chondrocytes with expanded chondrocytes enhanced cartilage tissue formation [22]. This co-culture model was applied to study the influence of cell-biomaterial interaction on cartilagenous tissue formation on PEOT/PBT scaffolds. PEOT/PBT 3DF scaffolds with 100% interconnectivity were fabricated with different porosity, pore volume, and copolymer composition. Specifically, 300/55/45 and 1000/70/30 were considered for their difference in physico-chemical properties and the differential influence this showed to have on cartilagenous tissue formation.

## Materials and Methods

### *Scaffolds fabrication*

Poly(ethylene oxide – terephthalate)/poly(butylene terephthalate) (PEOT/PBT) copolymers were obtained from IsoTis S.A. (Bilthoven, The Netherlands). The composition used in this study were 300/55/45 and 1000/70/30 where, following an aPEOTbPBTC nomenclature, a is the molecular weight in g/mol of the starting PEG blocks used in the copolymerization, while b and c are the weight fractions of the PEOT and PBT blocks, respectively.

3DF scaffolds were produced with a Bioplotter device (Envisiontec GmbH, Germany), which is basically an XYZ plotting machine as previously described by Landers et al [23, 24] and by our group [25, 26]. To make the extrusion of highly viscous PEOT/PBT fibers possible few modifications were done. The polymer was placed in a stainless steel syringe and heated at  $T = 200-210$  °C through a thermo-coupled cartridge unit, fixed on the "X"-mobile arm of the apparatus. When the polymer reached a molten phase, a nitrogen pressure of 4.5-5 Bars was applied to the syringe through a pressurized cap. Rectangular block models were deposited, layer by layer, through the extrusion of the polymer on a stage as a fiber in a CAD/CAM controlled manner. Scaffolds were then characterized by varying the fiber diameter (through the nozzle diameter or the deposition speed), the spacing between fibers in the same layer, the layer thickness and the configuration of the deposited fibers within the whole architecture. In particular, stainless steel Luer Lock

needles with an internal diameter (ID) of 200  $\mu\text{m}$  shortened to a length of 16 mm was used to extrude the polymeric filaments in this study. The deposition speed was set to 230 mm/min for 300/55/45 and to 280 mm/min for 1000/70/30. This resulted in extruded fibers with a diameter  $d_1$  of approximately 170  $\mu\text{m}$ . Three scaffold types were fabricated based on previous studies on the mechanical properties of PEOT/PBT 3DF scaffolds: 300/55/45 and 1000/70/30 (porosity = 74%) with similar, but not matching (NM) dynamic stiffness ( $E' = 1 \text{ MPa}$ ), as compared to articular bovine cartilage, and 1000/70/30 (porosity = 56%) mechanically matching (M) articular cartilage ( $E' = 10 \text{ MPa}$ ).

The rationale behind the scaffolds' design was first to compare 3D scaffolds with different physico-chemical properties, but identical structure, resulting in approximately similar dynamic stiffness. This aimed at assessing the net contribution of the polymers' physico-chemical properties on cartilage formation in a 3D scaffold model. At the same time the influence of high pore volume and low stiffness on cartilaginous tissue build up was studied. Next, a 3DF scaffold with low pore volume, resulting in matching the articular cartilage stiffness, was fabricated with 1000/70/30 for its potential capacity to support cell round morphology. This also allowed to compare the influence of low or high pore volume, that is matching or non-matching dynamic stiffness, on extra cellular matrix formation and scaffold degradation, and thus on the construct stability. For NM 300/55/45 and 1000/70/30 scaffolds the fiber spacing  $d_2$  was set to 600  $\mu\text{m}$ , the layer thickness  $d_3$  was set to 150  $\mu\text{m}$ , and the layer configuration was changed by 90° every two deposited layers (00-9090 configuration). For M 1000/70/30 scaffolds the fiber spacing  $d_2$  was fixed to 370  $\mu\text{m}$ , the layer thickness was fixed to 140  $\mu\text{m}$ , while the layer configuration was changed by 90° every single deposited layer (0-90 configuration).

### *Scaffolds Characterization*

Cylindrical samples of 4 mm in diameter by 4 mm in height were cored out in the “Z-direction” from the rectangular 3D fabricated blocks. Scaffolds geometry and architecture was characterized by environmental scanning electron microscopy (ESEM) analysis with a Philips XL 30 ESEM-FEG. The porosity of 3DF scaffolds was calculated as [23, 26]:

$$P = 1 - \frac{V_{\text{scaffold}}}{V_{\text{cube}}} = 1 - \frac{\pi}{4} \cdot \frac{1}{\frac{d_2}{d_1}} \cdot \frac{1}{\frac{d_3}{d_1}} \quad (1)$$

where P is the scaffold porosity,  $d_1$  the fiber diameter,  $d_2$  the fiber spacing and  $d_3$  the layer thickness, within each different structure.



### ***Cell Isolation and Culture***

Primary chondrocytes are referred to when chondrocytes were applied immediately after isolation. For chondrocytes isolation, full thickness articular cartilage was dissected from the patellar femoral groove of adult bovine. Dissected cartilage was incubated for 20-22 hrs in collagenase type II solution containing 0.15% collagenase (Worthington), Dulbecco's modified Eagle's medium (Gibco) supplemented with penicillin (100 U/ml) and streptomycin (100 µg/ml). Suspension was filtered through a 100 µm mesh nylon filter (cell strainer Nucleon) and cells were washed 2 times with PBS supplemented with penicillin (100U/ml) and streptomycin (100µg/ml). For expansion chondrocytes were plated at a density of  $3.5 \times 10^4$  cells/cm<sup>2</sup> and cultured in proliferation medium (PM) containing DMEM supplemented with 10% fetal bovine serum, 1x non-essential amino acids (Sigma-Aldrich), 10 mM HEPES buffer (Biowhitaker), 0.2 mM Ascorbic acid-2-phosphate (InVitrogen), 0.4 mM proline (Sigma-Aldrich), 100 U/ml penicillin (InVitrogen) and 100 µg/ml streptomycin (InVitrogen). Medium was refreshed every 3-5 days and cells were cultured in an incubator at 37 °C and 5% CO<sub>2</sub>. After 2-3 passages (9-12 population doublings), expanded cells were mixed with primary chondrocytes for seeding onto a porous scaffold.

### ***Cell seeding and culturing on 3DF scaffolds***

Cylindrical scaffolds were sterilized in isopropanol for 4 hours, rinsed in PBS extensively, incubated overnight in PM and blotted dry prior to seeding. Primary and expanded chondrocytes were mixed at a 20/80 ratio, centrifuged at 300g for 5 min and re-suspended in 54 µl of PM containing 300 µg/ml fibronectin. Scaffolds were seeded with 54 µl of cell suspension containing  $3 \times 10^6$  cells for 1 hr, after which medium was carefully added. Constructs were cultured statically in PM for 4 weeks in an incubator at 37 °C and 5% CO<sub>2</sub>.

### ***Biochemical Analysis***

Constructs (n=3) for quantitative analysis of sulphated glycosaminoglycans (GAGs) and cell number were washed with PBS and frozen overnight at -80 °C. Subsequently they were digested with 1 mg/ml proteinase K (Sigma-Aldrich) in Tris/EDTA buffer (pH 7.6) containing 18.5 µg/ml iodoacetamide and 1 µg/ml pepstatin A (Sigma-Aldrich) for >16 hrs at 56 °C. GAG content was spectrophotometrically determined with 9-dimethylmethylene blue chloride (DMMB) (Sigma-Aldrich) staining in PBE buffer (14.2 g/l Na<sub>2</sub>HPO<sub>4</sub> and 3.72 g/l Na<sub>2</sub>EDTA, pH 6.5) with a micro plate reader (Bio-TEK instruments) at an absorbance of 520 nm. Cell number was determined via quantification of total DNA with CyQuant DNA kit according to the manufacturer's description (Molecular probes) and fluorescent plate reader (Perkin-Elmer). Quantitative total GAG and total DNA were normalized for differences in wet weight of the scaffolds.

### *Scanning Electron microscopy (SEM) Analysis*

Tissue constructs were also analyzed by SEM. Samples were fixed overnight in 0.14 M cacodylate buffer (pH = 7.2 – 7.4) containing 0.25% glutaraldehyde (Merck). Scaffolds were subsequently dehydrated in sequential ethanol series and critical point dried from liquid carbon dioxide using a Balzers CPD 030 machine. Specimens were then gold sputtered (Cressington) and studied under the SEM.

### *Mechanical Characterization*

A dynamic mechanical analysis (DMA) instrument (Perkin Elmer 7e) was used to measure the dynamic stiffness of the 3DF scaffolds before and after culturing (n=6). Cylindrical fixtures were chosen to test the specimens and evaluate their behavior as a whole structure along their compression axis, in the “Z-direction”.

Scaffolds were loaded with a dynamic force varying from 100 mN to 150 mN in a dynamic stress experiment. More specifically, a starting force of 100 mN was applied and then continuously increased to 150 mN with a sinusoidal loading ramp of 5 mN/min, at a constant frequency of 1Hz. The dynamic stiffness was calculated by the instrument software (Pyris). The tests were conducted under wet conditions: a synovium-like fluid was prepared as a 3% (w/v) solution of poly(vinyl pyrrolidone) (PVP) in de-ionized water [26]. This was done to simulate the physiological environment of articular cartilage. Scaffolds were soaked in PVP-solution, before loading. The temperature was 37 °C during all of the experiments.

### *Statistical Analysis*

Statistical Analysis was performed using a two-tailed Student’s t-test with two sample equal variance, where the confidence level was set to 0.05 for statistical significance, unless otherwise specified. Values in this study are reported as mean and standard deviation.

## **Results**

### *Scaffolds Characterization*

SEM analysis revealed a fiber diameter d1 of  $170 \pm 15 \mu\text{m}$ , a fiber spacing d2 of  $605 \pm 12 \mu\text{m}$  for the NM scaffolds and of  $377 \pm 3 \mu\text{m}$  for the M scaffold, and a layer thickness d3 of  $148 \pm 10 \mu\text{m}$  for the NM scaffolds and of  $140 \pm 7 \mu\text{m}$  for the M scaffold. This corresponded to rectangular pores of  $435 \pm 2 \mu\text{m}$  in the X-Y plane by  $148 \pm 10 \mu\text{m}$  in the Z plane for the NM scaffolds, and of  $202 \pm 7 \mu\text{m}$  in the X-Y plane by  $140 \pm 7 \mu\text{m}$  in the Z plane for the M scaffold (Figure 1). The porosity of the NM scaffolds was  $74 \pm 2\%$ , while the porosity of the M scaffold was  $56 \pm 4\%$ .

## Tissue Formation

Seeding efficiency results at day 1 showed that on NM 300/55/45 (74%) and M 1000/70/30 (56%) the amount of DNA was significantly 25% higher compared to

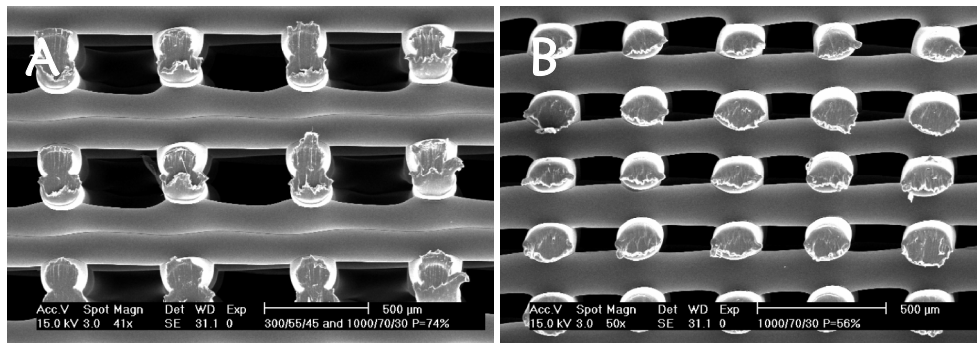


**Figure 1** – SEM micrographs of scaffolds architecture in terms of pore volume for (a) 300/55/45 and 1000/70/30 NM with a porosity of 74% and a starting stiffness of 1 Mpa, and for (b) 1000/70/30 M with a porosity of 56% and a starting stiffness of 10 MPa.

NM 1000/70/30 (74%) (Figure 2A). ESEM evaluation showed that at day 1, chondrocytes regained or maintained a spherical morphology after fibronectin mediated aggregation seeding on all scaffolds (figure 2B). Subsequently, seeded cells were distributed more homogeneously in these two types of scaffolds, than in the NM 1000/70/30. Interestingly, after 4 weeks of culture tissue formed contained significantly 35% more GAG on M 1000/70/30 (56%) compared to NM 300/55/45 (74%) and NM 1000/70/30 (74%) (Figure 3). The amount of DNA in the constructs was significantly lower only on NM 1000/70/30 (74%) compared to NM 300/55/45 (74%) and M 1000/70/30 (74%). Consequently, GAG/DNA was highest in tissue formed on M 1000/70/30 (56%). At this time point, while on 300/55/45 cells and tissue appeared as stretched structures which align with the scaffold surface and form long fibers, in 1000/70/30 (NM and M) cells still appeared to be spherical and tissue formed is condensed without any extrusions (Figures 4g, 4h, 4i). Additionally, it seems that ECM formed is filling the pores to a higher degree in the M 1000/70/30 (56%) scaffold as compared to NM 300/55/45 (74%) (Figure 5). This together with the quantitative GAG data indicates more cartilaginous tissue formation in M 1000/70/30 (56%) scaffolds. Table 1 summarizes DNA, GAG, and DNA/GAG measured in the constructs here considered.

### *Cartilage Construct Mechanical properties*

The dynamic stiffness of the constructs and of empty scaffolds soaked and incubated in medium was measured at different time points to examine the contribution of tissue formation and of scaffold degradation during culture. The dynamic stiffness of NM 300/55/45 tissue constructs increased from  $1.01 \pm 0.13$  MPa prior to culture, to  $1.41 \pm 0.23$  MPa at day 1, and to  $1.68 \pm 0.09$  MPa at day 28 (Figure 6). No

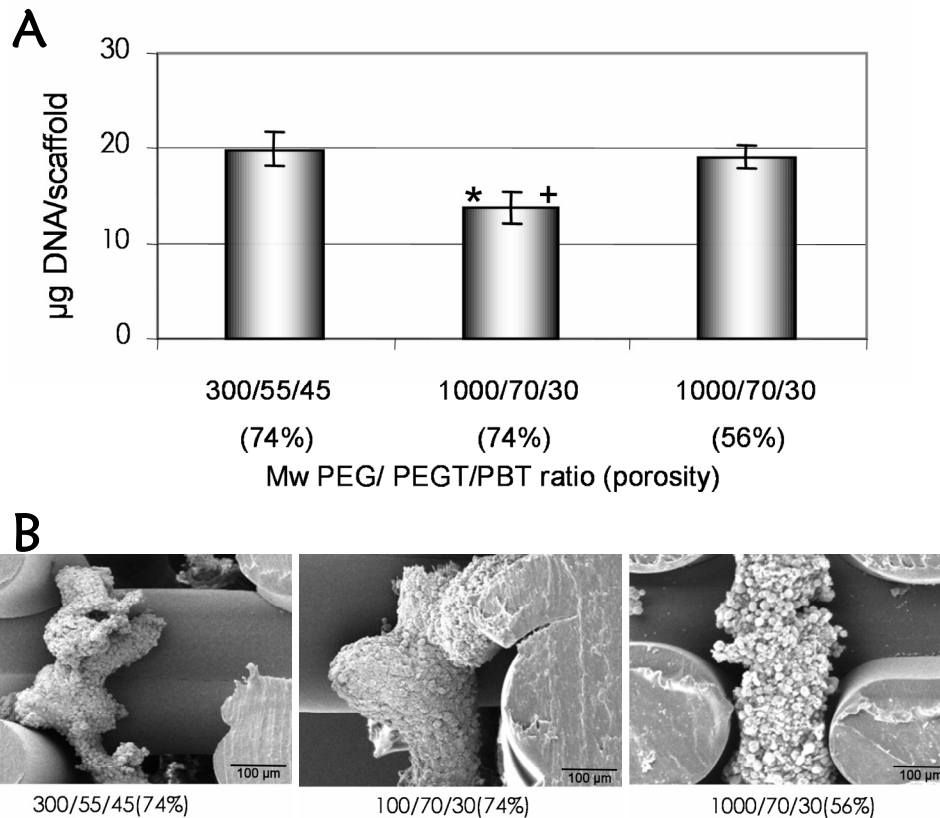
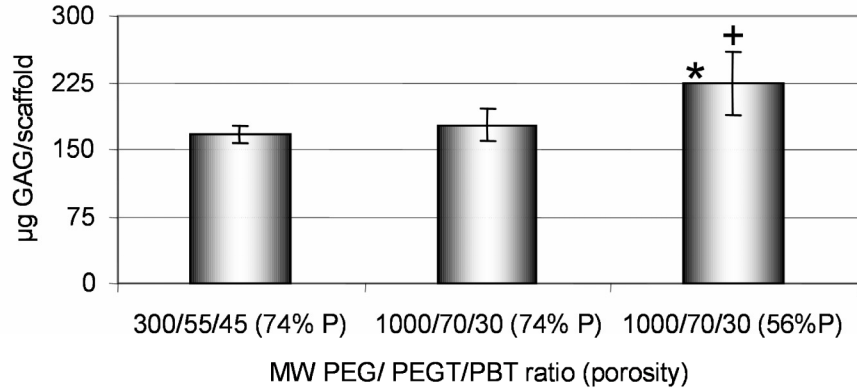


**Figure 2** – Seeding efficiency (a) and ESEM pictures (b) of 3DF PEGT/PBT scaffolds seeded with chondrocytes (day 1). (a) Quantitative DNA assay results representing the relative amount of cells after 1 day of static seeding. Cells seeded are 20/80 primary/expanded chondrocytes. Scaffold composition is described as Mw PEG/ ratio PEOT/PBT (porosity %). \* = significantly different from 300/55/45 (74%), + = significantly different from 1000/70/30 (74%). (b) ESEM micrographs of the 3DF constructs showing a maintained or recovered rounded morphology in all the scaffolds due to fibronectin aggregation. Scale bar: 100  $\mu$ m

significant change in the stiffness was measured for NM 300/55/45 empty scaffolds left in culture media at 37 °C during the whole culture period. Similarly, the dynamic stiffness of NM 1000/70/30 cartilage constructs increased from  $1.06 \pm 0.13$  MPa before culturing, to  $1.4 \pm 0.2$  MPa at day 1, and to  $2.75 \pm 0.2$  MPa at day 28. A slight decrease in stiffness of NM 1000/70/30 empty scaffolds was measured as  $0.92 \pm 0.18$  MPa after 28 days. Interestingly, the dynamic stiffness of M 1000/70/30 cartilage constructs increased from  $10.18 \pm 1.04$  MPa prior to culture, to  $13.40 \pm 1.3$  MPa at day 1, and to  $13.51 \pm 2.56$  MPa at day 28. A consistent decrease in the stiffness of M 1000/70/30 empty scaffolds was also measured as  $7.75 \pm 2.15$  MPa after 28 days. Since the dynamic stiffness of this construct remained constant during culture, it can be inferred that a similar speed of tissue formation and of scaffold degradation occurs for the matching 1000/70/30 architecture. In line

with the previous findings, tissue formed in the M 1000/70/30 scaffold contributed more to dynamic stiffness of the construct, compared tissue formed onto NM configurations (Figure 7). Specifically, the net tissue formed stiffness increased from  $0.4 \pm 0.18$  MPa to  $0.54 \pm 0.06$  MPa for NM 300/55/45, from  $0.34 \pm 0.06$  MPa to  $1.47 \pm 0.15$  MPa for NM 1000/70/30, and from  $3.22 \pm 0.29$  MPa to  $5.06 \pm 1.74$  MPa for M 1000/70/30.



Matching  
Cartilage

**Figure 3** – Total glycosaminoglycans (GAG) of in vitro cultured PEOT/PBT constructs (4 wks). Composition scaffold is described as Mw PEG/ PEOT/PBT ratio (porosity). Constructs were seeded with 20% primary chondrocytes and 80% expanded chondrocytes with fibronectin aggregation and cultured for 4 weeks. \* = significantly different from 300/55/45 (74%), + = significantly different from 1000/70/30 (74%).

Scaffold Composition	total GAG (µg)	Total DNA (µg)	GAG/DNA (µg/µg)
300/55/45 (74%)	166.3 ± 9.1	41.5 ± 4.3	4.0 ± 0.5
1000/70/30 (74%)	176.6 ± 18.2	34.0 ± 3.9 *	5.2 ± 0.8
1000/70/30 (56%)	223.3 ± 35.6 * +	36.9 ± 3.9 +	6.1 ± 1.2

**Table 1** – Total glycosaminoglycans (GAG), total DNA and GAG/DNA of in vitro cultured PEOT/PBT constructs (4 wks).

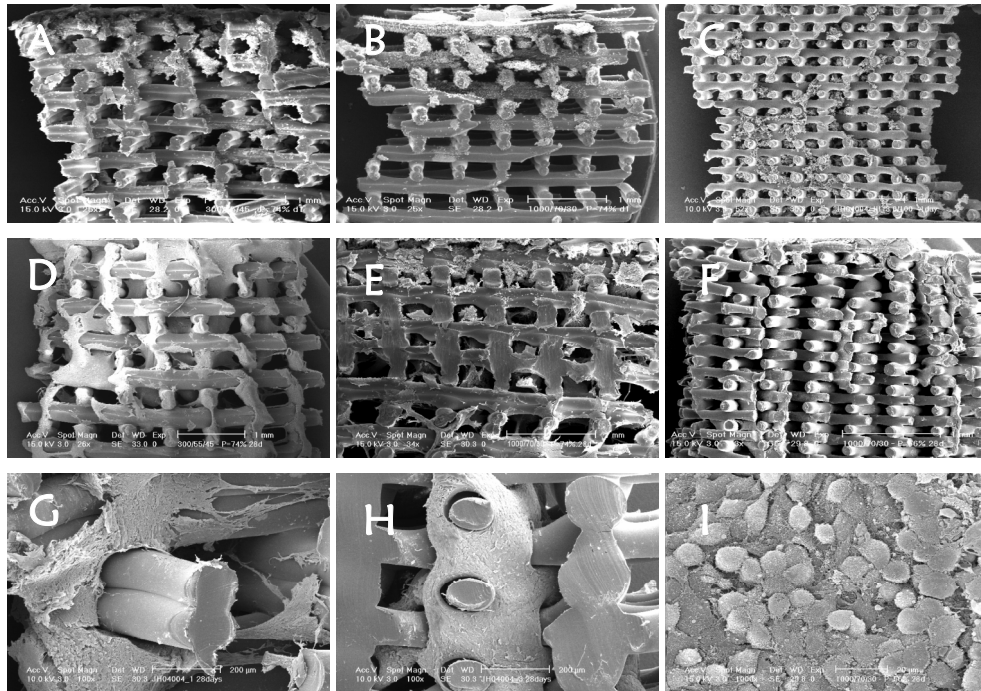


**Figure 4** – SEM analysis of cell distribution and matrix formation on NM (a, b, d, e) and M (c, f) constructs at day 1 (a, b, c) and at day 28 (d, e, f). Cells attach better to 300/55/45 NM (d) but dedifferentiate (g), while they are better entrapped and more homogeneously distributed in 1000/70/30 NM and M (e, f), where they maintain their phenotype (h, i). Scale bar: (a – f) 1 mm; (g, h) 200  $\mu$ m; (i) 20  $\mu$ m.

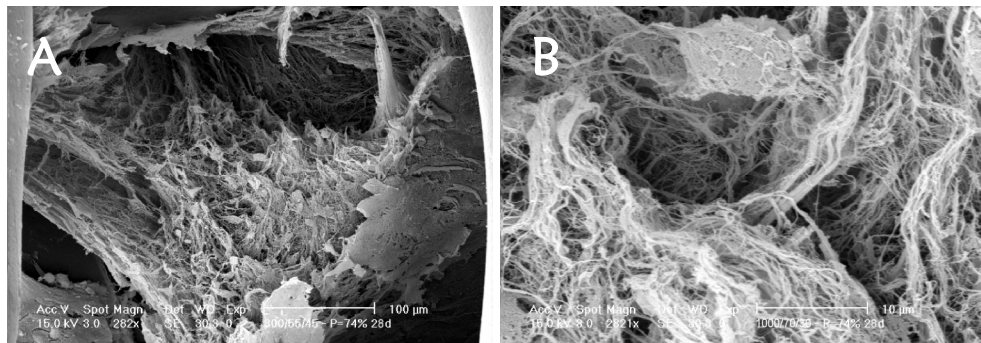


**Figure 5** – SEM micrographs show extra cellular matrix (ECM) formation after 28 days both in 300/55/45 NM (a) and 1000/70/30 NM and M (b), respectively. Scale bar: (a) 100  $\mu$ m; (b) 10  $\mu$ m.

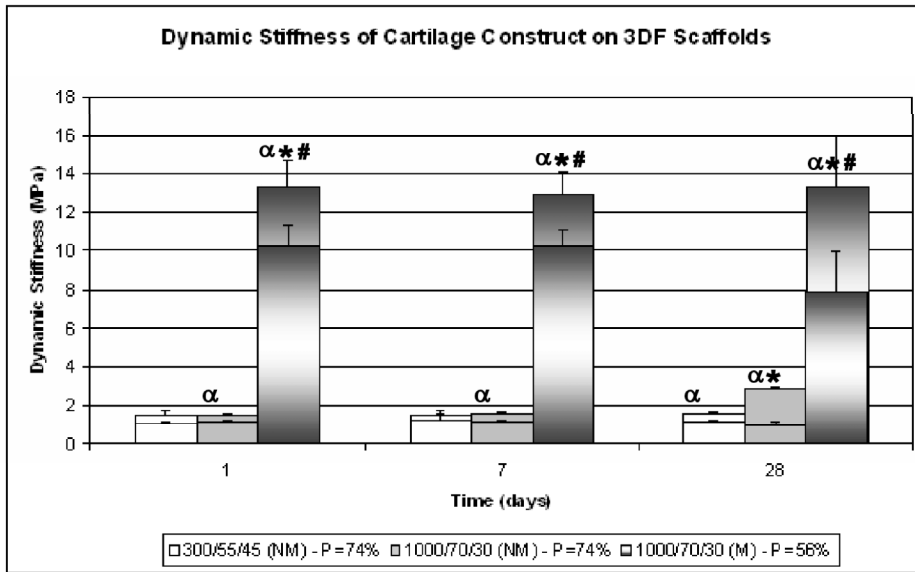


**Figure 6** – Dynamic Stiffness of cartilage constructs (higher bars) and of empty scaffolds (lower bars) at day 1, 7, and 28. ( $\alpha$ ) indicate significant differences of the cartilage constructs with respect to the empty scaffolds; (\*) point at significant differences with respect to 300/55/45 NM; (#) show significant differences as compared to 1000/70/30 NM.

Matching  
Cartilage

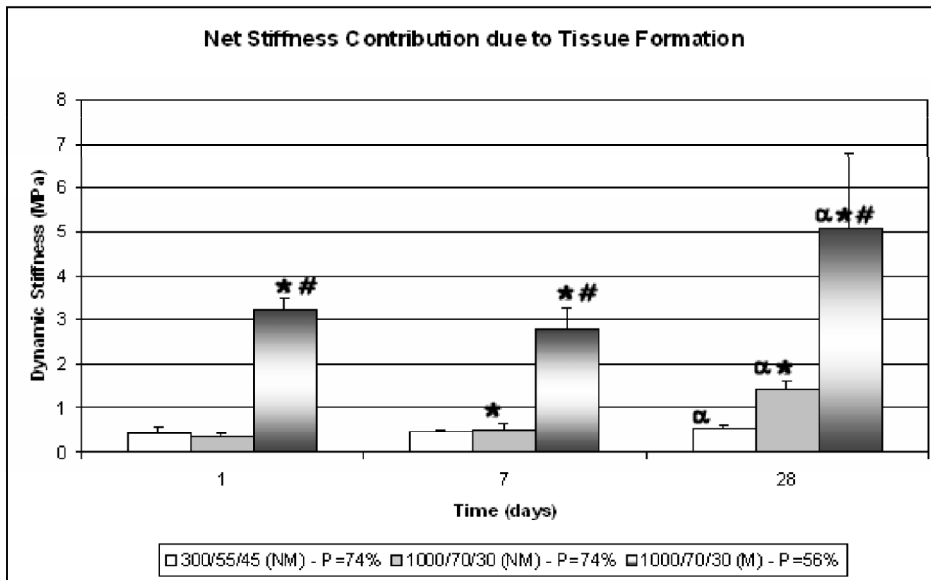


**Figure 7** – Net stiffness of the Tissue formed on the scaffolds, calculated as the difference between the stiffness of the constructs and the stiffness of empty scaffolds maintained in cartilage medium at physiological values for the same culture period. ( $\alpha$ ) indicate significant differences during culture time; (\*) show significant differences from 300/55/45 NM; (#) point at significant differences from 1000/70/30 NM.

## Discussion and Conclusions

Previous work from our group showed that the oxygen tension goes down rapidly from 1 to 2 mm of scaffold depth during chondrocyte culture in 3DF scaffolds as well as compression molded CM scaffolds (both 80% porosity) [20, 21]. However, cell distribution and matrix deposition of articular chondrocytes from immature origin was still enhanced in 3DF scaffolds (80% porosity) compared to CM scaffold. In the here described study the difference in tissue formation of chondrocytes from mature origin in 3DF scaffolds with a porosity of either 74% or 56% was examined. If porosity does not hamper homogenous cartilage tissue formation it is possible to manufacture 1000/70/30 scaffolds – having favorable surface properties – made matching mechanical properties of cartilage.

Therefore, 3D fiber deposited PEOT/PBT scaffolds with different physico-chemical properties, but similar mechanical properties resulted from high pore volume architecture were first fabricated to evaluate the influence of the polymer composition on tissue formation. Next, 3DF scaffolds with favorable surface properties and with matching mechanical properties of cartilage resulted from a low pore volume architecture were also fabricated to assess the influence of pore volume and architecture on cartilage regeneration. While porosity and pore volume decreased, interconnectivity of pores was not impaired (Fig. 1) resulting in increased mechanical stability of the M 1000/70/30 scaffold compared to the NM 1000/70/30. In this study, we showed that at low porosity (56%) in M 1000/70/30 cartilage tissue formed by mature bovine chondrocytes homogeneously distributed throughout the scaffold and the amount of GAG is significantly enhanced compared to higher porous NM 300/55/45 or NM 1000/70/30 scaffolds. Two factors appear to play an important role with increased cartilagenous tissue formation on low porosity M 1000/70/30 scaffolds: seeding efficiency and pore interconnectivity. Seeding efficiency on more protein adhesive surfaces like 300/55/45 is depending on cell attachment, while on less protein adhesive surfaces like 1000/70/30 chondrocytes have shown to maintain a spherical morphology and do not attach. Previously, chondrocytes treated with fibronectin prior to seeding showed to aggregate and enhance cartilage tissue formation [27, 28]. In the study here described, it was shown that fibronectin cell aggregation increased seeding efficiency on M 1000/70/30 with a lower porosity compared to NM 1000/70/30 with a higher porosity. From this, we concluded that more aggregates were captured and sustained in M 1000/70/30 as a result of the lower porosity of this scaffold. Second, pores were fully interconnected for all 3 scaffolds. Tissue formation of chondrocytes from an immature model is not hampered at low porosity in clinical relevant size scaffolds as previously mentioned [19]. From the results shown here, we conclude that low porosity does not hinder cartilage tissue formation by chondrocytes originating from a mature model throughout a scaffold. We conclude that the high interconnectivity of the pores allows for a decreased porosity thus preventing detrimental nutrient or oxygen limitations in the scaffold. Next, we studied the net result of tissue formation and scaffold degradation in vitro on dynamic stiffness of



1000/70/30 and 300/55/45 (NM) and 1000/70/30 (M). We showed that the dynamic stiffness of 300/55/45 scaffolds without cells remained unchanged over 28 days. In contrast, dynamic stiffness of both NM and M 1000/70/30 showed to decrease respectively of 15 and 24% when incubated in medium for 28 days. This is in agreement with what has been previously shown by Deschamps et al. [10], where degradation of scaffolds with a high water uptake like 1000/70/30 occurred faster due to more rapid hydrolysis compared to scaffolds like 300/55/45 that take up less water.

Surprisingly, the dynamic stiffness already increased of 0.4, 0.34, and 3.22 MPa when NM300/55/45, NM1000/70/30 and M 1000/70/30 were seeded with cells, respectively. Recently it has been shown that the shear modulus of a single mammalian cell (the shear modulus can be assumed to correlate with the stiffness by a factor varying between 0.5 and 1, depending on the Poisson's ratio) ranges between 20 and 60 Pa [29, 30]. In an ideal situation all the seeded cells are distributed homogeneously throughout a scaffold. If we consider cells as a biological "material", this would result in a corresponding homogeneous stress distribution on loading. Thus, if we consider the Voigt-Reuss model to calculate the modulus of the scaffold-cell composite [31, 32], the theoretical contribution of the seeded cells to the modulus of the construct would be negligible, considering that cells fill the pores of the scaffolds. However, in this case cells were aggregated with fibronectin prior seeding. It might be that fibronectin and aggregated cells contributed to the stiffness of the construct at an early stage. Welsh and Tirrell showed that the stiffness of protein engineered fibronectin varies with its molecular weight from 0.1 MPa to 0.321 MPa [33]. Furthermore, few researchers showed that when cells are exposed to fibronectin or fibronectin coated surfaces their intrinsic stiffness is significantly higher [34, 35]. This might explain the contribution of cells to the dynamic stiffness of the NM constructs here investigated. However, it does not explain the higher contribution of cells in M 1000/70/30 scaffolds with a higher initial dynamic stiffness compared to the other scaffolds with a lower initial dynamic stiffness. From quantitative data shown in Figure 2 it is clear that the amount of cells in M 1000/70/30 is not significantly different from the amount of cells in NM 300/55/45. However, the increase in dynamic stiffness after seeding is approximately 10-fold more for the first construct compared to the latter. One of the major differences between these scaffolds besides the stiffness is their porosity. From a pure material point of view, if we again consider cells as biological "materials", we can expect a higher contribution to the dynamic stiffness by a given number of cells seeded and entrapped into a scaffold with low porosity as compared to a scaffold with high porosity [36, 37]. This is due to the power [36] or exponential [17] relationship that links the static or dynamic stiffness, respectively, to the porosity of a cellular solid. For a scaffold with high porosity, a reduction in porosity results in a small increase of the scaffold's stiffness. For scaffolds with a low porosity, a small decrease may cause a significant increase in stiffness. This suggests that the contribution of the cells to the mechanical properties in M 1000/70/30 with 56% porosity is much higher than in NM 300/55/45 or NM1000/70/30 with 74% porosity. Moreover, since in the case of M 1000/70/30 the dynamic stiffness of the cartilagenous construct remains substantially constant during time and the stiffness of empty scaffolds

decreases in time, a similar speed of tissue formation and scaffold degradation rate could be inferred.

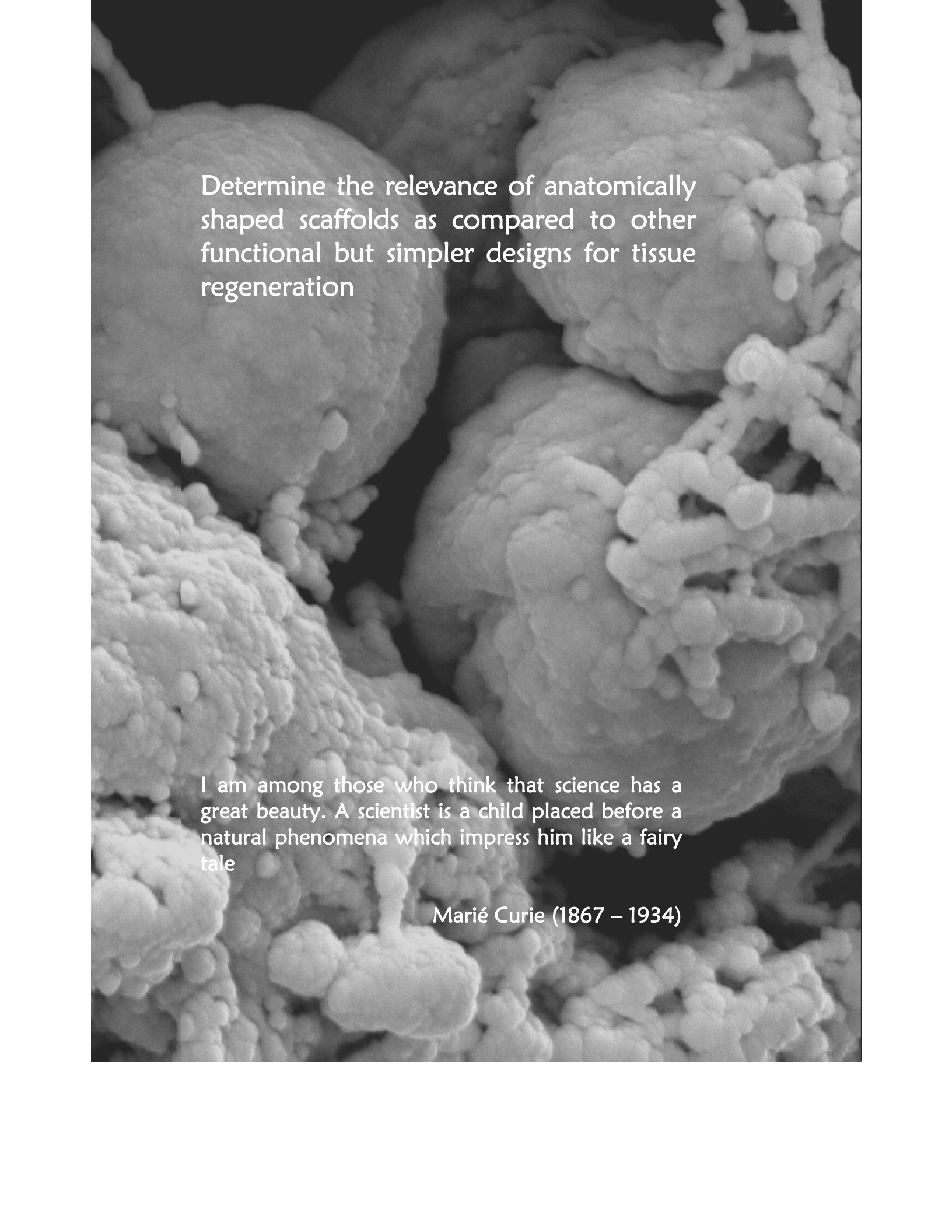
Finally, results showed that the dynamic stiffness of both M and NM 1000/70/30 constructs significantly increased as compared to NM 300/55/45 constructs. When taking into account that both M and NM 1000/70/30 degraded in medium, it is clear that scaffolds with this physicochemical composition support cartilaginous tissue formation with extra cellular matrix composition contributing substantially more to the mechanical properties of a construct. Taken together, these findings suggest that by accurately controlling the pore volume and the total porosity of a 3D scaffold with a completely interconnected pore network, it is possible to improve cell aggregated seeding efficiency and cartilage tissue formation. In the specific case of 1000/70/30 this was associated to appropriate physicochemical properties for sustaining chondrocyte rounded morphology and to a dynamic stiffness matching articular cartilage. 3DF scaffolds with low pore volume and low porosity made with 1000PEOT70PBT30 could, therefore, be interesting candidate to regenerate articular cartilage in long-term applications.

#### Reference:

- [1] Lutolf MP, Hubbell JA. Synthetic biomaterials as instructive extracellular microenvironments for morphogenesis in tissue engineering. *Nat Biotechnol* 2005;23(1):47-55.
- [2] Hutmacher DW. Scaffold design and fabrication technologies for engineering tissues--state of the art and future perspectives. *J Biomater Sci Polym Ed* 2001;12(1):107-24.
- [3] Muschler GF, Nakamoto C, Griffith LG. Engineering principles of clinical cell-based tissue engineering. *J Bone Joint Surg Am* 2004;86-A(7):1541-58.
- [4] Orner BP, Derda R, Lewis RL, Thomson JA, Kiessling LL. Arrays for the combinatorial exploration of cell adhesion. *J Am Chem Soc* 2004;126(35):10808-9.
- [5] Stevens MM, George JH. Exploring and engineering the cell surface interface. *Science* 2005;310(5751):1135-8.
- [6] Jeschke B, Meyer J, Jonczyk A, Kessler H, Adamietz P, Meenen NM, Kantlehner M, Goepfert C, Nies B. RGD-peptides for tissue engineering of articular cartilage. *Biomaterials* 2002;23(16):3455-63.
- [7] Sohier J, Haan RE, de Groot K, Bezemer JM. A novel method to obtain protein release from porous polymer scaffolds: emulsion coating. *J Control Release* 2003;87(1-3):57-68.
- [8] Lee JE, Kim KE, Kwon IC, Ahn HJ, Lee SH, Cho HC, Kim HJ, Seong SC, Lee MC. Effects of the controlled-released TGF-beta 1 from chitosan microspheres on chondrocytes cultured in a collagen/chitosan/glycosaminoglycan scaffold. *Biomaterials* 2004;25(18):4163-4173.
- [9] Moroni L, de Wijn JR, van Blitterswijk CA. Three-dimensional fiber-deposited PEOT/PBT copolymer scaffolds for tissue engineering: Influence of porosity, molecular network mesh size, and swelling in aqueous media on dynamic mechanical properties. *J Biomed Mater Res A* 2005;75:957-965.

- [10] Deschamps AA, Claase MB, Sleijster WJ, de Bruijn JD, Grijpma DW, Feijen J. Design of segmented poly(ether ester) materials and structures for the tissue engineering of bone. *J Control Release* 2002;78(1-3):175-86.
- [11] Bezemer JM, Grijpma DW, Dijkstra PJ, van Blitterswijk CA, Feijen J. A controlled release system for proteins based on poly(ether ester) block-copolymers: polymer network characterization. *J Control Release* 1999;62(3):393-405.
- [12] van Dijkhuizen-Radersma R, Peters FL, Stienstra NA, Grijpma DW, Feijen J, de Groot K, Bezemer JM. Control of vitamin B12 release from poly(ethylene glycol)/poly(butylene terephthalate) multiblock copolymers. *Biomaterials* 2002;23(6):1527-36.
- [13] Malda J, Woodfield TB, van der Floodt F, Wilson C, Martens DE, Tramper J, van Blitterswijk CA, Riesle J. The effect of PEGT/PBT scaffold architecture on the composition of tissue engineered cartilage. *Biomaterials* 2005;26(1):63-72.
- [14] Mahmood TA, Shastri VP, van Blitterswijk CA, Langer R, Riesle J. Tissue engineering of bovine articular cartilage within porous poly(ether ester) copolymer scaffolds with different structures. *Tissue Eng* 2005;11(7-8):1244-53.
- [15] Woodfield TB, Miot S, Martin I, van Blitterswijk CA, Riesle J. The regulation of expanded human nasal chondrocyte re-differentiation capacity by substrate composition and gas plasma surface modification. *Biomaterials* 2006;27(7):1043-53.
- [16] Mahmood TA, de Jong R, Riesle J, Langer R, van Blitterswijk CA. Adhesion-mediated signal transduction in human articular chondrocytes: the influence of biomaterial chemistry and tenascin-C. *Exp Cell Res* 2004;301(2):179-88.
- [17] Moroni L, Poort G, Van Keulen F, de Wijn JR, van Blitterswijk CA. Dynamic mechanical properties of 3D fiber-deposited PEOT/PBT scaffolds: An experimental and numerical analysis. *J Biomed Mater Res A* 2006(78):605-614.
- [18] Woodfield TB, Bezemer JM, Pieper JS, van Blitterswijk CA, Riesle J. Scaffolds for tissue engineering of cartilage. *Crit Rev Eukaryot Gene Expr* 2002;12(3):209-36.
- [19] VunjakNovakovic G, Obradovic B, Martin I, Bursac PM, Langer R, Freed LE. Dynamic cell seeding of polymer scaffolds for cartilage tissue engineering. *Biotechnol Prog* 1998;14(2):193-202.
- [20] Malda J, Woodfield TB, van der Floodt F, Kooy FK, Martens DE, Tramper J, van Blitterswijk CA, Riesle J. The effect of PEGT/PBT scaffold architecture on oxygen gradients in tissue engineered cartilaginous constructs. *Biomaterials* 2004;25(26):5773-80.
- [21] Malda J, van Blitterswijk CA, van Geffen M, Martens DE, Tamper J, Riesle J. Low oxygen tension stimulates the redifferentiation of dedifferentiated adult human nasal chondrocytes. *Osteoarthritis and Cartilage* 2004;12(4):306-313.
- [22] Hendriks JAA, de Bruijn E, van Blitterswijk CA, Riesle J. A powerful tool in cartilage tissue engineering; coculturing primary chondrocytes with expanded chondrocytes enhances chondrogenesis. *ORS Transactions of 51st annual meeting* 2006.
- [23] Landers R, Pfister A, Hubner U, John H, Schmelzeisen R, Mullhaupt R. Fabrication of soft tissue engineering scaffolds by means of rapid prototyping techniques. *Journal of materials science* 2002;37:3107-3116.

- [24] Landers R, Hubner U, Schmelzeisen R, Mulhaupt R. Rapid prototyping of scaffolds derived from thermoreversible hydrogels and tailored for applications in tissue engineering. *Biomaterials* 2002;23:4437-47.
- [25] Woodfield TB, Malda J, de Wijn J, Peters F, Riesle J, van Blitterswijk CA. Design of porous scaffolds for cartilage tissue engineering using a three-dimensional fiber-deposition technique. *Biomaterials* 2004;25(18):4149-61.
- [26] Moroni L, de Wijn JR, van Blitterswijk CA. 3D fiber-deposited scaffolds for tissue engineering: influence of pores geometry and architecture on dynamic mechanical properties. *Biomaterials* 2006;27(7):974-85.
- [27] Stewart MC, Saunders KM, Burton-Wurster N, Macleod JN. Phenotypic stability of articular chondrocytes in vitro: the effects of culture models, bone morphogenetic protein 2, and serum supplementation. *J Bone Miner Res* 2000;15(1):166-74.
- [28] Robinson EE, Foty RA, Corbett SA. Fibronectin matrix assembly regulates alpha5beta1-mediated cell cohesion. *Mol Biol Cell* 2004;15(3):973-81.
- [29] Hoffman BD, Massiera G, Van Citters KM, Crocker JC. The consensus mechanics of cultured mammalian cells. *Proc Natl Acad Sci U S A* 2006.
- [30] Kaazempur Mofrad MR, Abdul-Rahim NA, Karcher H, Mack PJ, Yap B, Kamm RD. Exploring the molecular basis for mechanosensation, signal transduction, and cytoskeletal remodeling. *Acta Biomater* 2005;1(3):281-93.
- [31] Voigt W. *Lehrbuch der Krystallphysik*. Leipzig, Germany: B.G. Teubner 1910.
- [32] Reuss A. *Zeitschrift für Angewandte Mathematik und Mechanik*. 1929;9:49-58.
- [33] Welsh ER, Tirrell DA. Engineering the extracellular matrix: a novel approach to polymeric biomaterials. I. Control of the physical properties of artificial protein matrices designed to support adhesion of vascular endothelial cells. *Biomacromolecules* 2000;1(1):23-30.
- [34] Takai E, Costa KD, Shaheen A, Hung CT, Guo XE. Osteoblast elastic modulus measured by atomic force microscopy is substrate dependent. *Ann Biomed Eng* 2005;33(7):963-71.
- [35] Bhadriraju K, Hansen LK. Extracellular matrix- and cytoskeleton-dependent changes in cell shape and stiffness. *Exp Cell Res* 2002;278(1):92-100.
- [36] Woesz A, Stampfl J, Fratzl P. Cellular solids beyond the apparent density - an experimental assessment of mechanical properties. *Advanced Engineering Materials* 2004;6(3):134-138.
- [37] Gibson LJ, Ashby MF. *Cellular Solids - structure and properties*, 2<sup>nd</sup> edition. Cambridge University Press, Cambridge 1997.

A scanning electron micrograph (SEM) showing a complex, porous, and interconnected scaffold structure. The structure consists of numerous small, rounded, interconnected components that form a dense, three-dimensional network. The overall appearance is highly textured and resembles a natural or biological material, possibly a bio-scaffold or a porous ceramic. The lighting highlights the intricate details of the interconnected fibers and nodes.

Determine the relevance of anatomically shaped scaffolds as compared to other functional but simpler designs for tissue regeneration

I am among those who think that science has a great beauty. A scientist is a child placed before a natural phenomena which impress him like a fairy tale

Marié Curie (1867 – 1934)



# Chapter 6

## Anatomical 3D Fiber-Deposited Scaffolds for Tissue Engineering: Designing a Neo-Trachea

L. Moroni <sup>a,\*</sup>, M. Curti <sup>b</sup>, M. Welti <sup>b</sup>, S. Korom <sup>b</sup>, W. Weder <sup>b</sup>, J.R. de Wijn <sup>a</sup>, C.A. van Blitterswijk <sup>a</sup>

<sup>a,\*</sup> Institute for BioMedical Technology (BMTI), University of Twente, P.O. Box 217, 7500 AE Enschede, The Netherlands. E-mail: l.moroni@tnw.utwente.nl

<sup>b</sup> Division of Thoracic Surgery, Laboratory of Tissue Engineering, University Hospital, Raemistrasse 100, CH-8091 Zurich, Switzerland.

### Abstract

The advantage of using anatomically shaped scaffolds as compared to modeled designs was investigated and assessed in terms of cartilage formation in an artificial tracheal construct. Scaffolds were rapid prototyped with a technique named three dimensional fiber deposition (3DF). Anatomical scaffolds were fabricated from a patient-derived computer tomography (CT) dataset, and compared to cylindrical and toroidal tubular scaffolds. Lewis rat tracheal chondrocytes were seeded on 3DF scaffolds and cultured for 21 days. MTT and sulphated glycosaminoglycans (GAG) assays were performed to measure the relative number of cells and the extracellular matrix (ECM) formed. After 3 weeks of culture, the anatomical scaffolds revealed a significant increase in ECM synthesis and a higher degree of differentiation as shown by the GAG/MTT ratio and by SEM analysis. Interestingly, a lower scaffold's pore volume and porosity resulted in more tissue formation and a better cell differentiation, as evidenced by GAG and GAG/MTT values. Scaffolds were compliant and did not show any signs of luminal obstruction *in vitro*. These results promote anatomical scaffolds as functional matrices for tissue regeneration not only to help regain the original shape, but also for their improved capacity to support larger tissue formation.

**Keywords:** Anatomical scaffolds, pore volume, porosity, cartilage, trachea regeneration.

## Introduction

Employing novel rapid prototyping techniques for tissue-engineer-based scaffold fabrication has led to the production of improved and more functional 3D matrices [1-4]. Rapid prototyped 3D scaffolds possess a completely interconnected and periodical pore network, which can be varied in dimension and shape layer by layer with a controlled CAD/CAM approach. They can be comprised of different materials, typically different polymers [5-7] or composites of polymers and ceramics [8-10], they can combine gradients of porosities [11, 12], and they can be shaped and designed to optimize their structural and mechanical properties for a specific purpose, resulting in multifunctional constructs [13-15]. Their complete interconnected porous network provides better nutrient delivery in the deeper parts of a tissue engineered construct with consequently better survival rate of cells as compared to conventional fabricated scaffolds, e.g. scaffolds from porogen based techniques [16, 17].

Several studies focused on the development of different rapid prototyping techniques [2, 18-20] and on scaffolds optimization [14, 21, 22]. Little is known on the effect of the scaffold shape design on tissue regeneration. From a clinical point of view, an appealing solution to engineer a specific tissue would consist in seeding cells on an anatomically shaped scaffold that can be rapid prototyped from a computerized tomography (CT) or from a magnetic resonance imaging (MRI) dataset of a patient [13]. Anatomical scaffolds have been so far considered only for the advantage to regain the same shape of the regenerated tissue. However, no study has demonstrated a possible benefit of an anatomical scaffold for tissue development as compared to other designs. It is possible that due to the better structural control over the architecture in simplified – still functional - modeled shapes, a better tissue development would be expected than in complex shapes derived from the anatomical design. In this case possible structural imperfections can result in the fabricated scaffolds because of resolution limitations.

Therefore the aim of this study was to assess whether the design of the scaffold (anatomical vs. geometrical) influences the dynamics of tissue formation in the constructs. For this purpose a rather complicated tissue structure such as a tracheal segment was considered and the regeneration of its cartilaginous part was studied. The trachea is a tubular conduit which can be divided in ring subunits comprised of hyaline cartilage covered by a layer of epithelial cells and mucosa in the inner side, and a layer of muscle cells in the outer side. Three different designs were considered: a cylindrical tube, a toroidal ring tube, and an anatomical tube fabricated from the acquisition of a CT scan dataset of a human trachea. Furthermore, two different scaffold porosities were considered to evaluate the optimal structure in terms of construct compliability and tissue formation. Rat chondrocytes were chosen as the cellular matrix and cultured on these dimensionally adapted scaffolds for 3 weeks. The distribution and the amount of cells and extracellular matrix present on the scaffolds were considered as determinants for a better scaffold performance. 3DF scaffolds were fabricated with block-copolymers of polyethyleneoxide-terephthalate (PEOT) and polybutylene-terephthalate (PBT). These polyether-ester multiblock



copolymers are thermoplastic elastomers with favorable physical properties like elasticity, toughness and strength in combination with easy processability. The properties are derived mainly from a phase separated morphology in which soft, hydrophilic PEO segments at environmental temperatures are physically cross-linked by the presence of hard, semi crystalline PBT segments. These cross-links are reversible and can be broken at temperatures above their glass transition- or melting point, which provides to the material its good processability. PEOT/PBT copolymers have been studied for *in vitro* and *in vivo* biocompatibility [23-26] and has found commercial clinical applications (PolyActive™, IsoTis Orthopaedics S.A.) as cement stoppers and bone fillers in orthopedic surgery [27, 28]. As they are polyether-esters, their degradation takes place in aqueous media by hydrolysis and oxidation with a rate that varies from very low for high PBT contents to medium and high for larger contents of PEOT and longer PEO segments [29-31]. Similarly, by varying the PEOT/PBT weight ratio and the length of the PEO segments, a series of copolymers that cover a wide range of mechanical properties with different abilities to swell in aqueous media can be obtained.

## Materials and Methods

### *Materials Characterization*

A Poly(ethylene oxide – terephthalate)/poly(butylene terephthalate) (PEOT/PBT) copolymer was obtained from IsoTis S.A. (Bilthoven, The Netherlands). The copolymer composition used in this study was specifically 300PEOT55PBT45 where, following an aPEOTbPBTc nomenclature, a is the molecular weight in g/mol of the starting PEG blocks used in the copolymerization, while b and c are the weight ratios of the PEOT and PBT blocks, respectively.

### *Scaffolds Design*

Three different designs were considered to evaluate the effect of the scaffold macroscopic topology on tracheal cartilage formation: cylindrical tubes (C), toroidal cylindrical tubes (T), and anatomical tracheal segments (A). The scaffolds had a lumen of approximately 5.5 mm and a wall thickness of 2.5 mm, resulting in an outer diameter of 10.5 mm. The height of the scaffolds was set to 4 cm. Cylindrical and toroidal tubes were designed with Rhinoceros® software. The Anatomical tracheal segment was obtained from a computerized tomography (CT) human dataset. The dataset was processed with Rhinoceros® software, and converted to the same format and dimensions as the other models. The models were downscaled to have approximately the same dimensions of a Lewis rat tracheal segment. The rat trachea and rat chondrocytes were chosen as a model to investigate the effect of the scaffold shape design.

### *Scaffolds Fabrication*

PEOT/PBT 3DF scaffolds were manufactured with a Bioplotter device (Envisiontec GmbH, Germany), essentially an XYZ plotter device as previously described [15, 32]. Few modifications were done to extrude highly viscous polymeric fibers. The polymers were put in a stainless steel syringe and heated at  $T = 210\text{ }^{\circ}\text{C}$  through a thermo stated cartridge unit, fixed on the “X”-mobile arm of the apparatus. When the molten phase was attained, a nitrogen pressure of 4 Bars was applied to the syringe through a pressurized cap. The scaffold models were loaded on the Bioplotter CAM (PrimCAM, Switzerland) software and deposited layer by layer, through the extrusion of the polymer on a stage as a fiber. The deposition speed was set to 240 mm/min. Scaffolds were then characterized by the fiber diameter (through the nozzle diameter), the spacing between fibers in the same layer, the layer thickness and the configuration of the deposited fibers within the whole architecture. In this study the used nozzle was a stainless steel Luer Lock needle with internal diameter (ID) of  $250\text{ }\mu\text{m}$ , shortened to a length of 16.2 mm for all the scaffold designs. The fiber spacing and the layer thickness were set at  $600\text{ }\mu\text{m}$  and at  $150\text{ }\mu\text{m}$ , respectively. This resulted in scaffolds’ porosity of 75%. Scaffolds with a lower porosity of 62% were also fabricated by decreasing the fiber spacing to  $400\text{ }\mu\text{m}$  to evaluate the influence of porosity on cell attachment and tissue formation. A 0-90 scaffold architecture was chosen, where fibers were deposited with  $90^{\circ}$  orientation steps between successive layers. Table 1 summarizes the designs and the fabrication parameters considered.

	id (mm)	th (mm)	h (mm)	T ( $^{\circ}\text{C}$ )	p (bar)	V (mm/min)	d1 ( $\mu\text{m}$ )	d2 ( $\mu\text{m}$ )	d3 ( $\mu\text{m}$ )	P (%)
C 75	4.5	2.5	40	210	4	240	$170 \pm 15$	$605 \pm 12$	$148 \pm 10$	$74.7 \pm 1.8$
VT 75										
AT 75										
C 62								$398 \pm 25$		$61.5 \pm 1.45$
VT 62										
AT 62										

**Table 1** – 3DF scaffolds geometrical and structural parameters.

### *Gas Plasma Treatment*

3DF fabricated scaffolds were argon gas plasma treated to improve cell attachment, as previously described [33]. Briefly, the samples were put in a cylindrical, radio-frequency glow-discharge chamber (Harrik Scientific Corp, USA). A vacuum of 0.01 mbar was applied to the chamber and subsequently flushed 4 times with argon (Ar, purity  $\geq 99.999\%$ , Hoekloos B.V., The Netherlands). The scaffolds were then treated under an Ar plasma (0.1-0.2 mbar) for 30 minutes.

### *Scaffolds Characterization*

Cross sections of the scaffolds were taken as samples and characterized by scanning electron microscopy (SEM) analysis with a Philips XL 30 ESEM-FEG. Samples were gold sputter (Carrington) before SEM analysis. The porosity of 3DF scaffolds was

both experimentally evaluated by liquid pycnometry and calculated from SEM measurements as described elsewhere [15, 32]:

$$P = 1 - \frac{V_{\text{scaffold}}}{V_{\text{cube}}} = 1 - \frac{\pi}{4} \cdot \frac{1}{\frac{d_2}{d_1}} \cdot \frac{1}{\frac{d_3}{d_1}} \quad (1)$$

where P is the scaffold porosity, d1 the fiber diameter, d2 the fiber spacing and d3 the layer thickness.

### ***Cell Culture***

Chondrocytes were harvested from 8-10 week old Lewis rats (pooled cells from n=4), weighing 200-250 g (Harlan, The Netherlands). Rats received human care in accordance with the "Guide for the Care and Use of Laboratory Animals" prepared by Council, and published by the National Academy Press, revised 1996. Donor anaesthesia was induced by isoflurane (Attane; Minrad inc, U.S.A.) inhalation and continued by intraperitoneal injection of 50 mg/kg sodium pentobarbital (Nembutal; Abbott Lab, U.S.A.). The animals were then euthanized by exsanguination of the great abdominal vessels, and the knee joints were resected under sterile conditions. After scraping of the articulating surfaces, chondrocytes were isolated via collagenase digestion. Cells were plated onto polystyrene cell culture flasks (Corning Inc., USA) and cultured in a humidified incubator at 37 °C with 5% CO<sub>2</sub>. Cells were trypsinized using trypsin/EDTA solution (0.05%/0.02% PAN Biotech) for 2-5 min at 37 °C and serially passaged upon reaching confluency. After the third or fourth passage the expanded chondrocytes were collected and dynamically seeded onto the scaffolds under a rotating flow at a density of 7.5 millions per scaffold. The constructs were left in the humidified incubator for 21 days (n=6). The culture medium contained HEPES (Invitrogen)-buffered DMEM (Invitrogen) supplemented with 10% fetal bovine serum (FBS, Sigma-Aldrich), 0.2 mM ascorbic acid 2-phosphate (Invitrogen), 0.1 mM non-essential amino acids (Sigma-Aldrich), 0.4 mM proline (Sigma-Aldrich), 100 units/ml penicillin (Invitrogen), and 100 µg/ml streptomycin (Invitrogen). Constructs were cultured at 37 °C in a humid atmosphere with 5% CO<sub>2</sub>. Medium was refreshed twice a week and subsets of chondrocytes were used for further subculturing or cryopreservation upon reaching near confluence.

### ***Biochemical Analysis***

3-(4,5-dimethylthiazol-2yl)-2,5-dyphenyltetrazolium bromide (MTT) and glycosaminoglycans (GAG) assays (Cyquant Assay, Invitrogen) were performed after 21 days of culture. MTT assay determines viable cells and is based on the mitochondrial conversion of the tetrazolium salt. Briefly, a modified assay was employed to quantitatively measure the viable chondrocytes growing on the scaffolds [34]. After 21 days of culture, 250 µl of medium and 20 µl of MTT

solution were added to each well, incubated at 37 °C for 1 h, and the supernatant discarded and replaced by 400  $\mu$ l isopropanol with 10% formic acid. Samples were incubated at 37 °C for an additional 5 min, vortexed for 10 min, and the MTT absorbency values of the resulting solution measured using an ELISA reader (Dynatech, Billingham, UK) at a wavelength of 570 nm.

GAG amount was determined spectrophotometrically (EL 312e Bio-TEK Instruments) after reaction with dimethylmethylene blue dye (DMMB, Sigma-Aldrich) by measuring absorbance at 520 nm. Samples were previously digested with papain type III (Sigma) solution (25 mg/ml) containing 0.1 M  $\text{NaH}_2\text{PO}_4$ , 5mM EDTA, 5mM cysteine HCL at 56 °C for 15 h. The final amount was calculated using a standard of chondroitin sulphate B (Sigma-Aldrich).

Statistical Analysis was performed using a Student's t-test (SPSS 8.0 software), where the confidence level was set to 0.05 for statistical significance. Values in this study are reported as mean and standard deviation.

### *Tissue Morphology Analysis*

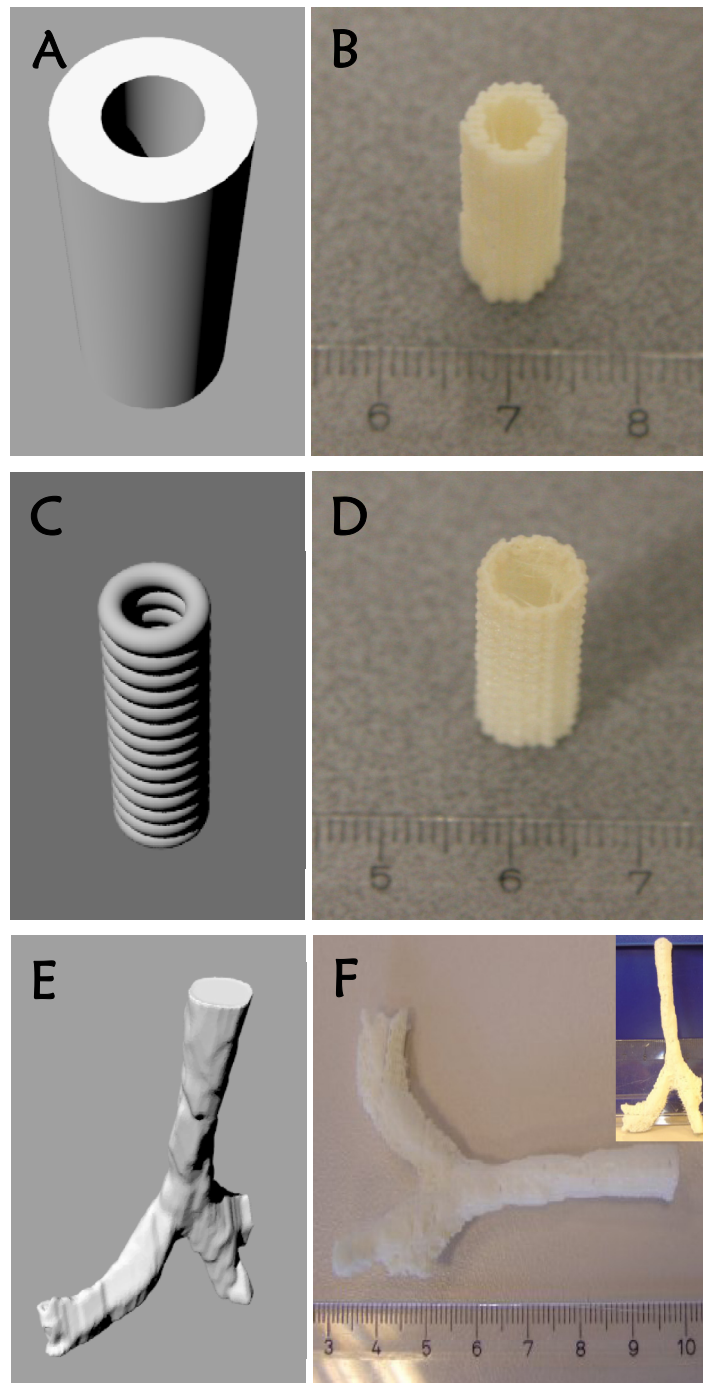
Constructs were analyzed by SEM to detect cell distribution and attachment, and extra cellular matrix formation. Samples were fixed overnight in 0.14 M cacodylate buffer (pH = 7.2 – 7.4) containing 0.25% glutaraldehyde (Merck). Scaffolds were subsequently dehydrated in sequential ethanol series, and critical point dried from liquid carbon dioxide using a Balzers CPD 030 machine. Samples were then gold sputtered prior SEM Analysis.

## Results

### *Scaffolds Characterization*

3DF tubular scaffolds with cylindrical, toroidal, and anatomical designs were successfully fabricated. Figure 1 presents a comparison between the designed models and the fabricated scaffolds. In the particular case of the anatomical scaffolds, although the tracheo-bronchial tree with both left and right main bronchus was also prototyped, only the tracheal part reaching from the sub-glottic to the pre-carinal region was used (comprising 4 cm of length).

SEM analysis revealed a significant consistency between the theoretical and real values of fiber diameter, fiber spacing, and layer thickness for all the scaffolds processed. Figure 2 shows the square pore architecture of the surface and of the cross section. The fiber diameter  $d_1$  was measured as  $170 \pm 15 \mu\text{m}$ . The fiber spacing  $d_2$  was  $605 \pm 12 \mu\text{m}$ , while the layer thickness  $d_3$  was  $148 \pm 10 \mu\text{m}$ . This corresponded to a scaffold porosity of  $74.7 \pm 1.8\%$ . The calculated porosities were similar to the values experimentally measured by liquid pycnometry. In this case, the porosity was  $79.2 \pm 0.06\%$  for the cylindrical tubes,  $78.49 \pm 0.63\%$  for the toroidal ones, and  $78.79 \pm 0.26\%$  for the anatomical scaffolds. When the set fiber



Anatomical  
3DF Scaffolds

**Figure 1** – 3DF scaffold designs (a, c, e) and corresponding fabricated prototypes (b, d, f). In the case of the anatomical scaffold (e, f) tubular tracheal segments with the same dimensions as the cylindrical (a, b) and the toroidal (c, d) scaffolds were considered by removing the bronchial bifurcation.

spacing was decreased to  $400\ \mu\text{m}$ , the measured value was  $398 \pm 25\ \mu\text{m}$ , resulting in a scaffold porosity of  $61.5 \pm 1.45\%$ . All the scaffolds produced had almost completely interconnected pores and no layer delamination phenomena occurred. However, an increasing amount of local imperfections with increasing of scaffold complexity was noticed and consisted in the production of thin fibers, which were produced at the end of each layer when the nozzle moved back to the starting position for the deposition of the successive layer.

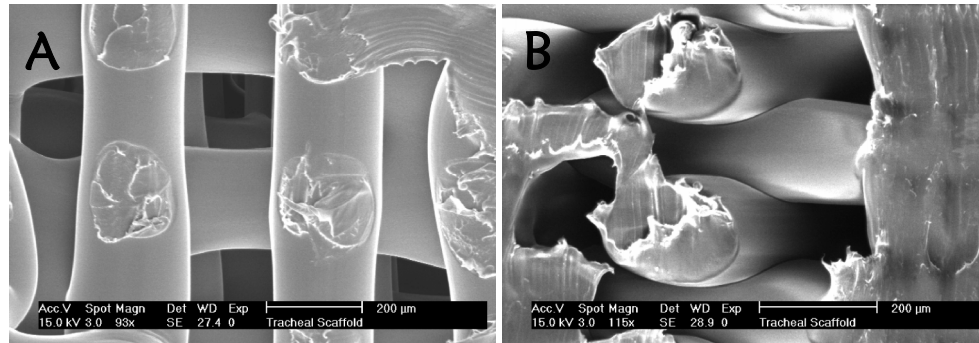


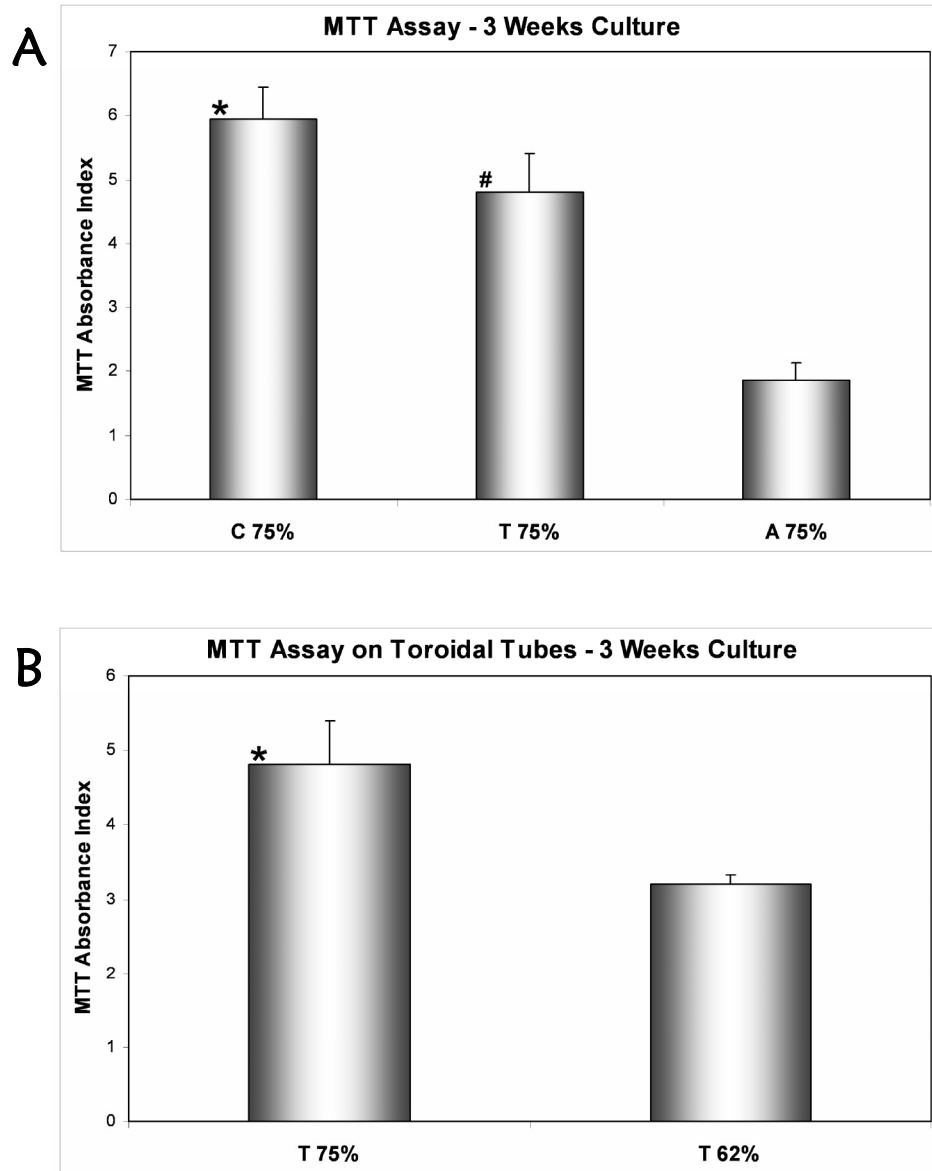
**Figure 2** – SEM micrographs of the surface (a) and of the cross section (b) of 3DF scaffolds. Scale bar:  $200\ \mu\text{m}$ .

### *Tissue Formation*

After 3 weeks of culture in the designed 3DF tracheal scaffolds, the MTT activity and the GAG formation were measured. Figure 3 shows the MTT activity for different scaffolds geometry (fig. 3A) and for different porosities (Fig. 3B). Interestingly, the MTT absorbance level significantly decreased from the cylindrical design to the toroidal and to the anatomical ones, suggesting a different cell attachment and cell entrapment efficiency of the scaffolds depending from their geometry. MTT activity was measured as  $5.95 \pm 0.5$  for the cylindrical tubes,  $4.8 \pm 0.6$  for the toroidal tubes, and  $1.86 \pm 0.28$  for the anatomical tubes. When scaffolds with the same shape but different porosities were considered, a significantly decrease of the MTT index was measured with decreasing porosity. For instance, in the case of the toroidal tubes the index decreased from  $4.8 \pm 0.6$  to  $3.21 \pm 0.12$ .

Even more interestingly, GAG formation significantly increased for the anatomical scaffold as compared to the cylindrical and the toroidal constructs, as shown in figure 4. GAG was  $37.72 \pm 11.36\ \mu\text{g}$  for the cylindrical tubes,  $43.02 \pm 7.13\ \mu\text{g}$  for the toroidal tubes, and  $133.14 \pm 27.94\ \mu\text{g}$  for the anatomical tubes (fig. 4A). Analogously, with decreasing porosity but same scaffold shape GAG production increased. Albeit not significantly, GAG formation increased from  $43.02 \pm 7.13\ \mu\text{g}$  to  $53.52 \pm 11.88\ \mu\text{g}$  with decreasing the porosity of toroidal tubes. The higher level of GAG formation in anatomical scaffolds and in lower porous scaffolds was also accompanied to a higher degree of differentiation towards cartilage tissue. In fact, higher GAG/MTT was found as presented in figure 5. Specifically, GAG/MTT

increase from  $6 \pm 1.5 \mu\text{g}$  for cylindrical scaffolds, to  $8.3 \pm 1.4 \mu\text{g}$  for toroidal scaffolds, to  $70.9 \pm 15.7 \mu\text{g}$  for anatomical scaffolds. With decreasing porosity GAG/MTT increased from  $8.3 \pm 1.5 \mu\text{g}$  to  $17.9 \pm 4.5 \mu\text{g}$  for toroidal scaffolds.



Anatomical  
3DF Scaffolds

**Figure 3** – MTT assay after 3 weeks of culture for the different scaffolds design (a) and for the two scaffold's porosity (b) considered. (\*) shows significant differences as compared to T 75% and A 75% for different designs, and to T 62% for different porosities. (#) illustrates significant differences as compared to A 75%.

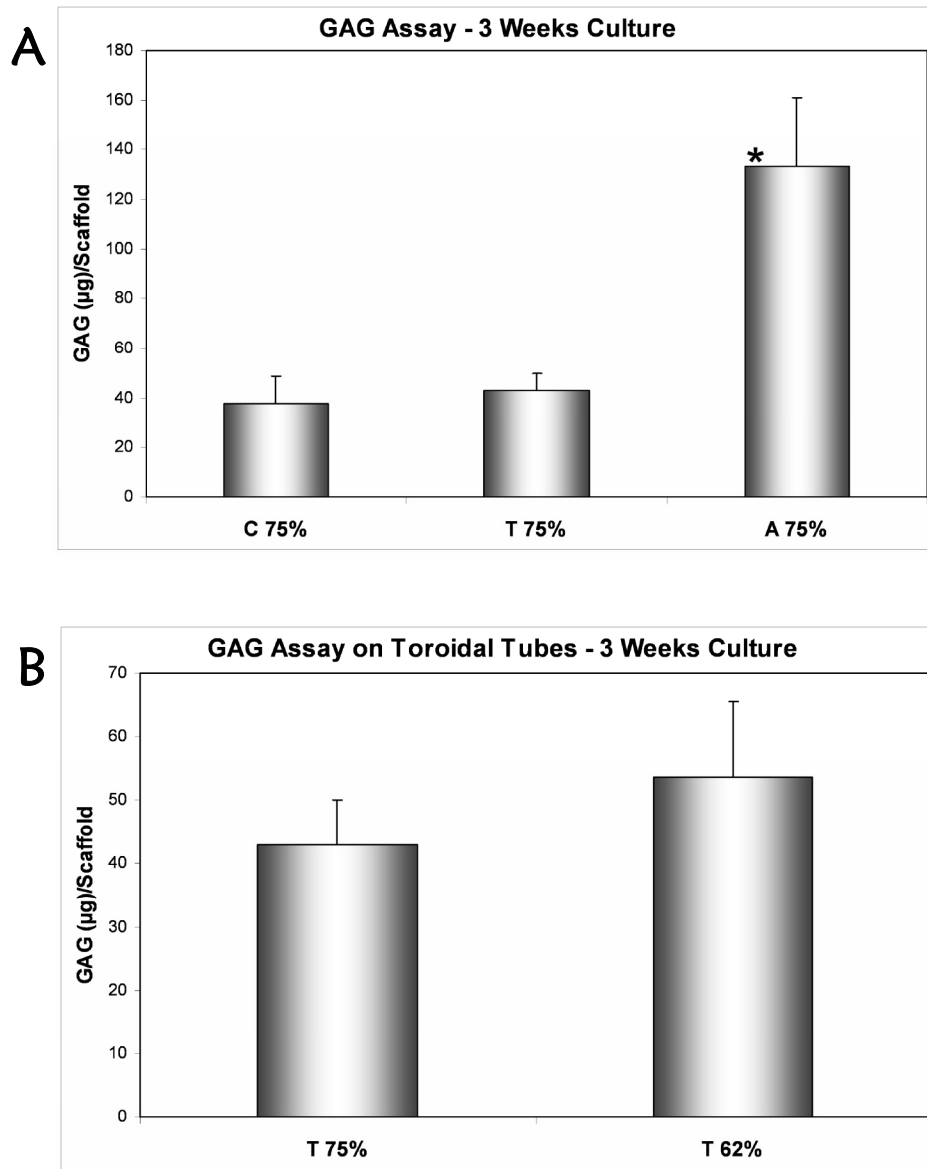


**Figure 4** – GAG assay after 3 weeks of culture for the different scaffolds design (a) and for the two scaffold's porosity (b) considered. (\*) shows significant differences with respect to C 75% and T 75%.

A qualitative confirmation of cell attachment and extra cellular matrix formation was detected by SEM analysis, as shown in figure 6. Chondrocytes attached and spread on all of the scaffolds considered and covered the whole surface of the tubular constructs. More rounded-shape cells were observed on anatomical scaffolds as compared to cylindrical and toroidal tubes (Figures 6D and 6E),



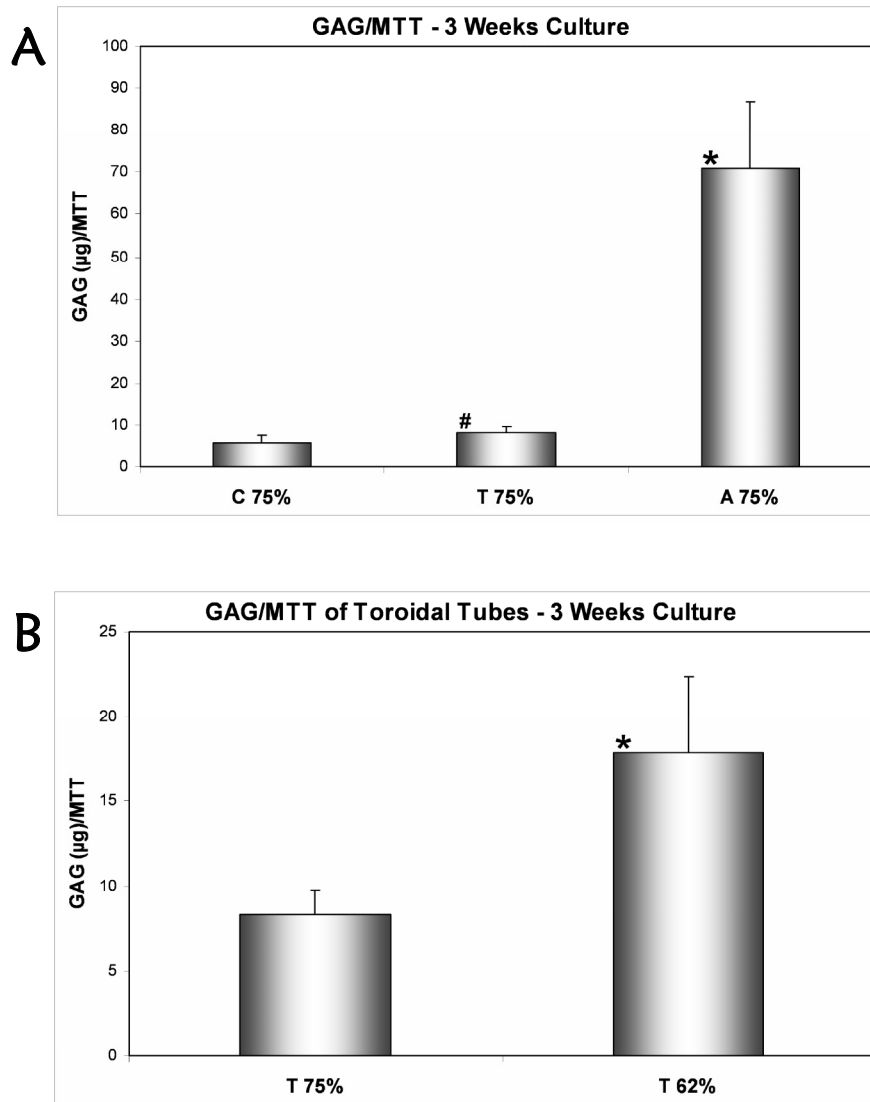


**Figure 5** – GAG/MTT ratio after 3 weeks of culture for the different scaffolds design (a) and for the two scaffold's porosity (b) considered. (\*) shows significant differences with respect to A 75% for different designs and to T 62% for different porosities.

which might suggest a higher cell differentiation. This was also associated with an increasing amount of thin fibers due to the repositioning of the nozzle at the end of each deposited layer to start the deposition of the next one, as previously described. As shown in figure 6F, extracellular matrix formation was detected. In particular, a fibrillar network could be observed. Fibrils bundles varied from 75 nm to 225 nm in diameter with an average of  $130 \pm 46$  nm and might be associated to collagen production.

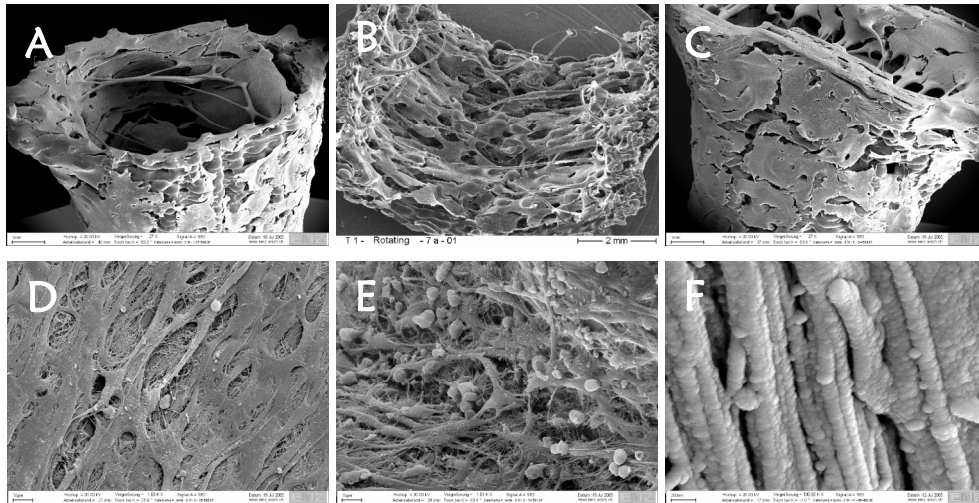


**Figure 6** – SEM micrographs illustrating the homogeneous coverage of 3DF scaffolds both on the inner and on the outer surface (a, b, c). Chondrocytes were slightly less spread on anatomical scaffolds (e) than on cylindrical or toroidal ones (d). Extra cellular matrix fibril formation was detected (f). (a, c) scale bar: 1 mm; (b) scale bar: 2 mm; (d, e) scale bar: 10 μm; (f) scale bar: 200 nm.

## Discussion

In the present study, we focused on the influence of the scaffold design on the reconstruction of the cartilage portion of a tracheal segment. A number of different designed 3DF scaffolds have been fabricated and the effect of the design evaluated for tracheal cartilage regeneration. Scaffolds showed an optimal resemblance as compared to the models. This is rather important for a complicated geometry like a three-dimensional anatomical trachea, whose model was obtained from a CT scan of a patient. Ultimately, provided the effectiveness of a CT/MRI anatomical model being better as compared to other scaffold design solutions, a custom-made and patient-dedicated scaffold could be envisioned and used to tissue engineer a specific tissue to regenerate [13]. Very interestingly, when tracheal rat chondrocytes were cultured to assess the influence of the scaffold design on tissue regeneration, a significant higher extracellular matrix production (sulphated GAGs) was measured for the anatomical model as compared to the toroidal and to the more simple cylindrical tubular structures. This was also accompanied by a significantly smaller amount of cells and, consequently, by a better cell differentiation degree as shown by the GAG/MTT ratio. It is possible that the increase in complexities and irregularities of the tubular structure of the scaffolds (figure 7) resulted in a more heterogeneous cell distribution due to shadow areas that are not reached by cells for attachment. This possibly implied the creation of local niches in the scaffolds where enhanced cell-cell contact would trigger a much higher production of extracellular matrix. Furthermore, the presence of thin fibers, formed during the relocation of the cartridge at the end of each deposited layer, resulted in an

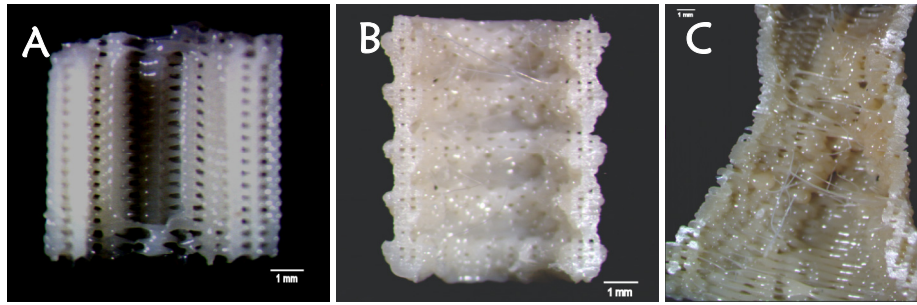


**Figure 7** – Optical microscopy pictures showing the internal structural geometry of the scaffolds for the (a) cylindrical, (b) toroidal, and (c) anatomical designs. Scale bar: 1 mm.

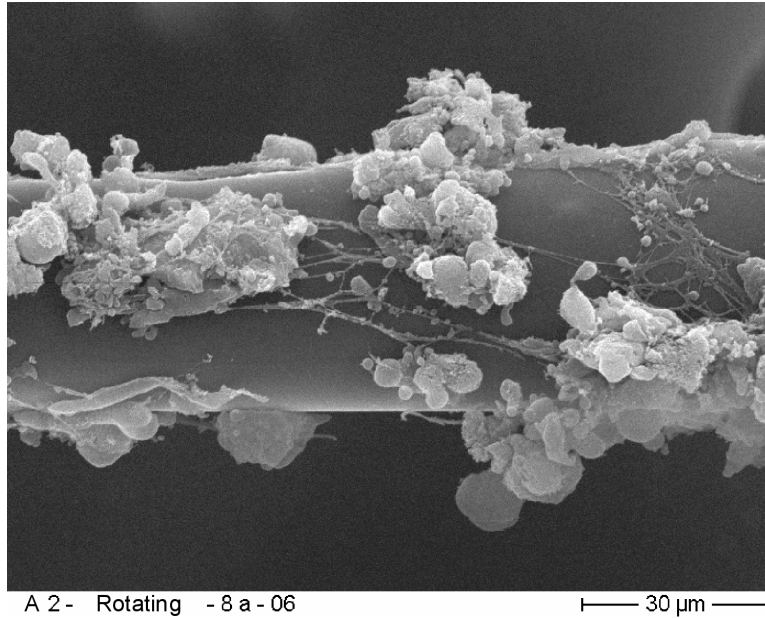


**Figure 8** – SEM micrograph showing rounded cells on thin fibers derived from resolution limitations during the movement of the nozzle at the end of a layer and before the deposition of the successive one. Scale bar: 30  $\mu\text{m}$ .

increasing amount of local imperfections with increasing of scaffold complexity. These fibers were found to be covered by more rounded cells, embedded in extracellular matrix (figure 8), as qualitatively analyzed by SEM. Specifically, a higher degree of chondrocyte differentiation in anatomical scaffolds was detected by SEM analysis, where a qualitatively higher number of cells appeared to have a rounded morphology (figure 6E). Moreover, fibril production was clearly visible and might give an indication of collagen fiber bundles formed by the cells. Collagen fibrils and fibril bundles of hyaline cartilage have been also analyzed extensively with SEM by Hughes *et al.* [35] in mice with similar structural characteristics and orientation. Furthermore, collagen type I and type II were shown to be detected when

chondrocytes were seeded and cultured on similar 3DF or compression molded scaffolds [11, 36, 37].

When scaffolds with a lower pore volume and, therefore, with a lower porosity were considered, a smaller amount of cells was measured. This was accompanied by a higher, although not significant, amount of GAG formed all over the scaffolds, and by a significantly higher GAG/MTT ratio. These findings are in contrast with one of the mainstays in scaffolding for tissue engineer applications. Scaffolds are normally intended to have a high porosity to improve nutrient flow and cell migration in the center of the construct. In “conventional” scaffolds - where conventional refers to fabrication techniques where the pores’ volume and shape is randomly generated and not controlled - nutrient supply is a major limitation for the success of the regenerated tissue due to the tortuosity of the pores, which might end in closed or partly closed cavities [17, 36]. This would result in cell death where nutrient flow is scarce or missing. In rapid prototyped scaffolds such a problem is partially solved or improved, as the periodicity and complete interconnectivity of the pore network induces a considerably better perfusion of the constructs [16]. Therefore, in these structures high porosity is not anymore a determinant for the success of the tissue regeneration as long as all the pores are large enough to be accessible for cells and for their nutrients. In this respect, a lower scaffolds pore volume and porosity resulted in a higher detailed resolution of the complex geometrical structure. This could offer more locations in the scaffolds where cell-cell contact could take place and stimulate more ECM production all over the constructs.

Several other studies have attempted to regenerate tracheal segments [38-46], and only few of these seems to have successfully reconstructed a functional part [39, 45, 46]. Trachea is a hierarchical tissue comprised of cartilage and mucosa. The success of a tissue engineered trachea strongly depends on the degree of epithelialization [39, 45]. A poor epithelialization might lead to stenosis of the construct and subsequent failure of the implant. In this respect, the compliability of the scaffold is also important to allow tissue deformation during movement and at the same time to prevent stenosis. In this study, epithelial cells were not co-cultured together with chondrocytes. Therefore, no conclusion can be drawn on the functionality of the engineered cartilage tracheal constructs here treated. Still, from the obtained results it seems that not only the scaffold structure, but also the scaffold design plays a role on tissue formation. If the scaffold structure can be ultimately related to the pore size and volume, its design is connected to the pore arrangement within the construct. Furthermore, PEOT/PBT scaffolds were seeded with different connective tissues in previously studies and were shown to support cell attachment, proliferation, and tissue formation [47, 48]. These results are encouraging for further studies, where epithelial and chondrocytes co-culture will be investigated on PEOT/PBT 3DF anatomical scaffolds and implanted *in vivo* to assess the functionality of such a complete construct. Moreover, the flexibility in scaffold design offered by a rapid prototyping technology like three dimensional fiber deposition gives the possibility to fine-tune the mechanical properties of the scaffold [7, 49] so that a compliant anatomical construct can be fabricated optimizing the risks for stenosis.

## Conclusions

The influence of 3DF scaffold design on cartilage formation for a tissue engineered trachea was investigated. After 3 weeks of culture, anatomically shaped scaffolds fabricated from a CT scan showed to support a smaller amount of cells, but more GAG production and a higher GAG/MTT ratio. SEM analysis revealed collagen fibril formation and full coverage of the scaffolds. From these results it appears that complex anatomically shaped scaffolds fabricated from real dataset of patients may very well be preferable over simple highly modeled designs in spite of and maybe even due to the inevitable higher degree of structural imperfections. Yet, anatomical scaffolds showed to support satisfactory tissue development for tracheal cartilage reconstruction and should be further considered for other tissue engineering applications.

## Acknowledgements

We are grateful to Dr. Riesle for critical review of the manuscript.

## References

- [1] Hutmacher DW, Sittering M, Risbud MV. Scaffold-based tissue engineering: rationale for computer-aided design and solid free-form fabrication systems. *Trends Biotechnol* 2004;22(7):354-62.
- [2] Yeong WY, Chua CK, Leong KF, Chandrasekaran M. Rapid prototyping in tissue engineering: challenges and potential. *Trends Biotechnol* 2004;22(12):643-52.
- [3] Yan Y, Xiong Z, Hu Y, Wang S, Zhang R, Zhang C. Layered manufacturing of tissue engineering scaffolds via multi-nozzle deposition. *Materials Letters* 2003;57:2623-2628.
- [4] Kim SS, Utsunomiya H, Koski JA, Wu BM, Cima MJ, Sohn J, Mukai K, Griffith LG, Vacanti JP. Survival and function of hepatocytes on a novel three-dimensional synthetic biodegradable polymer scaffold with an intrinsic network of channels. *Ann Surg* 1998;228(1):8-13.
- [5] Hutmacher DW, Schantz T, Zein I, Ng KW, Teoh SH, Tan KC. Mechanical properties and cell cultural response of polycaprolactone scaffolds designed and fabricated via fused deposition modeling. *J Biomed Mater Res* 2001;55(2):203-16.
- [6] Landers R, Hubner U, Schmelzeisen R, Mulhaupt R. Rapid prototyping of scaffolds derived from thermoreversible hydrogels and tailored for applications in tissue engineering. *Biomaterials* 2002;23:4437-47.
- [7] Moroni L, de Wijn JR, van Blitterswijk CA. Three-dimensional fiber-deposited PEOT/PBT copolymer scaffolds for tissue engineering: Influence of porosity, molecular network mesh size, and swelling in aqueous media on dynamic mechanical properties. *J Biomed Mater Res A* 2005;75:957-965.
- [8] Taboas JM, Maddox RD, Krebsbach PH, Hollister SJ. Indirect solid free form fabrication of local and global porous, biomimetic and composite 3D polymer-ceramic scaffolds. *Biomaterials* 2003;24(1):181-94.

- [9] Sherwood JK, Riley SL, Palazzolo R, Brown SC, Monkhouse DC, Coates M, Griffith LG, Landeen LK, Ratcliffe A. A three-dimensional osteochondral composite scaffold for articular cartilage repair. *Biomaterials* 2002;23(24):4739-51.
- [10] Schantz JT, Brandwood A, Hutmacher DW, Khor HL, Bittner K. Osteogenic differentiation of mesenchymal progenitor cells in computer designed fibrin-polymer-ceramic scaffolds manufactured by fused deposition modeling. *J Mater Sci Mater Med* 2005;16(9):807-19.
- [11] Woodfield TB, Van Blitterswijk CA, De Wijn J, Sims TJ, Hollander AP, Riesle J. Polymer scaffolds fabricated with pore-size gradients as a model for studying the zonal organization within tissue-engineered cartilage constructs. *Tissue Eng* 2005;11(9-10):1297-311.
- [12] Seitz H, Rieder W, Irsen S, Leukers B, Tille C. Three-dimensional printing of porous ceramic scaffolds for bone tissue engineering. *J Biomed Mater Res B Appl Biomater* 2005;74(2):782-8.
- [13] Hollister SJ. Porous scaffold design for tissue engineering. *Nat Mater* 2005;4(7):518-24.
- [14] Lin CY, Kikuchi N, Hollister SJ. A novel method for biomaterial scaffold internal architecture design to match bone elastic properties with desired porosity. *J Biomech* 2004;37(5):623-36.
- [15] Moroni L, de Wijn JR, van Blitterswijk CA. 3D fiber-deposited scaffolds for tissue engineering: Influence of pores geometry and architecture on dynamic mechanical properties. *Biomaterials* 2006;27:974-985.
- [16] Malda J, Woodfield TB, van der Vloodt F, Kooy FK, Martens DE, Tramper J, van Blitterswijk CA, Riesle J. The effect of PEGT/PBT scaffold architecture on oxygen gradients in tissue engineered cartilaginous constructs. *Biomaterials* 2004;25(26):5773-80.
- [17] Sachlos E, Czernuszka JT. Making tissue engineering scaffolds work. Review: the application of solid freeform fabrication technology to the production of tissue engineering scaffolds. *Eur Cell Mater* 2003;5:29-39; discussion 39-40.
- [18] Antonov EN, Bagratashvili VN, Whitaker MJ, Barry JJA, Shakesheff KM, Kononov AN, Popov VK, Howdle SM. Three-Dimensional Bioactive and Biodegradable Scaffolds Fabricated by Surface-Selective Laser Sintering. *Adv Mater* 2005;17:327-330.
- [19] Gratson GM, Xu M, Lewis JA. Microperiodic structures: direct writing of three-dimensional webs. *Nature* 2004;428(6981):386.
- [20] Vozzi G, Flaim C, Ahluwalia A, Bhatia S. Fabrication of PLGA scaffolds using soft lithography and microsyringe deposition. *Biomaterials* 2003;24(14):2533-40.
- [21] Hollister SJ, Maddox RD, Taboas JM. Optimal design and fabrication of scaffolds to mimic tissue properties and satisfy biological constraints. *Biomaterials* 2002;23(20):4095-103.
- [22] Yang S, Leong KF, Du Z, Chua CK. The design of scaffolds for use in tissue engineering. Part II. Rapid prototyping techniques. *Tissue Eng* 2002;8(1):1-11.
- [23] van Blitterswijk CA, van den Brink J, Leenders H, Bakker D. The effect of PEO ratio on degradation, calcification and bone bonding of PEO/PBT copolymer (PolyActive). *Cell and Materials* 1993;3:23-26.

- [24] Beumer GJ, van Blitterswijk CA, Ponec M. Degradative behaviour of polymeric matrices in (sub)dermal and muscle tissue of the rat: a quantitative study. *Biomaterials* 1994;15(7):551-9.
- [25] Beumer GJ, van Blitterswijk CA, Ponec M. Biocompatibility of a biodegradable matrix used as a skin substitute: an in vivo evaluation. *J Biomed Mater Res* 1994;28(5):545-52.
- [26] Bakker D, van Blitterswijk CA, Hesseling SC, Grote JJ. Effect of implantation site on phagocyte/polymer interaction and fibrous capsule formation. *Biomaterials* 1988;9(1):14-23.
- [27] Bulstra SK, Geesink RG, Bakker D, Bulstra TH, Bouwmeester SJ, van der Linden AJ. Femoral canal occlusion in total hip replacement using a resorbable and flexible cement restrictor. *J Bone Joint Surg Br* 1996;78(6):892-8.
- [28] Mensik I, Lamme EN, Riesle J, Brychta P. Effectiveness and Safety of the PEGT/PBT Copolymer Scaffold as Dermal Substitute in Scar Reconstruction Wounds (Feasibility Trial). *Cell Tissue Bank* 2002;3(4):245-53.
- [29] Deschamps AA, Claase MB, Sleijster WJ, de Bruijn JD, Grijpma DW, Feijen J. Design of segmented poly(ether ester) materials and structures for the tissue engineering of bone. *J Control Release* 2002;78(1-3):175-86.
- [30] Bezemer JM, Grijpma DW, Dijkstra PJ, van Blitterswijk CA, Feijen J. A controlled release system for proteins based on poly(ether ester) block-copolymers: polymer network characterization. *J Control Release* 1999;62(3):393-405.
- [31] van Dijkhuizen-Radersma R, Peters FL, Stienstra NA, Grijpma DW, Feijen J, de Groot K, Bezemer JM. Control of vitamin B12 release from poly(ethylene glycol)/poly(butylene terephthalate) multiblock copolymers. *Biomaterials* 2002;23(6):1527-36.
- [32] Landers R, Pfister A, Hubner U, John H, Schmelzeisen R, Mullhaupt R. Fabrication of soft tissue engineering scaffolds by means of rapid prototyping techniques. *Journal of materials science* 2002;37:3107-3116.
- [33] Woodfield TB, Miot S, Martin I, van Blitterswijk CA, Riesle J. The regulation of expanded human nasal chondrocyte re-differentiation capacity by substrate composition and gas plasma surface modification. *Biomaterials* 2005.
- [34] Zund G, Ye Q, Hoerstrup SP, Schoeberlein A, Schmid AC, Grunenfelder J, Vogt P, Turina M. Tissue engineering in cardiovascular surgery: MTT, a rapid and reliable quantitative method to assess the optimal human cell seeding on polymeric meshes. *Eur J Cardiothorac Surg* 1999;15(4):519-24.
- [35] Hughes LC, Archer CW, ap Gwynn I. The ultrastructure of mouse articular cartilage: collagen orientation and implications for tissue functionality. A polarised light and scanning electron microscope study and review. *Eur Cell Mater* 2005;9:68-84.
- [36] Malda J, Woodfield TB, van der Vloodt F, Wilson C, Martens DE, Tramper J, van Blitterswijk CA, Riesle J. The effect of PEGT/PBT scaffold architecture on the composition of tissue engineered cartilage. *Biomaterials* 2005;26(1):63-72.
- [37] Suh SW, Kim J, Baek CH, Kim H. Development of new tracheal prosthesis: autogenous mucosa-lined prosthesis made from polypropylene mesh. *Int J Artif Organs* 2000;23(4):261-7.

- [38] Suh SW, Kim J, Baek CH, Han J, Kim H. Replacement of a tracheal defect with autogenous mucosa lined tracheal prosthesis made from polypropylene mesh. *Asaio J* 2001;47(5):496-500.
- [39] Ziegelaar BW, Aigner J, Staudenmaier R, Lempart K, Mack B, Happ T, Sittinger M, Endres M, Naumann A, Kastenbauer E, Rotter N. The characterisation of human respiratory epithelial cells cultured on resorbable scaffolds: first steps towards a tissue engineered tracheal replacement. *Biomaterials* 2002;23(6):1425-38.
- [40] Yang L, Korom S, Welti M, Hoerstrup SP, Zund G, Jung FJ, Neuenschwander P, Weder W. Tissue engineered cartilage generated from human trachea using DegraPol scaffold. *Eur J Cardiothorac Surg* 2003;24(2):201-7.
- [41] Rotter N, Stolzel K, Endres M, Leinhase I, Ziegelaar BW, Sittinger M. Towards engineering of a tracheal equivalent: identification of epithelial precursor cells, differentiation and cocultivation techniques. *Med J Malaysia* 2004;59 Suppl B:35-6.
- [42] Kojima K, Vacanti CA. Generation of a tissue-engineered tracheal equivalent. *Biotechnol Appl Biochem* 2004;39(Pt 3):257-62.
- [43] Kojima K, Igotz RA, Kushibiki T, Tinsley KW, Tabata Y, Vacanti CA. Tissue-engineered trachea from sheep marrow stromal cells with transforming growth factor beta2 released from biodegradable microspheres in a nude rat recipient. *J Thorac Cardiovasc Surg* 2004;128(1):147-53.
- [44] Kim J, Suh SW, Shin JY, Kim JH, Choi YS, Kim H. Replacement of a tracheal defect with a tissue-engineered prosthesis: early results from animal experiments. *J Thorac Cardiovasc Surg* 2004;128(1):124-9.
- [45] Kamil SH, Eavey RD, Vacanti MP, Vacanti CA, Hartnick CJ. Tissue-Engineered Cartilage as a Graft Source for Laryngotracheal Reconstruction. *Arch Otolaryngol Head Neck Surg* 2005;130:1048-1051.
- [46] Wang H, Pieper J, Peters F, van Blitterswijk CA, Lamme EN. Synthetic scaffold morphology controls human dermal connective tissue formation. *J Biomed Mater Res A* 2005;74(4):523-32.
- [47] van den Bogaardt AJ, Ulrich MM, van Galen MJ, Reijnen L, Verkerk M, Pieper J, Lamme EN, Middelkoop E. Upside-down transfer of porcine keratinocytes from a porous, synthetic dressing to experimental full-thickness wounds. *Wound Repair Regen* 2004;12(2):225-34.
- [48] Moroni L, Poort G, Van Keulen F, de Wijn JR, van Blitterswijk CA. Dynamic mechanical properties of 3D fiber-deposited PEOT/PBT scaffolds: An experimental and numerical analysis. *J Biomed Mater Res A* 2006(78):605-614.





Unravel the influence of fiber  
dimensions and texture on cell faith  
and on release of incorporated  
compounds

Always do what you are afraid to do

Ralph Waldo Emerson (1803 – 1882)



# Chapter 7

## Fiber Diameter and Texture of Electrospun PEOT/PBT Scaffolds Influence Human Mesenchymal Stem Cell Proliferation and Morphology, and the Release of Incorporated Compounds

L. Moroni <sup>a,\*</sup>, R. Licht <sup>a</sup>, J. de Boer <sup>a</sup>, J.R. de Wijn <sup>a</sup>, C.A. van Blitterswijk <sup>a</sup>

<sup>a,\*</sup> Institute for BioMedical Technology (BMTI), University of Twente, P.O. Box 217, 7500 AE Enschede, The Netherlands. E-mail: l.moroni@tnw.utwente.nl

### Abstract

Electrospinning (ESP) has lately shown a great potential as a novel scaffold fabrication technique for tissue engineering. Scaffolds are produced by spinning a polymeric solution in fibers through a spinneret connected to a high voltage electric field. The fibers are then collected on a support, where the scaffold is created. Scaffolds can be of different shapes, depending on the collector geometry, and have high porosity and high surface per volume ratio, since the deposited fibers vary from the microscale to the nanoscale range. Such fibers are quite effective in terms of tissue regeneration, as cells can bridge the scaffold pores and fibers, resulting in a fast and homogeneous tissue growth. Furthermore, fibers can display a nanoporous ultrastructure due to solvent evaporation. The aim of this study was to characterize electrospun scaffolds from poly(ethylene oxide terephthalate)-poly(butylene terephthalate) (PEOT/PBT) copolymers and to unravel the mechanism of pore formation on the fibers. The effect of different fiber diameters and of their surface nanotopology on cell seeding, attachment and proliferation was studied. Smooth fibers with diameter of 10  $\mu\text{m}$  were found to support an optimal cell seeding and attachment within the micrometer range analyzed. Moreover, a nanoporous surface significantly enhanced cell proliferation and cells spreading on the fibers. The fabrication of ESP scaffolds with incorporated dyes with different molecular dimensions is also reported and their release measured. These findings contribute to the field of cell-material interaction and lead to the fabrication of “smart” scaffolds which can direct cells morphology and proliferation, and eventually release biological signals to properly conduct tissue formation.

**Keywords:** Electrospinning, nanoporosity, cell attachment, cell morphology, drug release.

## Introduction

Electrospinning is a relatively old technique used in polymer technology to spin small diameter fibers [1-3], which has recently found applications in tissue engineering as a scaffold fabrication tool [4-7]. It consists of spinning fibers from a material solution, typically a polymer, by exploiting a high electric field generated between the solution depot and a collector unit. Depending on the thickness of the fibrous network deposited on the collector, it is possible to fabricate bi-dimensional or three-dimensional structures that can be used to entrap and release drugs, and/or to seed and culture cells for a specific tissue regeneration. The particular small dimension of the spun fibers, typically in the same range of extra cellular matrix (ECM) fibers, makes these structures appealing as they can mimic ECM and possibly influence cells to express the proper proteins and signals. Surface micro- and nano porosity is also another important characteristic of fibrous scaffolds. This contributes to the creation of a better milieu for the cells to express a correct ECM formation [8-10]. In this respect, electrospinning is an intriguing fabrication method, as the spun fibers can either be made porous [4, 11] or non porous [4, 12], depending on the chemical properties of the solvent used and on the device settings.

The chemistry of a scaffold plays a crucial role for drug release and tissue formation as well. Depending on the affinity between the biomaterial chemical structure and the drug, its release profile changes [13, 14]. Cell attachment and morphology is also affected by the chemical structure of the material. For instance, a higher surface energy (hydrophilic) material typically results in a higher number of attached cells, with a spread out and spindle-like shape; in contrast, a lower surface energy (hydrophobic) material reduces cell attachment and leads to a rounded morphology [15, 16]. In this respect, copolymers of poly(ethylene oxide terephthalate)-poly(butylene terephthalate) (PEOT/PBT) are versatile biomaterials, because of their controllable surface energies [17]. These polyether-ester multiblock copolymers belong to a class of materials known as thermoplastic elastomers which display good physical properties like elasticity, strength and toughness, in combination with easy processing. These properties result mainly from a phase-separated morphology of the copolymers, in which soft, hydrophilic PEO segments at environmental temperatures are physically cross-linked by the presence of hard, semi crystalline PBT segments. In contrast to chemically cross-linked materials, these cross-links are reversible and will be disrupted at temperatures above their glass transition- or melting-point which gives the material its good handling properties. By controlling the PEOT/PBT ratio, the characteristic dimension (mesh size) of the molecular network can be varied to obtain polymers with a broad range of surface energies [17, 18], swellability [17, 19], and, consequently, mechanical properties [19, 20]. This class of polymers have been extensively investigated for *in vitro* and *in vivo* biocompatibility [17, 21, 22] and used in clinical applications (PolyActive™, IsoTis OrthoBiologics S.A.) as cement stoppers and bone fillers in orthopedic surgery [23, 24]. Being polyether-esters, degradation occurs in aqueous media, by hydrolysis and oxidation, at a rate that varies from very low for high PBT contents to medium and high for larger contents of PEOT and longer PEO segments [17, 25].

The aim of this study was to characterize electrospun scaffolds of a PEOT/PBT copolymer in order to assess their possible use as constructs for tissue engineering and controlled drug release applications. 300PEOT55PBT45 was selected because it showed to promote different cells attachment [26-29] and to have a medium surface energy (contact angle of  $48 \pm 1^\circ$ ) [17]. For these purposes scaffolds with different fiber diameter and fiber morphology have been made and selected to investigate their influence on cell attachment and proliferation. Furthermore, a number of dyes have been incorporated in the polymer solution and their release studied as a model to show the possible use of these fibrous networks as drug delivery systems.

## Materials and Methods

### *Materials Characterization*

Poly(ethylene oxide – terephthalate)/poly(butylene terephthalate) (PEOT/PBT) copolymers were obtained from IsoTis S.A. (Bilthoven, The Netherlands). Following an aPEOTbPBTc classification, the composition used in this study was 300PEOT55PBT45 where, a is the molecular weight in g/mol of the starting PEG blocks used in the copolymerization, while b and c are the weight ratios of the PEOT and PBT blocks, respectively.

300PEOT55PBT45 was dissolved in different solvents to study their effect on the fibers in terms of pore formation, size and shape. Different weight/volume (w/v) concentrations were also analyzed to investigate the influence on fibers dimension and scaffolds porosity. All the solvents were purchased from Sigma-Aldrich. In particular, chloroform ( $\text{CHCl}_3$ , boiling point  $T = 62^\circ\text{C}$ ), dichloromethane ( $\text{CH}_2\text{Cl}_2$ , boiling point  $T = 40^\circ\text{C}$ ), dichloroethane ( $\text{CH}_2\text{Cl}\cdot\text{CH}_2\text{Cl}$ , boiling point  $T = 82\text{-}84^\circ\text{C}$ ), dioxane ( $\text{C}_4\text{H}_8\text{O}_2$  boiling point  $T = 101^\circ\text{C}$ ), and two mixtures of chloroform with hexafluoroisopropanol (HFIP, boiling point  $T = 58^\circ\text{C}$ ) (78%/22% v/v and 90%/10% v/v), and of chloroform with methanol ( $\text{CH}_3\text{OH}$ , boiling point  $T = 65^\circ\text{C}$ ) (96%/4% v/v and 92%/8% v/v) were used. The concentration of the polymer solutions varied from 20% to 14% for chloroform, from 18% to 14% for dichloromethane, while the polymer concentration was set to 16% for dichloroethane, to 10% for dioxane, and to 18% and 20% for the solvents mixtures.

### *Scaffold fabrication*

Scaffold mats were manufactured from the polymers and the polymeric blends with an electrospinning (ESP) apparatus. This device consists of a high voltage generator (NCE 30000, Heinzinger Electronic GmbH, Germany) connected to a syringe, in which the polymer solution is contained, and to a collector that determines the final shape of the scaffold with its geometry. When a high voltage is applied, an electric field is formed between the syringe needle (positive pole) and the collector (negative pole). The polymer solution is pressed out of the syringe by a pump at

variable flow rates depending on the electrostatic field strength. When the intensity of the electrostatic field is high enough to surpass the surface tension of the liquid drop at the tip of the needle, the drop is pulled out into a jetting filament and deposited as a dry fiber on the collector. This is due to the solvent evaporation along the pathway between the syringe and the collector. In our experimental set up the voltage could be varied up to 30 kV, the needles used had a diameter of 1.2 mm, 0.8 mm, and 0.5 mm, and the syringe pump had an adjustable flow rate between 0.19 ml/min and 1.8 ml/min. The voltage and the width of the air gap between needle and collector determine the strength of the electrostatic field. For all the experiments the voltage was kept constant at 12 kV, unless indicated otherwise.

### ***Scaffold Characterization***

Scaffolds architecture was characterized by scanning electron microscopy (SEM) analysis with a Philips XL 30 ESEM-FEG. The porosity was calculated as:

$$P = 1 - \rho \cdot \frac{M}{V} \quad (1)$$

where P is the scaffold porosity,  $\rho$  the density of the polymeric system used, M the weight and V the volume of the fabricated scaffolds. The effect of the solvents used, of the polymer solution concentration, of the flow rate, and of the electrostatic field strength was investigated on pore formation and size and fiber dimension.

### ***Cell culture***

Bone marrow aspirates (5-15 ml) were obtained from two donors that had given written informed consent. Human mesenchymal stem cells (hMSC) were isolated and proliferated as previously described [30]. Briefly, aspirates were plated at a density of  $5 \times 10^5$  nucleated cells per  $\text{cm}^2$  and cultured in hMSC proliferation medium, which consists of minimal essential medium ( $\alpha$ -MEM, Life Technologies), 10% heat-inactivated foetal bovine serum (FBS, Cambrex), 0.2 mM ascorbic acid (Asap, Life Technologies), L-glutamine (Life Technologies), 100 U/ml penicillin (Life Technologies), 10  $\mu\text{g}/\text{ml}$  streptomycin (Life Technologies) and 1 ng/ml basic fibroblast growth factor (bFGF, Instruchemie, The Netherlands). Cells were grown at 37 °C in a humid atmosphere with 5%  $\text{CO}_2$ . Medium was refreshed twice a week and cells were used for further subculturing or cryopreservation upon reaching near confluence.

300PEOT55PBT45 electrospun discs with dimensions of 6 mm in diameter by 0.1 mm in thickness were obtained from fiber mats spun from 16% and 20% w/v chloroform solutions, and from 20% chloroform/HFIP mixture solution (90%/10%). These solutions gave scaffolds with an average smooth fiber diameter of 1  $\mu\text{m}$  and 4  $\mu\text{m}$  (16%  $\text{CHCl}_3$ ), 10  $\mu\text{m}$  (20%  $\text{CHCl}_3$ /HFIP 90/10 mixture –  $V = 15$  kV), 21  $\mu\text{m}$  (20%  $\text{CHCl}_3$  – air gap width = 10 cm), and 10  $\mu\text{m}$  with nanopores approximately

200 nm in size (20%  $\text{CHCl}_3$  – air gap width = 15 cm). Three dimensional scaffolds with fiber diameter of 270  $\mu\text{m}$  fabricated with a rapid prototyping device described elsewhere [31] were also seeded as a reference. Cells were seeded at a density of 5000 cells/scaffold and 25000 cells/scaffold in triplicates.

Cell counting was performed enzymatically using an Alamar blue assay. Culture medium was replaced with medium containing 10% Alamar blue solution (Biosource) and cells were incubated at 37 °C for 4h. Fluorescence was measured in a 200  $\mu\text{l}$  sample at 590 nm in an ELISA plate reader (Greiner) in duplicates. Cell morphology and attachment was investigated with SEM. The samples were fixed overnight in 0.14M cacodylate buffer (pH = 7.2 – 7.4) containing 0.25% glutaraldehyde (Merck). Then, samples were dehydrated in sequential ethanol series and critical point dried from liquid carbon dioxide using a Balzers CPD 030 Critical Point Dryer. The constructs were then sputter coated (Cressington) prior to SEM analysis.

A one-way statistic analysis of variance (ANOVA) was used with a significant level  $p$  of 0.05 to determine differences between cell numbers on the various scaffolds.

### ***Dye Incorporation and Release***

To investigate the possibility of incorporating drugs in electrospun PEOT/PBT scaffolds, dyes with different molecular weight ( $M_w$ ) and chemical conformation were incorporated in a 18% w/v 300PEOT55PBT45 solution in chloroform. Pyrrogalol red ( $M_w = 400.37$  g/mol), methylene blue ( $M_w = 319.19$  g/mol), and copper acetate ( $M_w = 199.93$  g/mol) were obtained from Sigma-Aldrich and used for this purpose. Furthermore, ESP scaffolds containing methylene blue only with an average smooth fiber diameter of 1  $\mu\text{m}$ , 10  $\mu\text{m}$ , and 10  $\mu\text{m}$  with nanoporous fiber surface were fabricated from the solution previously described to investigate the influence of fiber diameter and surface texture on dye release. The dyes were dissolved in the polymer solutions with a concentration of 4.92 mg/ml. After dye incorporation, the solutions were spun with the electrospinning device. Square scaffolds with a side of 1.8 cm and a thickness of approximately 1 mm were immersed in a phosphate buffered saline solution (PBS) at room temperature. The release was detected with a spectrophotometer (El 312e, BioTek Instruments) at the characteristic absorption wave lengths of the dyes.

## **Results**

### ***Scaffolds Characterization***

The effect of the solvents used, of the polymer solution concentration, and of the air gap (varying both the electrostatic field strength and the “time of flight” of the drying fibers) was investigated on pore formation and size and on fiber dimensions at constant voltage applied ( $V = 12$  kV), as summarized in Table 1.

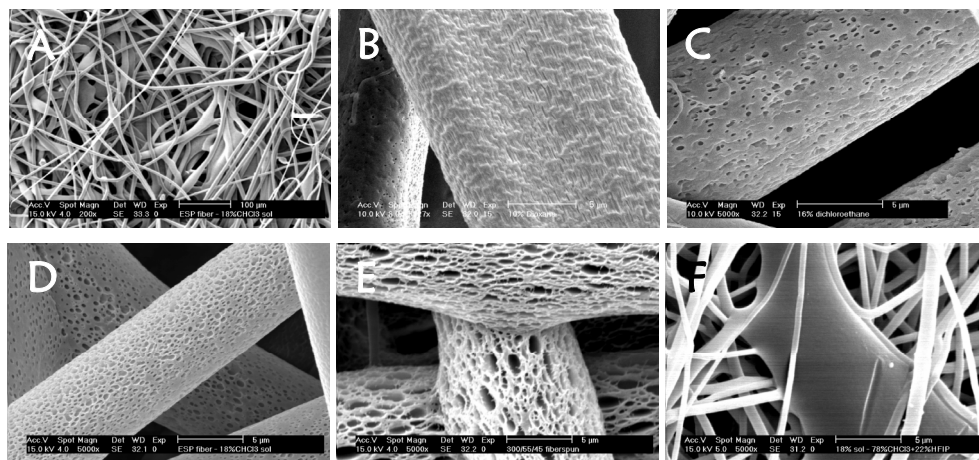


**Figure 1** – SEM micrographs of a 300PEOT55PBT45 electrospun scaffold (a, scale bar: 100  $\mu\text{m}$ ) and different fiber pore morphology obtained. (b) dioxane; (c) dichloroethane; (d) chloroform; (e) dichloromethane; (f) mixture of chloroform and HFIP. Scale bar: 5  $\mu\text{m}$ .

### *Effect of Solvents on Porous Fiber Formation*

#### Electrospun Scaffolds

The morphology and dimensions of porous and non porous fibers forming a 300PEOT55PBT45 ESP scaffold are shown in figure 1. By decreasing the boiling point of the solvents used to form the polymer solutions, the pore morphology became more irregular (figures 1b, 1c, 1d, and 1e). An effect of the boiling point can also be seen on pore size. With increasing solvent boiling point, the pore size decreased. For fibers spun from a 16% solution, the pore size varied from  $1.23 \pm 0.73 \mu\text{m}$  for dichloromethane (boiling point  $T = 40 \text{ }^\circ\text{C}$ ), to  $803 \pm 178 \text{ nm}$  for chloroform (boiling point  $T = 62 \text{ }^\circ\text{C}$ ), and to  $346 \pm 288 \text{ nm}$  for dichloroethane (boiling point  $T = 82\text{-}84 \text{ }^\circ\text{C}$ ). If dioxane was used as a solvent, an elongated morphology of the pores formed was found with dimensions of  $786 \pm 297 \text{ nm}$  along the fiber direction and of  $72 \pm 16 \text{ nm}$  along the perpendicular direction (figure 1b). In this case, a 10% polymer solution was used, as increasing the polymer concentration would result into a too thick gel that would fail to be spun. The polymer solution with dichloroethane and with dioxane would become gels at room temperature, for which reason the gels were heated to  $50 \text{ }^\circ\text{C}$  and  $60 \text{ }^\circ\text{C}$  respectively to let them liquefy, before and during electrospinning. If HFIP was used together with chloroform in a 22%/78% v/v mixture for a 20% polymer solution, no pore formation occurred (figure 1f), due most likely to the better solvent properties of HFIP for PEOT/PBT copolymers. If methanol was added to chloroform, an orientation effect of the deposited fibers was observed for an 8%/92% mixture, as depicted in figure 2. A lower degree in fiber orientation was observed if the methanol volume ratio was reduced to 4% in the solvent mixture. These results suggest a relation between pore and fiber formation, and the intrinsic solvents properties of the chemicals used to form the PEOT/PBT polymer solutions.



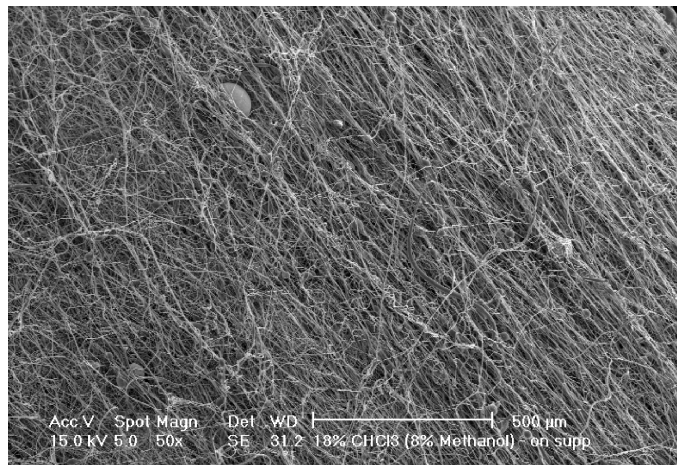
Polymer Concentration (%)	Air Gap (cm) - Electric Field (kV/cm)		Fiber Diameter (µm)		Pore Dimension (nm)		Interfiber Pore Size (µm)		Scaffold Porosity (%)	
	15	0.8	Dichloromethane	Chloroform	Dichloromethane	Chloroform	Dichloromethane	Chloroform	Dichloromethane	Chloroform
10	15	0.8	-	-	-	-	-	-	-	-
14	15	0.8	0.5 ± 0.25	0.76 ± 0.7	-	0	72 ± 16	34.1 ± 7.7	88 ± 2	88 ± 2
16	25	0.48	2.25 ± 1.75	0.96 ± 0.66	-	803 ± 178	-	-	90 ± 2	86 ± 3
16	15	0.8	2.25 ± 1.75	0.96 ± 0.66	7.4 ± 4.1	0	346 ± 288	41.13 ± 24.4	90 ± 2	86 ± 3
18	25	0.48	10 ± 8	10 ± 7	7.4 ± 4.1	0	-	-	89 ± 8	83 ± 5
18	15	0.8	10 ± 8	10 ± 7	-	997 ± 680	-	83.68 ± 41.43	89 ± 8	83 ± 5
20	25	0.48	-	21.4 ± 6	-	0	-	114.8 ± 46.4	-	-
20	15	0.8	-	21.4 ± 6	-	220 ± 50	-	105.74 ± 21.93	-	-

Table 1 – Electrospun scaffolds characterization. The flow rate was fixed at 0.39 ml/min.

Electrospun Scaffolds

### *Effect of Polymer Concentration and Air Gap on the Fiber Pore Size*

Pore formation and dimension were also connected to the polymer solution concentration and to the width of the air gap during electrospinning. Apparently, pore formation occurred until a lower limit of the air gap width was reached, depending on the polymer solution concentration. Pores were created



**Figure 2** – SEM micrographs of an ESP scaffold with oriented fibers, spun from an 18% PEOT/PBT solution in a chloroform/methanol mixture (92%/8%).

Electrospun  
Scaffolds

on the ESP fibers for solution concentrations higher than 16% at air gap larger than 20 cm. When the air gap was set to 25 cm, the pore size decreased with increasing polymer concentration from  $803 \pm 178$  nm to  $455 \pm 315$  nm for chloroform solutions, and from  $1.23 \pm 0.73$   $\mu\text{m}$  to  $997 \pm 680$  nm for dichloromethane solutions (Table 1). If the air gap was lower than 20 cm, pores were formed only for solutions with a concentration higher than 20%. In this case, the pore size decreased from  $455 \pm 315$  nm to  $220 \pm 50$  nm for chloroform solutions, when the air gap decreased from 25 cm to 15 cm, as shown in figure 3.

### *Effect of Polymer Concentration and Flow Rate on Fiber Size*

To characterize 300PEOT55PBT45 ESP scaffolds, the influence of the flow rate and the polymer concentration on fiber dimensions and scaffold porosity was considered. Only dichloromethane and chloroform were used as solvents to assess the link between the above mentioned parameters and the fiber size. Fiber diameters varied from  $155 \pm 46$  nm to  $14.55 \pm 2.55$   $\mu\text{m}$  for dichloromethane when the flow rate increased from 0.27 ml/min to 1.8 ml/min, as shown in figure 4. A range of fiber diameters from  $55 \pm 24$  nm to  $18.57 \pm 1.56$   $\mu\text{m}$  was obtained for chloroform

Effect of Air Gap on Fiber Pore Size

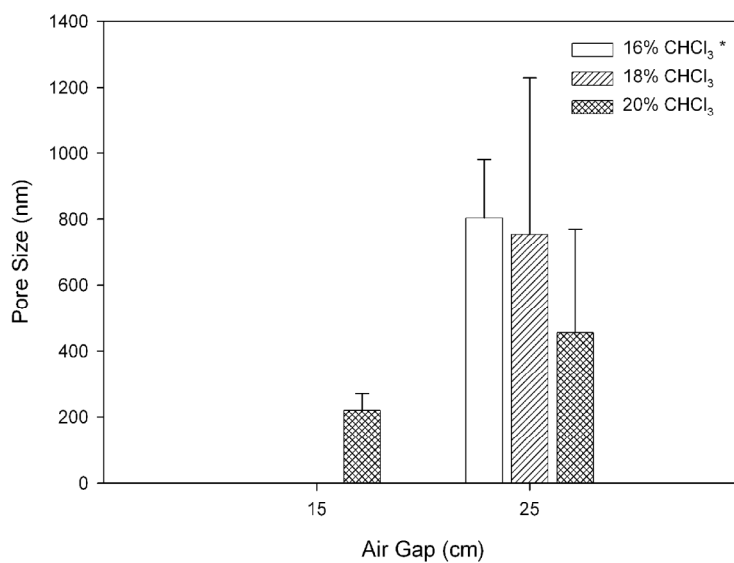


**Figure 3** – Effect of the air gap width on the pore size in the fibers. (\*) Larger gap widths are required for the formation of pores on fibers from lower concentration solvents.

Effect of Flow Rate on ESP Fiber Dimensions

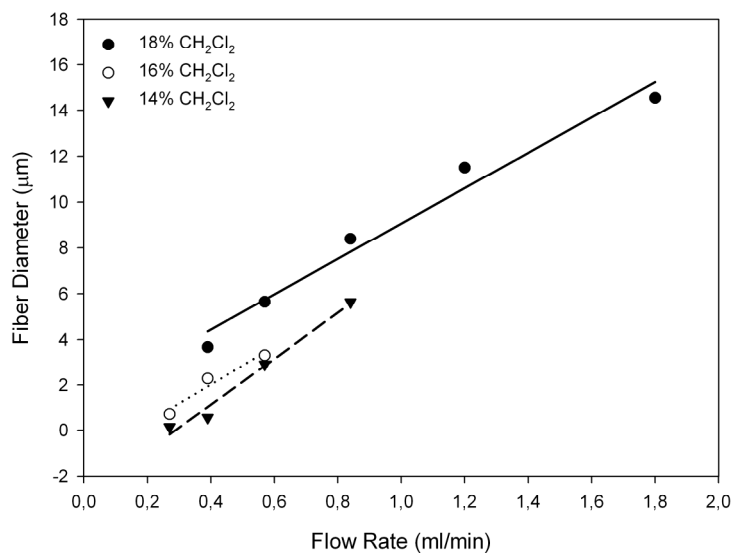


**Figure 4** – Dependence of fiber diameter on flow rate. Dichloromethane is shown here. Analogous trends were found when chloroform was used as a solvent.

Electrospun Scaffolds

solutions when the flow rate changed from 0.27 ml/min to 0.84 ml/min. In this case, a higher flow rate was not considered since jet instability occurred. In a similar way, the fiber diameter increased from  $560 \pm 320$  nm to  $3.67 \pm 0.5$   $\mu\text{m}$  for dichloromethane and from  $204 \pm 31$  nm to  $4.95 \pm 0.34$   $\mu\text{m}$  for chloroform when the solution concentration was increased from 14% to 18% and the flow rate was fixed to 0.39 ml/min (figure 5). This corresponded to an increase of scaffold porosity from  $89 \pm 8\%$  to  $93 \pm 2\%$  for dichloromethane and from  $83 \pm 5\%$  to  $88 \pm 2\%$  for chloroform. The interfiber pore size was also measured (Table 1) for chloroform polymer solutions and found to increase from  $34.1 \pm 7.7$   $\mu\text{m}$  to  $114.8 \pm 46.4$   $\mu\text{m}$  with solution concentrations increasing from 14% to 20% w/v.

#### Effect of Polymer Solution Concentration on ESP Fiber Dimensions

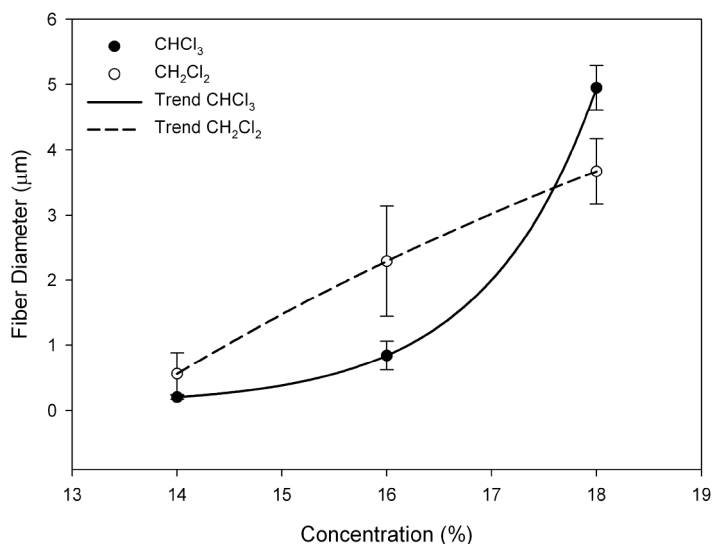


**Figure 5** – Influence of polymer concentration on fiber diameter. The flow rate was fixed at 0.39 ml/min.

#### *Beaded Electrospun Scaffolds*

The fabricated scaffolds were always comprised of fibers if spun from dichloromethane polymer solutions, while a mixture of fibers and spherical beads was observed for chloroform solutions with a concentration lower or equal to 16%, as shown in figure 6. The lower the concentration, the higher the number of beads present in the scaffold. These droplets appeared to be porous, and their porosity also depended from the polymer solution concentration and the electric field. When the beads were formed, their size varied from  $9.31 \pm 5.28$   $\mu\text{m}$  for a 16% solution concentration to  $40 \pm 20$   $\mu\text{m}$  for a 14% solution concentration. At the same time the pore size increased from  $475 \pm 225$  nm to  $585 \pm 390$  nm (figure 7). If the solution concentration was fixed to 16% and the air gap varied from 25 cm to 15

cm, the pore dimensions in the beads decreased from  $1475 \pm 525$  nm to  $475 \pm 225$  nm.

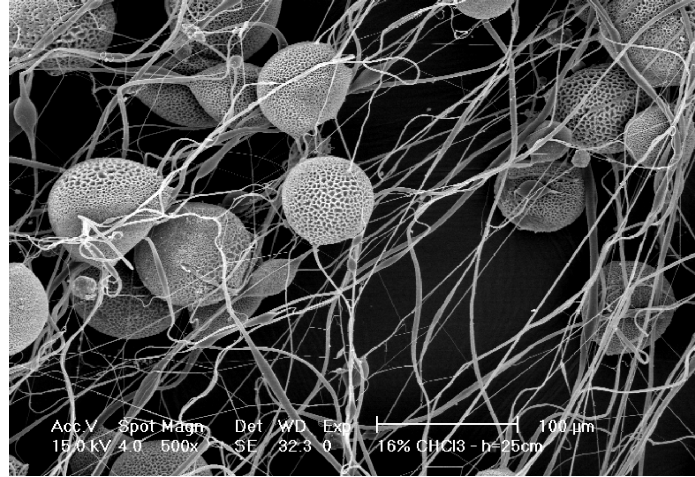


**Figure 6** – SEM micrograph of an electrospun PEOT/PBT beaded scaffold from a 16% w/v chloroform solution, showing interspersed porous beads and fibers. Scale bar: 100  $\mu$ m.

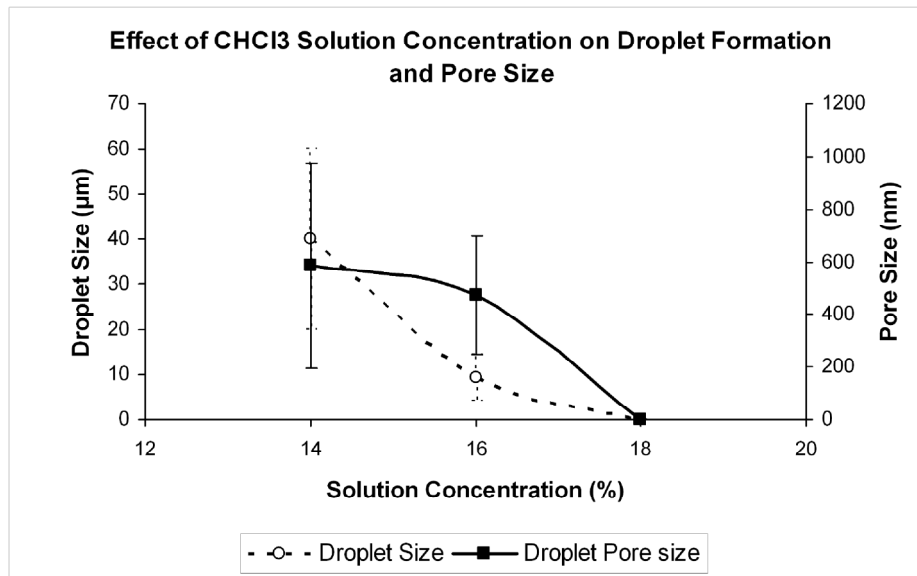


**Figure 7** – Influence of polymer concentration on bead formation and pore size on the formed beads with a fixed air gap of 15 cm.

Electrospun Scaffolds

## Cell Culture

To investigate the effect of fiber diameter and of fiber surface topology on cell attachment and proliferation, hMSC were seeded and cultured on ESP scaffolds for 14 days, and their relative number measured with an Alamar blue assay (Figure 8) after 3, 7, and 14 days. After 3 days of culture more cells were detected on the 10  $\mu\text{m}$  fiber scaffolds than on any other fiber diameter, suggesting that this diameter appears to be the most efficient for cell seeding or attachment. The

Effect of Fiber Diameter and Topology on HMSC Proliferation

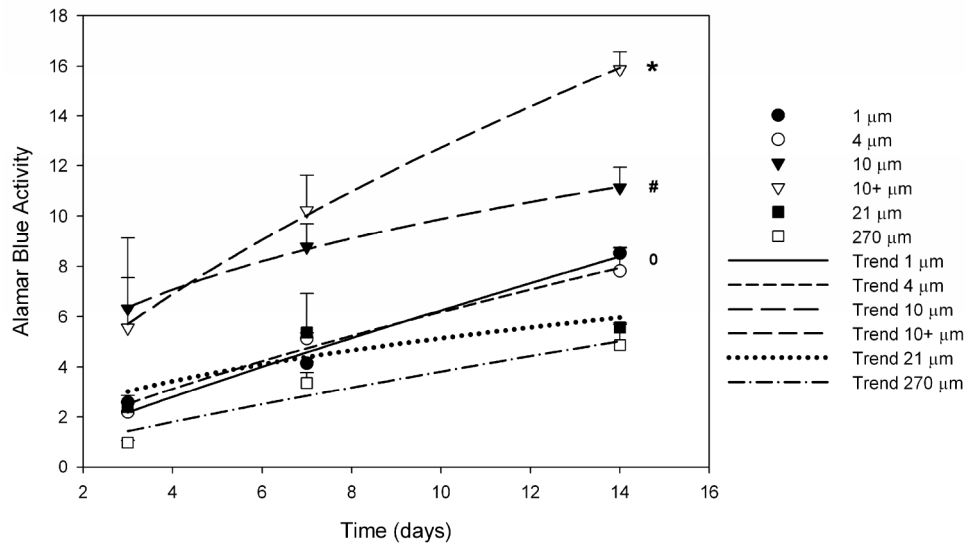


**Figure 8** – Effect of the fiber diameter and surface topography on cell attachment and proliferation. (\*) indicates significant difference between nanoporous and smooth surface; (#) shows significant difference of 10  $\mu\text{m}$  fiber diameter with respect to the other fiber diameters; (o) depicts significant differences between 1  $\mu\text{m}$  and 4  $\mu\text{m}$  fiber diameter with respect to 21  $\mu\text{m}$  and 270  $\mu\text{m}$ . Significance level  $p < 0.05$  ( $n=3$ ). Analogous trends were detected with the second donor and with higher cell density.

rate of proliferation can be inferred from the slopes of the Alamar blue activity versus time curves. For the smooth fiber scaffolds, the slope was similar for all the fiber diameters, suggesting that this parameter does not influence cell proliferation. In contrast, the slope of the curve for a nano-porous 10  $\mu\text{m}$  fiber scaffold was higher than in the case of a smooth 10  $\mu\text{m}$  fiber scaffold, suggesting that surface topography influences proliferation of human mesenchymal stem cells. This might entail a specific capacity of the cells to recognize an optimal fiber size for attachment and proliferation. Figure 9 shows cell attachment and proliferation on the ESP scaffolds. After 3 days, cells were found to aggregate on smooth fiber scaffolds (1  $\mu\text{m}$ , 4  $\mu\text{m}$ , 10  $\mu\text{m}$ , 21  $\mu\text{m}$ , and 270  $\mu\text{m}$ ), whereas they tended to spread on the nano-porous fiber scaffolds. Cells attached and grew on the surface and inside the scaffolds. These

trends were also measured for the other donor analyzed and a higher Alamar blue activity was detected for higher cell seeding density. After 14 days cells covered the entire scaffold surface and penetrated inside the fiber network.

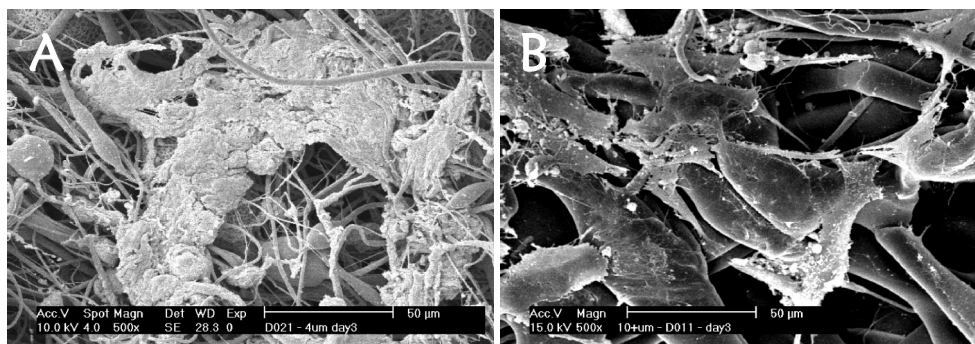


**Figure 9** – SEM micrographs of HMSC seeded and attached to 300PEOT55PBT45 scaffolds at day 3. (a) cell aggregates on smooth fibers; (b) cells spreading on nanoporous fibers. Scale bar: 50  $\mu\text{m}$ .

### ***Dye Release***

The release of pyrrogalol red and methylene blue incorporated in 300PEOT55PBT45 electrospun scaffolds is presented in figure 10. A burst release profile was observed within the first 24 hours for methylene blue and pyrrogalol red. After one month pyrrogalol red and methylene blue cumulative release corresponded to  $44.5 \pm 6.3\%$  and to  $29.13 \pm 5.6\%$  of the total dyes incorporated in the scaffolds, respectively. After a month, scaffolds still released the dyes in small amount. Copper acetate was also released from the scaffolds, but due to its precipitation in PBS it was not possible to quantitatively detect the amount delivered.

When incorporating methylene blue only in ESP scaffolds with different fiber diameters and surface topologies, the rate of dye release changed. With increasing fiber diameter from 1  $\mu\text{m}$  to 10  $\mu\text{m}$ , the cumulative release of methylene blue decreased from  $29.13 \pm 5.6\%$  to  $21.42 \pm 1.9\%$  of the total dye incorporated in one month. Interestingly, when nanoporosity was added to the surface of the 10  $\mu\text{m}$  wide fibers, an increase of the dye release rate occurred. In this case, the cumulative amount released was  $25.8 \pm 3.6\%$  of the total dye entrapped in the scaffolds.

## **Discussion**

### ***Electrospun Scaffold characterization***

The fabricated scaffolds were characterized by a wide range of fiber diameters combined or not with pore and/or beads formation, mainly depending on the spin flow rate, the polymer solution concentration, and the electric field. The voltage

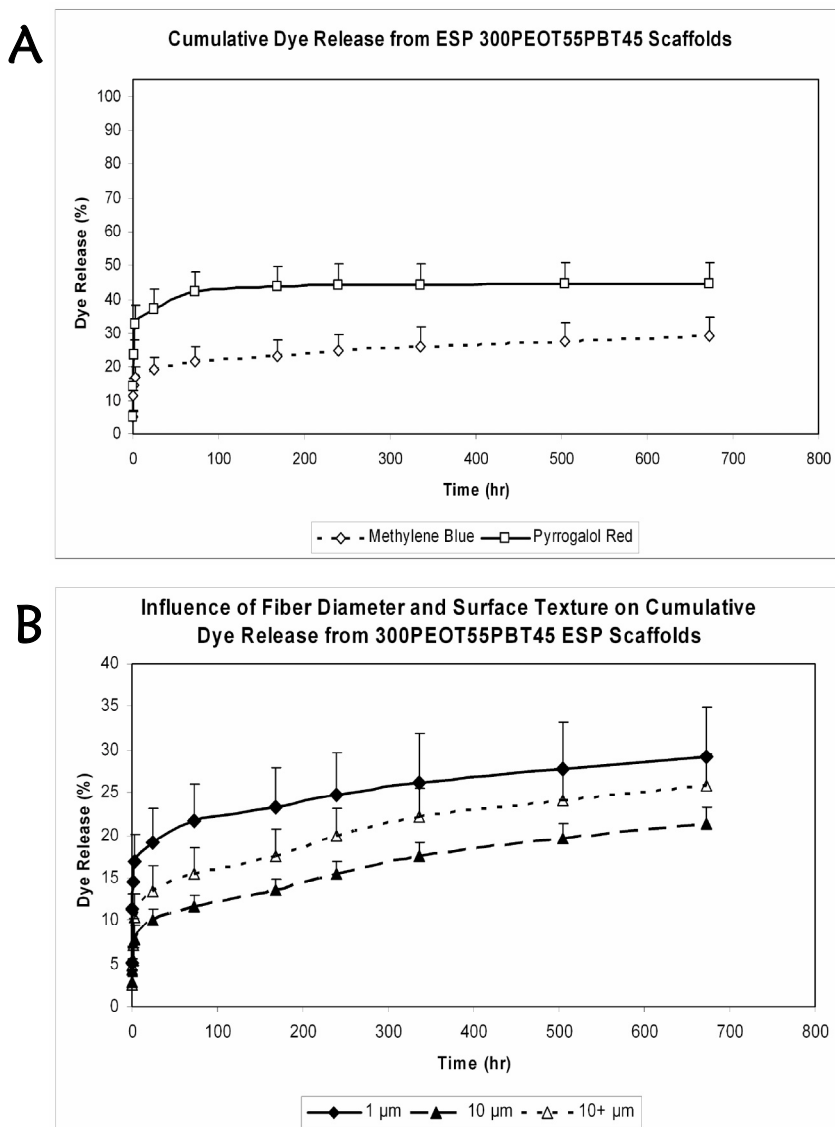


**Figure 10** – Cumulative dye release profile from electrospun 300PEOT55PBT45 scaffolds. (a) release of methylene blue and pyrragalol red from 1  $\mu\text{m}$  size fibrous ESP scaffolds; (b) influence of fiber diameter and of fiber topography on methylene blue cumulative release.

applied to make the scaffolds was fixed to 12 kV for simplicity, unless otherwise specified. The relationship between the applied voltage and the stability of the polymer jet and the consequent fiber diameter distribution has already been extensively studied by other researchers [2, 32]. In our case, electrospinning already occurred at 7 kV, but a more stable jet appeared to be at 12 kV. Increasing the voltage resulted in higher electrostatic forces on the apparatus and instability of the



jet that would split and splay, as also shown by Deitzel *et al* [32]. This produced a broader range of fiber diameters and beads formation, while the other parameters considered in this paper were fixed. Different needle diameters were also used to spin the fibers. Surprisingly, an increase of the needle diameter resulted in a decrease of the fiber diameter and in a more homogeneous distribution (data not shown). The needle diameter can be related to the jet length and, more precisely, to the distance from the needle tip where the Taylor cone becomes unstable and the spinning process begins, as proposed by Rutledge *et al* [33]. By increasing the needle diameter the jet length increases as well, resulting in a thinning of the Taylor cone. This would imply a smaller instability area from where the filaments start to be formed and, consequently, might be the reason for a decrease in the fiber diameter and for a more homogeneous distribution.

Electrospun fibers showed different morphological characteristics depending on the solvent used for the polymer solution. Porous and non porous fibers were generated, mainly depending on the chemical affinity between the solvent and the polymer. Specifically, only when HFIP was used in the solvent mixtures pore formation never occurred. This is due to the high affinity of HFIP with PEOT/PBT, among many other polymers. All the other solvents considered in this study formed less ideal and more colloidal solutions, where polymer and solvent rich regions are evenly distributed. To demonstrate it, the gelling time of 16% w/v polymer solutions in the different solvents used was measured and the results are presented in Table 2. All the solutions jellified eventually, except when a minimum amount of HFIP, corresponding to 10% of the solvent phase, was used. Pore formation appears to occur due to fast solvent evaporation and phase separation in polymer rich and poor areas, as also described by Bognitzki *et al* [11] and Rabolt *et al* [34].

Polymer Concentration (%)	Gelling Time (hr)				
	Dichloromethane	Chloroform	Dichloroethane	Dioxane	Chloroform90%/HFIP10%
16	167 ± 1	504 ± 6	0.1 ± 0.016	0.25 ± 0.05	No Gelling

**Table 2** – Gelling time of PEOT/PBT solutions at room temperature.

The fast evaporation gives the thickening mass less time to flow and level out the concentration differences in the polymer rich and poor phases. To partly corroborate this theory, we made 5  $\mu\text{m}$  thick films by spreading a 16% w/v solution of 300PEOT55PBT45 in  $\text{CH}_2\text{Cl}_2$  with a film applicator on a glass plate. Increasing the solvent evaporation speed resulted in an increase of the film surface texture, as analyzed by SEM (data not shown).

A lower boiling point of the solvent resulted in more irregular pore morphology and larger pore dimensions, which can also be explained by the fast evaporation mechanism. Likewise, the lower dissolving power of the lower boiling point solvents will create a tendency to form large phase separated areas in the solution. Matsuda *et al*. [12] also related the boiling point of solvents to the fiber morphology. In their case, a decrease of solvent boiling point resulted in less fusion or welding of the fibers at the contact points, but no pore formation on the fibers was observed. This might be due to the particular solvent mixture used and to the set up of the

electrospinning parameters. Yet, the fact that decreasing the boiling point led to a decrease of the fusion degree of the fibers can be related to the same physical phenomena. When dichloroethane and dioxane were used as solvents, the polymer solution had to be continuously stirred and heated to 50 °C or 60 °C, respectively, to be electrospun. In fact, thicker colloidal solutions were obtained from these solvents (Table 2). Larrondo *et al.* already reported the successful electrospinning of polymer melts [3, 35]. To our knowledge, this is the first time that gel systems were effectively electrospun, bridging the gap between polymer solutions and melts.

When methanol was added to chloroform in an 8%/92% v/v mixture, a high degree of orientation of the electrospun fibers on the grid used as a collector was observed (see figure 2). Reducing the methanol percentage in the mixture to 4%, fibers were still oriented along the main axis of the collecting grid, but the degree of orientation decreased. This orientation tendency can be related to the polarity of methanol, which under the applied electric field influences the fibers to orient along the direction, given by the collector grid. Furthermore, with methanol having a relatively low volatility the spun fibers probably reached the collector still in a wet phase, giving the polymer time to rearrange its structure not only in a favorite direction, but also in a non porous structure.

Pore formation and size also depended from the polymer solution concentration and from the air gap set for spinning. A lower limit for the air gap was found to create porous fibers (figure 3). Pore generation can be again connected to phase separation and solvent evaporation speed. The air gap between the syringe and the collector determines the travel distance between the syringe and the collector and a higher polymer concentration was required in the solution to generate porous fibers. When solvent evaporation was complete before the fiber was deposited, phase separation occurred during the time that the forming fibers were “in flight”. For smaller concentrations the fibers were still wet at the collector where a slower solvent evaporation took place so that the polymeric structure could rearrange into a continuous and non porous fiber. If the air gap was increased and, thus, the electrostatic field strength decreased the fibers had to travel at lower speed (electrostatic field strength) over a longer distance, which inferred a longer time for fast evaporation and phase separation. This resulted in pore formation, also for lower polymer concentrations, and in an increase in pore size.

The influence of the flow rate and of the polymer solution concentration was investigated to characterize the electrospun PEOT/PBT fibers. With increasing the flow rate and the polymer concentration an increase of the fiber dimension was observed (figures 4 and 5). This is expected, since a higher flow rate inferred a higher volume of spun solution, while a higher polymer concentration entailed a higher polymer weight percentage per volume of the solvent, resulting, therefore, in larger fibers. An analogous trend was also found by Deitzel *et al* [32], and Kidoaki *et al* [6] for electrospun polymer solutions. The increase of the fiber diameter also resulted in a decrease of the density of the scaffolds, due to a lower packing degree of the thicker fibers.

When chloroform solutions were electrospun, fibers were associated with beads for polymer concentrations lower than 16%. Beads were porous and increased in size with decreasing the solution concentration (figure 7). From SEM analysis it can be

also noted that an increase in beads number appeared to happen with decreasing the solution concentration. Beads formation was also observed by other researchers [7, 32, 36], and generally attributed to the jet instability due to a high field strength applied. The instability of the electrospun solution might have also occurred in our case. Although the electric field was kept constant, a decrease in the polymer concentration probably contributes to form jet instability, due to the lower viscosity of the solutions. Indeed spray drying where micro particles are formed exclusively is done at concentration lower than 6% [37]. The beads appeared to be porous. Both beads and pore size increased with decreasing polymer concentration and/or increasing the electric field. Similar explanations in terms of solvent evaporation rates can be given as in the case of porous fibers.

### *Cell Culture and drug release applications*

From the multitude of possibilities to vary electrospun fiber diameter and surface topology as discussed here, we selected five type of scaffolds with increasing fiber average diameter with and without nanopores and cultured them with hMSC to assess the influence of these two parameters on cell seeding, attachment and proliferation. Cells were also cultured on rapid prototyped scaffolds with fiber diameters of one to two orders of magnitude larger, as a comparison. The results suggest that a cell can significantly sense not only an optimal fiber dimension, but also the presence of nanotopography on the fiber surface. This might be due to a higher cell seeding efficiency already after 3 days on 10  $\mu\text{m}$  fiber scaffolds. Although in the case of ESP scaffolds with 1  $\mu\text{m}$  and 4  $\mu\text{m}$  fibers beads were present, SEM analysis showed that the ratio between fibers and beads appeared to be relatively high, resulting in a negligible effect of the presence of beads on cell behavior. Furthermore, a different cell behavior and morphology was found on fibers with or without nanopores where cells spread or aggregated maintaining a rounded shape, respectively. This might be explained by considering the radius of curvature of the single fibers. In relation to the cell dimensions of approximately 20  $\mu\text{m}$ , smaller diameters would offer higher curvatures. Subsequently, cells would tend to aggregate, keep a rounded shape and bridge more fibers together instead of spreading over the fiber surface. When the fiber diameter comes closer to the cell dimensions, the limiting effect of the fiber curvature would become less predominant, resulting in a significantly higher amount of cells on the scaffolds ( $p < 0.05$ ). Apparently, this phenomenon is optimal for a fiber diameter of approximately 10  $\mu\text{m}$ , since a further increase of the fiber diameter resulted in a decrease of cells attachment and proliferation. While this can be expected for fibers of 270  $\mu\text{m}$  that are organized into macroporous structures with a low efficiency to “sieve” and entrap cells, it is surprising for ESP fibers of 21  $\mu\text{m}$ . It might be possible that where this fiber diameter is quite close to the cell dimensions, cell motility is enhanced [38, 39], resulting in a lower proliferation rate. If nanoporous fibers are considered, a significantly higher cell activity was found with respect to non porous fibers with the same diameter. This was also coupled with lost of cell aggregation and with cell spreading. Nanopores, therefore, interacted with cells in such a way to stimulate a different biological response. A similar behavior was also found by other

researchers for different topology features on material substrates [40-42]. This difference between smooth and nano textured fibrous scaffolds can be very useful when influencing cell aggregation or spreading is desirable. For example in cartilage tissue engineering it is known that rounded and aggregated chondrocytes form more ECM with a higher content of collagen type II [29, 43, 44], while in bone tissue engineering spread osteoblasts perform better in terms of ECM formation [10, 45]. After 14 days almost all the available surface of the scaffolds was covered and cells penetrated also inside the construct.

ESP scaffolds were also tested for controlled drug release applications. Dyes with different molecular weight and chemical conformation were incorporated in 300PEOT55PBT45 polymer solutions, electrospun and released from the fabricated scaffolds. Dyes were considered as a model system for the release of small molecular weight compounds such as antibiotics. The cumulative release showed a burst effect, which might be due to the high specific surface of the fibers and to the dye molecules situated on or very near the surface. Copper acetate was also incorporated in ESP scaffolds to study its release from the polymeric fibers, since it is known to positively influence extracellular matrix formation [46]. The release of copper couldn't be detected quantitatively with a spectrometer analysis due to its precipitation in PBS. The weight of the precipitated dye compound was measured as good as possible and suggested a similar release profile as pyrogallol red and methylene blue, with a more moderate burst effect over the first 72 hours. This might be related to the smaller molecular dimension and to the different, ionic, chemical structure of the compound. Being the release mechanism of this copolymer family mainly based on diffusion [25, 47], the different compound chemical structure might have resulted in a different bonding degree to the polymer, which contributed to alter the release rate. An influence of fiber diameter and surface topography was found on the methylene blue release from ESP scaffolds. The cumulative amount of released dye decreased with increasing fiber diameter. This can be attributed to the correspondent lower fiber specific surface. However, when nanoporosity was incorporated on the surface of the fibers, the cumulative dye release increased as compared to smooth fibers with the same fiber diameter. The presence of nanoporosity resulted in a higher fiber surface available for diffusion. Furthermore, the dyes were only partly (<50%) released even after one month (Figure 10), indicating a strong bonding of these compounds to the polymer matrix the release of the remaining amount being dependent on the gradual degradation of the polymer [48, 49].

We showed in this investigation that electrospun PEOT/PBT scaffolds influence cell morphology and metabolic activity, and the release rate of incorporated compounds depending on fiber diameter and surface texture. In this respect a further tool to control the distribution and morphology of seeded cells or the release of drugs is to fabricate multiphase scaffolds, where different materials are selectively and regionally present in the construct. In the specific case of polymeric scaffolds, blends of two or more polymers can be made and studied for this purpose, as shown in figure 11. These systems would be even more useful in case of complex tissues, where different cell types are arranged in hierarchical structures such as the heart, the liver and the neural tissue, and where a selective different cell attachment

is desired, or in the case of co-culturing different cells type. If selective leaching is performed in a solvent-non solvent bath to remove one component of the blended polymer (figure 11b), scaffolds can be obtained where the increase of microporosity and surface roughness can enhance cell differentiation and extra cellular matrix formation [10, 42, 50]. Such a multiphase system could also be used to selectively release different biological agents in different time windows. An example of such a system is to electrospun water-in-oil polymer emulsions, where the drug is incorporated in water droplets and protected from the solvent [13]. Further studies will focus on the development of different releasing ESP networks and their incorporation in rapid prototyped scaffolds.

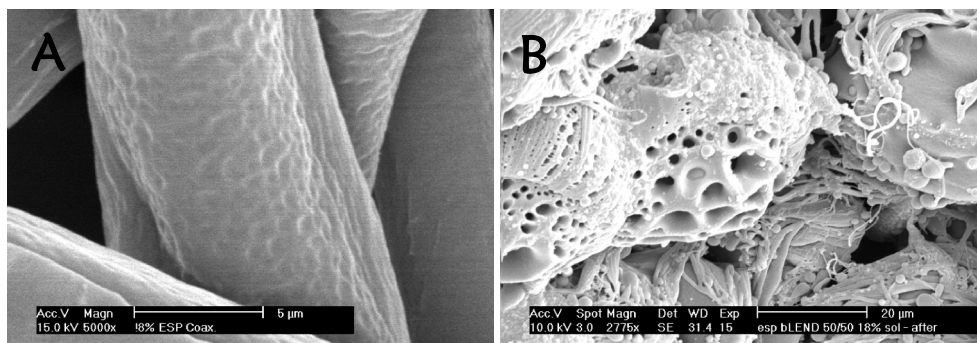


**Figure 11** – SEM micrographs of electrospun scaffolds from PEOT/PBT and P(BMA/MMA) or PCL blends in a random (a) and coaxial (b) distribution, and from PEOT/PBT – bovine serum albumin (BSA) emulsion (c). (a) ESP blend scaffolds after leaching out P(BMA/MMA), showing microporosity formation (pore size:  $761 \pm 508$  nm). Scale bar:  $20 \mu\text{m}$ ; (b) coaxial fiber with a PEOT/PBT shell ( $9.76 \pm 1.72 \mu\text{m}$ ) and a PCL core ( $8.06 \pm 1.16 \mu\text{m}$ ). Scale bar:  $5 \mu\text{m}$ ; (c) emulsion scaffold fiber dimension:  $1.5 \pm 0.7 \mu\text{m}$ . Scale bar:  $500 \mu\text{m}$ .

## Conclusions

Electrospun scaffolds of PEOT/PBT copolymers were successfully fabricated. A wide range of porous and non porous fibers can be obtained, depending on the solvent used and on the electrospinning settings. A set of ESP scaffolds with specific diameter and surface topography was selected to study their influence on cell attachment and activity. Fibers with a diameter of  $10 \mu\text{m}$  were found to have optimal cell attachment and proliferation. Furthermore, smooth or nanoporous fibers resulted in rounded aggregated or spread cells, respectively. After 14 days, the scaffolds were almost fully covered with cells, which also penetrated inside the fibril network. Dyes with different size and chemical structure were incorporated and released from the scaffolds in a burst and a first or higher order release pattern. These results suggest that PEOT/PBT electrospun scaffolds can offer a broad range of solutions for drug delivery and tissue engineering, in terms of the geometric and morphological properties of the fibril network they are formed of.

## Acknowledgements

This project was funded by the European Community project Intelliscaf GSRD\_2002\_00697. We are grateful to J. Sohier for the emulsion preparation and to F. Barrere for fruitful discussion on the manuscript.

## References:

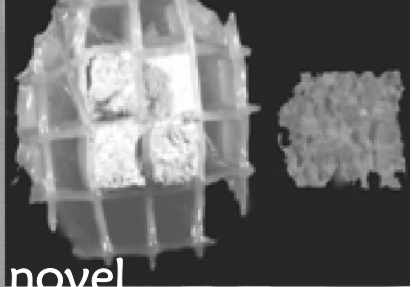
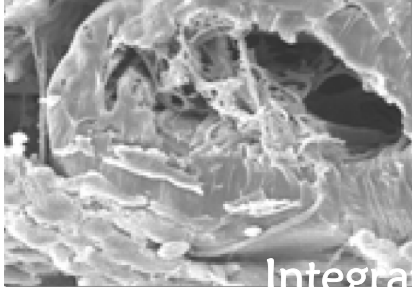
- [1] Taylor G. Electrically Driven Jets. *Proc R Soc London, Ser A* 1969;313:453-475.
- [2] Doshi J, Reneker D. Electrospinning Process and Applications of Electrospun Fibers. *J of Electrostatic* 1995;35:151-160.
- [3] Larrondo L, Manley R. Electrostatic Fiber Spinning from Polymer Melts. I. Experimental Observations on Fiber Formation and Properties. *J Polym Sci: Pol Phys Ed* 1981;19:909-920.
- [4] Kwon IK, Kidoaki S, Matsuda T. Electrospun nano- to microfiber fabrics made of biodegradable copolyesters: structural characteristics, mechanical properties and cell adhesion potential. *Biomaterials* 2005;26(18):3929-39.
- [5] Li WJ, Tuli R, Huang X, Laquerriere P, Tuan RS. Multilineage differentiation of human mesenchymal stem cells in a three-dimensional nanofibrous scaffold. *Biomaterials* 2005;26(25):5158-66.
- [6] Kidoaki S, Kwon IK, Matsuda T. Mesoscopic spatial designs of nano- and microfiber meshes for tissue-engineering matrix and scaffold based on newly devised multilayering and mixing electrospinning techniques. *Biomaterials* 2005;26(1):37-46.
- [7] Min BM, Lee G, Kim SH, Nam YS, Lee TS, Park WH. Electrospinning of silk fibroin nanofibers and its effect on the adhesion and spreading of normal human keratinocytes and fibroblasts in vitro. *Biomaterials* 2004;25(7-8):1289-97.
- [8] Mrksich M. What can surface chemistry do for cell biology? *Curr Opin Chem Biol* 2002;6(6):794-7.
- [9] Curtis A, Wilkinson C. Topographical control of cells. *Biomaterials* 1997;18(24):1573-83.
- [10] Boyan BD, Lossdorfer S, Wang L, Zhao G, Lohmann CH, Cochran DL, Schwartz Z. Osteoblasts generate an osteogenic microenvironment when grown on surfaces with rough microtopographies. *Eur Cell Mater* 2003;6:22-7.
- [11] Bognitzki M, Czado W, Frese T, Schaper A, Hellwig M, Steinhart M, Greiner A, Wendorff J. Nanostructured Fibers via Electrospinning. *Adv Mater* 2001;13(1):70-72.
- [12] Matsuda T, Ihara M, Inoguchi H, Kwon IK, Takamizawa K, Kidoaki S. Mechano-active scaffold design of small-diameter artificial graft made of electrospun segmented polyurethane fabrics. *J Biomed Mater Res A* 2005;73(1):125-31.
- [13] Sohier J, Haan RE, de Groot K, Bezemer JM. A novel method to obtain protein release from porous polymer scaffolds: emulsion coating. *J Control Release* 2003;87(1-3):57-68.
- [14] Nof M, Shea LD. Drug-releasing scaffolds fabricated from drug-loaded microspheres. *J Biomed Mater Res* 2002;59(2):349-56.
- [15] Mahmood TA, de Jong R, Riesle J, Langer R, van Blitterswijk CA. Adhesion-mediated signal transduction in human articular chondrocytes: the influence of biomaterial chemistry and tenascin-C. *Exp Cell Res* 2004;301(2):179-88.

- [16] Jansen EJ, Sladek RE, Bahar H, Yaffe A, Gijbels MJ, Kuijjer R, Bulstra SK, Guldmond NA, Binderman I, Koole LH. Hydrophobicity as a design criterion for polymer scaffolds in bone tissue engineering. *Biomaterials* 2005;26(21):4423-31.
- [17] Deschamps AA, Claase MB, Sleijster WJ, de Bruijn JD, Grijpma DW, Feijen J. Design of segmented poly(ether ester) materials and structures for the tissue engineering of bone. *J Control Release* 2002;78(1-3):175-86.
- [18] Olde Riekerink MB, Claase MB, Engbers GH, Grijpma DW, Feijen J. Gas plasma etching of PEO/PBT segmented block copolymer films. *J Biomed Mater Res A* 2003;65(4):417-28.
- [19] Moroni L, de Wijn JR, van Blitterswijk CA. Three-dimensional fiber-deposited PEOT/PBT copolymer scaffolds for tissue engineering: Influence of porosity, molecular network mesh size, and swelling in aqueous media on dynamic mechanical properties. *J Biomed Mater Res A* 2005;75:957-965.
- [20] Woodfield TB, Malda J, de Wijn J, Peters F, Riesle J, van Blitterswijk CA. Design of porous scaffolds for cartilage tissue engineering using a three-dimensional fiber-deposition technique. *Biomaterials* 2004;25(18):4149-61.
- [21] Bakker D, van Blitterswijk CA, Hesselting SC, Grote JJ. Effect of implantation site on phagocyte/polymer interaction and fibrous capsule formation. *Biomaterials* 1988;9(1):14-23.
- [22] Beumer GJ, van Blitterswijk CA, Ponc M. Degradative behaviour of polymeric matrices in (sub)dermal and muscle tissue of the rat: a quantitative study. *Biomaterials* 1994;15(7):551-9.
- [23] Bulstra SK, Geesink RG, Bakker D, Bulstra TH, Bouwmeester SJ, van der Linden AJ. Femoral canal occlusion in total hip replacement using a resorbable and flexible cement restrictor. *J Bone Joint Surg Br* 1996;78(6):892-8.
- [24] Mensik I, Lamme EN, Riesle J, Brychta P. Effectiveness and Safety of the PEGT/PBT Copolymer Scaffold as Dermal Substitute in Scar Reconstruction Wounds (Feasibility Trial). *Cell Tissue Bank* 2002;3(4):245-53.
- [25] Bezemer JM, Grijpma DW, Dijkstra PJ, van Blitterswijk CA, Feijen J. A controlled release system for proteins based on poly(ether ester) block-copolymers: polymer network characterization. *J Control Release* 1999;62(3):393-405.
- [26] Malda J, Woodfield TB, van der Vloodt F, Wilson C, Martens DE, Tramper J, van Blitterswijk CA, Riesle J. The effect of PEGT/PBT scaffold architecture on the composition of tissue engineered cartilage. *Biomaterials* 2005;26(1):63-72.
- [27] Wang H, Pieper J, Peters F, van Blitterswijk CA, Lamme EN. Synthetic scaffold morphology controls human dermal connective tissue formation. *J Biomed Mater Res A* 2005;74(4):523-32.
- [28] Papadaki M, Mahmood T, Gupta P, Claase MB, Grijpma DW, Riesle J, van Blitterswijk CA, Langer R. The different behaviors of skeletal muscle cells and chondrocytes on PEGT/PBT block copolymers are related to the surface properties of the substrate. *J Biomed Mater Res* 2001;54(1):47-58.
- [29] Woodfield TB, Miot S, Martin I, van Blitterswijk CA, Riesle J. The regulation of expanded human nasal chondrocyte re-differentiation capacity by substrate composition and gas plasma surface modification. *Biomaterials* 2006;27(7):1043-53.

- [30] de Boer J, Siddappa R, Gaspar C, van Apeldoorn A, Fodde R, van Blitterswijk C. Wnt signaling inhibits osteogenic differentiation of human mesenchymal stem cells. *Bone* 2004;34(5):818-26.
- [31] Moroni L, de Wijn JR, van Blitterswijk CA. 3D fiber-deposited scaffolds for tissue engineering: Influence of pores geometry and architecture on dynamic mechanical properties. *Biomaterials* 2006;27:974-985.
- [32] Deitzel J, Kleinmeyer J, Harris D, Beck Tan N. The effect of processing variables on the morphology of electrospun nanofibers and textiles. *Polymer* 2001;42:261-272.
- [33] Rutledge G, Li Y, Fridrikh S, Warner S, Kalayci V, Patra P. Electrostatic Spinning and Properties of Ultrafine Fibers. *National Textile Center Annual Report* 2001:1-10.
- [34] Rabolt J, Galvin M, Kiich K, Pocham D, Sun J, Wagner N. Enhancing the Properties of Nanoscale Electrospun Polymer Fibers through Chemical Architecture, Surface Texturing and Optimization of Processing Protocols. *Nanoscale Science and Engineering Grantees Conference Proceeding* 2003:1-3.
- [35] Larrondo L, Manley R. Electrostatic Fiber Spinning from Polymer Melts. II. Examination of the Flow Field in an Electrically Driven Jet. *J Polym Sci: Pol Phys Ed* 1981;19:921-932.
- [36] Geng X, Kwon OH, Jang J. Electrospinning of chitosan dissolved in concentrated acetic acid solution. *Biomaterials* 2005;26(27):5427-32.
- [37] Xie J, Marijnissen JC, Wang CH. Microparticles developed by electrohydrodynamic atomization for the local delivery of anticancer drug to treat C6 glioma in vitro. *Biomaterials* 2006;27(17):3321-32.
- [38] Smilenov LB, Mikhailov A, Pelham RJ, Marcantonio EE, Gundersen GG. Focal adhesion motility revealed in stationary fibroblasts. *Science* 1999;286(5442):1172-4.
- [39] Dalby MJ, Childs S, Riehle MO, Johnstone HJ, Affrossman S, Curtis AS. Fibroblast reaction to island topography: changes in cytoskeleton and morphology with time. *Biomaterials* 2003;24(6):927-35.
- [40] Curtis AS, Gadegaard N, Dalby MJ, Riehle MO, Wilkinson CD, Aitchison G. Cells react to nanoscale order and symmetry in their surroundings. *IEEE Trans Nanobioscience* 2004;3(1):61-5.
- [41] Dalby MJ, Riehle MO, Sutherland DS, Agheli H, Curtis AS. Morphological and microarray analysis of human fibroblasts cultured on nanocolumns produced by colloidal lithography. *Eur Cell Mater* 2005;9:1-8; discussion 8.
- [42] Chung TW, Liu DZ, Wang SY, Wang SS. Enhancement of the growth of human endothelial cells by surface roughness at nanometer scale. *Biomaterials* 2003;24(25):4655-61.
- [43] Malda J, van den Brink P, Meeuwse P, Grojec M, Martens DE, Tramper J, Riesle J, van Blitterswijk CA. Effect of oxygen tension on adult articular chondrocytes in microcarrier bioreactor culture. *Tissue Eng* 2004;10(7-8):987-94.
- [44] Barry JJ, Gidda HS, Scotchford CA, Howdle SM. Porous methacrylate scaffolds: supercritical fluid fabrication and in vitro chondrocyte responses. *Biomaterials* 2004;25(17):3559-68.
- [45] Chim H, Ong JL, Schantz JT, Hutmacher DW, Agrawal CM. Efficacy of glow discharge gas plasma treatment as a surface modification process for three-dimensional poly (D,L-lactide) scaffolds. *J Biomed Mater Res A* 2003;65(3):327-35.



- [46] Rodriguez JP, Rios S, Gonzalez M. Modulation of the proliferation and differentiation of human mesenchymal stem cells by copper. *J Cell Biochem* 2002;85(1):92-100.
- [47] Bezemer JM, Radersma R, Grijpma DW, Dijkstra PJ, Feijen J, van Blitterswijk CA. Zero-order release of lysozyme from poly(ethylene glycol)/poly(butylene terephthalate) matrices. *J Control Release* 2000;64(1-3):179-92.
- [48] van Dijkhuizen-Radersma R, Peters FL, Stienstra NA, Grijpma DW, Feijen J, de Groot K, Bezemer JM. Control of vitamin B12 release from poly(ethylene glycol)/poly(butylene terephthalate) multiblock copolymers. *Biomaterials* 2002;23(6):1527-36.
- [49] Sohier J, van Dijkhuizen-Radersma R, de Groot K, Bezemer JM. Release of small water-soluble drugs from multiblock copolymer microspheres: a feasibility study. *Eur J Pharm Biopharm* 2003;55(2):221-8.
- [50] Boyan BD, Hummert TW, Dean DD, Schwartz Z. Role of material surfaces in regulating bone and cartilage cell response. *Biomaterials* 1996;17(2):137-46.



Integrate conventional and novel fabrication technologies together to create multifunctional 3D scaffolds

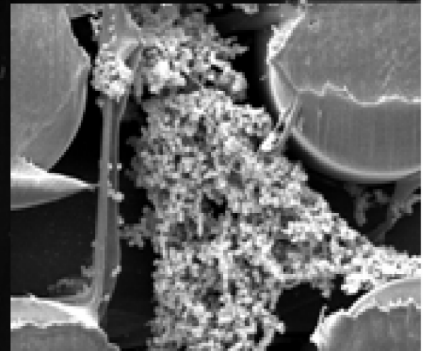
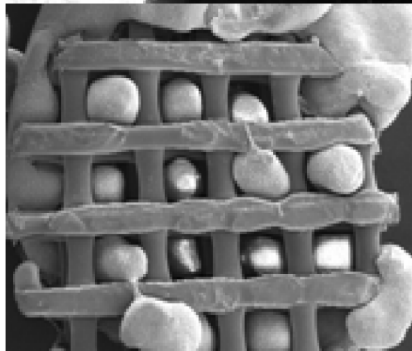


Nothing shocks me. I am a scientist

Harrison Ford as Indiana Jones (1942 – )

Audaces fortuna iuvat

Virgilio (70 B.C. – 19 B.C.)



# Chapter 8

## Design of Biphasic Polymeric 3D Fiber Deposited Scaffolds for Drug Release and Tissue Engineering Applications

L. Moroni <sup>a,\*</sup>, J. Hendriks <sup>a,b</sup>, R. Schotel <sup>b</sup>, J. Sohier <sup>a</sup>, J.R. de Wijn <sup>a</sup>, C.A. van Blitterswijk <sup>a</sup>

<sup>a,\*</sup> Institute for BioMedical Technology (BMTI), University of Twente, P.O. Box 217, 7500 AE Enschede, The Netherlands. E-mail: l.moroni@tnw.utwente.nl

<sup>b</sup> CellcoTec N.V., Prof. Bronkhorstlaan 10D, 3723 MB Bilthoven, The Netherlands

### Abstract

We present here a novel system to create rapid prototyped 3D fibrous scaffolds with a shell-core fiber architecture where the core polymer supplies the mechanical properties and the shell polymer acts as a coating providing the desired physicochemical surface properties for tissue engineering applications. By exploiting viscous encapsulation, a rheological phenomenon often undesired in molten polymeric blends flowing through narrow ducts, fibers with a shell – core configuration can be extruded. Hollow fibers can also be obtained by selective dissolution of the inner core polymer. The core diameter and the shell thickness can be controlled by varying the polymers in the blend, the blend composition, and the extrusion nozzle diameter. Simultaneous with extrusion, the extrudates are organized into three-dimensional matrices with different architectures and custom-made shapes by three-dimensional fiber deposition, a rapid prototyping tool which has recently been applied for the production of scaffolds for tissue engineering purposes. Poly[(ethylene oxide) terephthalate-co-poly(butylene) terephthalate] (PEOT/PBT) 3D fiber deposited (3DF) scaffolds with solid, shell-core, and hollow fiber architecture were fabricated and examined for cartilage tissue regeneration and controlled drug delivery applications.

**Keywords:** shell-core fibers; hollow fibers; viscous encapsulation; rapid prototyping; tissue engineering; drug delivery.

### Introduction

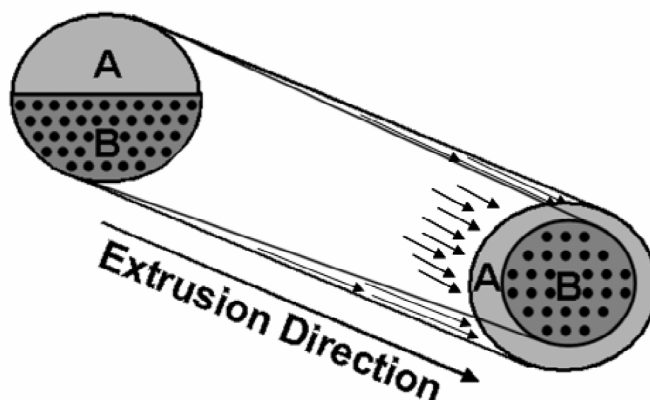
Biomaterial porous scaffolds are generally investigated for drug controlled release and tissue engineering applications as three dimensional (3D) means to vehicle medical treatments in specific locations [1-4] and to guide cell attachment, proliferation and differentiation into the tissue to regenerate [5-9]. Beyond the fact

that these constructs must be biocompatible and possibly biodegradable and/or bioresorbable, they also have to offer an initial and adequate mechanical support for the seeded cells to integrate with the surrounding tissue, to facilitate regaining the original shape of the treated defect and to provide the appropriate chemistry to direct cells and the extra cellular matrix (ECM) produced by them into the proper original tissue structure and architecture. Among the scaffold fabrication techniques currently available, rapid prototyping systems appear to be the most promising to satisfy the first requirements, as they can process a wide number of biomaterials [10, 11] in a custom-made shape and with matching mechanical properties in comparison with the specific application considered [12-14]. The outcomes are 3D scaffolds that normally possess fine tunable porosity, pore size and shape, and have a completely interconnected pore network, which allows a more efficient cell migration and nutrient perfusion than scaffolds fabricated with conventional techniques [15, 16]. Within rapid prototyping systems, 3D fiber deposition (3DF) has lately been investigated by our group to fabricate custom-made scaffolds and to modulate their mechanical properties for tissue engineering applications showing encouraging results [17-19]. In contrast, scaffolds fabricated with conventional techniques can be still shaped with custom-made molds, but it is more difficult to control their mechanical properties, pore size, shape and interconnectivity. In the resulting tortuous spongy-like structure nutrient perfusion is mostly limited to 0.5-1 mm in depth, thus leading to an heterogeneous distribution of cells in the scaffold after few weeks of culture [15, 20]. In this respect, important achievements have been obtained with salt leached or meshed scaffolds seeded with immature chondrocytes [21-24]. Yet, if mature cells are used their response can be quite different as compared to immature cells and tissue formation is still hampered in the middle of scaffolds fabricated with porogen- or mesh-based techniques [25, 26].

The physico-chemical properties of a scaffold are also relevant for drug release and tissue formation. Depending on the affinity between the biomaterial chemical structure and the drug, its release profile changes [2, 27]. Cell attachment and morphology are affected by the material chemical structure. For instance, a rather hydrophilic material typically results in a higher number of attached cells, with a spread and spindle-like shape; in contrast, a more hydrophobic material causes less cell attachment and rounded shape morphology [28]. Attached cell density and morphology ultimately bias the quality of the regenerated tissue in a long term. A way to control the release profile of a specific drug or the distribution and morphology of seeded cells is to fabricate multiphase scaffolds, where different materials are selectively and regionally present in the construct. In the specific case of polymeric scaffolds, blends of two or more polymers can be made and studied for this purpose. These systems would be useful when engineering complex tissues where different cell types are arranged in hierarchical structures such as the heart, the liver and the neural tissue [29, 30]. Such scaffolds are also suitable to engineer tissues for which it is determinant to maintain the original cell morphology like for chondrocytes in cartilage tissue engineering [28, 31, 32]. Studies on polymeric blends for tissue engineering applications have been done by different groups [33-36], but the investigations focused on exploiting the second polymer phase in the blend to create macro and micro porous scaffolds.

In this scenario, the aim of this study was to investigate a novel method to create biphasic shell-core fibers with controlled shell thickness and core diameter, and to simultaneously organize them into 3D scaffolds by means of precise deposition tools such as rapid prototyping technologies. Shell-core fibers are made by extrusion of a blend of two or more miscible and immiscible molten polymers and by exploiting a typical rheological phenomenon known as viscous encapsulation [37]. When the two components of the polymer blend have a significant difference in viscosity in the molten state the polymer with lower viscosity tends to shift, when flowing through a narrow duct – such as the nozzle of an extruder -, towards the walls of the duct during extrusion. This is due to the higher shear stresses present at the walls to which the lower viscosity polymer adapts more easily due to its higher capacity to distort. This separation of the components will produce a stratification - or, eventual, a “canalization” effect resulting in a shell-core structure, as depicted in figure 1. If a shell-core structure is created, the scaffolds can be seen as

### Viscous Encapsulation during Extrusion



**Viscosity A < Viscosity B**

**Figure 1** – Schematic draw of the viscous encapsulation phenomenon. Arrows show the encapsulation of the high viscosity polymer by the low viscosity polymer, due to higher shear stress (longer arrows) along the capillary walls.

a coated structure, where for instance one polymer gives the main mechanical properties and organization to the scaffold, and the other polymer(s) work as a coating to improve the surface properties of the construct. Else, if the difference in viscosity of the polymers in the blend is not significant a random distribution is obtained. In this case the fabricated scaffolds might be still used as “smart” constructs, where the different polymeric phases selectively influence attachment of different cells.

A third possible scaffold system comprising hollow fibers can also be created by using immiscible polymers and applying a selective leaching out technique, that is soaking the scaffolds in a solution that is only a solvent for the core polymer to generate the hollow cavities. These fibers are of a great interest in material science because of their multiple applications in different fields, like environmental [38, 39], electronic [40, 41], biomedical technologies [42, 43], and gene therapy [44, 45]. They find use for microfiltration, photonics, and biomedical instruments, among others. In tissue engineering, 3D hollow fiber scaffolds can provide, for example, a 3D system of reservoirs for drug release or a network for tissue in growth. The conventional fabrication processes used to cast them consist mainly in chemical or thermal phase inversion [46-48]. Among novel techniques, electrospinning and self-assembly has recently been proved to produce nanometer size hollow fibers [49-52]. With these techniques it is possible to some extent to control the hollowness of the fibers and to organize them by weaving technologies into three-dimensional (3D) structures [53]. However, it is difficult to obtain a precise control of the hollow cavities diameter and simultaneously a spatial organization in a 3D fashion. Furthermore, hollow fibers are individually drawn and small variations in the settings can result in irregularities in the lumen and shell size [54, 55].

It is here that this technique to fabricate shell-core and hollow fibers brings its novelty, as it makes use of a commonly unwanted phenomenon in polymeric blends processing. The first endeavor of our investigation was to determine in a set of biocompatible polymers a precise melt viscosity range in which viscous encapsulation occurs during extrusion. Biocompatible polymers with different solubility characteristics were chosen for the ultimate purpose of using the resulting hollow fibers in tissue engineering applications [56-61]. Block-copolymers of polyethyleneoxide-terephthalate (PEOT) and polybutylene-terephthalate (PBT), polybutylmethacrylate-methylmethacrylate (P(BMA/MMA)) and polycapro-lactone (PCL) have been investigated as models. PEOT/PBT are polyether-ester multiblock copolymers belonging to a class of materials known as thermoplastic elastomers which have already been broadly investigated for tissue engineering and drug delivery applications, because by varying the molecular weight of the starting PEG segments and the weight ratio of PEOT and PBT blocks it is possible to tailor-make properties, such as wettability [62], swelling [19, 27, 63], biodegradation rate [62], protein adsorption [28], and mechanical properties [17, 18], in combination with easy processability [63]. These copolymers have shown to be extensively biocompatible both *in vitro* and *in vivo* [56, 57, 64] and reached clinical applications (PolyActive™, IsoTis Orthopaedics S.A.) as cement stoppers and bone fillers in orthopedic surgery [65, 66]. Polymethylmethacrylate (PMMA) and copolymers [58, 67, 68] have found extensive use as bone cements for hip prosthesis implants, while polycapro-lactone is considered as one of the polymer standard in tissue engineering for its good biocompatibility, bioresorbability, and mechanical properties [59-61].

Examples of how 3DF scaffolds with shell-core and hollow fiber architecture can be used in tissue engineering with a particular regard to cartilage tissue formation and in controlled drug delivery applications are presented and discussed as possible smart biomaterials devices. Being viscous encapsulation a general rheological

phenomenon for polymer blends during co-extrusion, the principles treated in this paper will find applications for other polymeric systems as well.

## Materials and Methods

### *Materials Characterization*

Poly(ethylene oxide – terephthalate)/poly(butylene terephthalate) (PEOT/PBT) copolymers were acquired from IsoTis S.A. (Bilthoven, The Netherlands). The composition used in this study were 300/55/45 and 1000/70/30 where, following an aPEOTbPBTc nomenclature (a/b/c), a is the molecular weight in g/mol of the starting PEG blocks used in the copolymerization, while b and c are the weight ratios of the PEOT and PBT blocks, respectively. 1000/70/30 with three different molecular weights (1000/70/30, 1000/70/30-M, and 1000/70/30-L) were obtained. The difference in molecular weight was characterized by their melting indices, the higher molecular weight composition having a smaller melting index.

Poly(butylmethacrylate-methylmethacrylate) (PBMA/MMA) and Poly(caprolactone) (PCL) were purchased from Sigma-Aldrich, with different molecular weights. For P(BMA/MMA) 100.000 g/mol and 150.000 g/mol were used, while for PCL 12.000 g/mol, 65.000 g/mol, and 130.000 g/mol were employed.

The viscosity of the molten polymers was measured with a melting index system (ASTM D1238-73), which determines the grams of polymer flowing under a fixed weight in 10 minutes. A higher melting index corresponded to a lower viscosity. To form the polymeric blends, the polymers were grinded into particles less than 400  $\mu\text{m}$  in size and mixed in a 35/65, 50/50, and 65/35 ratio to reach continuity of the two polymers in the blend. An annealing step of two hours in an oven above the polymers glass temperature ( $T = 80\text{ }^{\circ}\text{C}$ ) was performed in order to obtain a better coarsening of the particles, as shown by Sarazin et al [33, 35]. Blends of immiscible polymers 300/55/45 and 1000/70/30 with P(BMA/MMA) and with PCL of the different given molecular weights, and blends of P(BMA/MMA) with PCL were made. Blends of 300/55/45 with 1000/70/30, which as polymers from the same PEOT/PBT family are miscible, were also obtained.

### *Scaffolds fabrication*

3D scaffolds were manufactured from the polymers and the polymeric blends with a Bioplotter device (Envisiontec GmbH, Germany), essentially an XYZ plotter device as previously described [17-19]. Few modifications were done to extrude highly viscous polymeric fibers. The polymers were put in a stainless steel syringe and heated at  $T = 190\text{-}220\text{ }^{\circ}\text{C}$  through a thermoset cartridge unit, fixed on the “X”-mobile arm of the apparatus. Temperature increased with increasing the viscosity of the processed blend. When the molten phase was attained, a nitrogen pressure of 5 Bars was applied to the syringe through a pressurized cap. Rectangular block models were loaded on the Bioplotter CAM software and plotted layer by layer, through the extrusion of the polymeric system on a stage as a fiber. The deposition speed

varied between 180 mm/min and 230 mm/min, depending on the viscosity of the blend or of the single polymer to extrude. Scaffolds were then characterized by varying the fiber diameter (through the nozzle diameter), the spacing between fibers in the same layer, the layer thickness and the configuration of the deposited fibers within the whole architecture. The used nozzles were stainless steel Luer Lock needles with internal diameter (ID) of 800  $\mu\text{m}$ , 400  $\mu\text{m}$  and 200  $\mu\text{m}$ , shortened to a length of 16.2 mm. The fiber spacing was set to 1800  $\mu\text{m}$ , 800  $\mu\text{m}$ , and 600  $\mu\text{m}$ , while the layer thickness to 625  $\mu\text{m}$ , 225  $\mu\text{m}$ , and 150  $\mu\text{m}$ , respectively for the different needles used. The architecture was changed by plotting fibers with 90° orientation steps between two successive layers or by modifying the fiber orientation after one or after two plotted layers (referred to as 0-90 or 00-9090 configurations).

Compression molded scaffolds were also fabricated as a reference for the 3D scaffolds characterization. Briefly, for each composition 4 grams of polymer blends were molten at  $T = 190\text{ }^{\circ}\text{C}$  in a stainless steel mould and left to cool down at room temperature under a pressure of 5bars. Solid sheets with the same dimensions as the 3D scaffolds were then obtained.

### *Scaffolds Characterization*

Cylindrical samples of 4 mm in diameter by 4 mm in height were cored out in the “Z-direction” from the rectangular 3D plotted blocks. Scaffolds geometry and architecture was characterized by environmental scanning electron microscopy (ESEM) analysis with a Philips XL 30 ESEM-FEG. The porosity of 3D plotted shell-core scaffolds was calculated as [18]:

$$P = 1 - \frac{V_{\text{scaffold}}}{V_{\text{cube}}} = 1 - \frac{\pi}{4} \cdot \frac{1}{\frac{d_2}{d_1}} \cdot \frac{1}{\frac{d_3}{d_1}} \quad (1)$$

where P is the scaffold porosity, d1 the fiber diameter, d2 the fiber spacing and d3 the layer thickness, within each different structure.

PEOT/PBT scaffolds with hollow fibers were obtained by soaking for three days 3D shell-core scaffolds in a solvent specific for the core polymer. Acetone (Sigma, The Netherlands) was used for P(BMA/MMA) core polymers, while 100% acetic acid (Sigma, The Netherlands) was used for PCL. Scaffolds were washed and left to dry for a day and then placed in a vacuum oven at 50  $^{\circ}\text{C}$  to leach out the remaining traces of the solvent. The ratio between the hollow core diameter (d) and the fiber diameter (D) was considered as an index to measure the blend composition after extrusion and compared it with before scaffold fabrication.

A polarized incident light optical microscope (PLM) was also used to analyze the structure of the 3D scaffolds fabricated with the 300/55/45 – 100/70/30 blend. The samples were embedded in Poly(methylmethacrylate) (PMMA) and then sectioned with a Leyca saw microtome (sp 1600). Thin sections (100  $\mu\text{m}$ ) were fixed with UV-glue on a glass slide and examined with PLM. In this case, the swelling ratio Q of



solid polymeric samples and of the 3DF scaffolds was also measured [19]. Briefly, cylindrical specimens with the same dimension above mentioned were put in PBS at 37 °C and left for three days to reach a swollen equilibrium state.  $Q$  was calculated as:

$$Q = 1 + \frac{\rho \cdot (M_{\text{swollen}} - M_{\text{dry}})}{M_{\text{dry}}} \quad (2)$$

where  $\rho$  was taken for simplicity as 1.2 g/ml for all the compositions,  $M_{\text{swollen}}$  is the scaffold equilibrium wet weight, and  $M_{\text{dry}}$  is the scaffold dry weight. The swollen weight was measured after having blotted the scaffolds with a tissue and after having expelled the water from the pores by applying pressurized air.

3DF scaffolds for culture experiments were sterilized in isopropanol (IPASEPT 70, VWR International) for 15 minutes, thoroughly washed with a phosphate buffered saline (PBS) solution (Gibco-BRL) three times, and incubated over night in culture medium prior cell seeding.

### ***Cell Seeding and Culture***

Chondrocytes were isolated via collagenase digestion from articular cartilage harvested from an 18-month old bovine knee joint [69]. Primary cells were aggregated with 300  $\mu\text{g/ml}$  of fibronectin (Invitrogen), statically seeded at a density of 3 millions in 50  $\mu\text{l}$  of medium and cultured on PEOT/PBT 3DF scaffolds ( $\varnothing$ 4 mm and 4 mm thick) with solid, shell-core, and hollow fiber architecture ( $n=6$ ).

Two sets of independent experiments were done to evaluate the shell-core or the hollow fiber 3D scaffolds as compared to solid fiber ones. In a first experiment, 300/55/45, 1000/70/30, and 1000/70/30-L – 300/55/45 shell-core 3DF scaffolds fabricated with 00-9090 architecture were selected and cultured for 3 weeks. This architecture was chosen as it displays more homogeneous pore size in all the directions as compared to a 0-90 configuration. Solid and shell-core fiber scaffolds were compared to assess the influence of different physico-chemical properties on cell morphology and tissue formation. In a second experiment, 300/55/45 3DF scaffolds with solid and hollow fibers were cultured for 4 weeks. Solid and hollow fiber scaffolds were compared to evaluate the difference in cell entrapment and ECM formation.

The culture medium contained HEPES (Invitrogen)-buffered DMEM (Invitrogen) supplemented with 10% fetal bovine serum (FBS, Sigma-Aldrich), 0.2 mM ascorbic acid 2-phosphate (Invitrogen), 0.1 mM non-essential amino acids (Sigma-Aldrich), 0.4 mM proline (Sigma-Aldrich), 100 units/ml penicillin (Invitrogen), and 100  $\mu\text{g/ml}$  streptomycin (Invitrogen). Constructs were cultured at 37 °C in a humid atmosphere with 5%  $\text{CO}_2$ . Medium was refreshed twice a week.

### ***Biochemical Analysis***

DNA and glycosaminoglycans (GAG) assays were performed at the end of the culture periods. Constructs were digested overnight at 56 °C in a Tris-EDTA buffered solution containing 1 mg/ml proteinase K, 18.5 µg/ml pepstatin A, and 1 µg/ml iodoacetamide (Sigma-Aldrich). Quantification of total DNA was done with Cyquant dye kit according to the manufacturers description (Molecular Probes) using a spectrofluorometer (LS 50B, Perkin Elmer). GAG amount was determined spectrophotometrically (EL 312e Bio-TEK Instruments) after reaction with dimethylmethylene blue dye (DMMB, Sigma-Aldrich) by measuring absorbance at 520 nm. The final amount was calculated using a standard of chondroitin sulphate B (Sigma-Aldrich).

### ***Histology Analysis***

Samples were fixed overnight in 0.14 M cacodylate buffer (pH = 7.2 – 7.4) containing 1.5% glutaraldehyde (Merck). Scaffolds were subsequently dehydrated in sequential ethanol series, plastic embedded in glycol-methacrylate (Merck) and cut using a microtome to yield 5 µm sections. Slices were stained with safranin-O (Sigma-Aldrich) to visualize extracellular matrix (sulphated glycosaminoglycans - GAG), and counterstained with haematoxylin (Sigma-Aldrich) and fast green (Merck) to visualize nuclei and cytoplasm of the cells. Mounted slides were examined under a light microscope (Nikon Eclipse E400) and representative images captured using a digital camera (Sony Corporation, Japan) and Matrix Vision software (Matrix Vision GmbH, Germany). Tissue constructs on scaffolds were also analyzed by SEM. Specimens were fixed and dehydrated as described above and critical point dried from liquid carbon dioxide using a Balzers CPD 030 machine. Samples were then gold sputtered and studied under the SEM.

### ***Mechanical Characterization***

To compare the dynamic stiffness of solid 300/55/45, 1000/70/30, and shell-core 1000/7030-L – 300/55/45 3DF scaffolds before and after culturing, dynamic mechanical analysis (DMA; Perkin Elmer 7e) was performed. For each configuration three samples were analyzed. Cylindrical fixtures were chosen to test the specimens and evaluate their behavior as a whole structure along their compression axis, in the “Z-direction”.

Scaffolds and cartilage constructs were loaded with a dynamic force varying from 1.5N to 2.5N in a dynamic stress experiment. More specifically, a starting force of 1.5N was applied and then continuously increased to 2.5N with a sinusoidal loading ramp of 50mN/min, at a constant frequency of 1Hz. The dynamic stiffness was calculated by the instrument software (Pyris). The tests were conducted under wet conditions: a synovium-like fluid was prepared as a 3% (w/v) solution of polyvinylpyrrolidone (PVP) in de-ionized water. This was done to simulate the physiological environment of articular cartilage. Scaffolds were soaked in PVP-solution, before loading. The temperature was 37 °C during all of the experiments.

### *Lysozyme loading*

To assess the different drug release capacities of 300/55/45 3D scaffolds, cylindrical hollow and full (control) fiber 3DF scaffolds were immersed in a 55mg/ml lysozyme solution for three hours, under vacuum. The release was detected through a  $\mu$ BCA assay (Pierce) with a spectrometer (EI 312e, BioTek Instruments) at 570 nm. Control scaffolds were just normal 3DF PEOT/PBT scaffolds. A hollow reservoir construct with the same geometry was also tested. Hollow reservoirs were obtained after protein adsorption by dipping the hollow scaffolds in a 16% weight/volume 1000/70/30 solution in chloroform (Sigma, The Netherlands) and evaporating the solvent to close the fibers at their ends.

### *Statistical Analysis*

Statistical Analysis was performed using a Student's t-test, where the confidence level was set to 0.05 for statistical significance. Values in this study are reported as mean and standard deviation. To evaluate the effect of the polymers' surface on chondrocyte morphology ten micrographs on different and randomly chosen pores for each scaffold were considered. Cell morphology was classified by five independent observers as spread (S), mostly spread (S-), mostly rounded (R-), and rounded (R). A non parametric Mann-Whitney test was carried out to assess the independency of the cell morphology on 300/55/45 from the cell morphology on 1000/70/30.

## Results

### *Scaffolds Characterization*

The melting indexes of the polymers considered in this study are presented in table 1. Values changed from  $2.7 \pm 0.2$  g/10min for PCL with a molecular weight of 130.000 g/mol to  $395 \pm 36$  g/10min for PCL with a molecular weight of 12.000 g/mol. All the other polymers had a melting index within this range. For polymeric blends, the ratio of their melting indexes was more relevant. In particular, under the rheological parameters of our 3D depositing process viscous encapsulation and the formation of a shell-core fiber construct was found for:

$$2.5 \leq \frac{M.I.(A)}{M.I.(B)} \leq 10.5 \quad (3)$$

where M.I.(A) is the melting index of the less viscous polymer A, and M.I.(B) is the melting index of the more viscous polymer B in the blend. Figure 2 shows an example of the shell-core structure before and after selective leaching to eventually

**Biphasic  
3DF Scaffolds**

Polymer/M.I. Ratio	300/55/45	1000/70/30	1000/70/30-low Mw	1000/70/30-middle Mw	PBMA Mw100	PBMA Mw150	PCL Mw12	PCL Mw65	PCL Mw130
300/55/45	*	0,8	0,37	0,66	1,1	5,62	0,071	1,6	10,4
1000/70/30	1,27	*	nd	nd	1,4	7,12	0,09	2	13,14
1000/70/30-low Mw	2,7	nd	*	nd	2,96	15,16	0,2	4,28	27,96
1000/70/30-middle Mw	1,52	nd	nd	*	1,66	8,53	0,107	2,41	15,74
PBMA Mw100	0,91	0,72	0,34	0,6	*	nd	0,064	1,44	9,44
PBMA Mw150	0,18	0,14	0,06	0,12	nd	*	0,013	0,28	1,84
PCL Mw12	14,1	11,13	5,23	9,34	15,5	30	*	nd	nd
PCL Mw65	0,63	0,5	0,23	0,41	0,7	3,54	nd	*	nd
PCL Mw130	0,1	0,07	0,03	0,06	0,1	0,5	nd	nd	*

**Table 1** – Melting Index ratio of the investigated polymers reported as row/column values. In grey the ratio values that were found to give viscous encapsulation. nd = not determined.

Needle Internal Diameter (µm)	Fibre Diameter (µm)	Shell Thickness (µm)	Core Diameter (µm)	Fibre Spacing (µm)	Layer Thickness (µm)	Structural Porosity (%)	Total Porosity (%)
800	752 ± 20	82 - 642	110 - 670	1850 ± 77	614 ± 71	61	62 - 71
400	348 ± 4	68 ± 14	280 ± 18	766 ± 11	227 ± 20	45	75
250	165 ± 35	107 ± 26	58 ± 17	565 ± 17	144 ± 10	74	78

**Table 2** – Characterization of the shell-core structure of 3DF scaffold fibers depending on the nozzle diameter. The 3DF scaffolds fiber spacing, layer thickness, structural and total porosities were also measured. A 50/50 weight ratio blend of 300/55/45 and P(BMA/MMA) with Mw = 150 kg/mol was used.

create the hollow fibers. Figure 2c gives the morphology of a 3D matrix obtained by compression molding. Here, the absence of shear stresses due to the constrained compression of the molten blend resulted in a dispersion of the two polymers. After selective leaching a porous random three-dimensional matrix is achieved with no stratification effects.

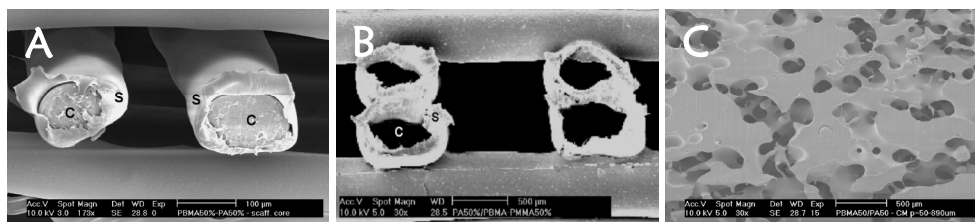


**Figure 2** – SEM micrographs of 50%/50% 300PEOT55PBT45 - P(BMA/MMA) 3DF matrix before (a) and after (b) leaching out P(BMA/MMA). The shell (S) – core (C) structure is clearly visible. (c) 50%/50% 300PEOT55PBT45 - P(BMA/MMA) compression molded scaffold after selective leaching of P(BMA/MMA) shows the dependence of viscous encapsulation on shear stresses. (a) scale bar: 100  $\mu\text{m}$ ; (b) scale bar: 200  $\mu\text{m}$ ; (c) scale bar: 500  $\mu\text{m}$ .

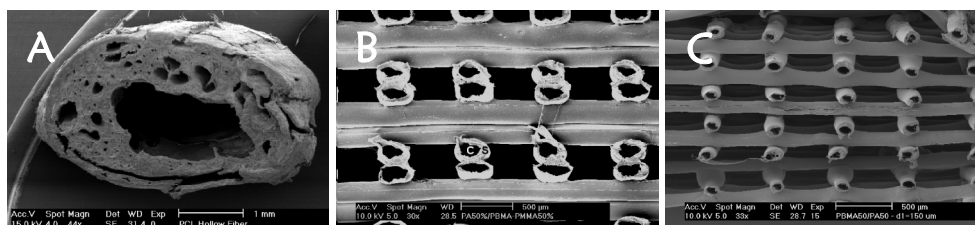


**Figure 3** – SEM micrographs of hollow fibrous scaffolds with different hollow cavity diameter and shell thickness. (a) scale bar: 1 mm; (b, c) scale bar: 500  $\mu\text{m}$ .

The possibilities to control the diameter of the inner hollow cavity and the thickness of the shell were also analyzed. The melting index ratio, the weight ratio in the blend, and the extrusion nozzle diameter were found to be especially of influence in this respect. By increasing the melting index ratio or the percentage of the lower viscosity polymer in the blend, the diameter of the hollow cavities decreased. Conversely, with increasing the nozzle diameter, the diameter of the hollow cavities increased to a point where stratification and consequently multiple cavities occurred within the same fiber, as illustrated in figure 3. As an exemplification, table 2 summarizes how the lumen diameter and the shell thickness vary with the nozzle internal diameter. ESEM analysis revealed fiber diameters of  $752 \pm 20 \mu\text{m}$ ,  $348 \pm 4 \mu\text{m}$ , and  $165 \pm 35 \mu\text{m}$  for needle diameters of 800  $\mu\text{m}$ , 400  $\mu\text{m}$ , and 200  $\mu\text{m}$ , respectively. In deposited scaffolds, the fiber spacing  $d_2$  was measured to be  $1850 \pm 77 \mu\text{m}$ ,  $766 \pm 11 \mu\text{m}$ , and  $565 \pm 17 \mu\text{m}$ , while the layer thickness  $d_3$  was  $614 \pm 71 \mu\text{m}$ ,  $227 \pm 20 \mu\text{m}$ ,  $144 \pm 10 \mu\text{m}$ , respectively. The overall porosity before scaffold treatment was measured to be  $61 \pm 3\%$ ,  $45 \pm 4\%$ , and  $74 \pm 8\%$ , respectively. By varying these parameters, it was possible to modulate the hollow cavity diameter from  $42 \pm 6 \mu\text{m}$  to  $684 \pm 219 \mu\text{m}$ , while the shell wall thickness varied from  $37 \pm$

17  $\mu\text{m}$  to  $649 \pm 52 \mu\text{m}$ . Ratios lower than 2.5 resulted in blends where more random rearrangements occurred. Ratios higher than 10.5 resulted in blends where co-extrusion of the components was not longer possible. The deposited fibers were composed of a single polymer, which changed from the low viscosity component to the high viscosity one during extrusion.

d/D - 35/65 Blend		d/D - 50/50 Blend		d/D - 65/35 Blend	
Theoretical	Measured	Theoretical	Measured	Theoretical	Measured
0.752	0.643 - 1	0.707	0.56 - 0.804	0.642	0.451 - 0.702

**Table 3** – Characterization of the blend composition before and after extrusion (volume fractions assumed to be approximately equal to weight fractions).

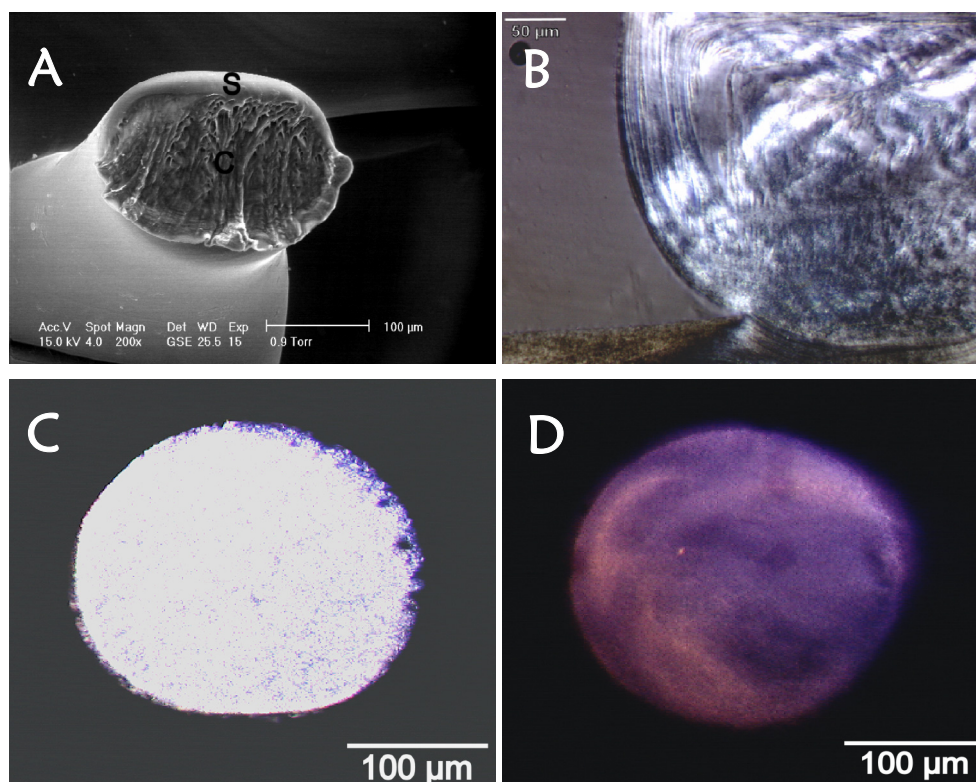


**Figure 4** – ESEM (a) and PLM (b) micrographs of 50%/50% blend of 1000/70/30 and 300/55/45. (a) detail of a fiber after 3 weeks in water, scale bar: 100  $\mu\text{m}$ . The shell (S) – core (C) structure is depicted. (b) PLM image, showing the outer amorphous 1000/70/30 and the inner birefringent 300/55/45 phases. A homogeneous outer shell layer can be clearly detected; scale bar: 50  $\mu\text{m}$ . In comparison are shown cross-sections of a 300/55/45 (c) and of a 1000/70/30 (d) fiber. Scale bar: 100  $\mu\text{m}$ .

A shell-core structure and subsequently a hollow fiber construct were clearly formed for 50/50 and 65/35 blend ratios. After a stabilization time of the blend in the

molten state, the extruded fibers appeared to have roughly the same composition as the original blend (table 3). The ratio between the hollow core diameter  $d$  and the fiber diameter  $D$  represent the extruded blend composition, which can be compared with the theoretical composition. The lower limit for the less viscous - shell - component appeared to be 35 wt% since blends with a smaller than 35/65 ratio lost integrity in most of the samples after leaching of the high viscosity component. Also with miscible polymers – from the PEOT/PBT family – shell-core fibers could be made through viscous encapsulation, provided the melting index ratio was within the appropriate range, as shown in figure 4. An outer shell layer of 1000/70/30 on a 300/55/45 core can be seen with environmental scanning electron microscopy (ESEM), especially when the sample is observed in a wet environment after swelling. Since hydrophilic 1000/70/30 swells more than hydrophobic 300/55/45, it is possible, by analyzing the thickness of the shell layer and of the core fiber before and after swelling, to determine which polymer corresponds to the shell and which to the core. ESEM analysis revealed a fiber diameter  $d_1$  of  $264 \pm 27 \mu\text{m}$ , a fiber spacing  $d_2$  of  $783 \pm 33 \mu\text{m}$ , and a layer thickness  $d_3$  of  $227 \pm 20 \mu\text{m}$ . The core diameter was measured as  $196 \pm 24 \mu\text{m}$ , and the shell thickness as  $56 \pm 18 \mu\text{m}$ . This corresponded to a scaffold porosity of  $70\% \pm 2\%$ . Table 4

Polymer	Q - Solid	Q - 3DF Scaffold	M.I. (g/10min)	M.I. Ratio
300/55/45	$1.06 \pm 0.01$	$1.14 \pm 0.01$	$28 \pm 2$	-
1000/70/30	$1.715 \pm 0.005$	$1.76 \pm 0.02$	$35.5 \pm 4.5$	$1.26 \pm 0.06$
1000/70/30-L	$1.715 \pm 0.005$	$1.76 \pm 0.02$	$75.5 \pm 3.84$	$2.7 \pm 0.04$
1000/70/30-300/55/45	$1.31 \pm 0.007$	$1.55 \pm 0.03$	-	-

**Table 4** – Volume swelling ratio, melting index and relative ratios of 300/55/45 and two compositions of 1000/70/30 differing by molecular weight; (L) indicates a lower molecular weight.

introduces the different swelling capacities of the copolymers related to their melting indexes. Viscous encapsulation was found to happen only when 1000/70/30-L was used. The swelling ratio  $Q$  of the solid material was measured as  $1.06 \pm 0.01$  for 300/55/45,  $1.715 \pm 0.005$  for 1000/70/30, and  $1.31 \pm 0.007$  for the 1000/70/30-L – 300/55/45 blend. An intermediate value of the swelling ratio for the 50/50 w/w is as expected. The confinement exercised by the 300/55/45 domains on the 1000/70/30 regions may result in “pre-stressed” 300/55/45 areas because of the swelling pressure exercised by the 1000/70/30 domains. The swelling ratio of the scaffolds was slightly higher as compared to solid materials and measured as  $1.14 \pm 0.01$  for 300/55/45,  $1.76 \pm 0.02$  for 1000/70/30, and  $1.55 \pm 0.03$  for the 1000/70/30-L-300/55/45 blend. This is due to better water uptake capacity of the copolymers in a filament shape, because of the higher surface to volume ratio. Also, polarized light microscopy analysis revealed that there is not a complete separation of the two polymers, but that domains of the amorphous 1000/70/30 are also present inside the semi-crystalline birefringent 300/55/45 core of the fiber. Finally, a triphasic polymeric blend was formed and processed to achieve further instructive properties of the 3D scaffolds. The blend was formed

from 50% of highly viscous P(BMA/MMA) core polymer, and the remaining 50% was comprised of 25% of 300/55/45 and 25% of 1000/70/30, the latter two being

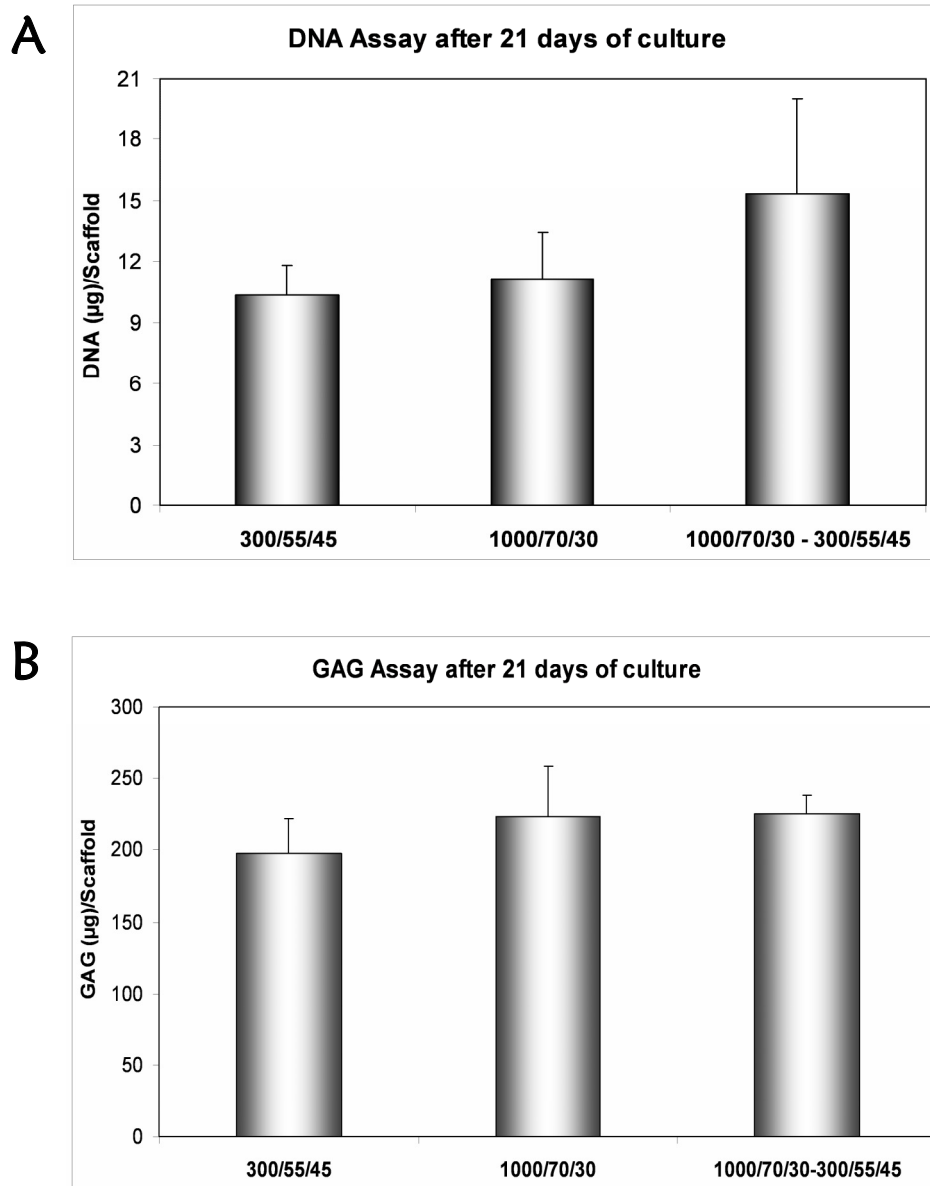


**Figure 5** – DNA (a) and GAG (b) assay results. Primary chondrocytes were seeded and cultured (21 days) on respectively 300/55/45, 1000/70/30 and 1000/70/30-L – 300/55/45 scaffolds (n=6).

known to have different physico-chemical properties which are of importance for drug release rates or cell morphology in cultures. The fabricated fibers showed three



distinct phases, and when the core polymer was dissolved a scaffold with 300/55/45 hollow fibers coated with 1000/70/30 was obtained (data not shown).

### *1000/70/30-L – 300/55/45 Shell-Core 3DF Scaffolds*

#### *Tissue Formation*

3DF scaffolds fabricated with 300/55/45, 1000/70/30, and 1000/70/30-L-300/55/45 blended copolymers were seeded with bovine primary articular chondrocytes and cultured for 21 days. No significant difference was detected in the amount of DNA and GAG present in the different constructs, as illustrated in figure 5. Specifically, DNA amount was  $10.36 \pm 1.43 \mu\text{g}$  in 300/55/45,  $11.17 \pm 2.3 \mu\text{g}$  in 1000/70/30, and  $15.3 \pm 4.66 \mu\text{g}$  in 1000/70/30 – 300/55/45. GAG was quantified as  $197.20 \pm 24.6 \mu\text{g}$  in 300/55/45,  $223 \pm 35.6 \mu\text{g}$  in 1000/70/30, and  $225 \pm 13.2 \mu\text{g}$  in 1000/70/30 – 300/55/45. Histological sections of the constructs confirmed cartilage specific GAG formation, as they were stained for safranin-O and cells were organized in lacunae surrounded by extra cellular matrix, which is typical for cartilage organization (Figure 6). More interestingly, after 3 weeks of culture ESEM analysis revealed spread chondrocyte morphology in 300/55/45, while rounded chondrocyte morphology was maintained in the shell-core fibrous scaffold, due to the outer 1000/70/30-L shell layer (Figure 7). Cells adhered on 300/55/45 fibers (Figures 7a and 7c), while staying aggregated and forming interconnected strands of tissue when in contact with 1000/70/30-L (Figures 7b and d). A similar cell morphology was detected on 1000/70/30 alone scaffolds (data not shown). Table 5 summarized the percentage of cells observed to be either spread, mostly spread, mostly rounded, or rounded. The statistics performed on the different categories always revealed independency of cell morphology on 300/55/45 and 1000/70/30, confirming the qualitative morphology findings by SEM. Extra cellular matrix formation could also be detected around the chondrocytes and in the scaffold pores (Figures 7e and 7f).

(%)	300/55/45	1000/70/30
<b>S</b>	68	8
<b>S-</b>	28	4
<b>R-</b>	2	46
<b>R</b>	2	42

**Table 2** – Cell Morphology analysis on 1000/70/30-L-300/55/45 and on 300/55/45 3DF scaffolds. Cells were classified as spread (S), mostly spread (S-), mostly rounded (R-), or rounded (R) and results expressed in percentages for class belonging. Cell morphology on 1000/70/30 scaffolds was similar as on the blended ones.

#### *Cartilage Construct Mechanical Properties*

The dynamic stiffness of empty scaffolds and cartilage constructs after 21 days of culture was measured. As shown in figure 8, at day 0 the dynamic stiffness of

1000/70/30-L-300/55/45 was higher than the stiffness of 300/55/45 and 1000/70/30, having the same scaffold structure and architecture. After 21 days of culture, the dynamic stiffness of the constructs was significantly higher than the stiffness of the empty scaffolds for all the conditions examined. Specifically the dynamic stiffness increased from  $0.95 \pm 0.07$  MPa to  $1.72 \text{ MPa} \pm 0.3$  MPa for 300/55/45, from  $0.996 \pm 0.16$  MPa to  $1.3 \pm 0.015$  MPa for 1000/70/30, and from  $1.85 \pm 0.13$  MPa to  $2.26 \pm 0.3$  MPa for 1000/70/30-L – 300/55/45. The dynamic stiffness of the shell-core construct was also significantly higher than the stiffness of the 300/55/45 and of the 1000/70/30 constructs.

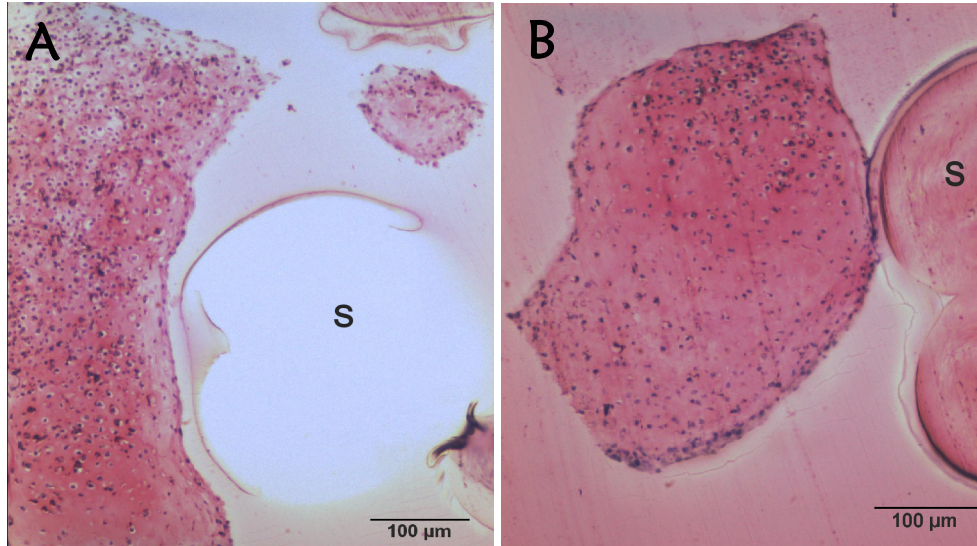


**Figure 6** – Histological sections of 300/55/45 (a) and 1000/70/30-L-300/55/45 (b) constructs, showing sulphated GAG formation with safranin-O staining. Scaffold architecture: 00-9090. S denotes 3DF scaffold fibers. Scale bar: 100  $\mu\text{m}$ .

Biphasic  
3DF Scaffolds

### *300/55/45 3DF Hollow Fiber Scaffolds*

#### *Tissue Engineering and Drug Delivery Applications*

Bovine primary articular chondrocytes cultured for 28 days in 3DF hollow fiber scaffolds were found to grow and form extracellular matrix (ECM) not only in the scaffold macropores, but also inside the hollow cavities as depicted in figure 9. This resulted in a significantly higher amount ( $p < 0.05$ ) of attached cells and of ECM formed, as compared to 3DF solid fiber scaffolds with the same architecture, due to a higher surface availability and likely due to a higher cell entrapment efficiency. Specifically the measured DNA amount increased from  $10.82 \pm 1.51$  ng for solid fiber scaffolds to  $16.46 \pm 3.4$  ng for hollow fiber scaffolds. GAG amount increased from  $272.97 \pm 67.72$   $\mu\text{g}$  for solid fiber scaffolds to  $564.56 \pm 85.48$   $\mu\text{g}$  for hollow fiber ones. Taking further advantage of the hollow cavities would consist of incorporating biological agents, which could be released in a controlled fashion. As

shown in figure 10 for a model protein like lysozyme, when the protein was adsorbed on the scaffold a burst or sustained release could be achieved with hollow fibers, respectively open or end-capped.

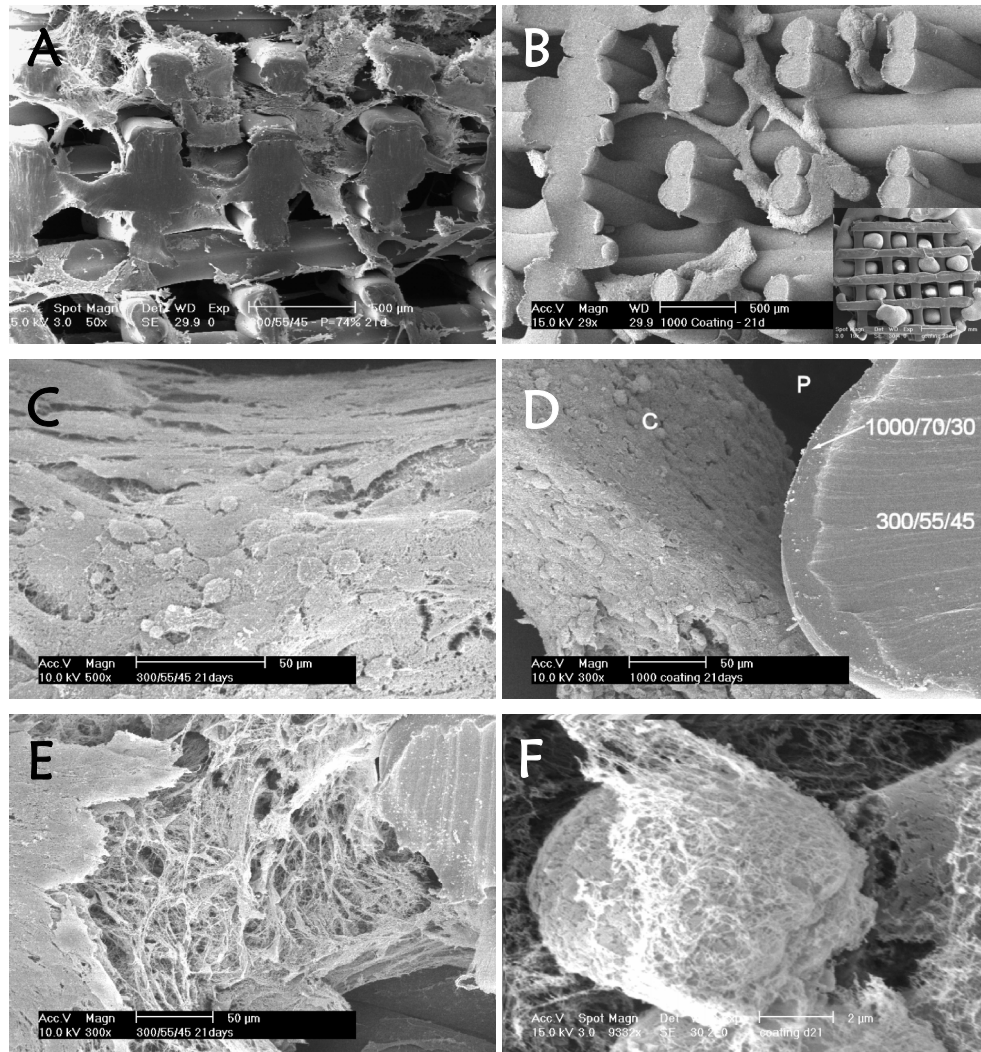


**Figure 7** – ESEM micrographs of 300/55/45 (a, c, e) and 1000/70/30-L-300/55/45 (b, d, f) constructs after 21 days of culture. Spread cell morphology (a, c) can be seen in 300/55/45 scaffolds, while rounded morphology (b, d) is kept in the shell-core fibrous scaffold (analogous results obtained for 1000/70/30 scaffolds). ECM formation (e,f) can be detected for both the constructs. Insert in micrograph (b) is indicative of a relatively more homogeneous cell distribution in the shell-core scaffolds as compared to 300/55/45 ones. C shows chondrocytes aggregation, while P denotes the pore space. Scaffold architecture: 00-9090. (a, b) scale bar: 500  $\mu\text{m}$ ; (c, d, e) scale bar: 50  $\mu\text{m}$ ; (f) scale bar: 2  $\mu\text{m}$ .

Biphasic  
3DF Scaffolds

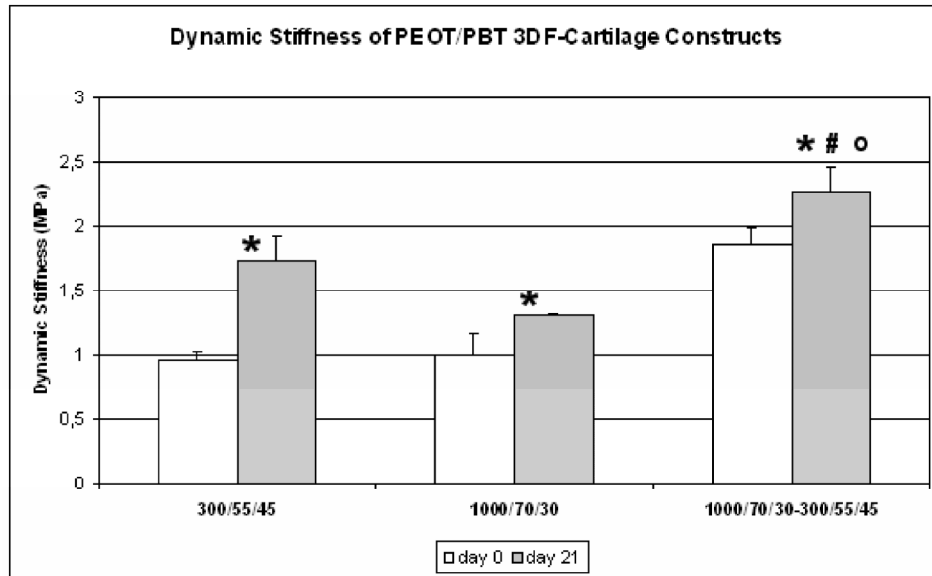


**Figure 8** – Dynamical stiffness measurement of empty scaffolds and cartilage constructs after 21 days of culture. (\*) shows significant differences with respect of empty scaffolds; (#) indicates significant differences from 300/55/45, while (o) from 1000/70/30. 00-9090 scaffold architecture was considered (n=6).

### Biphasic 3DF Scaffolds

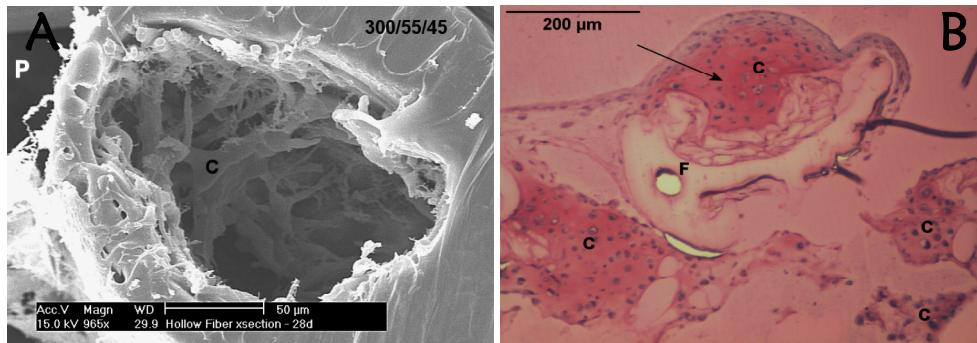


**Figure 9** – SEM (a) and optical microscope (b) micrographs showing chondrocytes (C) and ECM formation (arrow - pink staining) inside and outside the hollow fibers (P = Pore; F = Fiber). Scale bar: (a) 50  $\mu\text{m}$ ; (b) 200  $\mu\text{m}$ .

## Discussion

### *Shell-Core 3DF Scaffold Fabrication*

Biphasic polymeric 3D scaffolds have been fabricated with a Bioplotter and showed to have potential applications in tissue engineering and controlled drug release. A shell-core fiber structure was obtained by exploiting a phase separation

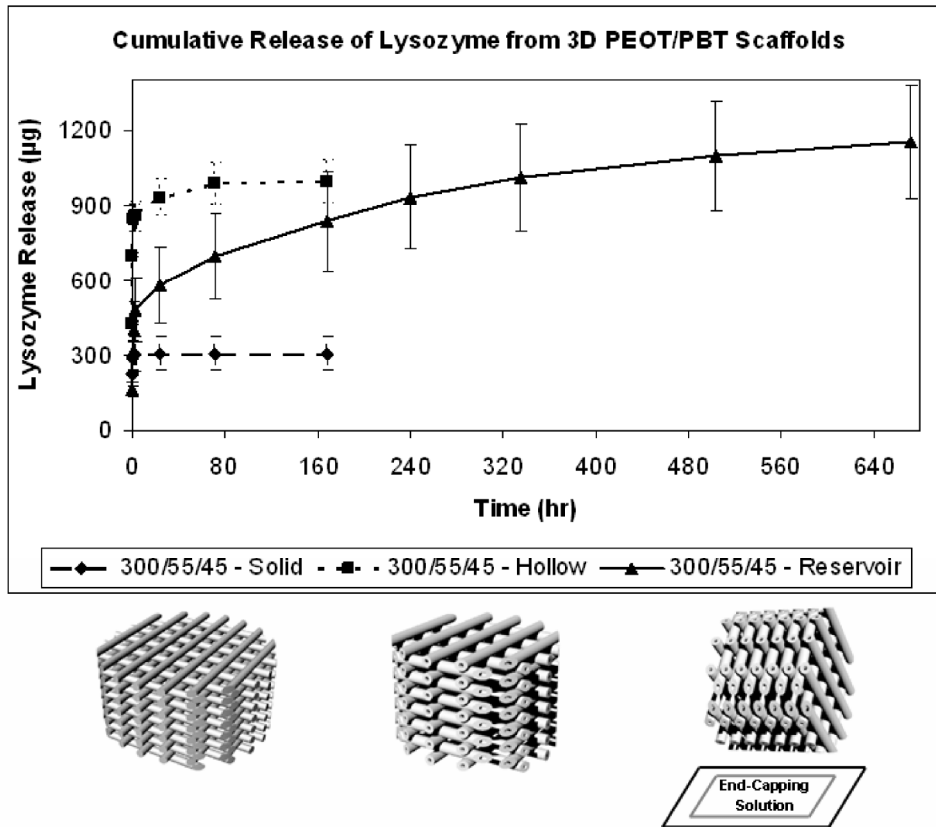


**Figure 10** – Lysozyme cumulative release profile from a 300/55/45 3DF solid, hollow and reservoir (end-capped) scaffold over one month. A higher amount of protein is released in a burst fashion in hollow fibers scaffolds as compared to solid fibers. If hollow fibers are end-capped with 1000/70/30 membranes the same amount of protein is released in a sustained manner.

phenomenon known as viscous encapsulation [37], in which the less viscous component of a blend tends to shift to the wall of a capillary when subjected to the shear stresses during flow. Viscous encapsulation occurred for a specific range of polymer viscosity ratios, determined through their melting index. It was strongly influenced by the diameter of the nozzle from which the blended fibers were extruded. A smaller core diameter was obtained when the melting index ratio increased from 2.5 to 10.5 and for smaller nozzles diameter. This might be due to the consequent increase of the flow rate of the low viscosity polymer, which indicates a preferential extrusion of this component on top of the effect of viscous encapsulation. If a polymeric blended scaffold is fabricated through compression molding, a randomized structure is obtained and microporosity is achieved when one of the polymers is leached out by solvent extraction as shown in figure 2. For a melting index ratio lower than 2.5, a random laminar mixture of the polymers is obtained. Viscous encapsulation did not occur due to the small difference in viscosity of the components. This is due to the similar shear rates experienced by the

two polymers, resulting in comparable velocities and in the production of secondary flows, as also shown by Dooley *et al* [37]. In this case, if one of the two phases was extracted with a solvent, the scaffold integrity was lost because of the removal of the extracted polymer from the fiber connections. If no polymer extraction is performed, such scaffolds could be employed in tissue engineering applications as biphasic polymeric constructs to attach cells selectively, for instance, by exploiting the different cells-surface interaction properties of the two polymers [28]. In contrast, ratios higher than 10.5 resulted in blends where co-extrusion of the components was no longer possible. The deposited fibers were composed of a single polymer, which changed from the low viscosity component to the high viscosity one during extrusion.

Viscous encapsulation also occurred in a certain range of blend composition. The core diameter decreased with the increase of the percentage of the low viscosity component PEOT/PBT, resulting in a consequent increase of the shell thickness. The composition of the blends after scaffold fabrication was consistent with the original blends composition, as shown by analyzing the hollowness index  $d/D$  presented in table 3. Only for a 35/65 blend the leached scaffolds often lost their integrity. This was due to the higher amount of the “core”-fiber polymer and to its higher viscosity. When these scaffolds were leached, the resulting structure was too fragile and would collapse on itself. As the 50/50 composition gave the most regular hollow fiber scaffolds, this blend was chosen to show improved cell and drug release properties of the biomaterial constructs.

#### ***1000/70/30-L – 300/55/45 Shell-Core 3DF Scaffolds Study***

Shell-core biphasic polymeric constructs were tested to assess their influence on cartilage tissue formation. 300/55/45, 1000/70/30, and 1000/70/30 with a lower molecular weight coated on 300/55/45 PEOT/PBT scaffolds were cultured with primary adult bovine chondrocytes. Despite a similar amount of cells attachment (DNA) and ECM formation (GAG) measured in all the considered scaffolds, 50/50 blended 1000/70/30-L-300/55/45 and 1000/70/30 scaffolds showed a more homogeneously distributed tissue formation as compared to 300/55/45 constructs. It seems that the scaffold polymeric composition is not a critical parameter to trigger GAG production specific for cartilaginous tissue. However, the fact that cells remained aggregated and maintained their round morphology in the shell-core scaffolds indicates that the 1000/70/30-L shell provides an environment supporting chondrocyte differentiation. This is in agreement with the findings of Mahmood *et al*. [28] and Woodfield *et al* [70] where chondrocytes cultures on 1000/70/30 not only maintained their rounded morphology but were found to produce a significantly higher amount of collagen type II.

The shell-core scaffolds had a higher dynamic stiffness than 300/55/45 and 1000/70/30 alone with the same structure and architecture, which might be explained by the contribution of the up taken water from 1000/70/30 after swelling in the medium to the scaffold dynamic stiffness [19]. When dynamically compressed, the response of the structure is not only given by the intrinsic stiffness of the dry material, but also by the fluid phase absorbed by 1000/70/30 and by the fluid

component that is pumped in and out of the porous scaffold. It is for this component that 1000/70/30 and 300/55/45 porous scaffolds can have a similar structural stiffness, being different polymers [71]. This same fluid component can be responsible for the higher stiffness of the shell-core structure, due to the stress of the swollen stratified 1000/70/30-L fibrils exerted on the 300/55/45 non swollen fibrils. Such a stress would cause the “pre-stress” of 300/55/45 domains. After 21 days of culture the dynamic stiffness of the constructs significantly increased for all of the compositions. The stiffness of the shell-core fibrous construct was significantly higher than the stiffness of the 300/55/45 and 1000/70/30 constructs, which is also due to the higher stiffness of the scaffold prior to culture.

The results obtained are encouraging as they show it is possible to maintain spherical chondrocyte morphology, which is a prerequisite for chondrogenesis. It also seems that these scaffolds can sustain a relatively homogeneous cartilage tissue formation in critical thick scaffolds when adult cells are used. Several studies have focused on how to optimize culture conditions in salt leached or meshed scaffolds and successfully achieved the regeneration of functional tissue engineered articular cartilage [21-24, 31, 72, 73]. In these cases, however, “immature” young cells characterized by a much higher proliferation capacity were used and might be responsible for the beneficial response even in scaffolds with critical thickness. When a more mature cell population was used in polymeric foams or meshes, limitations in cartilage formation at the center of the constructs occurred [7, 25, 26], which might be due to a different capacity of the cells to attach and migrate in the middle of the construct associated with a lower nutrient flow characteristic of these scaffolds. Therefore, the possibility to use a more open and interconnected structure like a rapid prototyped scaffold that allows a better nutrient perfusion and cell migration seems to be ideal as also supported by other recent studies [7, 16, 17, 74, 75]. In this setting, the shell-core structure here presented might offer a further improvement in combining the desired requirements for a scaffold and might be an optimal solution for cartilage tissue engineering, since it couples the better cell-interaction properties of 1000/70/30 at the interface with chondrocytes, while preserving the mechanical stability of 300/55/45. An additional improvement of the scaffolds would imply the incorporation of growth factors into the 1000/70/30 shell layer by diffusion, due to the swellability of this polymer. In summary, these findings coupled with the possibility to modulate the mechanical properties through 3DF to achieve a mechanically matching scaffold with respect to the tissue to regenerate make of 1000/70/30-L–300/55/45 an interesting alternative for tissue engineering applications.

### ***300/55/45 3DF Hollow Fiber Scaffolds***

Among the manifold applications which hollow fiber three-dimensional matrices can find, they can be very useful in tissue engineering and controlled release applications. If modeled with a proper architecture within a 3D construct, the hollow fibers result in constructs with less material per volume, which is of interest when the scaffold material has to resorb in the course of time. Moreover, the cavities can be useful to guide tissue in growth. Hollow fibers supported a higher amount of attached cells

and a higher amount of ECM formed as compared to 300/55/45 3DF solid fiber scaffolds. Interestingly, chondrocytes were able to penetrate inside the hollow cavities. Cell seeding was performed perpendicularly to the hollow fibers opening. Therefore, during cell seeding the scaffolds surface exposed for cell attachment is the same in the two configurations. It is possible that only in a successive moment, probably due to capillary forces and cell migration, chondrocytes were capable to enter the hollow fibers, resulting in a higher cell entrapment capacity of these scaffolds.

In this study the response of chondrocytes when seeded on 3DF hollow fibers scaffolds with a specific hollow cavity diameter of  $280 \pm 18 \mu\text{m}$  and a shell thickness of  $68 \pm 14 \mu\text{m}$  was evaluated. It may be that by increasing or decreasing the lumen diameter, an increase or a decrease of attached cells and, consequently, of ECM produced could be found. Different cell populations might also respond in a different way when cultured on these scaffolds. Further investigations need to be performed in these directions to evaluate whether there is an optimal hollow fiber dimension and to assess any variation on the behavior of other cells. Additional applications where hollow fibers could be useful to guide tissue in growth are neural and vascular tissue engineering where they could be used to form a network of nerves or capillaries, respectively. Furthermore, if computerized tomography (CT) or magnetic resonance image (MRI) datasets of a patient are available, the fabrication of anatomical custom-made hollow fibers 3DF scaffolds can be envisioned where this would be desirable from a clinical point of view. Alternatively, the organized hollow fiber scaffolds could be used in a bioreactor unit where the hollow fibers act as the perfusion capillaries while maintaining the porous structure of the scaffold for cell attachment, proliferation, and eventual differentiation [26, 76-79].

Hollow fiber 3DF scaffolds were also able to release a much higher quantity of adsorbed lysozyme, with respect of solid fiber scaffolds. This was most probably due to the increase in available surface of the hollow constructs. However if the ends of the fibers were left open, a burst effect was detected over the first 24 hours, thus confining the controlled release. Therefore, the hollow fibers were closed by dipping the scaffolds in a 1000/70/30 solution. The result was a controlled lysozyme release over a month, which was likely due to the end-capping 1000/70/30 membranes that allow protein diffusion [80]. In fact, being PEOT/PBT physical hydrogels, it is possible to control the release of incorporated biological factors by diffusion out of the polymer via the copolymer composition of the hollow fibers and/or of the end capping membranes [2, 81, 82]. To prove that 3DF hollow fiber scaffolds can release biofactors in a controlled fashion lysozyme was used. Many other biological compounds of interest for tissue engineering applications could be also used. In this respect, growth factors like TGF- $\beta$ , BMP, and IGF have already been reported as beneficial when released in a controlled manner [83-85]. The ability of these scaffolds would allow, for instance, to trigger dedifferentiated or undifferentiated cells to a specific lineage contributing to stimulate the proper tissue formation.



## Conclusions

We have demonstrated a new method to create shell-core and hollow fibers with controllable cavity diameter and shell thickness. This technique also allows to organize them in a three-dimensional scaffold by means of a rapid prototyping device called three-dimensional fiber deposition. This new type of shell-core and hollow fiber 3D scaffolds have shown to be instructive for tissue engineering and controlled drug release applications and might raise new interests as multifunctional constructs to better direct the faith of cells and of the developing tissues.

## Acknowledgements

This project was funded by the European Community project Intelliscaf G5RD\_2002\_00697. The authors are grateful to J. Riesle for critical revision of the study. A.A. van Apeldoorn was also helpful for technical support with ESEM.

## Reference:

- [1] Lutolf MP, Hubbell JA. Synthetic biomaterials as instructive extracellular microenvironments for morphogenesis in tissue engineering. *Nat Biotechnol* 2005;23(1):47-55.
- [2] Sohler J, Haan RE, de Groot K, Bezemer JM. A novel method to obtain protein release from porous polymer scaffolds: emulsion coating. *J Control Release* 2003;87(1-3):57-68.
- [3] Nof M, Shea LD. Drug-releasing scaffolds fabricated from drug-loaded microspheres. *J Biomed Mater Res* 2002;59(2):349-56.
- [4] Whang K, Goldstick TK, Healy KE. A biodegradable polymer scaffold for delivery of osteotropic factors. *Biomaterials* 2000;21(24):2545-51.
- [5] Tsang VL, Bhatia SN. Three-dimensional tissue fabrication. *Adv Drug Deliv Rev* 2004;56:1635-47.
- [6] Sherwood JK, Riley SL, Palazzolo R, Brown SC, Monkhouse DC, Coates M, Griffith LG, Landeen LK, Ratcliffe A. A three-dimensional osteochondral composite scaffold for articular cartilage repair. *Biomaterials* 2002;23(24):4739-51.
- [7] Malda J, Woodfield TB, van der Vloodt F, Wilson C, Martens DE, Tramper J, van Blitterswijk CA, Riesle J. The effect of PEGT/PBT scaffold architecture on the composition of tissue engineered cartilage. *Biomaterials* 2005;26(1):63-72.
- [8] Langer R, Vacanti JP. Tissue engineering. *Science* 1993;260(5110):920-6.
- [9] Kim SS, Utsunomiya H, Koski JA, Wu BM, Cima MJ, Sohn J, Mukai K, Griffith LG, Vacanti JP. Survival and function of hepatocytes on a novel three-dimensional synthetic biodegradable polymer scaffold with an intrinsic network of channels. *Ann Surg* 1998;228(1):8-13.
- [10] Hutmacher DW. Scaffold design and fabrication technologies for engineering tissues--state of the art and future perspectives. *J Biomater Sci Polym Ed* 2001;12(1):107-24.
- [11] Yeong WY, Chua CK, Leong KF, Chandrasekaran M. Rapid prototyping in tissue engineering: challenges and potential. *Trends Biotechnol* 2004;22(12):643-52.

- [12] Hollister SJ. Porous scaffold design for tissue engineering. *Nat Mater* 2005;4(7):518-24.
- [13] Taboas JM, Maddox RD, Krebsbach PH, Hollister SJ. Indirect solid free form fabrication of local and global porous, biomimetic and composite 3D polymer-ceramic scaffolds. *Biomaterials* 2003;24(1):181-94.
- [14] Lin CY, Kikuchi N, Hollister SJ. A novel method for biomaterial scaffold internal architecture design to match bone elastic properties with desired porosity. *J Biomech* 2004;37(5):623-36.
- [15] Sachlos E, Czernuszka JT. Making tissue engineering scaffolds work. Review: the application of solid freeform fabrication technology to the production of tissue engineering scaffolds. *Eur Cell Mater* 2003;5:29-39; discussion 39-40.
- [16] Malda J, Woodfield TB, van der Vloodt F, Kooy FK, Martens DE, Tramper J, van Blitterswijk CA, Riesle J. The effect of PEGT/PBT scaffold architecture on oxygen gradients in tissue engineered cartilaginous constructs. *Biomaterials* 2004;25(26):5773-80.
- [17] Woodfield TB, Malda J, de Wijn J, Peters F, Riesle J, van Blitterswijk CA. Design of porous scaffolds for cartilage tissue engineering using a three-dimensional fiber-deposition technique. *Biomaterials* 2004;25(18):4149-61.
- [18] Moroni L, de Wijn JR, van Blitterswijk CA. 3D fiber-deposited scaffolds for tissue engineering: influence of pores geometry and architecture on dynamic mechanical properties. *Biomaterials* 2006;27(7):974-85.
- [19] Moroni L, de Wijn JR, van Blitterswijk CA. Three-dimensional fiber-deposited PEOT/PBT copolymer scaffolds for tissue engineering: influence of porosity, molecular network mesh size, and swelling in aqueous media on dynamic mechanical properties. *J Biomed Mater Res A* 2005;75(4):957-65.
- [20] Muschler GF, Nakamoto C, Griffith LG. Engineering principles of clinical cell-based tissue engineering. *J Bone Joint Surg Am* 2004;86-A(7):1541-58.
- [21] Martin I, Padera RF, Vunjak-Novakovic G, Freed LE. In vitro differentiation of chick embryo bone marrow stromal cells into cartilaginous and bone-like tissues. *J Orthop Res* 1998;16(2):181-9.
- [22] Martin I, Vunjak-Novakovic G, Yang J, Langer R, Freed LE. Mammalian chondrocytes expanded in the presence of fibroblast growth factor 2 maintain the ability to differentiate and regenerate three-dimensional cartilaginous tissue. *Exp Cell Res* 1999;253(2):681-8.
- [23] Vunjak-Novakovic G, Freed LE, Biron RJ, Langer R. Effects of mixing on the composition and morphology of tissue-engineered cartilage. *Aiche Journal* 1996;42(3):850-860.
- [24] Freed LE, Hollander AP, Martin I, Barry JR, Langer R, Vunjak-Novakovic G. Chondrogenesis in a cell-polymer-bioreactor system. *Exp Cell Res* 1998;240(1):58-65.
- [25] Miot S, Scandiucci de Freitas P, Wirz D, Daniels AU, Sims TJ, Hollander AP, Mainil-Varlet P, Heberer M, Martin I. Cartilage tissue engineering by expanded goat articular chondrocytes. *J Orthop Res* 2006;24(5):1078-85.
- [26] Demartean O, Wendt D, Braccini A, Jakob M, Schafer D, Heberer M, Martin I. Dynamic compression of cartilage constructs engineered from expanded human articular chondrocytes. *Biochem Biophys Res Commun* 2003;310(2):580-8.

- [27] van Dijkhuizen-Radersma R, Peters FL, Stienstra NA, Grijpma DW, Feijen J, de Groot K, Bezemer JM. Control of vitamin B12 release from poly(ethylene glycol)/poly(butylene terephthalate) multiblock copolymers. *Biomaterials* 2002;23(6):1527-36.
- [28] Mahmood TA, de Jong R, Riesle J, Langer R, van Blitterswijk CA. Adhesion-mediated signal transduction in human articular chondrocytes: the influence of biomaterial chemistry and tenascin-C. *Exp Cell Res* 2004;301(2):179-88.
- [29] Risbud MV, Karamuk E, Moser R, Mayer J. Hydrogel-coated textile scaffolds as three-dimensional growth support for human umbilical vein endothelial cells (HUVECs): possibilities as coculture system in liver tissue engineering. *Cell Transplant* 2002;11(4):369-77.
- [30] Cao T, Ho KH, Teoh SH. Scaffold design and in vitro study of osteochondral coculture in a three-dimensional porous polycaprolactone scaffold fabricated by fused deposition modeling. *Tissue Eng* 2003;9 Suppl 1:S103-12.
- [31] Freed LE, Marquis JC, Nohria A, Emmanuel J, Mikos AG, Langer R. Neocartilage formation in vitro and in vivo using cells cultured on synthetic biodegradable polymers. *J Biomed Mater Res* 1993;27(1):11-23.
- [32] Barry JJ, Gidda HS, Scotchford CA, Howdle SM. Porous methacrylate scaffolds: supercritical fluid fabrication and in vitro chondrocyte responses. *Biomaterials* 2004;25(17):3559-68.
- [33] Sarazin P, Roy X, Favis BD. Controlled preparation and properties of porous poly(L-lactide) obtained from a co-continuous blend of two biodegradable polymers. *Biomaterials* 2004;25(28):5965-78.
- [34] Yuan Z, Favis BD. Macroporous poly(L-lactide) of controlled pore size derived from the annealing of co-continuous polystyrene/poly(L-lactide) blends. *Biomaterials* 2004;25(11):2161-70.
- [35] Sarazin P, Favis BD. Morphology control in co-continuous poly(L-lactide)/polystyrene blends: a route towards highly structured and interconnected porosity in poly(L-lactide) materials. *Biomacromolecules* 2003;4(6):1669-79.
- [36] Washburn NR, Simon CG, Jr., Tona A, Elgendy HM, Karim A, Amis EJ. Co-extrusion of biocompatible polymers for scaffolds with co-continuous morphology. *J Biomed Mater Res* 2002;60(1):20-9.
- [37] Dooley J. *Viscoelastic Flow Effects in Multilayer Polymer Coextrusion*: Technische Universiteit Eindhoven; 2002.
- [38] Lesage N, Sperandio M, Cabassud C. Performances of a hybrid adsorption/submerged membrane biological process for toxic waste removal. *Water Sci Technol* 2005;51(6-7):173-80.
- [39] Yeo A, Fane AG. Performance of individual fibers in a submerged hollow fiber bundle. *Water Sci Technol* 2005;51(6-7):165-72.
- [40] Yalin AP, DeFoort M, Willson B, Matsuura Y, Miyagi M. Use of hollow-core fibers to deliver nanosecond Nd:YAG laser pulses to form sparks in gases. *Opt Lett* 2005;30(16):2083-5.
- [41] Konorov SO, Serebryannikov EE, Fedotov AB, Miles RB, Zheltikov AM. Phase-matched waveguide four-wave mixing scaled to higher peak powers with large-core-area hollow photonic-crystal fibers. *Phys Rev E Stat Nonlin Soft Matter Phys* 2005;71(5 Pt 2):057603.

- [42] Abu-Absi SF, Seth G, Narayanan RA, Groehler K, Lai P, Anderson ML, Sielaff T, Hu WS. Characterization of a hollow fiber bioartificial liver device. *Artif Organs* 2005;29(5):419-22.
- [43] Ahn YH, Bensadoun JC, Aebischer P, Zurn AD, Seiger A, Bjorklund A, Lindvall O, Wahlberg L, Brundin P, Kaminski Schierle GS. Increased fiber outgrowth from xenotransplanted human embryonic dopaminergic neurons with co-implants of polymer-encapsulated genetically modified cells releasing glial cell line-derived neurotrophic factor. *Brain Res Bull* 2005;66(2):135-42.
- [44] Gardner TA, Ko SC, Yang L, Cadwell JJ, Chung LW, Kao C. Serum-free recombinant production of adenovirus using a hollow fiber capillary system. *Biotechniques* 2001;30(2):422-7.
- [45] Isayeva T, Kotova O, Krasnykh V, Kotov A. Advanced methods of adenovirus vector production for human gene therapy: roller bottles, microcarriers, and hollow fibers. *Bioprocessing J* 2003;2:75-81.
- [46] Niwa M, Kawakami H, Nagaoka S, Kanamori T, Morisaku K, Shinbo T, Matsuda T, Sakai K, Kubota S. Development of a novel polyimide hollow-fiber oxygenator. *Artif Organs* 2004;28(5):487-95.
- [47] Stokols S, Tuszynski MH. The fabrication and characterization of linearly oriented nerve guidance scaffolds for spinal cord injury. *Biomaterials* 2004;25(27):5839-46.
- [48] Hucker MJ, Bond IP, Haq S, Bleay S, Foreman A. Influence of manufacturing parameters on the tensile strengths of hollow and solid glass fibres. *Journal of Materials Science* 2002;37(2):309-315.
- [49] Li D, Xia Y. Electrospinning of Nanofibers: Reinventing the Wheel? *Adv Mater* 2004;16:1151-1170.
- [50] Loscertales IG, Barrero A, Marquez M, Spretz R, Velarde-Ortiz R, Larsen G. Electrically forced coaxial nanojets for one-step hollow nanofiber design. *J Am Chem Soc* 2004;126(17):5376-7.
- [51] Spreitzer G, Doctor J, Wright DW. Self-Assembled Beta-Sheet Architectures for Bone-Tissue Engineering. *Mat Res Soc Symp Proc* 2000;599:305-310.
- [52] Zhao JP, Gaddis CS, Cai Y, Sandhage KH. Free-standing microscale structures of nanocrystalline zirconia with biologically replicable three-dimensional shapes. *Journal of Materials Research* 2005;20(2):282-287.
- [53] Ko FK. Textiles and Garments for Chemical and Biological Protections. In: *Strategies to Protect the Health of Deployed U.S. Forces: Force Protection and Decontamination* 1999:182-216.
- [54] Gupta PK. Fibre Reinforcements for composite materials. *Comp Materials Series* 1988;2:19-69.
- [55] Imoto K, Sumi M, Toda G, Suganuma T. Optical Fiber Drawing Method with Gas-Flow Controlling System. *Journal of Lightwave Technology* 1989;7(1):115-121.
- [56] Beumer GJ, van Blitterswijk CA, Ponc M. Biocompatibility of a biodegradable matrix used as a skin substitute: an in vivo evaluation. *J Biomed Mater Res* 1994;28(5):545-52.
- [57] Bakker D, van Blitterswijk CA, Hesseling SC, Grote JJ. Effect of implantation site on phagocyte/polymer interaction and fibrous capsule formation. *Biomaterials* 1988;9(1):14-23.

- [58] Liu Q, de Wijn JR, van Blitterswijk CA. Covalent bonding of PMMA, PBMA, and poly(HEMA) to hydroxyapatite particles. *J Biomed Mater Res* 1998;40(2):257-63.
- [59] Peluso G, Petillo O, Anderson JM, Ambrosio L, Nicolais L, Melone MA, Eschbach FO, Huang SJ. The differential effects of poly(2-hydroxyethyl methacrylate) and poly(2-hydroxyethyl methacrylate)/poly(caprolactone) polymers on cell proliferation and collagen synthesis by human lung fibroblasts. *J Biomed Mater Res* 1997;34(3):327-36.
- [60] Wang PY. Compressed poly(vinyl alcohol)-polycaprolactone admixture as a model to evaluate erodible implants for sustained drug delivery. *J Biomed Mater Res* 1989;23(1):91-104.
- [61] Zein I, Hutmacher DW, Tan KC, Teoh SH. Fused deposition modeling of novel scaffold architectures for tissue engineering applications. *Biomaterials* 2002;23(4):1169-85.
- [62] Deschamps AA, Claase MB, Sleijsler WJ, de Bruijn JD, Grijpma DW, Feijen J. Design of segmented poly(ether ester) materials and structures for the tissue engineering of bone. *J Control Release* 2002;78(1-3):175-86.
- [63] Bezemer JM, Grijpma DW, Dijkstra PJ, van Blitterswijk CA, Feijen J. A controlled release system for proteins based on poly(ether ester) block-copolymers: polymer network characterization. *J Control Release* 1999;62(3):393-405.
- [64] Beumer GJ, van Blitterswijk CA, Ponc M. Degradative behaviour of polymeric matrices in (sub)dermal and muscle tissue of the rat: a quantitative study. *Biomaterials* 1994;15(7):551-9.
- [65] Bulstra SK, Geesink RG, Bakker D, Bulstra TH, Bouwmeester SJ, van der Linden AJ. Femoral canal occlusion in total hip replacement using a resorbable and flexible cement restrictor. *J Bone Joint Surg Br* 1996;78(6):892-8.
- [66] Mensik I, Lamme EN, Riesle J, Brychta P. Effectiveness and Safety of the PEGT/PBT Copolymer Scaffold as Dermal Substitute in Scar Reconstruction Wounds (Feasibility Trial). *Cell Tissue Bank* 2002;3(4):245-53.
- [67] Lau HK, Lee PC, Tang SC, Lim JK, Chow SP. Treatment of comminuted trochanteric femoral fractures with Dimon Hughston displacement fixation and acrylic cement--a preliminary report of sixteen cases. *Injury* 1983;15(2):129-35.
- [68] Larraz E, Elvira C, Roman JS. Design and properties of novel self-curing acrylic formulations for application in intervertebral disks restoration. *Biomacromolecules* 2005;6(4):2058-66.
- [69] Malda J, van Blitterswijk CA, Grojec M, Martens DE, Tramper J, Riesle J. Expansion of bovine chondrocytes on microcarriers enhances redifferentiation. *Tissue Eng* 2003;9(5):939-48.
- [70] Woodfield TB, Miot S, Martin I, van Blitterswijk CA, Riesle J. The regulation of expanded human nasal chondrocyte re-differentiation capacity by substrate composition and gas plasma surface modification. *Biomaterials* 2005.
- [71] Moroni L, Poort G, Van Keulen F, de Wijn JR, van Blitterswijk CA. Dynamic mechanical properties of 3D fiber-deposited PEOT/PBT scaffolds: An experimental and numerical analysis. *J Biomed Mater Res A* 2006(78):605-614.
- [72] Obradovic B, Carrier RL, Vunjak-Novakovic G, Freed LE. Gas exchange is essential for bioreactor cultivation of tissue engineered cartilage. *Biotechnol Bioeng* 1999;63(2):197-205.

- [73] Vunjak-Novakovic G, Martin I, Obradovic B, Treppo S, Grodzinsky AJ, Langer R, Freed LE. Bioreactor cultivation conditions modulate the composition and mechanical properties of tissue-engineered cartilage. *J Orthop Res* 1999;17(1):130-8.
- [74] Woodfield TB, Van Blitterswijk CA, De Wijn J, Sims TJ, Hollander AP, Riesle J. Polymer scaffolds fabricated with pore-size gradients as a model for studying the zonal organization within tissue-engineered cartilage constructs. *Tissue Eng* 2005;11(9-10):1297-311.
- [75] Miot S, Woodfield T, Daniels AU, Suetterlin R, Peterschmitt I, Heberer M, van Blitterswijk CA, Riesle J, Martin I. Effects of scaffold composition and architecture on human nasal chondrocyte redifferentiation and cartilaginous matrix deposition. *Biomaterials* 2005;26(15):2479-89.
- [76] Knazek RA, Gullino PM, Kohler PO, Dedrick RL. Cell culture on artificial capillaries: an approach to tissue growth in vitro. *Science* 1972;178(56):65-6.
- [77] Kawakami O, Miyamoto S, Hatano T, Yamada K, Hashimoto N, Tabata Y. Acceleration of aneurysm healing by hollow fiber enabling the controlled release of basic fibroblast growth factor. *Neurosurgery* 2006;58(2):355-64; discussion 355-64.
- [78] Janssen FW, Oostra J, Oorschot A, van Blitterswijk CA. A perfusion bioreactor system capable of producing clinically relevant volumes of tissue-engineered bone: in vivo bone formation showing proof of concept. *Biomaterials* 2006;27(3):315-23.
- [79] Gomes ME, Holtorf HL, Reis RL, Mikos AG. Influence of the porosity of starch-based fiber mesh scaffolds on the proliferation and osteogenic differentiation of bone marrow stromal cells cultured in a flow perfusion bioreactor. *Tissue Eng* 2006;12(4):801-9.
- [80] Bezemer JM, Radersma R, Grijpma DW, Dijkstra PJ, Feijen J, van Blitterswijk CA. Zero-order release of lysozyme from poly(ethylene glycol)/poly(butylene terephthalate) matrices. *J Control Release* 2000;64(1-3):179-92.
- [81] Sohier J, Vlugt TJ, Cabrol N, Van Blitterswijk C, de Groot K, Bezemer JM. Dual release of proteins from porous polymeric scaffolds. *J Control Release* 2006;111(1-2):95-106.
- [82] van Dijkhuizen-Radersma R, Roosma JR, Kaim P, Metairie S, Peters FL, de Wijn J, Zijlstra PG, de Groot K, Bezemer JM. Biodegradable poly(ether-ester) multiblock copolymers for controlled release applications. *J Biomed Mater Res A* 2003;67(4):1294-304.
- [83] Hunziker EB. Growth-factor-induced healing of partial-thickness defects in adult articular cartilage. *Osteoarthritis Cartilage* 2001;9(1):22-32.
- [84] Hunziker EB, Driesang IM, Morris EA. Chondrogenesis in cartilage repair is induced by members of the transforming growth factor-beta superfamily. *Clin Orthop Relat Res* 2001(391 Suppl):S171-81.
- [85] Uludag H, D'Augusta D, Golden J, Li J, Timony G, Riedel R, Wozney JM. Implantation of recombinant human bone morphogenetic proteins with biomaterial carriers: A correlation between protein pharmacokinetics and osteoinduction in the rat ectopic model. *J Biomed Mater Res* 2000;50(2):227-38.

# Chapter 9

## 3D Fiber Deposited-Electrospun Integrated Scaffolds Enhance Cartilage Tissue Formation

L. Moroni <sup>a,\*</sup>, R. Schotel <sup>b</sup>, D. Hamann <sup>a</sup>, J.R. de Wijn <sup>a</sup>, C.A. van Blitterswijk <sup>a</sup>

<sup>a,\*</sup> Institute for BioMedical Technology (BMTI), University of Twente, P.O. Box 217, 7500 AE Enschede, The Netherlands. E-mail: l.moroni@tnw.utwente.nl

<sup>b</sup> CellCoTec, Prof. Bronkhorstlaan 10D, 3723 MB Bilthoven, The Netherlands.

### Abstract

**D**espite the periodical and completely interconnected pore network that characterize rapid prototyped scaffolds, cell seeding efficiency remains still a critical factor for optimal tissue regeneration due to the current resolution limits in pore size. We present here a novel three-dimensional (3D) scaffold fabricated by combining 3D fiber deposition (3DF) and electrospinning (ESP). Scaffolds consisted of integrated 3DF macrofiber periodical and ESP microfiber random networks (3DFESP), where the 3DF construction provides structural integrity and mechanical properties and the ESP network works as a “sieving” and cell entrapment system, at the same time offering cues at the extracellular matrix (ECM) scale. Primary bovine articular chondrocytes were isolated, seeded, and cultured for 4 weeks on 3DF and 3DFESP scaffolds to evaluate the influence of the integrated ESP network on cell entrapment and on cartilage tissue formation. 3DFESP scaffolds showed a better cell entrapment as compared to 3DF scaffolds. This was accompanied by a higher amount of ECM (expressed in terms of sulphated glycosaminoglycans or GAG) and a significantly higher GAG/DNA ratio after 28 days. SEM analysis of the constructs revealed a rounded cell morphology on 3DFESP scaffolds, whereas a spread morphology was observed on 3DF scaffolds, suggesting a direct influence of fiber dimensions on cell differentiation. Furthermore, also ESP surface topology influenced cell morphology. Thus, the integration of 3DF and ESP techniques provide a new set of “smart” scaffolds for tissue engineering applications.

**Keywords:** rapid prototyping, electrospinning, scaffolds, cartilage, tissue engineering.

### Introduction

Rapid prototyped (RP) scaffolds are quite promising in tissue engineering, as they can be custom-shaped with a completely interconnected pore network [1-3]. Several studies focused on the development of different rapid prototyping techniques [4-10] and on scaffolds optimization [11-14]. In all of these techniques, pore volume and

architecture can be designed in a CAD/CAM controlled manner, resulting in a modulation of scaffold's mechanical properties [15] and in a proficient nutrient perfusion determinant for cell survival [16]. They can be comprised of different materials [17-20], they can combine gradients of porosities [21], and they can be designed to match specific tissue requirements, resulting in multifunctional constructs [20, 22, 23].

However, the scaffold's pore resolution poses still a limit in cell seeding efficiency and tissue formation. The pore size of RP scaffolds are relatively large as compared to cells dimensions and a high number of cells are needed to obtain a sufficient number of attached cells that produce enough extracellular matrix to functionalize the tissue engineered construct. This eventually results in expensive and extensive cell isolation, culture, and expansion processes, which may hamper the clinical relevance of RP scaffolds. A possible way to improve cell seeding efficiency is to aggregate cells [24-26] prior to seeding them onto the scaffolds, so that cell clumps will be better entrapped in the pores. Furthermore, cell aggregation is known to enhance cell-cell signaling [27], resulting in a better tissue formation [28]. Another possibility can be offered by introducing in RP scaffolds a micron scale fibril networks that have the double advantage to function as a "sieve" for cell entrapment and to provide extracellular matrix-like cues to cells. This can be achieved by integrating rapid prototyping with another novel technique like electrospinning (ESP). ESP fibers have typically dimensions varying from the nano- to the micro-scale, which results from the application of a high voltage electric field to a polymeric solution pumped into the field [29-31]. Depending on the pumping flow rate, the electric field intensity, and the polymer solution concentration, fibers of different diameter and surface topology can be obtained [31-34]. Furthermore, ESP scaffolds have been shown to influence cell proliferation rate and morphology depending on their size and surface texture [35-37].

Therefore, the aim of this study was to combine a rapid prototyping fabrication technique like 3D fiber deposition (3DF) with electrospinning (ESP) to fabricate integrated macro- and  $\mu$ -fiber polymeric scaffolds (3DFESP) and to assess the influence of the microfibrillar network on cell entrapment and differentiation into cartilage tissue. Three scaffolds construct were considered: 3DF scaffolds as such, and 3DFESP integrated scaffolds with two different ESP network densities determined by varying the electrospinning time. Primary bovine articular chondrocytes were seeded on the scaffolds and cultured for 4 weeks. The distribution and the amount of cells and extracellular matrix present on the scaffolds were considered as determinants for a better scaffold performance. 3DF and 3DFESP scaffolds were fabricated with block-copolymers of polyethyleneoxide-terephthalate (PEOT) and polybutylene-terephthalate (PBT). These polyether-ester multiblock copolymers are thermoplastic elastomers which display good physical properties like elasticity, toughness and strength in combination with easy processability. These properties result mainly from a phase separated morphology in which soft, hydrophilic PEO segments at environmental temperatures are physically cross-linked by the presence of hard, semi crystalline PBT segments. In contrast to chemically cross-linked materials, these cross-links are reversible and will be disrupted at temperatures above their glass transition- or melting point, which gives the material its good



processability. This class of polymers have been extensively studied for in vitro and in vivo biocompatibility [38-41] and found commercial clinical applications (PolyActive™, IsoTis Orthopaedics S.A.) as cement stoppers and bone fillers in orthopedic surgery [42, 43]. Being polyether-esters degradation occurs in aqueous media by hydrolysis and oxidation, the rate of which varying from very low for high PBT contents to medium and high for larger contents of PEOT and longer PEO segments [44, 45]. Similarly, by varying the PEOT/PBT ratio and the length of the PEO segments, a series of copolymers can be attained covering a wide range of mechanical properties with different abilities to swell in aqueous media.

## Materials and Methods

### *Materials Characterization*

Poly(ethylene oxide – terephthalate)/poly(butylene terephthalate) (PEOT/PBT) copolymers were obtained from IsoTis S.A. (Bilthoven, The Netherlands). The copolymer composition used in this study was 300PEOT55PBT45 where, following an aPEOTbPBTc nomenclature, a is the molecular weight in g/mol of the starting PEG blocks used in the copolymerization, while b and c are the weight ratios of the PEOT and PBT blocks, respectively.

### *Scaffolds Fabrication*

3D fiber deposited-electrospun integrated (3DFESP) scaffolds were manufactured by combining a Bioplotter device (Envisiontec GmbH, Germany) and a home-assembled electrospinning (ESP) apparatus. The Bioplotter is essentially an XYZ plotter device as previously described [6, 14]. Briefly, the polymers were put in a stainless steel syringe and heated at  $T = 190\text{ }^{\circ}\text{C}$  through a thermo-stated cartridge unit, fixed on the “X”-mobile arm of the apparatus. When the molten phase was achieved, a nitrogen pressure of 5 Bars was applied to the syringe through a pressurized cap. Rectangular block models were loaded on the Bioplotter CAM (PrimCAM, Switzerland) software and deposited layer by layer, through the extrusion of the polymer on a stage as a fiber. The deposition speed was set to 300 mm/min. Scaffolds were then characterized by the fiber diameter (through the nozzle diameter), the spacing between fibers in the same layer, the layer thickness and the configuration of the deposited fibers within the whole architecture. In this study, the nozzle internal diameter was  $400\text{ }\mu\text{m}$ , the fiber spacing was set to  $800\text{ }\mu\text{m}$ , the layer thickness was set to  $225\text{ }\mu\text{m}$ , and the scaffold architecture was determined by a 0-90 layer configuration where fibers were deposited with  $90^{\circ}$  orientation steps between successive layers.

Electrospun fibrous networks were fabricated from a 20% w/v polymer solution in a 90%/10% v/v chloroform/hexafluoroisopropanol mixture. The ESP device consists of a high voltage (0-30 kV) generator (NCE 30000, Heinzinger Electronic GmbH, Germany) connected to a syringe, where the polymer solution is contained, and to a collector plate. When a high voltage is applied, an electric field is formed between

the syringe needle (positive pole) and the collector (negative pole). The polymer solution is then pushed out of the syringe by a pump at variable flow rates depending on the electrostatic field strength. When the intensity of the electrostatic field is high enough to surpass the surface tension of the liquid drop at the tip of the needle, the drop is pulled out into a jetting filament and deposited as a dry fiber on the collector. The fibrous network is characterized by the voltage applied, the air gap (distance between the syringe needle and the collector plate), the pump flow rate, the syringe needle. In our experimental set up the voltage was kept constant at 15 kV, the air gap was fixed at 15 cm, the flow rate at 0.39 ml/min, and the needle used had an internal diameter of 0.9 mm.

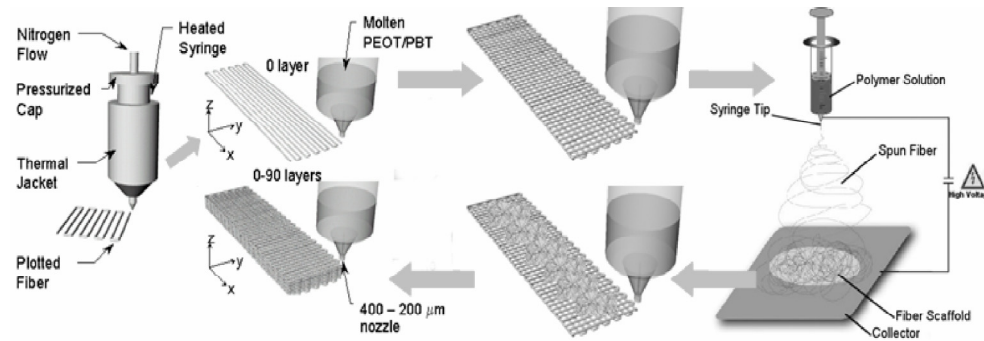


**Figure 1** – Schematic draw of the integration of 3DF and ESP fabrication techniques.

3DFESP scaffolds were fabricated by electrospinning a fibrous network layer every two layers of 3D fiber-deposited mesh until a scaffold height of 4 mm was reached (figure 1). Two different network densities were used to evaluate its influence on cell entrapment and tissue formation. The ESP fiber density was determined as the time frame used during electrospinning. Specifically, 3DFESP scaffolds with a fibrous network spun for 2 minutes (3DFESP-2) and for 30 seconds (3DFESP-30) were considered.

### *Scaffolds Characterization*

Cylindrical plugs of 4 mm in diameter by 4 mm in height were considered for characterization. The constructs were analyzed with a Philips XL 30 ESEM-FEG scanning electron microscopy (SEM). Samples were gold sputter (Carrington) before SEM analysis. The porosity of 3DF scaffolds was calculated following the theoretical approach by Landers et al [6]:

$$P = 1 - \frac{V_{\text{scaffold}}}{V_{\text{cube}}} = 1 - \frac{\pi}{4} \cdot \frac{1}{d_2} \cdot \frac{1}{d_3} \quad (1)$$

$$\frac{1}{d_1} \cdot \frac{1}{d_1}$$

where P is the scaffold porosity, d1 the fiber diameter, d2 the fiber spacing and d3 the layer thickness.

The porosity of ESP networks and 3DFESP scaffolds was experimentally measured by analyzing the mass and the volume of each structure, as:

$$P = 1 - \frac{M}{V} \cdot \frac{1}{\rho} \quad (2)$$

where, M and V are the measured mass and volume of the polymeric scaffolds, while  $\rho$  is the specific density of 300PEOT55PBT45 (1.2 g/cm<sup>3</sup>).

3D scaffolds for culture experiments were sterilized in isopropanol (IPASEPT 70, VWR International) for 15 minutes, thoroughly washed with a phosphate buffered saline (PBS) solution (Gibco-BRL) three times, and incubated over night in culture medium prior cell seeding.

### ***Cell Seeding***

Chondrocytes were isolated via collagenase digestion from articular cartilage harvested from an 18-month old bovine knee joint. Primary cells were aggregated with 300  $\mu$ g/ml of fibronectin (Invitrogen), statically seeded at a density of 3 millions in 50  $\mu$ l of medium and cultured on scaffolds for 1, 7, and 28 days (n=6). 3DF, 3DFESP-2, and 3DFESP-30 scaffolds of 4 mm in diameter and 4 mm in height fabricated with 0-90 architecture were considered. The culture medium contained HEPES (Invitrogen)-buffered DMEM (Invitrogen) supplemented with 10% fetal bovine serum (FBS, Sigma-Aldrich), 0.2 mM ascorbic acid 2-phosphate (Invitrogen), 0.1 mM non-essential amino acids (Sigma-Aldrich), 0.4 mM proline (Sigma-Aldrich), 100 units/ml penicillin (Invitrogen), and 100  $\mu$ g/ml streptomycin (Invitrogen). Constructs were cultured at 37 °C in a humid atmosphere with 5% CO<sub>2</sub>. Medium was refreshed twice a week and subsets of chondrocytes were used for further subculturing or cryopreservation upon reaching near confluence. Scaffolds were compared to evaluate the influence of the ESP network on chondrocytes entrapment in the pores, differentiation and morphology.

### ***Biochemical Analysis***

DNA and glycosaminoglycans (GAG) assay were performed after 1, 7, and 28 days of culture. Constructs were also digested overnight at 56 °C in a Tris-EDTA buffered solution containing 1 mg/ml proteinase K, 18.5  $\mu$ g/ml pepstatin A, and 1  $\mu$ g/ml iodoacetamide (Sigma-Aldrich). Quantification of total DNA was done with Cyquant dye kit according to the manufacturers description (Molecular Probes) using a spectrofluorometer (LS 50B, Perkin Elmer). GAG amount was determined spectrophotometrically (EL 312e Bio-TEK Instruments) after reaction with dimethylmethylene blue dye (DMMB, Sigma-Aldrich) by measuring absorbance at 520 nm. The final amount was calculated using a standard of chondroitin sulphate B (Sigma-Aldrich).

### *Histology Analysis*

Samples were fixed overnight in 0.14 M cacodylate buffer (pH = 7.2 – 7.4) containing 1.5% glutaraldehyde (Merck). Scaffolds were subsequently dehydrated in sequential ethanol series, plastic embedded in glycol-methacrylate (Merck) and cut using a microtome to yield 5  $\mu\text{m}$  sections. Slices were stained with safranin-O (Sigma-Aldrich) to visualize extracellular matrix (sulphated glycosaminoglycans - GAG), and counterstained with haematoxylin (Sigma-Aldrich) and fast green (Merck) to visualize cytoplasm and cells nuclei. Mounted slides were examined under a light microscope (Nikon Eclipse E400) and representative images captured using a digital camera (Sony Corporation, Japan) and Matrix Vision software (Matrix Vision GmbH, Germany). Tissue constructs on scaffolds were also analyzed by SEM. Specimens were fixed and dehydrated as described above and critical point dried from liquid carbon dioxide using a Balzers CPD 030 machine. Samples were then gold sputtered and studied under the SEM.

### *Statistical Analysis*

Statistical Analysis was performed using a Student's t-test, where the confidence level was set to 0.05 for statistical significance. Values in this study are reported as mean and standard deviation.

## Results

### *Scaffolds Characterization*

The surface and cross section of 3DFESP scaffolds is illustrated in figure 2. SEM analysis revealed a fiber diameter of  $268 \pm 32 \mu\text{m}$ , a fiber spacing of  $807 \pm 28 \mu\text{m}$ , and a layer thickness of  $227 \pm 20 \mu\text{m}$  for the 3DF scaffolds, and a fiber diameter of  $10 \pm 2.8 \mu\text{m}$  for the ESP network. This corresponded to a porosity of  $69 \pm 3\%$  for the 3DF scaffolds, and to a porosity of  $94 \pm 1.6\%$  for the ESP network. The porosity of the integrated 3DFESP scaffolds was measured as  $50 \pm 3\%$ . The scaffolds produced were 100% interconnected porous structures and no layer delamination phenomenon occurred.

### 3DF-ESP Scaffolds

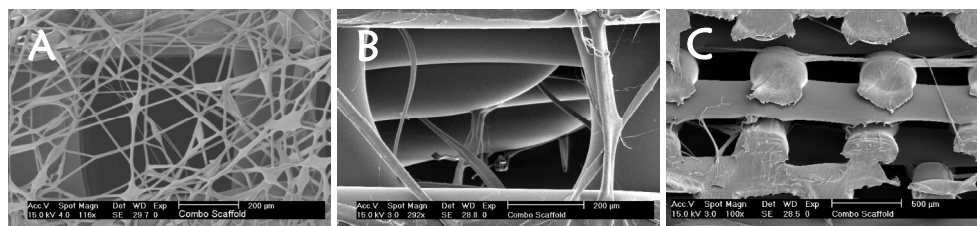


**Figure 2** – SEM micrographs of the surface (a, b) and of the cross section (c) of 3DFESP scaffolds. (a) ESP network spun for 2 minutes every two 3DF deposited layers (3DFESP-2); (b) ESP network spun for 30 seconds every two 3DF deposited layers (3DFESP-30); (c) cross section of a 3DFESP-30 scaffold. (a, b) scale bar: 200  $\mu\text{m}$ ; (c) scale bar: 500  $\mu\text{m}$ .

### *Cell Entrapment & Tissue Formation*

During the 4 weeks of culture on the 3DF and on the 3DFESP scaffolds, DNA amount and GAG formation were measured. Figure 3 shows the DNA amount for the different scaffolds considered in the study. At day 1 DNA significantly increased from 3DF to 3DFESP-2, suggesting a better cell entrapment in the pores of the 3DFESP scaffolds. With increasing ESP network density, DNA did not significantly change. Specifically, DNA was measured as  $5.21 \pm 0.94 \mu\text{g}$  for 3DF,  $7.57 \pm 1.86 \mu\text{g}$  for 3DFESP-30, and  $7.81 \pm 1.08 \mu\text{g}$  for 3DFESP-2 scaffolds. At day 7 a similar trend was found and the increase for 3DFESP-2 was significantly different as compared to 3DF scaffolds, indicating that cells were still more efficiently retained in the integrated scaffolds during the proliferation time. The cell amount, however, was found to be comparable between the scaffolds after 4 weeks of culture. This might imply a redistribution of the cells in the constructs due to extracellular matrix formation.

More interestingly, the GAG amount increased in the whole culture period with the same trend as for DNA, suggesting a better tissue formation in the integrated scaffolds as depicted in figure 4. The increase was significant for 3DFESP as compared to 3DF scaffolds all over the culture period. Specifically, GAG increased from  $160.29 \pm 46.43 \mu\text{g}$  for 3DF, to  $321.1 \pm 77.86 \mu\text{g}$  for 3DFESP-30, and to  $316.84 \pm 75.93 \mu\text{g}$  for 3DFESP-2 scaffolds over a month. Even more interestingly, a higher degree of differentiation was found for chondrocytes cultured on 3DFESP scaffolds, as shown in figure 5 from the GAG/DNA ratio. GAG/DNA significantly increased in 3DFESP scaffolds as compared to 3DF scaffolds alone during the month of culture. In particular, the increase was measured at day 1 as  $4.37 \pm 2.13$  for 3DF,  $5.87 \pm 1.11$  for 3DFESP-30,  $7.24 \pm 1.59$  for 3DFESP-2 scaffolds. At day 28 GAG/DNA ratios reached  $22.23 \pm 4.18$  for 3DF,  $54.26 \pm 12.72$  for 3DFESP-30, and  $54.77 \pm 8.11$  for 3DFESP-2.

A better chondrocytes differentiation into cartilage tissue in 3DFESP scaffolds can be also qualitatively detected by SEM analysis. After 28 days of culture, chondrocytes appeared completely spread and attached to the big fibers of 3DF scaffolds (figure 6A), whereas they remained aggregated and maintained a rounded shape morphology in 3DFESP scaffolds (figures 6B and 6C). This is already evident after 1 day of culture, when chondrocytes in contact with big 3DF fibers attach and spread on their surface, while chondrocytes entrapped in the small ESP fiber network keep their rounded morphology (figures 6D and 6E), suggesting an effect of the fiber size on cell morphology. Extracellular matrix formation can be also detected, as shown in figure 6F, and was confirmed by histology where the formed tissue responded to safranin-O staining (figure 7).

### **Discussion**

3DFESP integrated scaffolds were successfully produced by combining two novel scaffold fabrication technologies: 3D fiber deposition and electrospinning. The

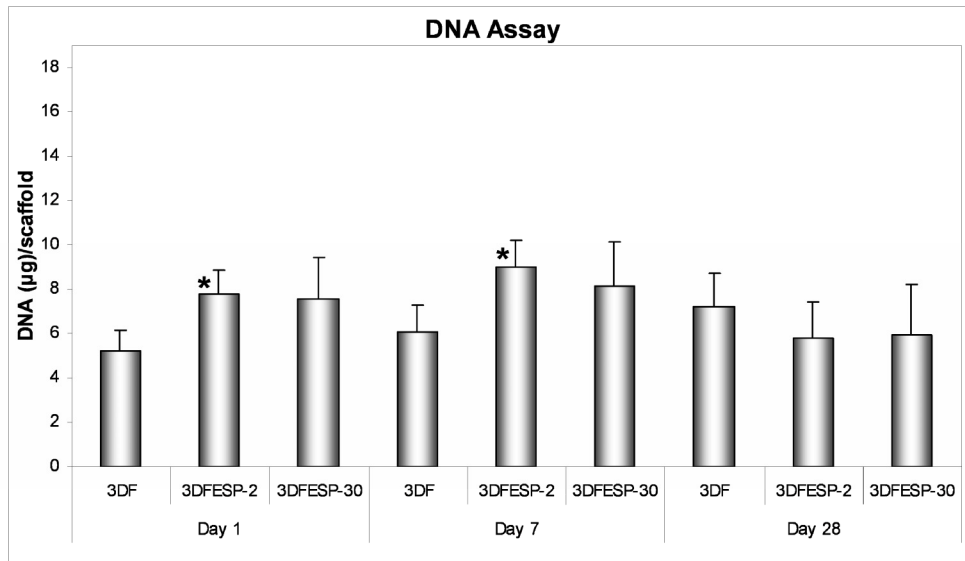


**Figure 3** – DNA assay on 3DF, 3DFESP-2, and 3DFESP-30 scaffolds after 1, 7, and 28 days of culture. (\*) shows significant differences with respect to 3DF scaffolds ( $p < 0.05$ ).

3DF-ESP  
Scaffolds

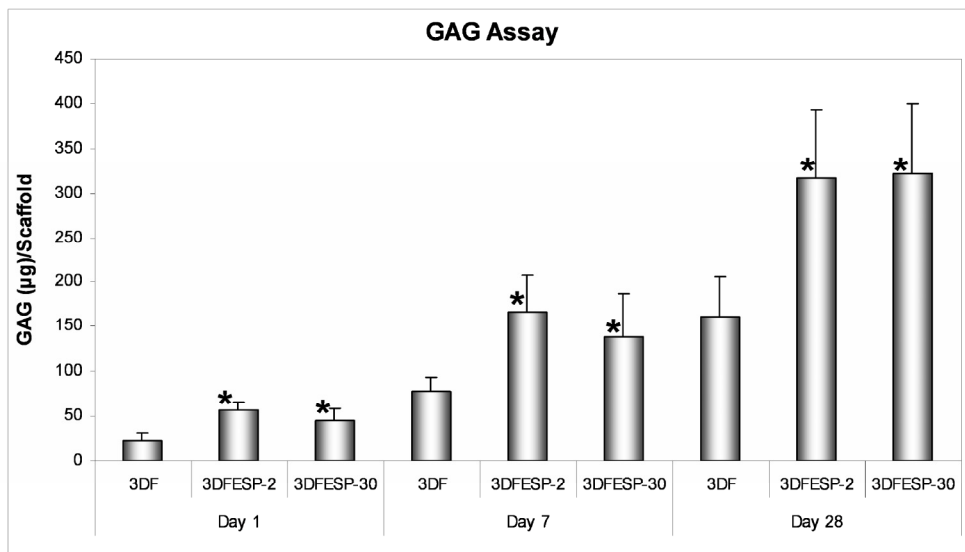


**Figure 4** – GAG assay on 3DF, 3DFESP-2, and 3DFESP-30 scaffolds after 1, 7, and 28 days of culture. (\*) indicates significant differences with respect to 3DF scaffolds ( $p < 0.05$ ).

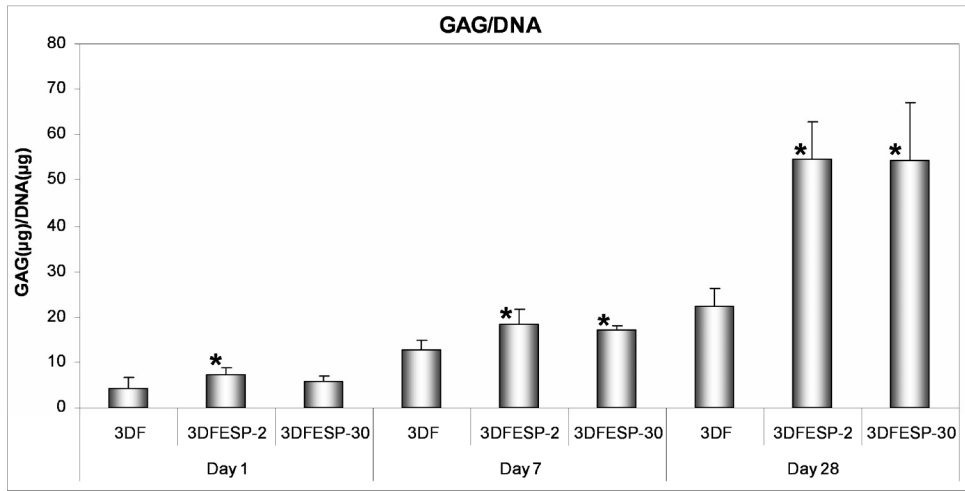


**Figure 5** – GAG/DNA ratio on 3DF, 3DFESP-2, and 3DFESP-30 scaffolds after 1, 7, and 28 days of culture. (\*) depicts significant differences with respect to 3DF scaffolds ( $p < 0.05$ ).

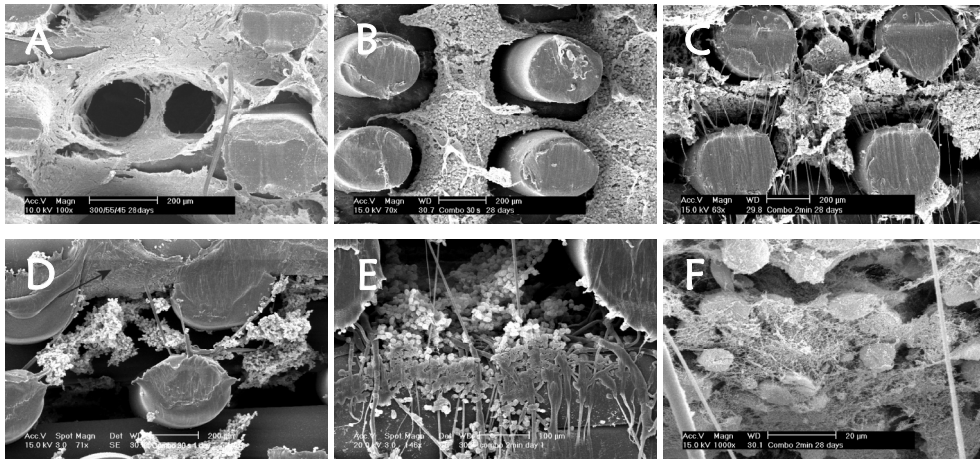


**Figure 6** – SEM pictures show chondrocytes distribution and morphology on 3DF (a), 3DFESP-30 (b, d), and 3DFESP-2 (c, e, f) scaffolds. After 28 days scaffolds pores were bridged by cells (a-c) and ECM (f). Chondrocytes were spread on 3DF scaffolds (a) and maintained their rounded morphology on 3DFESP scaffolds (b, c). Cell morphology was influenced by the fiber diameter (d, e) already at day 1. (a-d) scale bar: 200 µm; (e) scale bar: 100 µm; (f) scale bar: 20 µm.

scaffolds were characterized by a periodically interspersed network of rapid prototyped macrofibers and electrospun microfibers. Scaffolds with macrofibers of approximately 300 µm and microfibers of approximately 10 µm were used in this specific study. No delamination between layers of 3DF fibers or layers of 3DF and ESP fibers occurred, resulting in a stable scaffold construct. Moreover, being the integration principles adopted in this study relatively simple, such a system can be extended to different kind of polymers and other rapid prototyping devices. Further

3DF-ESP  
Scaffolds

investigations could also focus on the combination of different fiber diameter and surface texture. The two techniques offer, in fact, a wide versatility and range of solutions. The resolution limit of 3DF is currently 100  $\mu\text{m}$  and can be further downscaled by improving – for example – the extrusion mechanism [46, 47], while

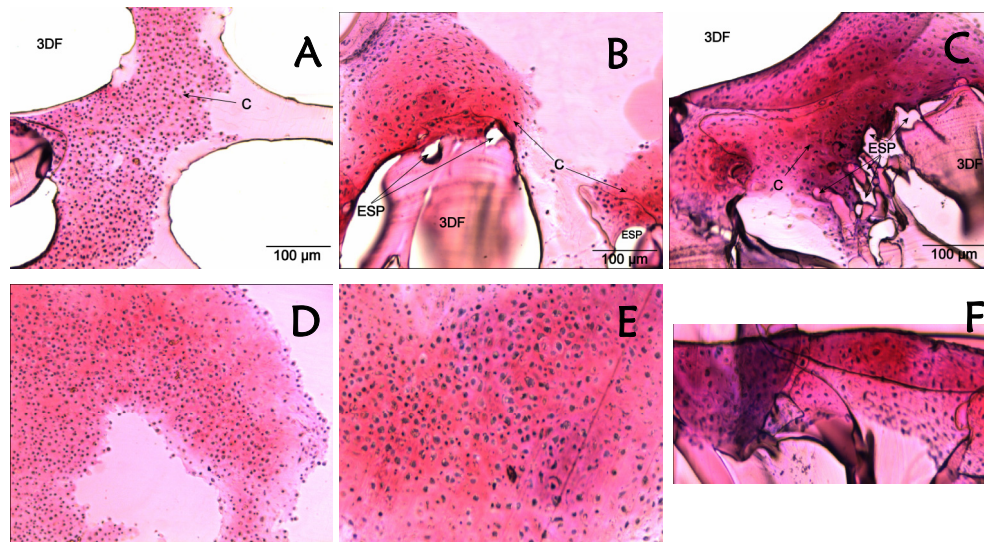


**Figure 7** – Histological cross sections show sulphated GAG formation in 3DF (a), 3DFESP-30 (b), and 3DFESP-2 (c) scaffolds by safranin-O staining. Inserts show staining in the middle of the scaffolds (d, e) and close to the ESP micron-size fibers (f). Differences in 3DF and ESP fiber coloration are due to partial or total dissolution of PEOT/PBT in the embedding material (glycol-methacrylate). C indicates cartilage formation (GAG), 3DF refers to the macro fibers, while ESP to the micro fibers. Scale bar: 100  $\mu\text{m}$ .

ESP fibers can be downscaled to few tenths of nanometers [48-50]. Furthermore, electrospun fibers can be fabricated with different surface morphology [32, 37, 51] and were shown to influence cell proliferation and morphology [37]. For instance, we also integrated in 3DF scaffolds an ESP network of nanoporous fibers with a fiber diameter of 10  $\mu\text{m}$  and rounded shaped nanopores of 220 nm. Seeded mesenchymal stem cells were found to attach, spread, and proliferate most preferably on the electrospun fibers, while almost no cell adhered to the 3DF macrofibers (figure 8). Another interesting possibility is the direct integration of the two techniques in a single apparatus, since electrospinning of molten polymers has been successfully demonstrated [30] and characterized [52] by Larrondo *et al.* We have started to look into this direction and we could extend molten polymer electrospinning to PEOT/PBT copolymers, as shown in figure 9. However, more efforts need to be put in the insulation of the rapid prototyping robot from the electrospinning high voltage collector. Yet, the combination of these varieties might give origin to multifunctional structures useful in application where a hierarchical structure and a time response of such a construct are desired.



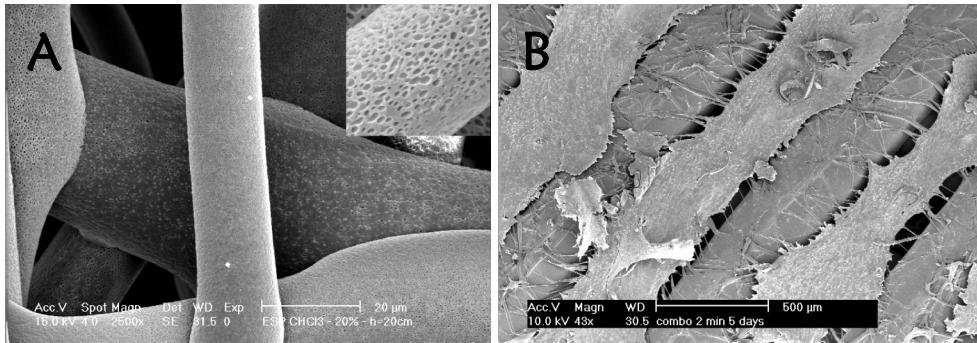


**Figure 8** – SEM micrographs showing (a) the nanopore surface topology of the ESP fibers and (b) stem cells selective attachment and spreading on the 10  $\mu\text{m}$  nanoporous electrospun network, which suggests an influence of fiber nanoporosity on cell morphology and a cell-fiber size preferential interaction. Scale bar: 500  $\mu\text{m}$ .

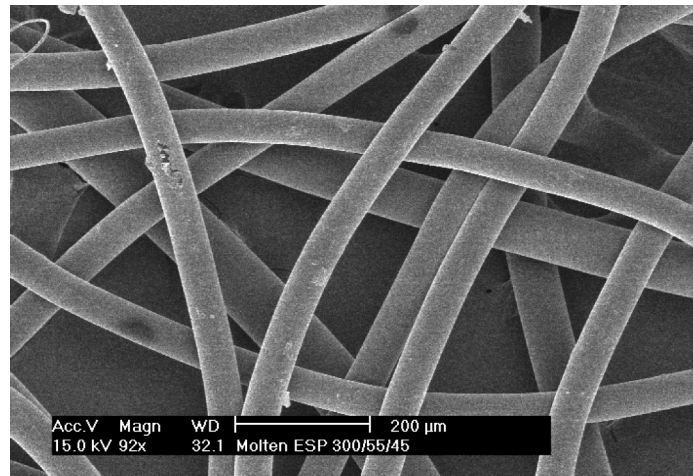


**Figure 9** – SEM micrographs of molten-electrospun 300PEOT55PBT45. Scale bar: 200  $\mu\text{m}$ .

As an example to show their improved functionality, these cellular structures were used as scaffolds for cartilage tissue engineering. Bovine primary chondrocytes were cultured for one month on 3DF and 3DFESP scaffolds with different ESP network density. Cells were better retained in 3DFESP. This can be deputed to the “sieving” effect of the ESP integrated network, which entraps cells within the scaffolds. The entrapment efficiency of 3DFESP constructs was enhanced after cell seeding and during cell proliferation (day 7), since the increase in DNA amount was significant as compared to 3DF scaffolds alone. Furthermore, a homogeneous distribution of cells could be detected throughout the entire scaffold. Therefore, it can be inferred that the pores of the electrospun network are accessible and do not obstruct cell migration in the scaffold. However, after 4 weeks DNA decreased in the 3DFESP scaffolds. This might be due to a redistribution of cells in favor of a higher extracellular matrix production, as also supported by a higher GAG formation in the

combined constructs. The production of more GAG can also be attributed to a better cell differentiation in the 3DFESP scaffolds, as analyzed by SEM and quantitatively confirmed by the GAG/DNA ratio. In fact, chondrocytes appeared to maintain a rounded morphology when in contact with smooth microfibers and started to spread already after 1 day only when in contact with smooth macrofibers (figure 6D and 6E). It is known that when chondrocytes maintain their natural spherical shape they produce more GAG and a higher collagen type II versus collagen type I ratio [53-56]. This is partly corroborated by the GAG/DNA ratio, which determines how much GAG is produced per cell. A higher value of this ratio implies a higher degree of differentiation of the cells. Therefore, a better articular cartilage tissue formation can be expected from the 3DFESP constructs. No significant difference was found by varying the ESP network density. A comparable amount of DNA was found during the cell attachment (day 1) and proliferation (day 7) stages when a higher density network (3DFESP-2) was integrated as compared to a lower density network (3DFESP-30). This was also reflected in a similar GAG formation and a comparable GAG/DNA ratio. Therefore, no implications between the density of the network chosen in this study and the efficiency of the cell “sieving” and entrapment effect can be drawn. These results make of 3DFESP a very promising new type of scaffolds for cartilage tissue formation. Since they combine a macrostructure that provides the required mechanical properties and a microstructure that supplies topological cues at the extracellular matrix level, 3DFESP scaffolds can also find applications for other engineered tissue. Furthermore, the possibility to incorporate biological factors in the ESP network [57, 58] gives the possibility to control layer by layer the differentiation of cell and the formation of hierarchically structured tissues.

## Conclusion

### 3DF-ESP Scaffolds

A novel type of scaffold (3DFESP) that combines a periodical rapid prototyped macrostructure with a random electrospun microstructure integrated in the same construct has been fabricated, characterized and evaluated for cartilage tissue engineering. 3DFESP showed a higher amount of entrapped cells during attachment and proliferation and a higher amount of extracellular matrix produced after 4 weeks of culture as compared to 3DF scaffolds alone. Furthermore, a better cell differentiation was supported by these constructs, as shown by the GAG/DNA ratio and by SEM analysis. Chondrocytes maintained their rounded morphology in 3DFESP scaffolds while they spread in 3DF scaffolds. Being the two fabrication technologies versatile to process different kind of materials with a number of topological superficial cues, these new kinds of scaffolds can be used to create different multifunctional 3D matrices that will improve the current status of tissue engineering applications.

## Acknowledgements

This project was funded by the European Community project Intelliscaf GSRD\_2002\_00697.

## References

- [1] Yeong WY, Chua CK, Leong KF, Chandrasekaran M. Rapid prototyping in tissue engineering: challenges and potential. *Trends Biotechnol* 2004;22(12):643-52.
- [2] Hutmacher DW, Sittinger M, Risbud MV. Scaffold-based tissue engineering: rationale for computer-aided design and solid free-form fabrication systems. *Trends Biotechnol* 2004;22(7):354-62.
- [3] Hollister SJ. Porous scaffold design for tissue engineering. *Nat Mater* 2005;4(7):518-24.
- [4] Giordano RA, Wu BM, Borland SW, Cima LG, Sachs EM, Cima MJ. Mechanical properties of dense polylactic acid structures fabricated by three dimensional printing. *J Biomater Sci Polym Ed* 1996;8(1):63-75.
- [5] Hutmacher DW. Scaffold design and fabrication technologies for engineering tissues--state of the art and future perspectives. *J Biomater Sci Polym Ed* 2001;12(1):107-24.
- [6] Landers R, Pfister A, Hubner U, John H, Schmelzeisen R, Mullhaupt R. Fabrication of soft tissue engineering scaffolds by means of rapid prototyping techniques. *J of Mater Sci* 2002;37:3107-3116.
- [7] Vozzi G, Flaim C, Ahluwalia A, Bhatia S. Fabrication of PLGA scaffolds using soft lithography and microsyringe deposition. *Biomaterials* 2003;24(14):2533-40.
- [8] Antonov EN, Bagratashvili VN, Whitaker MJ, Barry JJA, Shakesheff KM, Kononov AN, Popov VK, Howdle SM. Three-Dimensional Bioactive and Biodegradable Scaffolds Fabricated by Surface-Selective Laser Sintering. *Adv Mater* 2005;17:327-330.
- [9] Woodfield TB, Malda J, de Wijn J, Peters F, Riesle J, van Blitterswijk CA. Design of porous scaffolds for cartilage tissue engineering using a three-dimensional fiber-deposition technique. *Biomaterials* 2004;25(18):4149-61.
- [10] Smay JE, Gratson GM, Shepherd RF, Cesarano III J, Lewis JA. Directed Colloidal Assembly of 3D Periodic Structures. *Adv Mater* 2002;14(18):1279-1283.
- [11] Lin CY, Kikuchi N, Hollister SJ. A novel method for biomaterial scaffold internal architecture design to match bone elastic properties with desired porosity. *J Biomech* 2004;37(5):623-36.
- [12] Hollister SJ, Maddox RD, Taboas JM. Optimal design and fabrication of scaffolds to mimic tissue properties and satisfy biological constraints. *Biomaterials* 2002;23(20):4095-103.
- [13] Lin AS, Barrows TH, Cartmell SH, Guldberg RE. Microarchitectural and mechanical characterization of oriented porous polymer scaffolds. *Biomaterials* 2003;24(3):481-9.
- [14] Moroni L, de Wijn JR, van Blitterswijk CA. 3D fiber-deposited scaffolds for tissue engineering: Influence of pores geometry and architecture on dynamic mechanical properties. *Biomaterials* 2006;27:974-985.

- [15] Moroni L, de Wijn JR, van Blitterswijk CA. Three-dimensional fiber-deposited PEOT/PBT copolymer scaffolds for tissue engineering: Influence of porosity, molecular network mesh size, and swelling in aqueous media on dynamic mechanical properties. *J Biomed Mater Res A* 2005;75:957-965.
- [16] Malda J, Woodfield TB, van der Vloodt F, Kooy FK, Martens DE, Tramper J, van Blitterswijk CA, Riesle J. The effect of PEGT/PBT scaffold architecture on oxygen gradients in tissue engineered cartilaginous constructs. *Biomaterials* 2004;25(26):5773-80.
- [17] Li JP, de Wijn JR, Van Blitterswijk CA, de Groot K. Porous Ti(6)Al(4)V scaffold directly fabricating by rapid prototyping: Preparation and in vitro experiment. *Biomaterials* 2005.
- [18] Smay JE, Cesarano III J, Tuttle BA, Lewis JA. Directed Colloidal Assembly of Linear and Annulate Lead of Zirconia Titanate Arrays. *J Am Ceram Soc* 2005;87(2):293-295.
- [19] Sherwood JK, Riley SL, Palazzolo R, Brown SC, Monkhouse DC, Coates M, Griffith LG, Landeen LK, Ratcliffe A. A three-dimensional osteochondral composite scaffold for articular cartilage repair. *Biomaterials* 2002;23(24):4739-51.
- [20] Yan Y, Xiong Z, Hu Y, Wang S, Zhang R, Zhang C. Layered manufacturing of tissue engineering scaffolds via multi-nozzle deposition. *Materials Letters* 2003;57:2623-2628.
- [21] Woodfield TB, Van Blitterswijk CA, De Wijn J, Sims TJ, Hollander AP, Riesle J. Polymer scaffolds fabricated with pore-size gradients as a model for studying the zonal organization within tissue-engineered cartilage constructs. *Tissue Eng* 2005;11(9-10):1297-311.
- [22] Smith CM, Stone AL, Parkhill RL, Stewart RL, Simpkins MW, Kachurin AM, Warren WL, Williams SK. Three-dimensional bioassembly tool for generating viable tissue-engineered constructs. *Tissue Eng* 2004;10:1566-76.
- [23] Fan H, Lu Y, Stump A, Reed ST, Baer T, Schunk R, Perez-Luna VV, Lopez GP, Brinker CJ. Rapid prototyping of patterned functional nanostructures. *Nature* 2000;405(6782):56-60.
- [24] Furukawa KS, Suenaga H, Toita K, Numata A, Tanaka J, Ushida T, Sakai Y, Tateishi T. Rapid and large-scale formation of chondrocyte aggregates by rotational culture. *Cell Trans* 2003;12:475-9.
- [25] Kino-Oka M, Maeda Y, Yamamoto T, Sugawara K, Taya M. A kinetic modeling of chondrocyte culture for manufacture of tissue-engineered cartilage. *J Biosci Bioeng* 2005;99(3):197-207.
- [26] Martin I, Dozin B, Quarto R, Cancedda R, Beltrame F. Computer-based technique for cell aggregation analysis and cell aggregation in in vitro chondrogenesis. *Cytometry* 1997;28(2):141-6.
- [27] Gilbert SF. *Developmental Biology*. Sinauer Associates, Inc. 2000.
- [28] Loty S, Forest N, Boulekbache H, Sautier JM. Cytochalasin D induces changes in cell shape and promotes in vitro chondrogenesis: a morphological study. *Biol Cell* 1995;83(2-3):149-61.
- [29] Taylor G. Electrically Driven Jets. *Proc R Soc London, Ser A* 1969;313:453-475.

- [30] Larrondo L, Manley R. Electrostatic Fiber Spinning from Polymer Melts. I. Experimental Observations on Fiber Formation and Properties. *J Polym Sci: Pol Phys Ed* 1981;19:909-920.
- [31] Deitzel J, Kleinmeyer J, Harris D, Beck Tan N. The effect of processing variables on the morphology of electrospun nanofibers and textiles. *Polymer* 2001;42:261-272.
- [32] Kwon IK, Kidoaki S, Matsuda T. Electrospun nano- to microfiber fabrics made of biodegradable copolyesters: structural characteristics, mechanical properties and cell adhesion potential. *Biomaterials* 2005;26(18):3929-39.
- [33] Rutledge G, Li Y, Fridrikh S, Warner S, Kalayci V, Patra P. Electrostatic Spinning and Properties of Ultrafine Fibers. *National Textile Center Annual Report* 2001:1-10.
- [34] Boland E, Coleman B, Barnes C, Simpson D, Wnek G, Bowlin G. Electrospinning polydioxanone for biomedical applications. *Acta Biomaterialia* 2005:115-123.
- [35] Stevens MM, George JH. Exploring and engineering the cell surface interface. *Science* 2005;310(5751):1135-8.
- [36] Badami AS, Kreke MR, Thompson MS, Riffle JS, Goldstein AS. Effect of fiber diameter on spreading, proliferation, and differentiation of osteoblastic cells on electrospun poly(lactic acid) substrates. *Biomaterials* 2006;27(4):596-606.
- [37] Moroni L, Licht R, de Boer J, de Wijn JR, van Blitterswijk CA. Fiber diameter and texture of electrospun PEOT/PBT scaffolds influence human mesenchymal stem cell proliferation and morphology, and the release of incorporated compounds. *Biomaterials* 2006;27(28):4911-22.
- [38] Beumer GJ, van Blitterswijk CA, Ponc M. Degradative behaviour of polymeric matrices in (sub)dermal and muscle tissue of the rat: a quantitative study. *Biomaterials* 1994;15(7):551-9.
- [39] Beumer GJ, van Blitterswijk CA, Ponc M. Biocompatibility of a biodegradable matrix used as a skin substitute: an in vivo evaluation. *J Biomed Mater Res* 1994;28(5):545-52.
- [40] Bakker D, van Blitterswijk CA, Hesseling SC, Grote JJ. Effect of implantation site on phagocyte/polymer interaction and fibrous capsule formation. *Biomaterials* 1988;9(1):14-23.
- [41] van Blitterswijk CA, van den Brink J, Leenders H, Bakker D. The effect of PEO ratio on degradation, calcification and bone bonding of PEO/PBT copolymer (PolyActive). *Cell and Mater* 1993;3:23-26.
- [42] Bulstra SK, Geesink RG, Bakker D, Bulstra TH, Bouwmeester SJ, van der Linden AJ. Femoral canal occlusion in total hip replacement using a resorbable and flexible cement restrictor. *J Bone Joint Surg Br* 1996;78(6):892-8.
- [43] Mensik I, Lamme EN, Riesle J, Brychta P. Effectiveness and Safety of the PEGT/PBT Copolymer Scaffold as Dermal Substitute in Scar Reconstruction Wounds (Feasibility Trial). *Cell Tissue Bank* 2002;3(4):245-53.
- [44] Bezemer JM, Grijpma DW, Dijkstra PJ, van Blitterswijk CA, Feijen J. A controlled release system for proteins based on poly(ether ester) block-copolymers: polymer network characterization. *J Control Release* 1999;62(3):393-405.
- [45] Deschamps AA, Claase MB, Sleijster WJ, de Bruijn JD, Grijpma DW, Feijen J. Design of segmented poly(ether ester) materials and structures for the tissue engineering of bone. *J Control Release* 2002;78(1-3):175-86.

- [46] Rao RB, Krafcik KL, Morales AM, Lewis JA. Microfabricated deposition nozzles for direct-write assembly of three-dimensional periodic structures. *Advanced Materials* 2005;17(3):289-+.
- [47] Lewis JA, Gratson GM. Direct writing in three dimensions. *Materials Today* 2004;July/August:32-39.
- [48] Min BM, Lee G, Kim SH, Nam YS, Lee TS, Park WH. Electrospinning of silk fibroin nanofibers and its effect on the adhesion and spreading of normal human keratinocytes and fibroblasts in vitro. *Biomaterials* 2004;25(7-8):1289-97.
- [49] Yoshimoto H, Shin Y, Terai H, Vacanti J. A biodegradable nanofiber scaffold by electrospinning and its potential for bone tissue engineering. *Biomaterials* 2003;24:2077-2082.
- [50] van Dijkhuizen-Radersma R, Roosma JR, Sohler J, Peters FL, van den Doel M, van Blitterswijk CA, de Groot K, Bezemer JM. Biodegradable poly(ether-ester) multiblock copolymers for controlled release applications: An in vivo evaluation. *J Biomed Mater Res A* 2004;71(1):118-27.
- [51] Bognitzki M, Czado W, Frese T, Schaper A, Hellwig M, Steinhart M, Greiner A, Wendorff J. Nanostructured Fibers via Electrospinning. *Adv Mater* 2001;13(1):70-72.
- [52] Larrondo L, Manley R. Electrostatic Fiber Spinning from Polymer Melts. II. Examination of the Flow Field in an Electrically Driven Jet. *J Polym Sci: Pol Phys Ed* 1981;19:921-932.
- [53] Mahmood TA, de Jong R, Riesle J, Langer R, van Blitterswijk CA. Adhesion-mediated signal transduction in human articular chondrocytes: the influence of biomaterial chemistry and tenascin-C. *Exp Cell Res* 2004;301(2):179-88.
- [54] Woodfield TB, Miot S, Martin I, van Blitterswijk CA, Riesle J. The regulation of expanded human nasal chondrocyte re-differentiation capacity by substrate composition and gas plasma surface modification. *Biomaterials* 2005.
- [55] Miot S, Woodfield T, Daniels AU, Suetterlin R, Peterschmitt I, Heberer M, van Blitterswijk CA, Riesle J, Martin I. Effects of scaffold composition and architecture on human nasal chondrocyte redifferentiation and cartilaginous matrix deposition. *Biomaterials* 2005;26(15):2479-89.
- [56] Barry JJ, Gidda HS, Scotchford CA, Howdle SM. Porous methacrylate scaffolds: supercritical fluid fabrication and in vitro chondrocyte responses. *Biomaterials* 2004;25(17):3559-68.
- [57] Jiang H, Hu Y, Li Y, Zhao P, Zhu K, Chen W. A facile technique to prepare biodegradable coaxial electrospun nanofibers for controlled release of bioactive agents. *J Control Release* 2005;108(2-3):237-43.
- [58] Li C, Vepari C, Jin HJ, Kim HJ, Kaplan DL. Electrospun silk-BMP-2 scaffolds for bone tissue engineering. *Biomaterials* 2006;27(16):3115-24.

# Chapter 10

## Development of Tailor Made Hybrid Scaffolds for Osteochondral Tissue Engineering

L. Moroni <sup>a,\*</sup>, L.Paoluzzi <sup>b</sup>, J. Pieper <sup>c</sup>, J.R. de Wijn <sup>a</sup>, C.A. van Blitterswijk <sup>a</sup>

<sup>a,\*</sup> Institute for BioMedical Technology (BMTI), University of Twente, P.O. Box 217, 7500 AE Enschede, The Netherlands. E-mail: l.moroni@tnw.utwente.nl

<sup>b</sup> Mechanical Engineering Institute, Università Politecnica delle Marche, Ancona, Italy

<sup>c</sup> Isotis OrthoBiologics S.A., Irvine, U.S.A.

### Abstract

Scaffolds for osteochondral tissue engineering should provide mechanical stability when implanted in a joint, at the same time offering to the cells signals specific for chondral and bone regeneration and an open, accessible, and completely interconnected pore network for their attachment, proliferation, and migration. Biomaterial composites of polymers and ceramics are often considered to satisfy these requirements, but generally their synthesis may result in poor chemical bonding, despite the maintained or improved tissue forming properties. This may affect their mechanical properties and processability into 3D scaffolds. Therefore, the aim of this study was to design and fabricate hybrid 3D scaffolds with a novel concept based on biomaterials assembly. Rapid prototyped biphasic-calcium phosphate (BCP) ceramic particles were integrated into the pores of a polymeric 3D fiber-deposited matrix (3DFM) and infused with demineralised bone matrix (DBM) to obtain a construct that displays the mechanical robustness of ceramics and the flexibility of polymers and DBM foams. Results showed that the mechanical properties of these constructs could be modulated depending on the ceramic particle design while maintaining completely interconnectivity and accessibility of their pore network, characteristic of rapid prototyped structures. An osteochondral scaffold was then proposed by directly manufacturing a 3D fiber-deposited (3DF) structure optimized for cartilage regeneration on top of the bone hybrid scaffold. The two compartments were interlocked by a system of intertwined concentric fibers mimicking the tidemark region. These 3D scaffolds can be used for osteochondral tissue engineering as they couple mechanical stability and a fully open pore network to the chondral and bone forming properties of the single biomaterials combined in the assembly.

**Keywords:** rapid prototyping; assembly; ceramics; polymers; tissue engineering.

## Introduction

Osteochondral defects are typically derived from congenital diseases or traumatic events in young patients and from osteoarthritis in old individuals. This results in associated pain and joint instability. Although bone tissue has the capacity for regenerative growth, bone repair is impaired in many pathological situations and cartilage has a poor capacity to regenerate itself due to its avascular nature and to its intrinsic composition. Therefore, there is a critical need to develop technologies to promote bone and chondral healing. Autografts are used most to treat osteochondral defects. However, their clinical use involves some difficulties like septic complications, viral transmission, and patient morbidity in the location where new tissue is taken [1, 2]. A possible solution in terms of availability would be the use of allografts. Yet, these may be associated to risks of disease transmission, and difficulties in shaping. A significant additional limitation of allografts is related to a delay in remodelling by the host for the bony part and to a lack of integration with the surrounding tissue in the chondral site. Furthermore, in case of very large defects the allograft may remain in the implant site throughout the patient's life, creating an area more prone to fracture or infection [3-5].

These issues have justified the development of 3D scaffolds employed in a tissue engineering approach, which are an attractive alternative when used alone or in combination with cells to restore the joint functionality [5-7]. Osteochondral scaffolds typically comprise a cartilage and a bone compartment. The chondral scaffold is generally formed by polymeric foams or textile meshes [8-13], while bone substitutes includes either biomaterials mimicking the composition of bone, i.e. calcium phosphate ceramics simulating the bone mineral composition [14-17] or demineralized bone matrices (DBMs) matching the organic composition [18-21]. Despite the fact that these materials have demonstrated satisfying cartilage and bone forming capacities, their mechanical properties may not be always optimal for implanting in load bearing sites. In particular for the bony site, under high loads ceramics are often too brittle and can be subject to fracture, whereas DBMs are very flexible and may require the patient to be temporarily immobilised. A possible solution to overcome the mechanical drawbacks displayed by ceramics and DBMs is to combine and integrate them with a polymeric matrix. Studies to date have focused on the incorporation of ceramics and polymers by interspersing the polymeric phase into the ceramic one – and *vice versa* – to finally obtain a homogeneous composite scaffold [22-26]. However, this often results in scaffolds with poor polymeric-ceramic bonding and limited control over composite processability and mechanical properties. Furthermore, during the interspersion of the two phases some of the pores can be blocked, typically due to the use of solvents, resulting in a reduction of the scaffold's pore interconnectivity [4, 22]. In this respect, rapid prototyping techniques can offer an optimal solution in terms of modulating mechanical properties, as they demonstrated to effectively control the structural parameters of 3D scaffolds [27-30]. Moreover, these techniques can process a number of different biomaterials and require a minimal or no use of solvents.



Therefore, the aim of this study was to design, fabricate, and characterize tri-phasic hybrid scaffolds with a novel concept where the biomaterials are not chemically or physically bonded, but assembled in a single 3D construct with preserved pore network accessibility and interconnectivity. By integrating different rapid prototyping technologies and freeze-drying, it was possible to create scaffolds for osteochondral tissue engineering, where the chondral scaffold was directly connected to the bone compartment by 3D fiber-deposition (3DF). In particular, we focused on the mechanical improvement of the bony part of the scaffold. This was formed by a flexible polymeric porous matrix, into the pores of which ceramic particles of designed shapes were “captured” or press-fitted. The constructs were, then, infused in a DBM gel and freeze-dried to obtain a foamy interspersed phase that acted as mechanical “cushion” at the same time providing further bone regeneration properties. The bone scaffold was finally interlocked to an optimized 3DF scaffold for cartilage regeneration [31, 32] through a fibrous system made of intertwined concentric polymeric fibers, mimicking the tidemark area of the osteochondral natural architecture.

Block-copolymers of poly(ethylene oxide – terephthalate)/poly(butylene terephthalate) (PEOT/PBT) have been used to fabricate the polymeric matrix. These polyether-ester block copolymers are biodegradable thermoplastic elastomers, which have favorable physical properties such as elasticity, toughness and strength in combination with easy processability [33-35]. PEOT/PBT copolymers have demonstrated to have a satisfactory biocompatibility both *in vitro* and *in vivo* [36-38] and reached clinical applications (PolyActive™, IsoTis Orthopaedics S.A.) as cement stoppers and bone fillers in orthopedic surgery [39, 40]. Biphasic calcium phosphate (BCP) was used as a ceramic, given the osteoconductive and osteoinductive properties depending on its physicochemical properties and microstructure [41-45]. BCP is obtained by sintering a calcium deficient apatite above 700 °C. It consists of a more stable hydroxyapatite (HA)  $\text{Ca}_{10}(\text{PO}_4)_6(\text{OH})_2$  phase and of a more soluble beta-tricalcium phosphate ( $\beta$ -TCP)  $\text{Ca}_3(\text{PO}_4)_2$  phase. By controlling the ratio of the two phases, it is possible to optimize the release of calcium and phosphate ions from the soluble  $\beta$ -TCP phase in the body, which contributes to the formation of new bone. Demineralized bone matrices (DBM) are normally obtained by acid extraction of the mineralized component of bone, while maintaining the collagen and non-collagenous proteins. Among these proteins an important role in DBMs osteoinductivity is played by the presence of morphogenic factors, which contributes to direct the differentiation of local mesenchymal stem cells into the osteogenic lineage [46-48]. Since the hybrid constructs proposed here hypothetically combine the flexibility of polymers and DBMs with the mechanical strength of ceramics while maintaining the individual osteochondral formation capacities of PEOT/PBT copolymers, DBMs, and ceramics, they could find applications as tissue-engineered based scaffolds in load bearing sites.

## Materials and Methods

### *Materials Characterization*

Poly(ethylene oxide – terephthalate)/poly(butylene terephthalate) (PEOT/PBT) copolymers, solubilized demineralized bone matrix (DBM), and biphasic calcium phosphate (BCP) powder were obtained from IsoTis Orthopaedics S.A. (Bilthoven, The Netherlands). The copolymer composition used in this study were 1000PEOT70PBT30 for the 3DFM matrix of the bone compartment and 300PEOT55PBT45 for the cartilage compartment of the osteochondral scaffold where, following an aPEOTbPBTc nomenclature, *a* is the molecular weight in g/mol of the starting PEG blocks used in the copolymerization, while *b* and *c* are the weight ratios of the PEOT and PBT blocks, respectively.

### *Design of the Bone Compartment Scaffolds*

Tri-phasic scaffolds were fabricated by assembling BCP, 1000PEOT70PBT30, and DBM into monolithic constructs for the bone compartment of the osteochondral scaffold. Two different designs (A and B) were chosen to realize scaffolds. Design A consisted in fabricating a PEOT/PBT 3D fiber-deposited matrix (3DFM) that was used as a carrier for BCP rapid prototyped particles, which were press fitted into the scaffold pores. BCP particles were of pillar (side: 1.6 mm; height: 4.3 mm), truncated cone (large base diameter: 2 mm; small base diameter: 1.6 mm; height: 4 mm), spherical (diameter: 1.8 mm) and irregular (between 1.4 mm and 2 mm in their maximum dimension) shapes (figure 1a). More spherical and irregular particles were press fitted in the pores of the 3DFM scaffolds until covering the total thickness of the polymeric matrix. Different ceramic particle shapes were considered to assess the optimal amount of included BCP and the influence of the particle geometry on mechanical properties, while maintaining the flexibility of the construct. The 3DFM scaffold had a block shape, with a square base of 10 mm, and a height of 3.15 mm. Since 1000PEOT70PBT30 is known to swell in an aqueous environment [33-35], the scaffolds were under dimensioned to match exactly the BCP designed particles in a wet milieu.

In design B, a BCP cylinder (5 mm in diameter by 3 mm in height) was pre-soaked in a DBM gel (2.6% w/v in a 4.75% v/v methanol in demineralized water solution) and subsequently lyophilized. The cylinder was “sandwiched” by two discs of DBM foam (5 mm in diameter by 1 mm in height) and the construct was inserted in a hollow cylindrical container of PEOT/PBT made by three-dimensional fiber deposition (figure 1b). The polymeric hollow cylinder had an outer diameter of 6 mm, a wall thickness of 1 mm and a height of 6 mm. In both design A and B, the whole constructs were immersed again in the DBM gel and freeze-dried. Figure 1 illustrates the principle of the assembling procedure.

### *Fabrication of the Bone Compartment Scaffolds*

#### *Polymeric 3DFM Matrix*

1000PEOT70PBT30 3DFM scaffolds were manufactured with a Bioplotter device (Envisiontec GmbH, Germany), essentially an XYZ plotter device as previously described [35]. The device was modified to extrude highly viscous polymeric fibers. The polymer was put in a stainless steel syringe and heated at  $T = 190\text{ }^{\circ}\text{C}$  through a thermoset cartridge unit, fixed on the "X"-mobile arm of the apparatus. When the molten phase was achieved, a nitrogen pressure of 5 bars was applied to the syringe through a pressurized cap. The scaffold models were loaded on the Bioplotter CAM (PrimCAM, Switzerland) software and deposited layer by layer, through the extrusion of the polymer on a stage as a fiber. The deposition speed was set to 300 mm/min. Scaffolds were then characterized by the fiber diameter (through the nozzle diameter), the spacing between fibers in the same layer, the layer thickness and the configuration of the deposited fibers within the whole architecture. In design A, the nozzle used was a stainless steel Luer Lock needle with internal diameter (ID) of  $400\text{ }\mu\text{m}$ , shortened to a length of 16.2 mm. The fiber spacing was set to  $1650\text{ }\mu\text{m}$ , while the layer thickness to  $225\text{ }\mu\text{m}$ . A 0-90 scaffold architecture was chosen, where fibers were deposited with  $90^{\circ}$  orientation steps between successive layers. In design B, the hollow cylindrical scaffold was fabricated with a similar nozzle with respect to design A, but with a smaller ID of  $250\text{ }\mu\text{m}$ . The fiber spacing was decreased to  $600\text{ }\mu\text{m}$ , and the layer thickness to  $150\text{ }\mu\text{m}$ , while the fiber deposition architecture was maintained as a 0-90 architecture.

#### *Ceramic Particles*

Porous BCP designed particles were fabricated by an indirect rapid prototyping technique. First negative masks were designed with CAD/CAM software (RhinoCeros®) and fabricated with an acrylic photopolymerizable resin by photolithography (PreFAB, Envisiontec, Germany). The masks were then filled with a BCP slurry made by adding 32.8 grams of calcinated BCP powder (20 hours in an oven at  $1000\text{ }^{\circ}\text{C}$ ), 14.2 grams of non calcinated BCP powder, 20 grams of demineralized water, 1.2 grams of methylcellulose solution (2% w/v methylcellulose in demineralized water), 2.2 grams of ammonia, and 14.1 grams of  $300 - 500\text{ }\mu\text{m}$  sieved naphthalene particles, resulting in a 30% macro porosity of the BCP particles. The components were blended and vigorously stirred with a mixer for approximately 30 minutes, until a homogeneous slurry was obtained. The BCP particles were then obtained by debonding and sintering in a furnace (Nabertherm, Germany) at  $T = 1150\text{ }^{\circ}\text{C}$ . Irregular BCP particles with an average size between 1.4 mm and 2 mm were also used. These latter particles were fabricated by hydrogen peroxide foaming, as described elsewhere [16]. BCP particles were press fitted in the pores of the 3DF matrix by exploiting the swelling behavior of 1000PEOT70PBT30. The polymeric matrix was left in demineralized water for 24 hours to allow swelling prior to insertion of the BCP particles.

### ***3D Hybrid Scaffold Assembly***

DBM gel was obtained by mixing 2 grams of DBM powder into 80 grams of methanol solution (4.75% volume/volume in demineralized water). DBM foams were fabricated by placing the gel in square molds and freeze-drying (Virtis 25 SRC, The Netherlands). The scaffolds were finally immersed in the DBM gel and placed for 1 hour under vacuum (0.01 mbar) to let the gel impregnate the porous polymeric matrix and the BCP particles. After infiltration the final construct was freeze-dried to obtain a porous DBM matrix infiltrating and surrounding the scaffolds. This resulted in a final hybrid scaffold thickness of approximately 6 mm for each design.

### ***3D Osteochondral Scaffolds Fabrication***

The 300PEOT55PBT45 cartilage compartment of the osteochondral scaffold was deposited directly on top of the bone assembled 3D hybrid scaffold by 3DF. In a similar process to what previously explained, the polymer was placed in the extrusion syringe and heated through the thermoset cartridge to reach its molten state at  $T = 210\text{ }^{\circ}\text{C}$ . A nitrogen pressure of 5 bars was applied to extrude the polymeric fibers from a nozzle with an ID of  $250\text{ }\mu\text{m}$  and a length of 16.2 mm. The fiber spacing was set to  $600\text{ }\mu\text{m}$ , and the layer thickness to  $150\text{ }\mu\text{m}$ , while the fiber deposition architecture was maintained as a 0-90 architecture. The fibers were deposited at a speed of 230 mm/min. Since the two PEOT/PBT compositions (bone = 1000PEOT70PBT30 – cartilage = 300PEOT55PBT45) have different swelling properties, osteochondral scaffolds with and without an interlocking fibrous system were fabricated to assess the interface resistance of the construct. The interlocking system was made of intertwined concentric 1000PEOT70PBT30 and 300PEOT55PBT45 fibers at the interface between the bone and the chondral parts of the construct. The concentric fibers were extruded from needles with ID and length as above described. The fiber spacing was set to  $800\text{ }\mu\text{m}$ , and the layer thickness to  $135\text{ }\mu\text{m}$ . The fiber spacing was chosen to obtain a precise interlock of the fibers after swelling. The resulting osteochondral scaffolds had a diameter of 6 mm and a height of approximately 8 mm.

### ***Scaffolds Characterization***

Cylindrical plugs of 6 mm in diameter by 8 mm in height were taken as samples for characterization. The constructs were analyzed with an optical microscope (OM) to assess their integrity over time and by scanning electron microscopy (SEM) analysis with a Philips XL 30 ESEM-FEG. Samples were gold sputter coated (Carrington) before SEM analysis.

The porosity of the 3DF cartilage scaffold and of the bone scaffold in its separated components and as a final whole construct was experimentally measured by analyzing the mass and the volume of each structure, as:

$$P = 1 - \frac{M}{V} \cdot \frac{1}{\rho} \quad (1)$$

where  $M$  and  $V$  are the measured mass and volume of the scaffolds components, while  $\rho$  is the specific density of the materials (1.25 g/cm<sup>3</sup> for 1000PEOT70PBT30, 3.15 g/cm<sup>3</sup> for BCP, and assumed to be 1 g/cm<sup>3</sup> for DBM, since the mineral component was extracted). The composition of BCP particles was analyzed by x-ray diffraction (XRD) (Rigaku Miniflex, China) and Fourier Transform Infrared analysis (FTIR) (Spectrum 1000, Perkin Elmer, USA).

For the bone hybrid construct, the weight and volume percentage of BCP included in each scaffold was also measured as the ratio between the BCP particles weight and volume and the weight and volume of the final construct, respectively (table 1).

### ***Mechanical Characterization of the Bone Hybrid Scaffolds***

A DMA instrument (Perkin Elmer 7e) was used to evaluate the bending and compressive dynamic stiffness of the 3D assembled scaffolds of the bone compartment and of the single biomaterials used. In the dynamic bending test, three slabs of 15 mm in length by 5 mm in width by 6 mm in height were used as samples. In the case of the hybrid constructs, only scaffolds from design A were tested in the bending configuration as the intrinsic construction of scaffolds in design B did not allow for their bending characterization. A 3-point bending test was chosen for the characterization. Scaffolds were loaded with a dynamic force varying from 350 mN to 450 mN. A ramp of 5 mN/min at a constant frequency of 1Hz was applied. A lower range of forces was applied with respect to the compressive dynamic test to prevent sample deformation that impinged with the test setting.

In the compressive dynamic test, for each hybrid design and for each single biomaterial used three cylindrical samples of 6 mm in diameter by approximately 6 mm in height were tested. Cylindrical fixtures were chosen to test the specimens and evaluate their behavior as a whole structure along their compression axis, in the “z-direction”. Scaffolds were loaded with a dynamic force varying from 3.5N to 4.5N. A ramp of 50mN/min at a constant frequency of 1Hz was used. In the two test configurations, the dynamic stiffness, or storage modulus  $E'$ , was calculated in the elastic region of the composites. The theoretical modulus as proposed by the Reuss-Voigt model for a composite was also calculated [49, 50]. In this case we assumed the ceramic particles as mainly oriented along the longitudinal direction where compression occurs. The modulus can then be calculated as:

$$E = E_i V_i + E_m V_m \quad (2)$$

Where  $E$  is the modulus of the final construct,  $E_i$  and  $V_i$  are the modulus and the volume fraction of the inclusions (here considered as the BCP particles), while  $E_m$  and  $V_m$  are the modulus and the volume fraction of the polymeric matrix.

The stress and deformation at break were measured with a Zwick Z050 mechanical testing apparatus (Zwick, Germany), in a failure test under compression with a crosshead speed of 1mm/min.

### *Statistical Analysis*

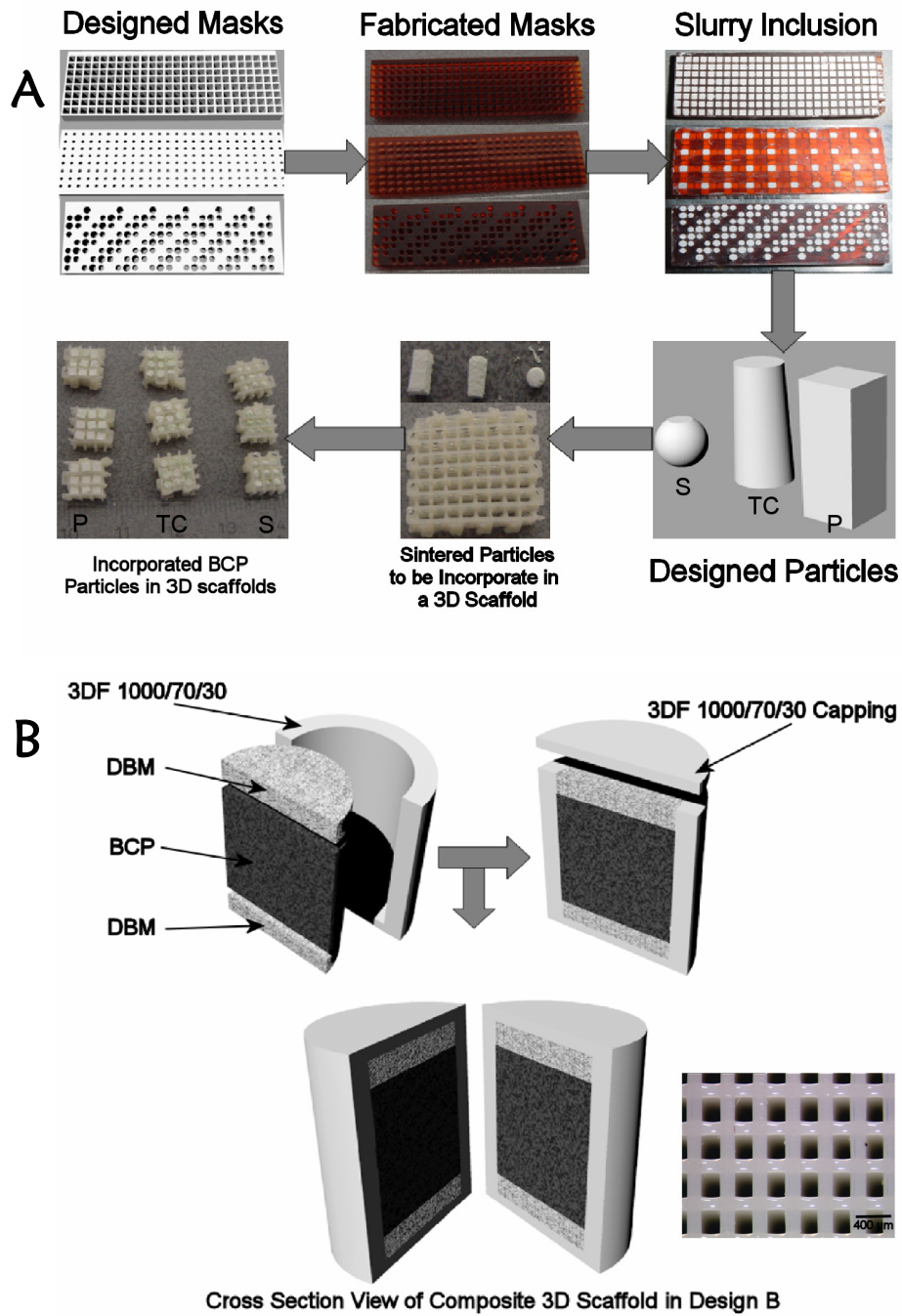
Statistical Analysis was performed using a Student's t-test, where the confidence level was set to 0.05 for statistical significance. Values in this study are reported as mean and standard deviation.

## **Results**

### *Bone Scaffolds Characterization*

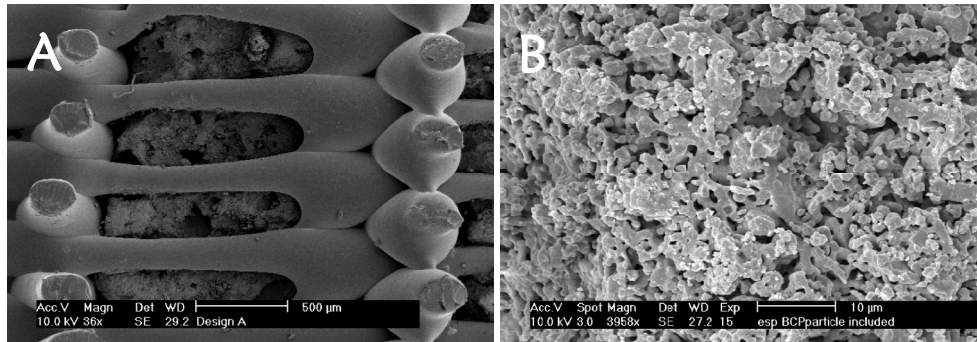
Figure 1 introduces the principles of scaffold assembly for designs A and B for the bone compartment of the osteochondral scaffold. The constructs were macroscopically examined by OM and found to keep their integrity both in a dry and in a wet (immersed in PBS) environment, after fabrication. The characteristic dimensions of 3DFM scaffolds – namely fiber diameter and spacing, and layer thickness – showed to be in good correlation with the parameters set on the device software. No fiber delamination occurred after BCP and DBM assembly. Shrinkage following sintering of BCP particles was shown to vary from  $7 \pm 0.7\%$  to  $18 \pm 1.9\%$ . The composition of the BCP particles was analyzed by XRD and was comprised of 24.6% of tricalcium phosphate (TCP) and 75.4% of hydroxyapatite (HA). FTIR spectra showed the typical pattern of BCP (not shown), as also described elsewhere [43].

Figure 2 shows the cross section of the assembled scaffold and the micro porosity of the BCP particles of a typical scaffold as in design A, analyzed by SEM. Table 1 introduces the weight and volume percentage of BCP included into the 3D PEOT/PBT matrix, depending on the particles geometry. The pillar particles were found to fit better in the pores of the 3DFM scaffolds, resulting in a maximum BCP weight percentage of  $61 \pm 3.15\%$ , which corresponded to a volume fraction of  $27.98 \pm 0.81\%$ . Figure 3 illustrates the cross section of a design B construct analyzed by SEM, where the macro porous structure of the BCP cylinder can be seen after DBM immersion (figure 3a). A particular section of the whole hybrid construct is depicted in figure 3b and shows the scaffold composition after assembling. For both the designs, a final infusion in a DBM gel was performed to ensure the integration of the different components assembled in the scaffolds, as previously described. The final constructs had a pore distribution from  $1.43 \pm 1.25 \mu\text{m}$  to  $1351 \pm 2.4 \mu\text{m}$  and a total porosity of  $79.35 \pm 1.9\%$  in design A, and a pore distribution from  $1.43 \pm 1.25 \mu\text{m}$  to  $531 \pm 237 \mu\text{m}$  and a total porosity of  $88.95 \pm 1.26\%$  in design B. Table 2 summarizes the pore size and porosity of the two presented scaffold designs.



Osteochondral Scaffolds

**Figure 1** – Schematic draw of the scaffold process fabrication for (a) design A and (b) design B. (b) Insert in design B shows an optical micrograph of the porous structure of the 3DF hollow cylinder; scale bar: 400  $\mu\text{m}$ . P = Pillar; TC = Truncated Cone; S = Spherical.



**Figure 2** – SEM micrographs of design A integrated 3D hybrid scaffolds. (a) BCP particles inserted in the pores of a 3DF 1000PEOT70PBT30 matrix. (b) microstructure of ceramic particles sintered at  $T = 1150\text{ }^{\circ}\text{C}$ . Scale bar: (a)  $500\text{ }\mu\text{m}$ ; (b)  $10\text{ }\mu\text{m}$ . Pillar particles are shown here as an exemplification.

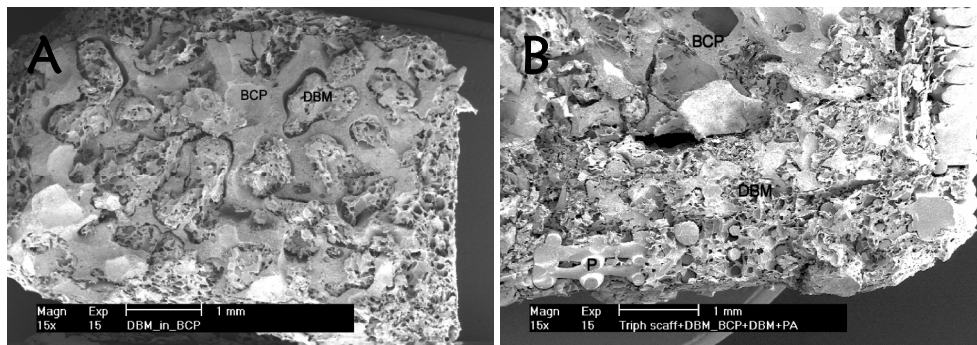


**Figure 3** – SEM micrographs of design B integrated 3D hybrid scaffolds. (a) BCP cylinder infused with DBM after freeze drying. (b) particular section of the whole construct after insertion of the two DBM foamy discs and the infused BCP cylinder in the hollow 3DFM scaffold and final DBM infusion and lyophilization shows the integration of all the components. Scale bar: 1 mm.

### *Osteochondral Scaffolds*

#### Osteochondral Scaffolds

Figure 4 shows the osteochondral constructs with and without the interlocking system. Due to the different swelling properties of the two PEOT/PBT compositions (bone = 1000PEOT70PBT30 – cartilage = 300PEOT55PBT45), instability at the interface of the two compartments may occur (figure 4a). Therefore, an interlocking fibrous system made of intertwined concentric 1000PEOT70PBT30 and 300PEOT55PBT45 fibers was deposited at the interface between the bone and the chondral parts of the construct (figure 4b and 4c). SEM analysis revealed a fiber diameter  $d_1$  of  $170 \pm 15\text{ }\mu\text{m}$ , a fiber spacing  $d_2$  of  $605 \pm 12\text{ }\mu\text{m}$ , and a layer thickness  $d_3$  of  $148 \pm 10\text{ }\mu\text{m}$  for the cartilage compartment scaffolds. This corresponded to a porosity of  $74 \pm 2\%$  and, consequently, to a dynamic stiffness of approximately 13 MPa, as calculated from previous studies [31].



Designed Particles	BCP (weight %)	BCP (volume %)
<b>Irregular</b>	38.32 ± 9.9	11.83 ± 2.5
<b>Sphere</b>	38.24 ± 1.45	14.12 ± 0.37
<b>Truncated cone</b>	46.96 ± 3.66	21.23 ± 0.95
<b>Pillar</b>	61.06 ± 3.15	27.98 ± 0.81

**Table 1** – BCP weight percentage included in the assembled scaffolds depending on particle design.

	Macropore Size (µm)	Micropore Size (µm)	Porosity (%)
<b>Design A</b>			79.35 ± 1.9
3DFM	1351 ± 2.4 (XY) - 228 ± 11 (Z)	-	82 ± 2.7
BCP	357 ± 122	1.43 ± 1.25	66 ± 2.3
DBM Infused	51.6 ± 29.5	-	90.06 ± 2.03
<b>Design B</b>			88.95 ± 1.26
3DFM	435 ± 3 (XY) - 148 ± 10 (Z)	-	78 ± 3
BCP	531 ± 237	1.43 ± 1.25	90 ± 1.8
DBM Discs	94.3 ± 19.6	-	91.53 ± 0.59
DBM Infused	51.6 ± 29.5	-	96.27 ± 0.77

**Table 2** – Pore size and porosity distribution of the single components and of the final scaffold constructs.

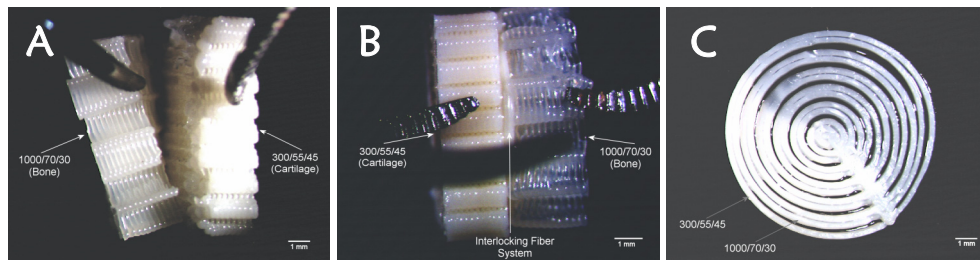


**Figure 4** – Optical microscopy images of the osteochondral 3D scaffolds without (a) and with (b) the interlocking concentric fiber system (c) under forceps solicitation. Scale bar: 1 mm.

### *Mechanical Characterization of the Bone 3D Scaffolds*

The 3D hybrid scaffolds fabricated for the bone compartment of the osteochondral construct were mechanically characterized by measuring the bending and compressive storage modulus (or dynamic stiffness,  $E'$ ) and the breaking stress and strain. In design A, the bending and compressive dynamic stiffness of the 3DFM constructs with and without the inclusion of BCP particles are shown in figures 5 and 6 respectively. In the bending test, the bending dynamic stiffness was  $0.134 \pm 0.035$  MPa for the bare 3DFM scaffold. When the designed BCP particles were press-fitted into the pores of the 3DFM scaffolds the bending test significantly increased to  $0.94 \pm 0.15$  MPa for irregular particles, to  $3.72 \pm 0.03$  MPa for spherical particles, to  $8.86 \pm 0.65$  MPa for truncated cones, and to  $18.99 \pm 0.14$  MPa for pillar particles ( $p < 0.05$ ). In the compression test (figure 6a), the compressive storage modulus  $E'$  significantly increased from  $0.692 \pm 0.16$  MPa for 3DFM bare matrices to  $0.935 \pm 0.165$  MPa for irregular particles, to  $17.38 \pm 5.38$  MPa for spherical particles, to  $26.2 \pm 4.76$  MPa for pillar particles, to  $37.96 \pm 6.14$  MPa for truncated conical particles. In the case of design B (figure 6b), the compressive storage modulus of the hollow 3DFM cylinder was measured as  $1.1 \pm 0.34$  MPa, while the stiffness of the whole construct was measured as  $7.8 \pm 1.68$  MPa ( $p < 0.05$ ). DBM had a bending modulus of  $0.132 \pm 0.034$  MPa and a compressive modulus of  $0.335 \pm 0.04$  MPa ( $p < 0.05$ ). BCP had a bending modulus of  $39.28 \pm 1.29$  MPa and a compressive modulus of  $47.36 \pm 5.34$  MPa ( $p < 0.05$ ). In case of the hybrid scaffolds in design A, the elastic moduli of the different construct configurations were also calculated with the theoretical model proposed by Voigt for composites and were found to be in the same range as the bending measured values, but not comparable to the compression ones (table 3). The bending ( $r^2 = 0.96$ ) and the Reuss-Voigt ( $r^2 = 0.99$ ) moduli seemed to increase with a power law, with increasing the BCP volume fraction, as shown in figure 7. However, this was not the case for the compression modulus ( $r^2 = 0.87$ ). The stress at break was also dependent on the design of the hybrid scaffolds. Stress changed from  $0.52 \pm 0.14$  MPa for irregular particles to  $14.01 \pm 1.19$  MPa for pillar particles. The strain varied from  $9.92 \pm 1.78\%$  to  $33.74 \pm 0.49\%$ , but did not appear to depend on the scaffold design, as presented in table 4. DBM and 3DFM alone did not break under compression.

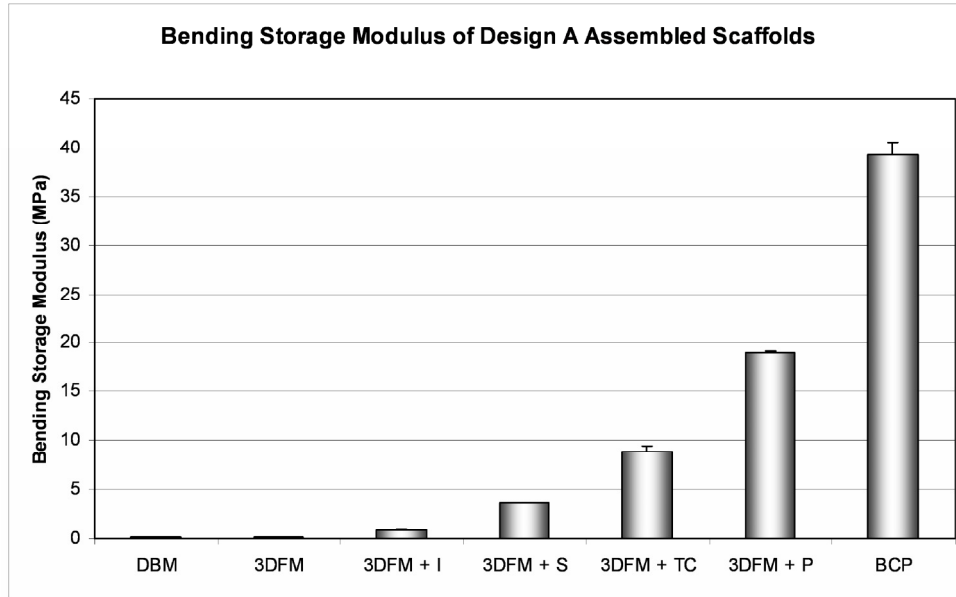


**Figure 5** – Influence of the scaffold design on the bending storage modulus in design A. The dynamic stiffness of the single components comprising the hybrid scaffold was also measured for comparison. All groups were significantly different from each other ( $p < 0.05$ ). Particle shape legend: I = Irregular; S = Spherical; P = Pillar; TC = Truncated Cone.

	$E'_{\text{bend exp}}$ (MPa)	$E'_{\text{comp exp}}$ (Mpa)	$E'_{\text{theor}}$ (MPa)
<b>Sphere</b>	$3.72 \pm 0.03$	$17.38 \pm 5.38$	6.99
<b>Truncated cone</b>	$8.86 \pm 0.65$	$37.97 \pm 6.14$	10.17
<b>Pillar</b>	$18.99 \pm 0.14$	$26.2 \pm 4.76$	13.19

**Table 3** – Comparison between the experimental and the theoretical (Reuss-Voigt model) values of the storage moduli of 3D scaffolds with custom-designed assembled BCP particles.

Osteochondral Scaffolds

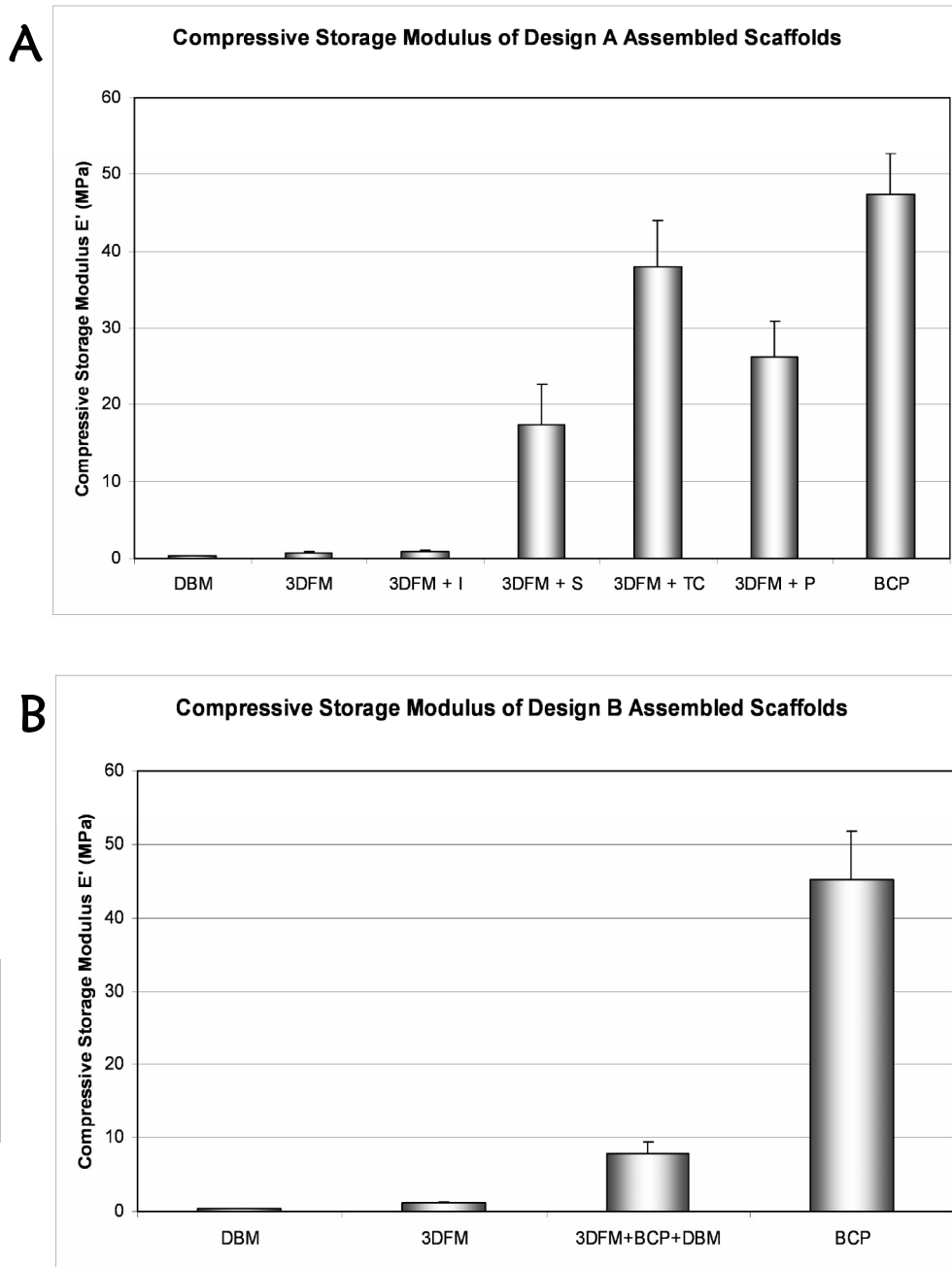


**Figure 6** – Influence of the scaffold design on the compressive dynamic stiffness in design A and B. The storage modulus of the single components forming the hybrid scaffold was also determined for comparison. All groups were significantly different from each other ( $p < 0.05$ ). Particle shape legend: I = Irregular; S = Spherical; P = Pillar; TC = Truncated Cone.

## Influence of BCP Volume Fraction on 3D Assembled Scaffolds' Stiffness

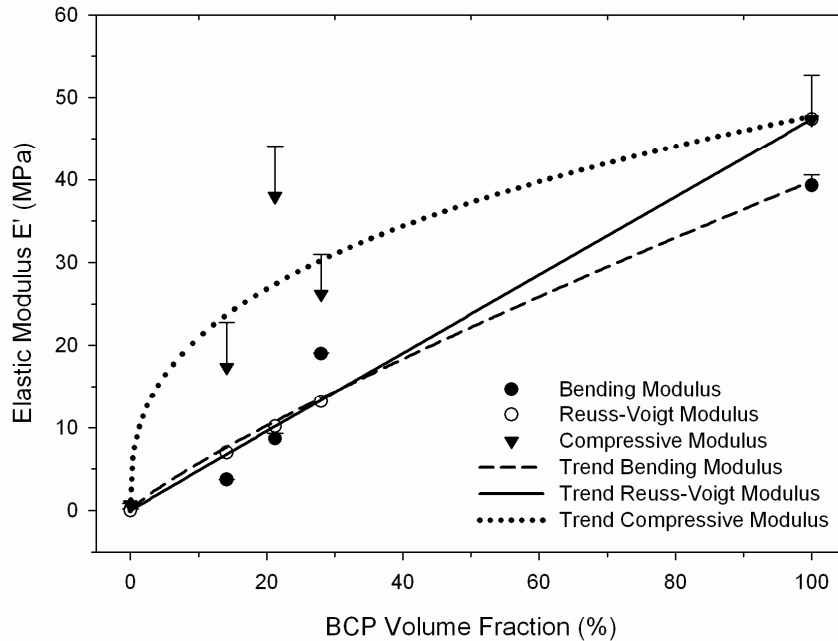


**Figure 7** – Influence of the BCP volume fraction on the bending, compressive, and Reuss-Voigt moduli. Bending modulus:  $r^2 = 0.96$ ; Reuss-Voigt modulus:  $r^2 = 0.99$ ; compressive modulus:  $r^2 = 0.87$ .

## Discussion

Osteochondral 3D scaffolds comprising a cartilage 3DF compartment and a bone 3D assembled compartment were successfully fabricated and showed to possess the mechanical flexibility of polymers and DBMs, and the strength of ceramics. Furthermore, the rapid prototyping approach used in the design allowed the creation of scaffolds with a completely interconnected and accessible pore network. Different tri-phasic 3D hybrid scaffolds were considered and characterized in terms of their structural and mechanical properties for the bone compartment. Whereas ceramics and DBMs have different mechanical drawbacks, the former being too brittle and the latter too flexible to be used in a high load bearing site, the hybrid composite of these two bone graft substitutes with a polymeric matrix was shown to have a variable stiffness depending on the ceramic particles and on the overall construct design. Since ceramics are typically characterized by their behavior at break, the breaking stress and strain of the composite scaffolds were also measured. The DBM foam discs and the final DBM infusion of the constructs functioned as energy “cushions” during compression, resulting in an increase in the breaking strain and a

variable stress which was most likely due to the corresponding increase in BCP content. Strain didn't seem to depend on scaffold design and showed approximately a 3-fold increase with respect to BCP scaffolds alone, while stress varied from a 14-fold decrease for irregular particles to a 2-fold increase for pillar particles as compared to BCP scaffolds alone (table 4). The variable increase of the stiffness and of the breaking stress might be linked to the different packing degree of the ceramic in the polymeric matrix, resulting in a progressively higher coupling of the two materials. The increasing fit with the polymer, thus, resulted in a more efficient strengthening of the construct, increasing the overall stiffness and the stress at break. At the same time, the presence of DBM and of the polymer introduced a higher flexibility in the constructs due to their intrinsic mechanical properties, causing an increase in the deformation at break.

	$\sigma_{\text{break}}$ [MPa]	$\epsilon_{\text{break}}$ [%]
Irregular	0.52 ± 0.14	33.5 ± 0.14
Sphere	1.8 ± 0.83	33.41 ± 0.05
Truncated Cones	4.8 ± 0.86	33.4 ± 0.02
Pillars	14.01 ± 1.19	33.74 ± 0.49
Design B	2.13 ± 0.93	26.38 ± 5.1
BCP	7.65 ± 1.25	9.92 ± 1.78
Cancellous Bone (*)	0.15 - 10.2	-
Cortical Bone (*)	90 - 193	-

**Table 4** – Stress and strain at break for design A (influence of particle design), design B, and BCP. (\*) Strength values for bone are taken from Athanasiou *et al.* [3].

With increasing BCP weight and/or volume percentage in the hybrid 3D scaffolds, the bending modulus increased accordingly. This can be expected as, with higher BCP content, the scaffolds are more densely packed, resulting in an increase of the stiffness given that BCP is the stiffest component in the assembled construct (figure 5). A similar trend was seen for the compressive stiffness, although the highest value was measured when truncated conical ceramic particles were press-fitted in the polymeric matrix (figure 6). The higher performance of these particles within the matrix, despite a non-correspondent higher weight percentage (table 1), might be due to a higher localization of the surface stresses in a cylindrical section as compared to the rectangular one characteristic of the pillar particles. The higher

localization is originated by a “confinement” or “focusing” effect of the ceramic particle in the polymeric matrix, which is dependent on the particle section and results in a stiffer response. This is theoretically quantified as a 10-20% increase for a cylindrical section as compared to a cubical one [51, 52] and falls within the variation experimentally measured for truncated conical and pillar particles. The experimental measured values of the bending stiffness were also in the same range of the calculated stiffness values from the Reuss-Voigt model. This might suggest that the assembly of the different biomaterials proposed here can be considered close to a composite when subjected to a flexion load, although it cannot be strictly defined as such since this is typically formed by chemically bonded materials. It is clear that the hybrid scaffolds do not mechanically respond as real composites when their mechanical behavior in compression is considered. In this case the theoretical and the experimental values do not follow the same power law. As previously explained, it might be that the different stress localization on ceramic particles with different shapes is predominant in compression as compared to a volumetric increase of BCP in the assembly.

As reviewed by Athanasiou *et al.* [3], cancellous bone has a bending modulus varying between 49 MPa and 336 MPa, and a compressive modulus varying between 12 MPa and 900 MPa. Cortical bone has a bending modulus ranging from 5.44 GPa to 15.8 GPa, and a compressive modulus ranging from 4.9 GPa to 27.6 GPa (figures 4b and 5c). The variations are related to different bone sources, different locations within the sources, and to different mechanical testing conditions. Cancellous bone has a strength varying between 0.15 MPa and 10.2 MPa, while cortical bone has a strength ranging from 90 MPa to 193 MPa. If the stiffness and stress/deformation at break of the different hybrid 3D assembled scaffolds are compared to the stiffness of cortical and cancellous bone, constructs with pillar or conical-cylindrical ceramic particles seems to better approach the mechanical behavior of cancellous bone. Cortical bone still has a much greater stiffness and strength as compared to the scaffolds here presented. Therefore, if mimicking the mechanical properties of the tissue to regenerate still holds as a requirement for scaffold fabrication in the specific case of cortical bone, it seems necessary to look for better performing biomaterials.

The osteochondral 3D scaffolds proposed here seem to be an appealing solution, as they combine cartilage and bone compartments mechanically matching the natural tissues to be regenerated with biomaterials that singularly showed to promote cartilage and bone tissue formation. The advantage of using a 3DFM polymeric matrix in the bony part of the construct is that it is possible to directly fabricate the osteochondral polymer structure of the scaffold by 3DF. Specifically, the chondral part of the scaffold can be fabricated on top of the bone hybrid scaffold with 300PEOT55PBT45, a PEOT/PBT composition that has been considered for cartilage tissue engineering [13, 32, 53]. Since the two PEOT/PBT compositions (bone = 1000PEOT70PBT30 – cartilage = 300PEOT55PBT45) have different swelling properties, an interlocking fibrous system made of intertwined concentric 1000PEOT70PBT30 and 300PEOT55PBT45 fibers was deposited at the interface between the bone and the chondral parts of the construct. This system also had the function to mimic the tidemark in the osteochondral natural architecture, as

1000PEOT70PBT30 calcifies and interconnects with the bony part. As shown qualitatively in figure 4, when the osteochondral scaffold was solicited simply with forceps, the presence of the interlocking system prevented the delamination of the two parts of the scaffold even after one month in culture medium at physiological conditions. Preliminary experiments showed that these osteochondral scaffolds are able to support cell attachment and proliferation (data not shown). Still, the synergistic effect of the integrated biomaterials remains to be demonstrated. Further investigations will focus on the biological effectiveness of combining polymers with ceramics and DBMs for bone and osteochondral regeneration. The stability of such a construct for the repair of osteochondral defects *in vitro* and *in vivo* will be also the object of further studies.

## Conclusions

A novel approach to make tri-phasic scaffolds for osteochondral tissue engineering was introduced based on biomaterials assembly. Hybrid three-dimensional scaffolds made of polymers, ceramics, and DBMs by integrating different scaffolds fabrication technologies were fabricated and found to couple the flexibility of polymers and DBMs with the mechanical strength of ceramics, at the same time maintaining a completely interconnected pore network. The mechanical properties of these constructs could be modulated depending on the assembly design and matched both the cartilage and the cancellous bone stiffness and strength. Given that the design rationale focused on using biomaterials that singularly found applications in bone and cartilage tissue engineering, the optimization of the hybrid constructs in this study makes these scaffolds promising candidates for osteochondral regeneration.

## Acknowledgements

This project was funded by the European Community project Intelliscaf GSRD\_2002\_00697. Critical discussion with Dr. H. Yuan on ceramics was highly appreciated. We are also grateful to Dr. T.B.F. Woodfield, L. Lelli, and G. Eccher for their significant input in reviewing the manuscript.

## References:

- [1] Guldberg VM. Natural history of autografts and allografts. Bone Implant Grafting, Older J editor. London: Springer 1992:9-12.
- [2] Hunziker EB. Articular cartilage repair: basic science and clinical progress. A review of the current status and prospects. Osteoarthritis and Cartilage 2001;10:432-463.
- [3] Athanasiou KA, Zhu C, Lanctot DR, Agrawal CM, Wang X. Fundamentals of biomechanics in tissue engineering of bone. Tissue Eng 2000;6(4):361-81.
- [4] Laurencin CT, Ambrosio AM, Borden MD, Cooper JA, Jr. Tissue engineering: orthopedic applications. Annu Rev Biomed Eng 1999;1:19-46.
- [5] Martin I, Miot S, Barbero A, Jakob M, Wendt D. Osteochondral tissue engineering. J Biomech 2006.



- [6] Shao XX, Hutmacher DW, Ho ST, Goh JC, Lee EH. Evaluation of a hybrid scaffold/cell construct in repair of high-load-bearing osteochondral defects in rabbits. *Biomaterials* 2006;27(7):1071-80.
- [7] Shao X, Goh JC, Hutmacher DW, Lee EH, Zigang G. Repair of large articular osteochondral defects using hybrid scaffolds and bone marrow-derived mesenchymal stem cells in a rabbit model. *Tissue Eng* 2006;12(6):1539-51.
- [8] Barry JJ, Gidda HS, Scotchford CA, Howdle SM. Porous methacrylate scaffolds: supercritical fluid fabrication and in vitro chondrocyte responses. *Biomaterials* 2004;25(17):3559-68.
- [9] Demartean O, Wendt D, Braccini A, Jakob M, Schafer D, Heberer M, Martin I. Dynamic compression of cartilage constructs engineered from expanded human articular chondrocytes. *Biochem Biophys Res Commun* 2003;310(2):580-8.
- [10] Freed LE, Marquis JC, Nohria A, Emmanuel J, Mikos AG, Langer R. Neocartilage formation in vitro and in vivo using cells cultured on synthetic biodegradable polymers. *J Biomed Mater Res* 1993;27(1):11-23.
- [11] Vunjak-Novakovic G, Obradovic B, Martin I, Bursac PM, Langer R, Freed LE. Dynamic cell seeding of polymer scaffolds for cartilage tissue engineering. *Biotechnol Prog* 1998;14(2):193-202.
- [12] Huang Q, Goh JC, Hutmacher DW, Lee EH. In vivo mesenchymal cell recruitment by a scaffold loaded with transforming growth factor beta1 and the potential for in situ chondrogenesis. *Tissue Eng* 2002;8(3):469-82.
- [13] Malda J, Woodfield TB, van der Vloodt F, Wilson C, Martens DE, Tramper J, van Blitterswijk CA, Riesle J. The effect of PEGT/PBT scaffold architecture on the composition of tissue engineered cartilage. *Biomaterials* 2005;26(1):63-72.
- [14] LeGeros RZ, Lin S, Rohanizadeh R, Mijares D, LeGeros JP. Biphasic calcium phosphate bioceramics: preparation, properties and applications. *J Mater Sci Mater Med* 2003;14(3):201-9.
- [15] Daculsi G, Laboux O, Malard O, Weiss P. Current state of the art of biphasic calcium phosphate bioceramics. *J Mater Sci Mater Med* 2003;14(3):195-200.
- [16] Yuan H, Yang Z, Li Y, Zhang X, De Bruijn JD, De Groot K. Osteoinduction by calcium phosphate biomaterials. *J Mater Sci Mater Med* 1998;9(12):723-6.
- [17] Wilson CE, Krut MC, de Bruijn JD, van Blitterswijk CA, Oner FC, Verbout AJ, Dhert WJ. A new in vivo screening model for posterior spinal bone formation: comparison of ten calcium phosphate ceramic material treatments. *Biomaterials* 2006;27(3):302-14.
- [18] Chakkalakal DA, Strates BS, Garvin KL, Novak JR, Fritz ED, Mollner TJ, McGuire MH. Demineralized bone matrix as a biological scaffold for bone repair. *Tissue Eng* 2001;7(2):161-77.
- [19] Mauney JR, Jaquiere C, Volloch V, Heberer M, Martin I, Kaplan DL. In vitro and in vivo evaluation of differentially demineralized cancellous bone scaffolds combined with human bone marrow stromal cells for tissue engineering. *Biomaterials* 2005;26(16):3173-85.
- [20] Peterson B, Whang PG, Iglesias R, Wang JC, Lieberman JR. Osteoinductivity of commercially available demineralized bone matrix. Preparations in a spine fusion model. *J Bone Joint Surg Am* 2004;86-A(10):2243-50.

- [21] Ozturk A, Yetkin H, Memis L, Cila E, Bolukbasi S, Gemalmaz C. Demineralized bone matrix and hydroxyapatite/tri-calcium phosphate mixture for bone healing in rats. *Int Orthop* 2006.
- [22] Kaito T, Myoui A, Takaoka K, Saito N, Nishikawa M, Tamai N, Ohgushi H, Yoshikawa H. Potentiation of the activity of bone morphogenetic protein-2 in bone regeneration by a PLA-PEG/hydroxyapatite composite. *Biomaterials* 2005;26(1):73-9.
- [23] Kay S, Thapa A, Haberstroh KM, Webster TJ. Nanostructured polymer/nanophase ceramic composites enhance osteoblast and chondrocyte adhesion. *Tissue Eng* 2002;8(5):753-61.
- [24] Kreklau B, Sittinger M, Mensing MB, Voigt C, Berger G, Burmester GR, Rahmanzadeh R, Gross U. Tissue engineering of biphasic joint cartilage transplants. *Biomaterials* 1999;20(18):1743-9.
- [25] Schek RM, Taboas JM, Hollister SJ, Krebsbach PH. Tissue engineering osteochondral implants for temporomandibular joint repair. *Orthod Craniofac Res* 2005;8(4):313-9.
- [26] Sherwood JK, Riley SL, Palazzolo R, Brown SC, Monkhouse DC, Coates M, Griffith LG, Landeen LK, Ratcliffe A. A three-dimensional osteochondral composite scaffold for articular cartilage repair. *Biomaterials* 2002;23(24):4739-51.
- [27] Zein I, Hutmacher DW, Tan KC, Teoh SH. Fused deposition modeling of novel scaffold architectures for tissue engineering applications. *Biomaterials* 2002;23(4):1169-85.
- [28] Hollister SJ. Porous scaffold design for tissue engineering. *Nat Mater* 2005;4(7):518-24.
- [29] Taboas JM, Maddox RD, Krebsbach PH, Hollister SJ. Indirect solid free form fabrication of local and global porous, biomimetic and composite 3D polymer-ceramic scaffolds. *Biomaterials* 2003;24(1):181-94.
- [30] Moroni L, de Wijn JR, van Blitterswijk CA. 3D fiber-deposited scaffolds for tissue engineering: Influence of pores geometry and architecture on dynamic mechanical properties. *Biomaterials* 2006;27:974-985.
- [31] Moroni L, Poort G, Van Keulen F, de Wijn JR, van Blitterswijk CA. Dynamic mechanical properties of 3D fiber-deposited PEOT/PBT scaffolds: An experimental and numerical analysis. *J Biomed Mater Res A* 2006(78):605-614.
- [32] Woodfield TB, Malda J, de Wijn J, Peters F, Riesle J, van Blitterswijk CA. Design of porous scaffolds for cartilage tissue engineering using a three-dimensional fiber-deposition technique. *Biomaterials* 2004;25(18):4149-61.
- [33] Deschamps AA, Claase MB, Sleijsler WJ, de Bruijn JD, Grijpma DW, Feijen J. Design of segmented poly(ether ester) materials and structures for the tissue engineering of bone. *J Control Release* 2002;78(1-3):175-86.
- [34] Bezemer JM, Grijpma DW, Dijkstra PJ, van Blitterswijk CA, Feijen J. A controlled release system for proteins based on poly(ether ester) block-copolymers: polymer network characterization. *J Control Release* 1999;62(3):393-405.
- [35] Moroni L, de Wijn JR, van Blitterswijk CA. Three-dimensional fiber-deposited PEOT/PBT copolymer scaffolds for tissue engineering: Influence of porosity, molecular network mesh size, and swelling in aqueous media on dynamic mechanical properties. *J Biomed Mater Res A* 2005;75:957-965.
- [36] Bakker D, van Blitterswijk CA, Hesselink SC, Grote JJ. Effect of implantation site on phagocyte/polymer interaction and fibrous capsule formation. *Biomaterials* 1988;9(1):14-23.

- [37] Beumer GJ, van Blitterswijk CA, Ponec M. Degradative behaviour of polymeric matrices in (sub)dermal and muscle tissue of the rat: a quantitative study. *Biomaterials* 1994;15(7):551-9.
- [38] Beumer GJ, van Blitterswijk CA, Ponec M. Biocompatibility of a biodegradable matrix used as a skin substitute: an in vivo evaluation. *J Biomed Mater Res* 1994;28(5):545-52.
- [39] Bulstra SK, Geesink RG, Bakker D, Bulstra TH, Bouwmeester SJ, van der Linden AJ. Femoral canal occlusion in total hip replacement using a resorbable and flexible cement restrictor. *J Bone Joint Surg Br* 1996;78(6):892-8.
- [40] Mensik I, Lamme EN, Riesle J, Brychta P. Effectiveness and Safety of the PEGT/PBT Copolymer Scaffold as Dermal Substitute in Scar Reconstruction Wounds (Feasibility Trial). *Cell Tissue Bank* 2002;3(4):245-53.
- [41] Rice JM, Hunt JA, Gallagher JA. Quantitative evaluation of the biocompatible and osteogenic properties of a range of biphasic calcium phosphate (BCP) granules using primary cultures of human osteoblasts and monocytes. *Calcif Tissue Int* 2003;72(6):726-36.
- [42] Habibovic P, Sees TM, van den Doel MA, van Blitterswijk CA, de Groot K. Osteoinduction by biomaterials--physicochemical and structural influences. *J Biomed Mater Res A* 2006;77(4):747-62.
- [43] Habibovic P, Yuan H, van der Valk CM, Meijer G, van Blitterswijk CA, de Groot K. 3D microenvironment as essential element for osteoinduction by biomaterials. *Biomaterials* 2005;26(17):3565-75.
- [44] Habibovic P, Yuan H, van den Doel M, Sees TM, van Blitterswijk CA, de Groot K. Relevance of osteoinductive biomaterials in critical-sized orthotopic defect. *J Orthop Res* 2006;24(5):867-76.
- [45] Mastrogiacomo M, Scaglione S, Martinetti R, Dolcini L, Beltrame F, Cancedda R, Quarto R. Role of scaffold internal structure on in vivo bone formation in macroporous calcium phosphate bioceramics. *Biomaterials* 2006;27(17):3230-7.
- [46] Urist MR. Bone: formation by autoinduction. *Science* 1965;150(698):893-9.
- [47] Reddi AH. Cell biology and biochemistry of endochondral bone development. *Coll Relat Res* 1981;1(2):209-26.
- [48] Urist MR, DeLange RJ, Finerman GA. Bone cell differentiation and growth factors. *Science* 1983;220(4598):680-6.
- [49] Voigt W. *Lehrbuch der Krystallphysik*. Leipzig, Germany: B.G. Teubner 1910.
- [50] Reuss A. *Zeitschrift für Angewandte Mathematik und Mechanik*. 1929;9:49-58.
- [51] Gutierrez AP, Canovas MF. The modulus of elasticity of high performance concrete. *Materials and Structure* 1995;28:559-568.
- [52] Gere JM, Timoshenko SP. *Mechanics of Materials*. Third Edition, PWS-KENT Publishing Company, Boston 1990.
- [53] Woodfield TB, Van Blitterswijk CA, De Wijn J, Sims TJ, Hollander AP, Riesle J. Polymer scaffolds fabricated with pore-size gradients as a model for studying the zonal organization within tissue-engineered cartilage constructs. *Tissue Eng* 2005;11(9-10):1297-311.



## General Discussion

If you have an apple and I have an apple, and we exchange apples, we both still only have one apple. But if you have an idea and I have an idea, and we exchange ideas, we each now have two ideas

George Bernard Shaw (1856 – 1950)

# Chapter 11

## General Discussion

The field of tissue engineering continuously grew since its creation in the early eighties and received a boost in the past decade that led to the commercialization of “first generation” products ranging from artificial skin to bone and cartilage. The attempts to regenerate other tissues showed promising achievements, such as artery regeneration in congenitally deformed children, nerve regeneration after trauma, or tissue engineered bladder replacement, just to mention a few. Yet, there is a need to improve the long-term functionality (years vs. month) and the reproducibility of the final outcomes for engineered tissue or regenerative medicine therapies. The word engineering tracks back its origin to the Latin word “ingenium”, which literally means “ingenuity” or “creativity”. This is at the base of the regenerative medicine field [1] and the work present in the recent literature – as pointed out in chapter 1 – and in this thesis support the new trend emerging in tissue engineering, for which integration of different technological platforms is leading to a new generation of artificial tissue prototypes. Here, we have proposed the creation of smart 3D scaffolds by combining and integrating different fabrication and material processing techniques, in some cases taking advantage of usually undesired phenomena like low resolution (chapter 6) or polymeric blend viscous encapsulation during their molten state (chapter 8). Among the multitude of choices in biomaterials, material processing, and scaffold fabrication techniques, a family of thermoplastic copolymers (PEOT/PBT) was chosen for their tailorable properties and processed with an extrusion-based rapid prototyping technique (3DF). These copolymers are typically characterized by three parameters. When using an *a/b/c* acronym, *a* refers to the molecular weight of the starting PEG blocks used in the copolymerization reaction with PBT, while *b* and *c* are the weight ratios of the resulting PEOT and PBT domains. The main results presented in this thesis are hereafter discussed following the general aims enlightened in the introduction.

### *Characterization of the Mechanical and Physicochemical Properties of 3D Scaffolds*

One of the mainstays in tissue engineering is that scaffolds should mimic the biomechanical properties of the tissues to be replaced. Ideally, the scaffolds should be made of a biodegradable material, whose degradation rate is coupled to tissue formation dynamics. In this way the mechanical support of the scaffold would be progressively overtaken by the newly formed tissue. To achieve biomechanically mimicking scaffolds with respect to cartilage, the viscoelastic behavior of the chosen polymers was first studied by dynamic mechanical analysis. Scaffolds were immersed in a wet environment matching the rheological properties of the synovium fluid. Scaffold porosity, pore size, and pore shape were varied to assess how these

parameters can control and modulate the mechanical properties of 3D scaffolds (chapters 2, 3, and 4). With increasing porosity and pore size, a decrease in the elastic response and an increase in the plastic response of the scaffolds were detected as expected. The same behavior also occurred when the pore shape was changed by decreasing the fiber deposition angle between two successive layers. This allowed creating a multidimensional matrix of structural and physico-chemical parameters which permits the selection of conditions to fabricate a scaffold with viscoelastic properties matching a specific tissue (chapter 3). Such a “decisional” system was also evaluated numerically, leading to the validation of a mathematical model that can be used to predict 3DF scaffolds dynamic stiffness, as discussed in chapter 4. Since the model depends on the dynamic stiffness of the solid material  $E'_0$  and on a specific scaffold coefficient  $\alpha$  characteristic of each architecture and copolymer composition, it might be possible to extend it to other thermoplastic polymers provided their  $E'_0$  and  $\alpha$  are known. Although 3D scaffolds manufactured with conventional fabrication techniques can be successfully made to match the mechanical properties of a desired tissue [2, 3], these properties are poorly correlated with the fabrication parameters [2, 4]. Furthermore, conventional scaffolds shed concerns on their complete pore network interconnectivity and tortuosity, which might hamper nutrient diffusion and cell migration in the center of constructs with a clinically relevant size [5, 6] as previously explained. In these chapters, it was demonstrated how rapid prototyped 3D scaffolds with mechanical properties mimicking a specific tissue are obtained in good correlation with the fabrication parameters, at the same time controlling the pore network interconnectivity and tortuosity. The scaffolds' viscoelastic properties were found to be highly dependent on the structural porosity, in agreement with the model theorized by Gibson *et al.* [7] and experimentally assessed by Woesz *et al.* [8] for cellular solids. In the model proposed here, however, the dynamic stiffness and the porosity of the scaffolds correlated better with an exponential fit than with a power scale as for cellular solids. This might be related to the dynamic analysis performed to mechanically characterize these structures, in combination with the presence of the fluid phase that is pumped in and out of the highly interconnected pore network of the scaffolds. An alternative appealing approach to modulate the mechanical properties of 3D scaffolds consists in applying the homogenization theory to solid free-form fabrication (SFF) [9, 10]. In this way, it is possible to calculate an optimal pore unit to maximize a set of desired properties. The optimal pore unit can be periodically repeated or organized together with other optimal pore units specific for other properties to achieve a hierarchical 3D structure during the scaffold fabrication process. This strategy has been successfully applied in the fabrication of scaffolds for bone tissue engineering, showing promising results [11, 12].

### ***Importance of Mimicking a Tissue Biomechanical Behavior***

A utilization of the prediction tool introduced in chapter 4 is shown in chapter 5 and adopted to study how to optimize a 3D scaffold structure for cartilage regeneration. Scaffolds with similar architecture – resulting in similar starting mechanical properties – but different physicochemical behavior (300/55/45 and

1000/70/30) were compared to a 3D scaffold with matching dynamic stiffness and physicochemical properties (1000/70/30) with respect to bovine articular cartilage. After one month of culture, cartilage formation was significantly higher in the matching scaffold than in the non-matching scaffolds. Interestingly, this finding was not strictly related to the matching or non-matching dynamic stiffness, but to the architectural configuration of the scaffolds. It was the lower pore volume and porosity of the structure that better entrapped cells resulting in a higher seeding efficiency and ECM formation in the matching scaffold. This was coupled to physicochemical properties that contributed to maintain the original rounded morphology of chondrocytes, whereas 300/55/45 supported a spread morphology having a higher surface energy. Several studies have focused on how to optimize culture conditions in conventional scaffolds and attained the regeneration of functional tissue engineered articular cartilage [13-19]. In these cases, cells derived from immature origin were used. The much higher proliferation capacity that characterizes these cells as compared to adult chondrocytes might be responsible for the favorable response even in critical size scaffolds. When a more mature cell population was used in foams or meshes, limitations in cartilage formation at the center of the constructs occurred [5, 6, 20]. This might be related to a different capacity of adult cells to attach and migrate in the middle of the construct associated with a lower nutrient flow characteristic of conventional scaffolds. Therefore, the possibility to use a more open and interconnected structure like a rapid prototyped scaffold that allows a better nutrient perfusion and cell migration seems to be ideal as also supported by other recent studies [3, 20-23]. Furthermore, the matching 1000/70/30 3D scaffold showed comparable degradation and tissue formation rates. These findings indicate that the optimization of the scaffold structure and physicochemical properties associated with low pore volume and porosity might lead to the tissue engineering ideal, where mature tissue grows and replaces the synthetic scaffold with the same dynamics. The fact that the particular scaffold structure displaying low pore volume and porosity also had a dynamic stiffness matching articular cartilage makes of 1000PEOT70PBT30 an appealing candidate to be further investigated when implanted in load bearing sites. Some concerns, however, might rise due to the poor handling properties of this PEOT/PBT composition when hydrated after few weeks in culture. It might be that, despite the encouraging results of the *in vitro* dynamical test, the structure will fail under the much higher stresses applied in an anatomical location during exercise.

### ***Relevance of Anatomically Shaped Scaffolds***

One of the advantages of rapid prototyping techniques as 3D scaffolds fabrication methods is to create anatomically shaped structures from datasets of patients. The data can be derived from CT and/or MRI scans of a specific anatomical part of the body to regenerate. An increasing amount of studies has been focusing on tissue regeneration on anatomical supports [24-28] with interesting results, since the landmark report of Cao *et al* [29]. Apart from the obvious benefit of regaining the original shape of the tissue or organ to repair, it has not been investigated so far whether anatomically shaped scaffolds might play a role in the dynamics of tissue

formation as compared to other simpler but yet functional designs. In this respect, a tracheal model was studied in chapter 6. The trachea with its complicated geometry was chosen to challenge the limited resolution capacity of 3DF. When compared to cylindrical and toroidal tubes, anatomically shaped scaffolds supported fewer cells and a higher production of ECM, as characterized by DNA and GAG assay respectively. Unexpectedly, with increasing complexity of the scaffold geometry the limitations of the rapid prototyping technique contributed to the improvement of cartilage formation. This was due to the significant formation of plastically drawn thin fibers during scaffold manufacturing when the nozzle moved from the end-point of a layer to the start-point of the successive layer. These fibers showed to sustain a rounded morphology of the seeded and attached chondrocytes, which might have resulted in the higher amount of ECM formed and in the higher degree of cell differentiation. Tracheal segment reconstruction has been a fervent field of tissue engineering [30-38], due to the possible complications of the current clinical techniques such as stenosis and/or infection. Only few of these appear to have successfully regenerated a functional part [31, 37, 38]. Trachea is a hierarchical tissue consisting of cartilage and mucosa. The accomplishment of a tissue engineered trachea is strongly related to the degree of epithelialization [31, 37]. A poor epithelialization might cause stenosis of the construct and the collapse of the implant. In this study, epithelial cells were not co-cultured with chondrocytes. Therefore, no conclusion can be drawn on the functionality of the engineered cartilage tracheal constructs discussed in this chapter. Still, from these results it seems that not only the scaffold structure, but also the scaffold design is determinant for tissue formation.

#### *Influence of Fiber Dimensions and Texture on Cell Faith and on Release of Incorporated Compounds*

As a logical consequence of the particularly interesting findings of chapter 6 related to the effect of thin fibers on tissue formation, the influence of fiber diameter and texture on cell morphology and proliferation was analyzed. Another novel scaffold fabrication technique – electrospinning (ESP) – was used for this purpose, since it allows the creation of micro- and nano-fibers with different surface topology [39]. These fibers are in the same scale of the extra cellular matrix (ECM) fibril network surrounding the cells in their natural environment, and, therefore, are considered to mimic the physical cues to which the cells are normally exposed. PEOT/PBT electrospun mats were first fabricated and characterized to control the fiber size and to unravel the mechanism of surface indentation and pore formation on the fibers during deposition. Human mesenchymal stem cells were then cultured on scaffolds with different fiber diameter and surface topology. As reported in chapter 7, it seemed that fibers of approximately 10  $\mu\text{m}$  in diameter showed an optimal cell seeding efficiency and a higher amount of cells after 2 weeks of culture. In addition, when nanoporosity was added to these fibers a higher proliferation rate and different cell morphology were found. Although these conclusions were found for human mesenchymal stem cells, the association of rounded or spread cells to smooth or nanotextured fibers respectively is rather intriguing as it might be used to direct a specific cell population into a desired morphology. The results also



confirmed the benefit of having thin smooth fibers for tracheal cartilage formation, as previously discussed for chapter 6. Li *et al.* [40] and Badami *et al.* [41] also studied the effect of thin fibers on chondrocytes and osteoprogenitor cells, respectively. Their results – although different as they compare fibers with different dimensions and fabricated with different polymers – are in line with what was found and discussed in this chapter, for which cells are capable to sense specific fiber dimensions and surface topologies singularly for each biomaterial used. Furthermore, a similar behavior was also discovered by other researchers when various topology features were created on flat material substrates by lithographic techniques [42-44], suggesting a stronger influence of surface topology on cells as compared to fiber dimensions. Some practical issues may still rise from the cell seeding efficiency on ESP scaffolds, due to the possible floating of the scaffolds when immersed in the culture media. An interesting solution in this direction has been proposed by Stankus *et al.* [45] and consisted in electrospraying cells concomitantly with electrospinning. Cells were demonstrated to be viable, to proliferate within the scaffold, and to differentiate into the desired tissue. Moreover, the possibility to incorporate drugs, proteins, and growth factors to release them in a sustained manner makes of ESP networks possible multifunctional structures that can be either used alone as 2D or 3D matrices or integrated in a 3D scaffold to mimic the ECM environment and function as a cell “sieving” system at the same time. In this direction – supporting the results presented in this chapter – a study from Li *et al.* [46] showed it was possible to incorporate a protein belonging to the bone morphogenic protein family (BMP-2) in silk ESP scaffolds preserving its activity. Incorporated scaffolds resulted in a higher bone formation.

### ***Integration of Fabrication Technologies to Create Multifunctional 3D Scaffolds***

A few examples of how different material processing and scaffold fabrication technologies can be integrated to generate multifunctional scaffolds have been illustrated and used in chapters 8, 9, and 10 for cartilage and bone tissue engineering. In chapter 8, a shell-core system of 3DF scaffolds was created by combining 3DF with a rheological phenomenon of molten polymeric blends known as viscous encapsulation. By fine-tuning the difference in viscosity of two or more polymers in a molten blend and exposing it to the shear stress field during extrusion, fibers with shell-core architecture were deposited and organized in a 3D scaffold by 3DF. With immiscible or even partially miscible polymers, a completely separated or at least a partially stratified fibrous structure can be obtained. In the former case selective leaching can be applied, resulting in the formation of a 3D scaffold with organized hollow fibers. These fibers were shown to significantly increase the amount of cartilage ECM formation as compared to solid fibers, while minimizing the amount of synthetic polymer. Despite these encouraging preliminary results, further studies should be directed to evaluate whether there is an optimal hollow fiber dimension in terms of tissue formation and to assess any variation on the behavior of other cells. These fibers could find multiple applications in tissue engineering such as tissue in-growth guides for neural and vascular tissue engineering, anatomical scaffolds derived from computerized tomography (CT) or magnetic resonance image (MRI)

datasets of a patient where a hollow fiber architecture would be desirable, or as an integrated perfusion system in a bioreactor unit while maintaining the porous structure of the scaffold for cell attachment, proliferation, and eventual differentiation [47-50]. Alternatively, the use of such hollow fibers end-capped by a polymeric thin membrane as a system of drug delivery reservoirs was proposed and showed to sustain the release of a model protein over a month. Such a system might be further up-graded for the release of more functional growth factors for specific tissue engineering applications. Eventually the incorporation of different biological compounds selectively present in different layers of the 3DF reservoir scaffold might be useful where the development of a hierarchical tissue requires the expression of different signals. Many different techniques are available to create hollow fibers [51-54]. With these techniques the hollowness of the fibers and their organization by weaving technologies into three-dimensional (3D) structures can be controlled to some extent [55]. Yet, it is difficult to achieve a precise control over the hollow cavities diameter and simultaneously a periodical, spatial organization in a 3D fashion as in the case of the technique here introduced. Additionally, hollow fibers are individually drawn and small variations in the setting parameters can result in irregularities in the lumen and shell size [56, 57].

In the case of shell-core scaffolds, it was shown how to exploit the shell layer as a coating that gives more favorable physicochemical properties to the structure, while the core polymer would offer the required mechanical properties. With PEOT/PBT copolymers it has been demonstrated that 1000/70/30 could maintain chondrocyte rounded morphology, while 300/55/45 displays better mechanical properties but supports dedifferentiated, spread chondrocyte morphology. Although it is possible to modulate the dynamic stiffness of 1000/70/30 to achieve a configuration with mechanical properties matching natural articular cartilage, some issues are still present on the stability of these scaffolds when implied in high load bearing areas like in the knee, as delamination of the fibers might occur as also previously discussed. However, if a 1000/70/30-300/55/45 shell-core scaffold was used the combination of the two polymers allowed to take advantage of the better physicochemical properties of 1000/70/30 for cartilage formation in the outer shell and of the mechanical stability of 300/55/45 in the inner core. Furthermore, the 3DF shell-core scaffold appeared to have a higher stiffness as compared to 1000/70/30 and 300/55/45 3D scaffolds, probably due to a pre-stress effect of the more swelling 1000/70/30 fibrils on the less swelling 300/55/45 fibrils mixed in the core of the fiber. The improvement of mechanical properties combined with a large ECM formation and maintained rounded chondrocyte morphology makes these constructs promising 3D systems for long-term applications in cartilage regeneration. When compared to other scaffolds coating techniques, these shell-core 3DF scaffolds showed to have a homogeneous and continuous shell coating for all of the fibers without the formation of membranes obstructing pores [58], which may result in a reduction of pore interconnectivity, and without breaking or flaking of the coating due to mechanical loading [59]. This may happen when the coating is transferred to the scaffold through a polymer solution in the former case, or through deposition from physiological solutions in the latter method. An alternative technique to transfer a homogeneous coating onto 3D scaffolds has been recently reported and

made use of self-assembly peptide solutions [60]. Albeit the interesting structure of the coating deposited on the fibers of the scaffolds, uncertainties over the strength of the coating still remain.

Chapter 9 introduced the integration of 3DF and ESP techniques to create a multifunctional system where the 3DF scaffold would give the mechanical stability and the pore organization for tissue development and the ESP networks would act as a cell sieve and provide topographical cues to the cells, as previously mentioned. 3DFESP scaffolds showed to entrap a significantly higher number of cells and to elicit more ECM formation as compared to 3DF scaffolds. Moreover, 3DFESP constructs maintained rounded chondrocyte morphology even if 300/55/45 was used. This can be attributed to the presence of the smooth micron-size ESP fibril network, as also investigated in chapter 7. No significant influence of the ESP network density could be detected. The work presented in this chapter can be considered as an integration of novel scaffold fabrication techniques, since it combines the improved porous organization of a rapid prototyping structure with the multifunctionality of an ESP mesh. Further improvements of this technique might involve the use of different biomaterials in different layers of the rapid prototyping and/or of the ESP constructs where the hierarchical architecture of the desired natural tissue may require the use of synthetic substitutes with appropriate physicochemical and mechanical properties for each specific region. This can be also combined with the incorporation of biofactors in the ESP fibers in the polymer solution, by electrospinning an emulsion, or by electrospinning a biphasic fluid with a coaxial needle where the biological compound is included in the core liquid phase. To expand the fibrillar network from bi-dimensional to three-dimensional, electrospinning can be substituted by phase inversion techniques. As shown in an example in figure 1, a three-dimensional fibrous network can be created within a PEOT/PBT 3DF scaffold by dipping it in a PCL solution, freezing it and extracting the solvent by freeze-drying. Depending on the freezing temperature it is also possible to control the pore dimensions on the fiber network formed. Eventually biological compounds could be dissolved in the polymer solution used to form the 3D network. An additional possibility would be to couple 3D scaffolds with self-assembling (SA) biomaterials to create a 3D nanofibrillar network in the scaffolds. The flexibility of emerging SA systems allows modifying them so that they can express specific peptide sequences related to the specific tissue engineering application [61-63]. Only a few studies focused on the integration of micro- or nano-fibers in macro-fiber 3D scaffolds fabricated by wet spinning and fiber bonding [64, 65]. In both cases, the inclusion of such fibers resulted in an increased number of attached cells and a better tissue formation, thus confirming our findings. In addition, in the study here reported the integration of thin fibers into rapid prototyped scaffolds allows combining the completely interconnected macro-pores of 3D scaffolds, resulting in controllable mechanical properties, with the ECM mimicking ESP matrix providing the appropriate physical cues to the cells for improved tissue formation.

Finally, chapter 10 proposed a novel concept to create 3D scaffolds for osteochondral tissue engineering. Assembled hybrid 3D scaffolds were made by integrating 3DF, indirect stereolithography, and freeze-drying. The hybrid construct

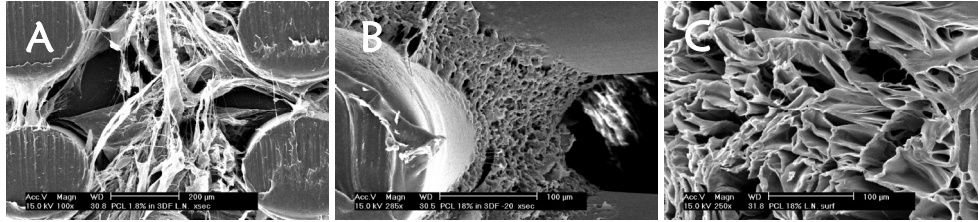


**Figure 1** – SEM micrographs of fibrillar 3D network formation by phase inversion and examples of different porosity range of the fibers. (a) non porous (1.8% w/v solution frozen at  $T = -196\text{ }^{\circ}\text{C}$ ); (b) pore size of  $9.27 \pm 3\text{ }\mu\text{m}$  (18% w/v solution frozen at  $T = -20\text{ }^{\circ}\text{C}$ ); (c) pore size of  $56.74 \pm 32.12\text{ }\mu\text{m}$  (18% w/v solution frozen at  $T = -196\text{ }^{\circ}\text{C}$ ). Pilot experiment, not published data. Scale bar: (a)  $200\text{ }\mu\text{m}$ ; (b, c)  $100\text{ }\mu\text{m}$ .

was mechanically characterized and various design options were considered for its use as the bone compartment. As ceramics are generally too brittle and demineralized bone matrices too flexible for direct implantation in a high load bearing bony site, the possibility to assemble them in a single 3D scaffold together with a polymeric matrix functioning as a carrier offers an attractive solution in terms of the final construct mechanical stability, while maintaining the biological bone forming properties of the biomaterials. 3D scaffolds were assembled following two different design approaches. In a first design, BCP particles were sintered in polymeric molds fabricated by photolithography with specific shapes and press-fitted into the pores of a 3DF 1000/70/30 matrix. In a second model, a BCP cylinder was inserted between two DBM foamy discs and the assembly was placed in a hollow 3DF cylindrical scaffold, which was eventually closed by a deposited 3DF membrane on top of the hollow cylinder. The constructs were finally immersed in a DBM gel and freeze-dried to obtain a foamy integrated structure in and outside the ceramic-polymeric assembly. The bending and compressive storage moduli of these scaffolds varied mainly with the different shapes of the ceramic particles, due to the redistribution of the applied stress on the different particles, and with increasing ceramic weight content. In a similar manner, the stress at break was modulated by changing the ceramic particle geometry, while the deformation at break was substantially constant, probably because of the “cushioning” contribution of the DBM foam in and out the 3D construct. The scaffold bone compartment was directly integrated to the cartilage compartment by 3D fiber-deposition. The chondral part of the scaffold was made of 300/55/45 to assure the mechanical stability of the whole construct. Having the two PEOT/PBT compositions (bone = 1000/70/30 – cartilage = 300/55/45) different swelling properties, an interlocking fibrous system made of intertwined concentric 1000/70/30 and 300/55/45 fibers was deposited at the interface between the bone and the chondral parts of the construct. This system also has the function to mimic the tidemark in the osteochondral natural architecture, as 1000/70/30 calcifies and interconnects with the bony part. 3DF osteochondral scaffolds showed also to support cell attachment and proliferation, and differentiation into bone and cartilage in the respective compartments [66]. This study emphasized that the combination of different

fabrication technologies can lead to the creation of a pool of different scaffolds with tailorable mechanical and physicochemical properties, at the same time maintaining a favorable biological response. Typical methods to fabricate composite scaffolds aim at interspersing the two phases to finally achieve a homogeneous construct [67-69]. However, this frequently results in scaffolds with poor polymer-ceramic bonding and limited control over the composite processability and mechanical properties [70, 71]. The interspersing of the two phases might also result in the obstruction of some of the scaffold pores, compromising pore interconnectivity [72]. When compared to these conventional methods, the approach discussed in chapter 10 makes use of rapid prototyping to combine polymer and ceramics into a 3D scaffold, while preserving pore interconnectivity and accessibility. Future studies should aim at assessing any eventual biological synergistic effect of the single biomaterials in the hybrid scaffolds, the ability of such constructs to support *in vivo* bone and cartilage formation, and their mechanical stability in a load bearing site. The work presented in this thesis attempted to highlight how important it is to combine biological, chemical, and mechanical stimuli for the success of novel medical treatments, with a particular regard to regenerative medicine. The key for a perfect combination of such signals seems to be the integration of the many different technological platforms available and in development to create multifunctional structures. The future direction to implement this integration should pass through an initial stage where cell-materials interactions are studied and detected in a high throughput system that can be named “materiomics”, as mentioned earlier in this book. Depending on the specific tissue to regenerate, an optimal biomaterial can be so chosen to elicit the appropriate cell response and eventually modified with specific ligands and/or by incorporating biological compounds. The combination of biomaterial processing techniques with scaffold fabrication technologies and the spatiotemporal incorporation and eventual controlled and sustained release of biofactors will contribute to create a new generation of “smart” scaffolds that will lead to long-term successful applications in regenerative medicine. A trend is emerging where no longer new techniques from different disciplines are only slowly diffusing into tissue engineering or regenerative medicine. Instead, the transfer is much quicker and involves simultaneous implementation of multiple novel techniques. It will not be long before this combinatorial approach will funnel back novel knowledge to the more basic disciplines.

#### References:

- [1] Williams DF. To engineer is to create: the link between engineering and regeneration. *Trends Biotechnol* 2006;24(1):4-8.
- [2] Lin AS, Barrows TH, Cartmell SH, Guldberg RE. Microarchitectural and mechanical characterization of oriented porous polymer scaffolds. *Biomaterials* 2003;24(3):481-9.
- [3] Miot S, Woodfield T, Daniels AU, Suetterlin R, Peterschmitt I, Heberer M, van Blitterswijk CA, Riesle J, Martin I. Effects of scaffold composition and architecture on human nasal chondrocyte redifferentiation and cartilaginous matrix deposition. *Biomaterials* 2005;26(15):2479-89.

- [4] Sachlos E, Czernuszka JT. Making tissue engineering scaffolds work. Review: the application of solid freeform fabrication technology to the production of tissue engineering scaffolds. *Eur Cell Mater* 2003;5:29-39; discussion 39-40.
- [5] Miot S, Scandiucci de Freitas P, Wirz D, Daniels AU, Sims TJ, Hollander AP, Mainil-Varlet P, Heberer M, Martin I. Cartilage tissue engineering by expanded goat articular chondrocytes. *J Orthop Res* 2006;24(5):1078-85.
- [6] Demartean O, Wendt D, Braccini A, Jakob M, Schafer D, Heberer M, Martin I. Dynamic compression of cartilage constructs engineered from expanded human articular chondrocytes. *Biochem Biophys Res Commun* 2003;310(2):580-8.
- [7] Gibson LJ, Ashby MF. *Cellular Solids - structure and properties*, 2<sup>nd</sup> edition. Cambridge University Press, Cambridge 1997.
- [8] Woesz A, Stampfl J, Fratzl P. Cellular solids beyond the apparent density - an experimental assessment of mechanical properties. *Adv Eng Mater* 2004;6:134-138.
- [9] Hollister SJ. Porous scaffold design for tissue engineering. *Nat Mater* 2005;4(7):518-24.
- [10] Hollister SJ, Maddox RD, Taboas JM. Optimal design and fabrication of scaffolds to mimic tissue properties and satisfy biological constraints. *Biomaterials* 2002;23(20):4095-103.
- [11] Lin CY, Kikuchi N, Hollister SJ. A novel method for biomaterial scaffold internal architecture design to match bone elastic properties with desired porosity. *J Biomech* 2004;37(5):623-36.
- [12] Lin CY, Schek RM, Mistry AS, Shi X, Mikos AG, Krebsbach PH, Hollister SJ. Functional bone engineering using ex vivo gene therapy and topology-optimized, biodegradable polymer composite scaffolds. *Tissue Eng* 2005;11(9-10):1589-98.
- [13] Martin I, Padera RF, Vunjak-Novakovic G, Freed LE. In vitro differentiation of chick embryo bone marrow stromal cells into cartilaginous and bone-like tissues. *J Orthop Res* 1998;16(2):181-9.
- [14] Martin I, Vunjak-Novakovic G, Yang J, Langer R, Freed LE. Mammalian chondrocytes expanded in the presence of fibroblast growth factor 2 maintain the ability to differentiate and regenerate three-dimensional cartilaginous tissue. *Exp Cell Res* 1999;253(2):681-8.
- [15] Freed LE, Marquis JC, Nohria A, Emmanuel J, Mikos AG, Langer R. Neocartilage formation in vitro and in vivo using cells cultured on synthetic biodegradable polymers. *J Biomed Mater Res* 1993;27(1):11-23.
- [16] Obradovic B, Carrier RL, Vunjak-Novakovic G, Freed LE. Gas exchange is essential for bioreactor cultivation of tissue engineered cartilage. *Biotechnol Bioeng* 1999;63(2):197-205.
- [17] Vunjak-Novakovic G, Martin I, Obradovic B, Treppo S, Grodzinsky AJ, Langer R, Freed LE. Bioreactor cultivation conditions modulate the composition and mechanical properties of tissue-engineered cartilage. *J Orthop Res* 1999;17(1):130-8.
- [18] Vunjak-Novakovic G, Freed LE, Biron RJ, Langer R. Effects of mixing on the composition and morphology of tissue-engineered cartilage. *Aiche Journal* 1996;42(3):850-860.
- [19] Freed LE, Hollander AP, Martin I, Barry JR, Langer R, Vunjak-Novakovic G. Chondrogenesis in a cell-polymer-bioreactor system. *Exp Cell Res* 1998;240(1):58-65.

- [20] Malda J, Woodfield TB, van der Vloodt F, Wilson C, Martens DE, Tramper J, van Blitterswijk CA, Riesle J. The effect of PEGT/PBT scaffold architecture on the composition of tissue engineered cartilage. *Biomaterials* 2005;26(1):63-72.
- [21] Malda J, Woodfield TB, van der Vloodt F, Kooy FK, Martens DE, Tramper J, van Blitterswijk CA, Riesle J. The effect of PEGT/PBT scaffold architecture on oxygen gradients in tissue engineered cartilaginous constructs. *Biomaterials* 2004;25(26):5773-80.
- [22] Woodfield TB, Malda J, de Wijn J, Peters F, Riesle J, van Blitterswijk CA. Design of porous scaffolds for cartilage tissue engineering using a three-dimensional fiber-deposition technique. *Biomaterials* 2004;25(18):4149-61.
- [23] Woodfield TB, Van Blitterswijk CA, De Wijn J, Sims TJ, Hollander AP, Riesle J. Polymer scaffolds fabricated with pore-size gradients as a model for studying the zonal organization within tissue-engineered cartilage constructs. *Tissue Eng* 2005;11(9-10):1297-311.
- [24] Schek RM, Taboas JM, Hollister SJ, Krebsbach PH. Tissue engineering osteochondral implants for temporomandibular joint repair. *Orthod Craniofac Res* 2005;8(4):313-9.
- [25] Landis WJ, Jacquet R, Hillyer J, Lowder E, Yanke A, Siperko L, Asamura S, Kusuhara H, Enjo M, Chubinskaya S, Potter K, Isogai N. Design and assessment of a tissue-engineered model of human phalanges and a small joint. *Orthod Craniofac Res* 2005;8(4):303-12.
- [26] Hutmacher DW, Ng KW, Kaps C, Sittinger M, Klaring S. Elastic cartilage engineering using novel scaffold architectures in combination with a biomimetic cell carrier. *Biomaterials* 2003;24(24):4445-58.
- [27] Alhadlaq A, Elisseeff JH, Hong L, Williams CG, Caplan AI, Sharma B, Kopher RA, Tomkoria S, Lennon DP, Lopez A, Mao JJ. Adult stem cell driven genesis of human-shaped articular condyle. *Ann Biomed Eng* 2004;32(7):911-23.
- [28] Mironov V, Boland T, Trusk T, Forgacs G, Markwald RR. Organ printing: computer-aided jet-based 3D tissue engineering. *Trends Biotechnol* 2003;21(4):157-61.
- [29] Cao Y, Vacanti JP, Paige KT, Upton J, Vacanti CA. Transplantation of chondrocytes utilizing a polymer-cell construct to produce tissue-engineered cartilage in the shape of a human ear. *Plast Reconstr Surg* 1997;100(2):297-302; discussion 303-4.
- [30] Suh SW, Kim J, Baek CH, Kim H. Development of new tracheal prosthesis: autogenous mucosa-lined prosthesis made from polypropylene mesh. *Int J Artif Organs* 2000;23(4):261-7.
- [31] Suh SW, Kim J, Baek CH, Han J, Kim H. Replacement of a tracheal defect with autogenous mucosa lined tracheal prosthesis made from polypropylene mesh. *Asaio J* 2001;47(5):496-500.
- [32] Ziegelaar BW, Aigner J, Staudenmaier R, Lempart K, Mack B, Happ T, Sittinger M, Endres M, Naumann A, Kastenbauer E, Rotter N. The characterisation of human respiratory epithelial cells cultured on resorbable scaffolds: first steps towards a tissue engineered tracheal replacement. *Biomaterials* 2002;23(6):1425-38.
- [33] Yang L, Korom S, Welti M, Hoerstrup SP, Zund G, Jung FJ, Neuenschwander P, Weder W. Tissue engineered cartilage generated from human trachea using DegraPol scaffold. *Eur J Cardiothorac Surg* 2003;24(2):201-7.

- [34] Rotter N, Stolzel K, Endres M, Leinhase I, Ziegelaar BW, Sittinger M. Towards engineering of a tracheal equivalent: identification of epithelial precursor cells, differentiation and cocultivation techniques. *Med J Malaysia* 2004;59 Suppl B:35-6.
- [35] Kojima K, Vacanti CA. Generation of a tissue-engineered tracheal equivalent. *Biotechnol Appl Biochem* 2004;39(Pt 3):257-62.
- [36] Kojima K, Igotz RA, Kushibiki T, Tinsley KW, Tabata Y, Vacanti CA. Tissue-engineered trachea from sheep marrow stromal cells with transforming growth factor beta2 released from biodegradable microspheres in a nude rat recipient. *J Thorac Cardiovasc Surg* 2004;128(1):147-53.
- [37] Kim J, Suh SW, Shin JY, Kim JH, Choi YS, Kim H. Replacement of a tracheal defect with a tissue-engineered prosthesis: early results from animal experiments. *J Thorac Cardiovasc Surg* 2004;128(1):124-9.
- [38] Kamil SH, Eavey RD, Vacanti MP, Vacanti CA, Hartnick CJ. Tissue-Engineered Cartilage as a Graft Source for Laryngotracheal Reconstruction. *Arch Otolaryngol Head Neck Surg* 2005;130:1048-1051.
- [39] Li D, Xia YN. Electrospinning of nanofibers: Reinventing the wheel? *Advanced Materials* 2004;16(14):1151-1170.
- [40] Li WJ, Jiang YJ, Tuan RS. Chondrocyte phenotype in engineered fibrous matrix is regulated by fiber size. *Tissue Eng* 2006;12(7):1775-85.
- [41] Badami AS, Kreke MR, Thompson MS, Riffle JS, Goldstein AS. Effect of fiber diameter on spreading, proliferation, and differentiation of osteoblastic cells on electrospun poly(lactic acid) substrates. *Biomaterials* 2006;27(4):596-606.
- [42] Curtis AS, Gadegaard N, Dalby MJ, Riehle MO, Wilkinson CD, Aitchison G. Cells react to nanoscale order and symmetry in their surroundings. *IEEE Trans Nanobioscience* 2004;3(1):61-5.
- [43] Dalby MJ, Riehle MO, Sutherland DS, Agheli H, Curtis AS. Morphological and microarray analysis of human fibroblasts cultured on nanocolumns produced by colloidal lithography. *Eur Cell Mater* 2005;9:1-8; discussion 8.
- [44] Chung TW, Liu DZ, Wang SY, Wang SS. Enhancement of the growth of human endothelial cells by surface roughness at nanometer scale. *Biomaterials* 2003;24(25):4655-61.
- [45] Stankus JJ, Guan JJ, Fujimoto K, Wagner WR. Microintegrating smooth muscle cells into a biodegradable, elastomeric fiber matrix. *Biomaterials* 2006;27(5):735-744.
- [46] Li C, Vepari C, Jin HJ, Kim HJ, Kaplan DL. Electrospun silk-BMP-2 scaffolds for bone tissue engineering. *Biomaterials* 2006;27(16):3115-24.
- [47] Knazek RA, Gullino PM, Kohler PO, Dedrick RL. Cell culture on artificial capillaries: an approach to tissue growth in vitro. *Science* 1972;178(56):65-6.
- [48] Kawakami O, Miyamoto S, Hatano T, Yamada K, Hashimoto N, Tabata Y. Acceleration of aneurysm healing by hollow fiber enabling the controlled release of basic fibroblast growth factor. *Neurosurgery* 2006;58(2):355-64; discussion 355-64.
- [49] Janssen FW, Oostra J, Oorschot A, van Blitterswijk CA. A perfusion bioreactor system capable of producing clinically relevant volumes of tissue-engineered bone: in vivo bone formation showing proof of concept. *Biomaterials* 2006;27(3):315-23.
- [50] Gomes ME, Holtorf HL, Reis RL, Mikos AG. Influence of the porosity of starch-based fiber mesh scaffolds on the proliferation and osteogenic differentiation of bone



- marrow stromal cells cultured in a flow perfusion bioreactor. *Tissue Eng* 2006;12(4):801-9.
- [51] Niwa M, Kawakami H, Nagaoka S, Kanamori T, Morisaku K, Shinbo T, Matsuda T, Sakai K, Kubota S. Development of a novel polyimide hollow-fiber oxygenator. *Artif Organs* 2004;28(5):487-95.
- [52] Stokols S, Tuszynski MH. The fabrication and characterization of linearly oriented nerve guidance scaffolds for spinal cord injury. *Biomaterials* 2004;25(27):5839-46.
- [53] Loscertales IG, Barrero A, Marquez M, Spretz R, Velarde-Ortiz R, Larsen G. Electrically forced coaxial nanojets for one-step hollow nanofiber design. *Journal of the American Chemical Society* 2004;126(17):5376-5377.
- [54] Zhao JP, Gaddis CS, Cai Y, Sandhage KH. Free-standing microscale structures of nanocrystalline zirconia with biologically replicable three-dimensional shapes. *Journal of Materials Research* 2005;20(2):282-287.
- [55] Ko FK. Textiles and Garments for Chemical and Biological Protections. In: *Strategies to Protect the Health of Deployed U.S. Forces: Force Protection and Decontamination* 1999:182-216.
- [56] Gupta PK. Fibre Reinforcements for composite materials. *Composite Materials Series* 1988;2:19-69.
- [57] Imoto K, Sumi M, Toda G, Suganuma T. Optical Fiber Drawing Method with Gas-Flow Controlling System. *Journal of Lightwave Technology* 1989;7(1):115-121.
- [58] Chen QZ, Boccaccini AR. Poly(D,L-lactic acid) coated 4555 Bioglass-based scaffolds: processing and characterization. *J Biomed Mater Res A* 2006;77(3):445-57.
- [59] Chim H, Hutmacher DW, Chou AM, Oliveira AL, Reis RL, Lim TC, Schantz JT. A comparative analysis of scaffold material modifications for load-bearing applications in bone tissue engineering. *Int J Oral Maxillofac Surg* 2006.
- [60] Harrington DA, Cheng EY, Guler MO, Lee LK, Donovan JL, Claussen RC, Stupp SI. Branched peptide-amphiphiles as self-assembling coatings for tissue engineering scaffolds. *J Biomed Mater Res A* 2006;78(1):157-67.
- [61] Zhang SG. Fabrication of novel biomaterials through molecular self-assembly. *Nature Biotechnology* 2003;21(10):1171-1178.
- [62] Hartgerink JD, Beniash E, Stupp SI. Self-assembly and mineralization of peptide-amphiphile nanofibers. *Science* 2001;294(5547):1684-8.
- [63] Harrington DA, Cheng EY, Guler MO, Lee LK, Donovan JL, Claussen RC, Stupp SI. Branched peptide-amphiphiles as self-assembling coatings for tissue engineering scaffolds. *J Biomed Mater Res A* 2006;78A(1):157-167.
- [64] Tuzlakoglu K, Bolgen N, Salgado AJ, Gomes ME, Piskin E, Reis RL. Nano- and micro-fiber combined scaffolds: a new architecture for bone tissue engineering. *J Mater Sci Mater Med* 2005;16(12):1099-104.
- [65] Williamson MR, Black R, Kietly C. PCL-PU composite vascular scaffold production for vascular tissue engineering: Attachment, proliferation and bioactivity of human vascular endothelial cells. *Biomaterials* 2006;27(19):3608-3616.
- [66] Hamann D, Moroni L, Paoluzzi L, van Blitterswijk CA. Osteochondral tissue engineering based on mesenchymal stem cells loaded on triphasic rapid prototyped scaffolds. *Tiss Eng and Reg Med Int Soc Proc* 2006.

- [67] Kay S, Thapa A, Haberstroh KM, Webster TJ. Nanostructured polymer/nanophase ceramic composites enhance osteoblast and chondrocyte adhesion. *Tissue Eng* 2002;8(5):753-61.
- [68] Sherwood JK, Riley SL, Palazzolo R, Brown SC, Monkhouse DC, Coates M, Griffith LG, Landeen LK, Ratcliffe A. A three-dimensional osteochondral composite scaffold for articular cartilage repair. *Biomaterials* 2002;23(24):4739-51.
- [69] Taboas JM, Maddox RD, Krebsbach PH, Hollister SJ. Indirect solid free form fabrication of local and global porous, biomimetic and composite 3D polymer-ceramic scaffolds. *Biomaterials* 2003;24(1):181-94.
- [70] Kreklau B, Sittinger M, Mensing MB, Voigt C, Berger G, Burmester GR, Rahmzadeh R, Gross U. Tissue engineering of biphasic joint cartilage transplants. *Biomaterials* 1999;20(18):1743-9.
- [71] Martin I, Miot S, Barbero A, Jakob M, Wendt D. Osteochondral tissue engineering. *J Biomech* 2006.
- [72] Kaito T, Myoui A, Takaoka K, Saito N, Nishikawa M, Tamai N, Ohgushi H, Yoshikawa H. Potentiation of the activity of bone morphogenetic protein-2 in bone regeneration by a PLA-PEG/hydroxyapatite composite. *Biomaterials* 2005;26(1):73-9.

# Summary

This thesis describes a library of novel 3D scaffolds designed and optimized for tissue engineering and regenerative medicine applications. Tissue engineering aims at restoring or regenerating a deamaged tissue by combining cells, derived from a patient biopsy, with a 3D porous matrix, functioning as a scaffold. After isolation and eventual *in vitro* expansion, cells are seeded on the 3D scaffolds and, depending on the strategy, implanted directly or at a later stage in the patient's body. 3D scaffolds generally need to satisfy a number of requirements: (i) biocompatibility, (ii) biodegradability and/or bioresorbability, (iii) suitable mechanical properties, (iv) adequate physicochemical properties to direct cell-material interactions matching the tissue to be replaced, (v) facilitate regaining the original shape of the damaged tissue and the integration with the surrounding environment. From the review of the literature proposed in chapter 1, it appears still a challenge to satisfy all the aforementioned requisites with the biomaterials and the scaffold fabrication technologies nowadays available. 3D scaffolds can be fabricated with various techniques, among which rapid prototyping and electrospinning seem to be the most promising. Rapid prototyping technologies allow manufacturing scaffolds with a controlled, completely accessible pore network – determinant for nutrient supply and diffusion – in a CAD/CAM fashion. Electrospinning (ESP) allows mimicking the extracellular matrix (ECM) environment of the cells and can provide fibrous scaffolds with instructive surface properties to direct cell faith into the proper lineage. Yet, these fabrication methods have some disadvantages if considered alone. Therefore, the aim of this thesis was to characterize rapid prototyped and ESP scaffolds and to propose few examples that highlight the importance of combining different scaffolds fabrication technologies and possibly different biomaterials to provide cells with mechanical, physicochemical, and biological cues at the macro, micro, and nano scale. If merged together, the solutions proposed in this book may satisfy all of the scaffolds' requirements for tissue engineering applications.

Rapid prototyped scaffolds were first characterized in terms of their mechanical and physicochemical properties in chapters 2, 3 and 4. A technique called 3D fiber deposition (3DF) was used. The mechanical properties of 3DF scaffolds were shown to be modulated, depending on the scaffold's total porosity, pore size and shape, and depending on the biomaterial composition processed. A mathematical model was also determined and numerically assessed, as discussed in chapter 4. This model can be used to predict the mechanical properties of 3D scaffolds and to optimize them to match the mechanical properties of the desired tissue (e.g. articular or meniscal cartilage) in terms of porosity, architecture, and physicochemical composition of the biomaterial. As an example, the model was used to choose scaffolds with specific mechanical and physicochemical properties for articular cartilage regeneration (chapter 5). Scaffolds with analogous architecture – resulting

also in comparable starting mechanical properties – but different physicochemical behavior were compared to a 3D scaffold with matching dynamic stiffness and physicochemical properties of bovine articular cartilage. After one month of culture, cartilage formation was significantly higher in the matching scaffold than in the non-matching scaffolds. Interestingly, this finding was not strictly related to the matching or non-matching dynamic stiffness, but to the architecture configuration of the scaffolds. It was the lower pore volume and porosity of the structure that better entrapped cells resulting in a higher seeding efficiency and ECM formation in the matching scaffold.

Rapid prototyping techniques can also fabricate anatomical scaffolds from a computer tomography (CT) or a magnetic resonance image dataset of a patient. Chapter 6 aimed at evaluating whether anatomically shaped scaffolds have a role in the dynamics of tissue formation as compared to other simpler but yet functional designs, apart from the evident benefit of regaining the natural shape of the tissue to be restored. A tracheal model was chosen for this purpose. After 3 weeks in culture, anatomical scaffolds sustained a higher production of ECM and a better cell differentiation. With increasing complexity of the scaffold geometry the limitations of the rapid prototyping technique contributed to the improvement of cartilage formation, due to the significant formation of plastically drawn thin fibers during scaffold manufacturing. These fibers showed to support a rounded morphology of the seeded and attached chondrocytes, which might have positively influenced tissue formation.

As a logical consequence of the findings of chapter 6 related to the effect of thin fibers on tissue dynamics, the influence of fiber diameter and texture on cell morphology and proliferation was analyzed by fabricating ESP scaffolds. As reported in chapter 7, cells were not only able to distinguish between different surface topologies, but also among different fiber diameters. The results shown in this chapter suggested that the physical cues obtained by ESP can influence cell morphology and might play a role in their differentiation into a specific lineage.

Few examples of how different material processing and scaffold fabrication technologies can be integrated to generate multifunctional scaffolds are introduced in chapters 8, 9, and 10. In chapter 8, a shell-core system of 3D scaffolds was created by combining 3DF with a rheological phenomenon of molten polymeric blends known as viscous encapsulation. By fine-tuning the difference in viscosity of two or more polymers in a molten blend and exposing it to the shear stress field during extrusion, fibers with a shell-core and with a hollow architecture were deposited and organized in a 3D scaffold. In both cases these scaffolds showed to support better cartilage regeneration when compared to standard 3D scaffolds. This resulted from the presence of a shell layer functioning as a coating designed to have better physicochemical properties for chondrocyte interactions, in the case of shell-core fiber 3D scaffolds. When hollow fiber scaffolds were used, a higher cell entrapment was associated to a lower amount of synthetic biomaterial compared to 3DF scaffolds with solid fibers. Furthermore, possible use of these constructs as tissue guiding matrices or as integrated systems for direct nutrient perfusion can be envisioned. Chapter 9 introduced the integration of 3DF and ESP techniques to generate a multifunctional system where the 3DF scaffold would provide the

mechanical stability and the pore organization for tissue development and the ESP networks would act as a cell sieve and supply topographical cues to the cells. The resulting integrated scaffolds displayed a significantly higher number of entrapped cells and elicited more ECM formation as compared to 3DF scaffolds alone. This was also associated with maintained rounded chondrocyte morphology, due to the presence of the smooth micron-size ESP fibril network. In chapter 10 a novel concept to create 3D scaffolds for osteochondral tissue engineering is discussed, where assembled hybrid 3D scaffolds were made by integrating 3DF, indirect stereolithography, and freeze-drying. As ceramics are generally too brittle and demineralized bone matrices too flexible for direct implantation in a high load bearing bony site, the possibility to assemble them in a single 3D scaffold together with a polymeric matrix functioning as a carrier offers an attractive solution in terms of the final construct mechanical stability, while maintaining the biological bone forming properties of the biomaterials. The hybrid constructs analyzed displayed modifiable mechanical properties, depending on the ceramic volume ratio and particle shape in the constructs.

Finally, chapters 11 summarizes and discusses the results presented in this thesis and offers few possible ideas for future developments.

# Samenvatting

Dit proefschrift beschrijft het ontwerp en de optimalisatie van drie dimensionale dragers voor toepassingen in de weefsel techniek (“tissue engineering”) en regeneratieve geneeskunde.

Met tissue engineering wordt beoogd beschadigd of ontbrekend weefsel te herstellen of te vervangen door cellen afkomstig uit een biopsie van de patiënt aan te brengen op een drie dimensionale poreuze matrix die “scaffold” (lett.: “steiger”) wordt genoemd. Na isoleren en eventueel expanderen van de cellen worden deze gezaaid op en in de 3D scaffold en, afhankelijk van de te volgen behandelstrategie, direct of op een later tijdstip geïmplantéerd in het lichaam van de patiënt. Deze scaffolds moeten aan een aantal eisen voldoen voor wat betreft: (i) biocompatibiliteit, (ii) biodegradeerbaarheid, - resorbeerbaarheid, (iii) de juiste mechanische eigenschappen, (iv) fysisch chemische eigenschappen die via cel-materiaal interacties de vorming van het gewenste weefsel kunnen bewerkstelligen en (v) geometrie waardoor herstel van de oorspronkelijke contouren van het weefsel en de integratie met het restweefsel kan worden bevorderd.

Een overzicht van de literatuur zoals gegeven in hoofdstuk 1 leert dat er nog een aanzienlijke uitdaging ligt om met de heden ten dage beschikbare materialen en technieken aan de boven omschreven voorwaarden te voldoen. Van de technieken waarmee de scaffolds kunnen worden gemaakt lijken “rapid prototyping” en elctrospinnen de meest belovende”. Rapid prototyping technologie – gebaseerd op CAD/CAM - maakt het mogelijk om scaffolds te maken met een volledig controleerbaar, open en toegankelijk porieën systeem dat nodig is voor voldoende aanvoer van nutriënten. Met electrospinnen (ESP) is het mogelijk de extracellulaire matrix (ECM) van de cellen na te bootsen en de scaffold van oppervlakte eigenschappen te voorzien die de celkweek in de richting van het gewenste type weefsel kan dirigeren. Toch hebben de genoemde technieken ieder voor zich weer bepaalde tekortkomingen.

Het was daarom het doel van dit onderzoek om door rapid prototyping en ESP verkregen scaffolds nader te karakteriseren en het belang te illustreren van het combineren van verschillende vervaardigingstechnieken en verschillende biomaterialen teneinde de cellen te voorzien van mechanische ,fysisch-chemische en biologische stimuli op macro, micro en nano niveau. Met de in dit proefschrift voorgestelde vervaardigingroutes zou aan alle denkbare eisen die vanuit tissue engineering aan scaffolds gesteld worden tegemoet gekomen kunnen worden.

In de hoofdstukken 2,3, en 4 worden de met rapid prototyping verkregen scaffolds allereerst gekarakteriseerd in termen van mechanische eigenschappen. Daarbij werd een techniek van 3D fiber deposition (3DF) toegepast. Aangetoond werd hoe de mechanische eigenschappen van 3DF scaffolds gecontroleerd kunnen worden met het porievolume, de poriegrootte en – vorm en met de fysisch-chemische

samenstelling van het materiaal. In hoofdstuk 4 wordt hiertoe ook een mathematisch model opgesteld en numeriek gevalideerd. Dit model kan gebruikt worden om van een scaffold de mechanische eigenschappen te voorspellen en te optimaliseren in termen van porositeitkenmerken en materiaaleigenschappen voor gebruik in een bepaald type weefsel (bijvoorbeeld articulaire of meniscus kraakbeen). Bij wijze van voorbeeld is dit model in hoofdstuk 5 gebruikt om scaffolds te ontwerpen met geschikte eigenschappen voor regeneratie van articulaire kraakbeen. Scaffolds met gelijksoortige poriearchitectuur en mechanische eigenschappen – maar met verschillende materiaaleigenschappen werden in celkweek vergeleken met een scaffold dat met runderkraakbeen overeenkomende dynamische stijfheid en fysisch-chemische eigenschappen bezat. Na een kweektijd van een maand was er significant meer kraakbeen gevormd in de scaffold die het meest met runderkraakbeen overeenkwam. Interessant was dat deze bevinding niet alleen gerelateerd was aan de overeenkomende stijfheid maar ook aan de poriearchitectuur. Het was met name een lager porievolume dat door beter vast te houden een hogere zaai-efficiëntie mogelijk maakte en daarmee een betere extra cellulaire matrix vorming. Via rapid prototyping technieken kunnen ook scaffolds worden vervaardigd op basis van Röntgen- of MRI scans van een patiënt (computer tomografie, CT-scans). In hoofdstuk 6 wordt nagegaan in hoeverre een anatomische vorm van scaffolds een rol speelt in de dynamiek van weefselvorming in vergelijking met weliswaar functionele maar meer modelmatige, simpelere vormen. Hiervoor werd een model van een trachea gekozen. Na 3 weken celkweek was er in het anatomische model meer extra cellulaire matrix gevormd en trad betere celdifferentiatie op. Met de toegenomen structuurcomplexiteit van het anatomische model bleek de aan de vervaardigingstechniek gerelateerde vorming van zeer dunne vezeltjes een beter kraakbeenvorming mogelijk te maken. Deze vezeltjes bleken een ronde morfologie van de er aan gehechte chondrocyten te stimuleren waardoor mogelijk de weefselvorming positief werd beïnvloed.

Als een logisch gevolg van de bevindingen van hoofdstuk 6 werd een studie gedaan naar de invloed van vezel diameter en oppervlakte structuur op celmorfologie en groeisnelheid met behulp van ESP scaffolds. In hoofdstuk 7 wordt beschreven hoe de cellen niet alleen reageerden op oppervlakte structuren maar ook op de vezeldiameter. De resultaten van deze studie suggereren dat de aan electrospinnen gerelateerde fysische kenmerken van de scaffolds een invloed kunnen hebben op de celmorfologie en daardoor wellicht een rol spelen bij de differentiatie naar het type weefsel.

In de hoofdstukken 8,9 en 10 worden een aantal voorbeelden gegeven van hoe met verschillende technieken en materiaalbehandelingen multifunctionele scaffolds zijn te vervaardigen. Hoofdstuk 8 beschrijft scaffolds van vezels met een schil-kern structuur verkregen door bij 3DF technologie gebruik te maken van een reologisch verschijnsel bij polymeermengsels dat visceuze encapsulatie wordt genoemd. Door een smelt van een polymeermengsel waarin de componenten verschillende viscositeiten bezitten te onderwerpen aan de schuifspanningen van het 3DF extrusieproces worden vezels verkregen met een schil-kern- of holle structuur en tegelijkertijd geordend in een scaffold. In beide gevallen werd een betere

kraakbeenvorming geconstateerd dan in het geval van scaffolds met standaard vezels.

In het geval van de schil-kern vezels werd dat bereikt door speciale eigenschappen van de schil die als een coating om de vezel zat en in het geval van de holle vezels was het een betere cel “vangst” bij zaaien gecombineerd met een kleinere hoeveelheid materiaal per volume eenheid dan bij massieve vezels het geval is. Met deze structuren worden scaffolds met weefselsturende eigenschappen voorstelbaar evenals systemen met geïntegreerde nutriënten perfusie.

In hoofdstuk 9 worden scaffolds beschreven die verkregen zijn door een combinatie van 3DF en ESP technieken. Hierbij zorgt de 3DF structuur voor mechanische stevigheid en de voor weefselvorming geschiktste poriestructuur terwijl het er doorheen geweven ESP netwerk fungeert als celzeef en door oppervlaktestructuren van de microvezels de celmorfologie beïnvloedt. De zo verkregen geïntegreerde scaffolds maakten een betere zaai-efficiëntie mogelijk en daarmee een betere vorming van extracellulaire matrix.

Hoofdstuk 10 beschrijft een nieuw concept om scaffolds voor osteochondrale toepassingen te vervaardigen door integratie van 3DF, indirecte stereolithografie en vriesdrogen. Waar keramiek in het algemeen te bros en gedemineraliseerde botmatrix te week is om op een mechanisch zwaar belaste plaats te functioneren, vormt de mogelijkheid om deze materialen te integreren in een polymere 3DF matrix een aantrekkelijke manier om de voor botvorming gunstige mechanische en biologische eigenschappen van deze materialen te combineren in één construct. Met het volumepercentage van de keramische deeltjes alsmede met geometrie ervan konden de mechanische eigenschappen van deze constructen worden ingesteld.

In hoofdstuk 11, tenslotte, worden de resultaten uit dit proefschrift samengevat en besproken alsmede een aantal ideeën voor mogelijke toekomstige ontwikkelingen.



# Riassunto

Il lavoro di ricerca descritto in questa tesi presenta una serie di scaffold tridimensionali (3D) innovativi, disegnati e ottimizzati per applicazioni di ingegneria tissutale e medicina rigenerativa. L'ingegneria dei tessuti si prefigge lo scopo di riparare o rigenerare tessuti umani associando una popolazione di cellule con una matrice 3D porosa che funzioni come scaffold. Dopo aver isolato, ed eventualmente espanso, le cellule con tecniche in vitro, queste vengono seminate sugli scaffold che, a seconda della strategia considerata, possono essere impiantati subito o in un secondo momento nel corpo del paziente. Gli scaffold 3D devono tipicamente soddisfare una serie di requisiti: (i) biocompatibilità, (ii) biodegradabilità e/o biorisorbibilità, (iii) adeguate proprietà meccaniche, (iv) adatte proprietà fisico-chimiche per dirigere le interazioni cellule-materiale durante la formazione tissutale, (v) recupero della forma originale del tessuto danneggiato e integrazione con l'ambiente circostante. Dalla revisione della letteratura nel campo dell'ingegneria tissutale proposta nel capitolo 1, risulta ancora problematico soddisfare tutti i requisiti precedentemente menzionati con i biomateriali e le tecniche di fabbricazione degli scaffold oggi disponibili. Gli scaffold 3D possono essere prodotti con varie tecnologie, tra le quali la prototipizzazione rapida e l'elettrospinning sembrano essere le più promettenti. Tramite la prototipizzazione rapida (RP), per mezzo di metodiche CAD/CAM, è possibile creare scaffold caratterizzati da una rete porosa controllata e completamente accessibile, che è fondamentale per l'approvvigionamento di nutrienti e per la loro diffusione. L'elettrospinning (ESP) permette di imitare sinteticamente la matrice extracellulare (ECM) in cui le cellule sono situate, e in tal modo fornisce delle proprietà superficiali utili per influenzare la differenziazione delle cellule nel corretto fenotipo. Tuttavia, se considerate separatamente, queste tecniche di fabbricazione presentano alcuni svantaggi.

Lo scopo degli studi qui presentati è quello di caratterizzare scaffold fabbricati tramite RP ed ESP, e di proporre alcuni esempi che mettano in luce l'importanza di integrare diverse tecniche di produzione di scaffold e, possibilmente, diversi biomateriali che forniscano alle cellule adeguati segnali meccanici, fisico-chimici e biologici a livello macro, micro e nanoscopico. Se combinate assieme, le soluzioni qui proposte potrebbero soddisfare tutti i requisiti richiesti per gli scaffold da utilizzare in ingegneria tissutale.

Nei capitoli 2, 3 e 4 sono state determinate le proprietà meccaniche e fisico-chimiche di scaffold RP. Gli scaffold sono stati prodotti tramite una tecnica chiamata deposizione 3D di fibre (3DF). Le proprietà meccaniche degli scaffold 3DF possono essere modulate secondo la porosità, le dimensioni e le forme dei pori e secondo la composizione chimica del biomateriale usato. Come discusso nel capitolo 4, è stato

possibile formulare un modello matematico validato numericamente. Tale modello può essere usato per predire le proprietà meccaniche degli scaffold 3D e come strumento per ottimizzare la porosità, l'architettura e la composizione fisico-chimica di tali strutture in modo da imitare le proprietà meccaniche del tessuto da rigenerare (e.g. cartilagine articolare o meniscale). Ad esempio, il modello è stato usato per scegliere scaffold con precise proprietà meccaniche e fisico-chimiche per la rigenerazione della cartilagine articolare (capitolo 5). Scaffold con architettura simile – risultante in proprietà meccaniche simili – e diverse proprietà fisico-chimiche sono stati paragonati a scaffold con rigidità dinamica e comportamento fisico-chimico uguali a quelli della cartilagine articolare bovina. Dopo un mese di coltura, la formazione cartilaginea è stata significativamente più elevata in questi ultimi scaffold. Questi risultati non sono tanto correlati alla rigidità meccanica degli scaffold, quanto all'architettura degli scaffold. L'inferiore volume dei pori e l'inferiore porosità degli scaffold con simili proprietà rispetto alla cartilagine bovina sono risultati in una migliore capacità di intrappolamento delle cellule nei pori, e di conseguenza in una migliore efficienza di semina e formazione di ECM.

Le tecniche di prototipizzazione rapida permettono anche la fabbricazione di scaffold anatomici tramite un set di immagini di un paziente derivanti da tomografia computerizzata (CT) o da risonanza magnetica (MRI). Nel capitolo 6 è stato valutato il ruolo dell'anatomicità degli scaffold sulla formazione del tessuto cartilagineo tracheale rispetto a scaffold con geometria più semplice ma ugualmente funzionale. Un segmento tracheale è stato scelto per testare i limiti di risoluzione della tecnica 3DF. A parte l'ovvio beneficio di ricreare la forma naturale del tessuto danneggiato, gli scaffold anatomici hanno sostenuto una più elevata produzione di ECM ed una migliore differenziazione delle cellule nel tessuto cartilagineo dopo tre settimane di coltura. Paradossalmente, al crescere della complessità della geometria degli scaffold le limitazioni in risoluzione della tecnica 3DF hanno contribuito a una migliore formazione tissutale, a causa della formazione di fibrille estruse plasticamente durante la produzione degli scaffold. Queste fibrille supportano una morfologia sferica dei condrociti adesi, il che potrebbe aver influenzato positivamente la crescita tissutale.

A conseguenza dei risultati ottenuti nel capitolo 6 relativi all'effetto delle fibrille sulla dinamica di rigenerazione cartilaginea, l'influenza delle dimensioni e della topologia superficiale di fibre polimeriche sulla morfologia e proliferazione delle cellule è stata analizzata fabbricando scaffold tramite ESP. Come descritto nel capitolo 7, le cellule sono state capaci di distinguere non solo tra diverse topologie superficiali, ma anche tra fibre di diverso diametro. I risultati ottenuti suggeriscono che gli stimoli fisici presenti sulle fibre e creati tramite ESP possono influenzare la morfologia cellulare e potrebbero avere un ruolo nella loro differenziazione in uno specifico tessuto.

Nei capitoli 8, 9 e 10 sono trattati studi che mostrano come diverse tecnologie di lavorazione di materiali e diverse tecniche di fabbricazione di scaffold posso essere integrate per creare scaffold multifunzionali. Nel capitolo 8, scaffold bifasici formati da fibre rivestite da un altro biomateriale sono stati prodotti combinando 3DF con un fenomeno reologico noto come incapsulazione viscosa. Sfruttando la differenza di viscosità tra due o più polimeri in una miscela polimerica fusa e sottoponendola a

un campo di sforzi di taglio durante l'estrusione, è stato possibile fabbricare fibre bifasiche o cave e organizzarle in uno scaffold 3D. Le fibre cave sono state ottenute tramite dissolvimento selettivo dell'anima interna delle fibre bifasiche. In entrambi i casi gli scaffold hanno dimostrato una migliore rigenerazione cartilaginea a confronto con scaffold 3D standard a fibre solide monofasiche. Inoltre, questi scaffold potrebbero anche essere utili come matrici per guidare la rigenerazione tissutale (e.g. nervi o capillari) o come capillari integrati in scaffold 3D per la diretta perfusione di nutrienti. Nel capitolo 9 viene introdotta la fabbricazione di nuovi scaffold ottenuti dall'integrazione delle tecniche 3DF e ESP per la creazione di un sistema multifunzionale in cui gli scaffold 3D forniscono stabilità meccanica e una rete porosa organizzata per lo sviluppo tissutale, mentre il network ESP agisce da filtro per intrappolare le cellule e fornir loro opportuni stimoli fisici. Tali nuovi scaffold, se paragonati a scaffold 3DF, hanno mostrato un aumento significativo delle cellule adese e intrappolate nei pori, e quindi un conseguente aumento della ECM formata. Ciò è associato al mantenimento della morfologia sferica dei condrociti, dovuta alla presenza di fibre lisce e micrometriche caratteristiche del network ESP. Nel capitolo 10 viene presentato un nuovo concetto di assemblaggio di diversi biomateriali per la creazione di scaffold ibridi volti alla ricostruzione di difetti osteocondrali. Tali scaffold ibridi sono stati ottenuti dall'integrazione di 3DF, prototipizzazione rapida indiretta e freeze-drying. Poiché i materiali ceramici sono tipicamente troppo fragili e la matrice ossea demineralizzata troppo flessibile per poter essere direttamente impiantati in siti ossei ad alto carico, la possibilità di assemblarli in un singolo scaffold 3D, assieme ad una matrice polimerica funzionante da vettore, offre una soluzione interessante perché combina la stabilità meccanica del costruito finale alle proprietà di rigenerazione ossea dei singoli biomateriali usati. Questi scaffold ibridi hanno dimostrato di avere una rigidità meccanica modulabile secondo il volume specifico di ceramica presente e della loro forma all'interno della struttura.

Infine, nel capitolo 11 sono riassunti e discussi i risultati presenti in questa tesi e sono descritte alcune possibili idee per sviluppi futuri.

# Curriculum Vitae

Lorenzo Moroni was born on July 13<sup>th</sup>, 1976 in Milano, Italy. His childhood was spent in between the metropolitan city, the mountains of Aosta Valley, and the sea coast of Liguria at the border with France. After his graduation from the Renato Donatelli scientific high school (Milano, Italy) in 1995, he enrolled at the Polytechnic University of Milan. He obtained a Master of Science degree in Biomedical Engineering in 2001. The last part of his studies was conducted within the Erasmus program at the Chalmers University of Technology in Gothenburg – Sweden – where he achieved a second Master of Science degree in Nanoscale Science and Technology in 2002. His final master thesis was entitled “Poly Lactide–co-glycolide polymer microfabrication process for tissue engineering: novel patterned scaffold for cell cultivation and a capsule design for vascular endothelial growth factor controlled release”, under the supervision of Prof. M.C. Tanzi, P. Apell, and L.P. Lee at University of California at Berkeley (USA) where the experimental part of the project was performed.



In January 2003, he accepted a PhD position at the Institute for Biomedical Technology, University of Twente (Enschede, The Netherlands), in collaboration with IsoTis S.A. (Irvine, USA). The research was performed under the supervision of Prof. C.A. van Blitterswijk and Dr. J.R. de Wijn, the results of which are described in this thesis entitled “A Mechanistic Approach to Design Smart 3D Scaffolds for Tissue Engineering”. At the beginning of 2007, he will start a post-doc at the Johns Hopkins University in the Biomaterials & Tissue Engineering group of Dr. J. Elisseeff.